



**Nevada Department of Transportation**

**Report No. 743-18-803**

**Galena Creek Bridge Health Monitoring  
Instrumentation**

**June 2022**

## Disclaimer

This work was sponsored by the Nevada Department of Transportation. The contents of this report reflect the views of the authors, who are responsible for the facts and the accuracy of the data presented herein. The contents do not necessarily reflect the official views or policies of the State of Nevada at the time of publication. This report does not constitute a standard, specification, or regulation.

## TECHNICAL REPORT DOCUMENTATION PAGE

1. Report No. 743-18-803		2. Government Accession No.		3. Recipient's Catalog No.	
4. Title and Subtitle Galena Creek Bridge Health Monitoring Instrumentation				5. Report Date April 2, 2022	
				6. Performing Organization Code NV State Vendor Code: D35000813	
7. Author(s) Jee Woong Park; Ryan J. Sherman; Hamza Aslam; Erol Kalkan				8. Performing Organization Report No.	
9. Performing Organization Name and Address University of Nevada, Las Vegas 4505 S Maryland Parkway Box 404015 Las Vegas, NV 89154				10. Work Unit No.	
				11. Contract or Grant No. 743-18-803	
12. Sponsoring Agency Name and Address Nevada Department of Transportation 1263 South Stewart Street Carson City, NV 89712				13. Type of Report and Period Covered Final Report	
				14. Sponsoring Agency Code	
15. Supplementary Notes NA					
16. Abstract  <p>This abstract documents and presents a research study/implementation project of structural health monitoring (SHM) systems on the Galana Creek Bridge, supported by the Nevada Department of Transportation under Project Agreement No: P743-18-803. Full-scale SHM systems, in combination with smart monitoring software, were designed and implemented on the northbound structure of the bridge to monitor the response and behavior of the bridge to various loadings in real time. Two SHM systems, which are a primary seismic monitoring system and a secondary exploratory system, were installed to measure the structural response to seismic activity as well as to routine traffic, thermal expansion and contraction, and wind events. The seismic system consisted of 33 accelerometers and a triaxial seismograph, while the exploratory system included an array of temperature, wind, displacement, and tilt sensors. The software implemented generates a comprehensive report on each predefined triggered event and sends real-time notifications to proper authorities within NDOT on the condition of the bridge following the trigger event. Ultimately, this project serves as an SHM testbed for NDOT and contributes to the advancement of SHM as a bridge safety and management tool.</p>					
17. Key Words Structural Health Monitoring, SHM, bridge monitoring, seismic monitoring, real-time monitoring, accelerometer				18. Distribution Statement No restrictions. This document is available through the: National Technical Information Service Springfield, VA 22161	
19. Security Classif. (of this report) Unclassified		20. Security Classif. (of this page) Unclassified		21. No. of Pages 1	
				22. Price \$299,782	

# **FINAL REPORT**

## **Galena Creek Bridge Health Monitoring Instrumentation**

Prepared for:

Nevada Department of Transportation  
Carson City, NV

Prepared by:

Jee Woong Park, PhD  
University of Nevada, Las Vegas  
Las Vegas, NV

Ryan J. Sherman, PhD, PE and Hamza Aslam  
Georgia Institute of Technology  
Atlanta, GA

Erol Kalkan, PhD, PE  
QuakeLogic Inc.  
Roseville, CA

June 2022



## **ACKNOWLEDGEMENTS**

The authors are grateful for the financial support by the Nevada Department of Transportation (NDOT) to conduct this work. In addition, the authors would like to acknowledge all NDOT personnel who assisted with the coordination and execution of the field installation as well as the research assistants and technical support staff from the universities and QuakeLogic who provided unwavering support in completion of the project.

# TABLE OF CONTENTS

<b>LIST OF FIGURES .....</b>	<b>VII</b>
<b>LIST OF TABLES .....</b>	<b>IV</b>
<b>ABSTRACT .....</b>	<b>VI</b>
<b>EXECUTIVE SUMMARY .....</b>	<b>IV</b>
SUMMARY OF RESEARCH NEED .....	IV
RESEARCH FINDINGS/CONCLUSION .....	IV
<b>CHAPTER 1. INTRODUCTION .....</b>	<b>1</b>
1.1 RESEARCH NEED AND OVERARCHING PROJECT GOAL.....	1
1.2 RESEARCH OBJECTIVES .....	2
1.3 REPORT ORGANIZATION .....	3
<b>CHAPTER 2. BACKGROUND .....</b>	<b>4</b>
2.1 DESCRIPTION OF THE GALENA CREEK BRIDGE .....	4
2.1.1 <i>Materials</i> .....	7
2.1.2 <i>Superstructure</i> .....	7
2.1.3 <i>Substructure</i> .....	15
2.1.4 <i>Bearings</i> .....	17
2.2 PREVIOUS RESEARCH ON THE GALENA CREEK BRIDGE .....	18
2.2.1 <i>Seismic Time-History Analysis</i> .....	18
2.2.2 <i>Investigation of Load, Time-Dependent, and Temperature-Dependent Effects</i> .....	19
2.2.3 <i>Dynamic Characterization and Baseline Testing</i> .....	20
2.3 NEVADA DEPARTMENT OF TRANSPORTATION REPORTS.....	22
2.3.1 <i>Bridge Inspection Report, 2018</i> .....	22
2.3.2 <i>Load Rating Report, 09/13/2016</i> .....	23
<b>CHAPTER 3. STRUCTURAL HEALTH MONITORING SYSTEM HARDWARE.....</b>	<b>25</b>
3.1 PRIMARY SEISMIC SYSTEM INSTRUMENTATION .....	27
3.1.1 <i>Accelerometers</i> .....	27
3.1.2 <i>Sensor Installation and Wiring</i> .....	31
3.2 SECONDARY EXPLORATORY SYSTEM INSTRUMENTATION .....	35
3.2.1 <i>Displacement sensors</i> .....	35
3.2.2 <i>Tilt Meter</i> .....	38

3.2.3	<i>Temperature gauges</i> .....	39
3.2.4	<i>Wind Sensor</i> .....	40
3.3	DATA RECORDERS .....	40
3.4	FREE-FIELD STATION .....	42
<b>CHAPTER 4.</b>	<b>CONTROL SOFTWARE, DASHBOARD, AND REPORT</b> .....	<b>44</b>
4.1	CONTROL SOFTWARE .....	44
4.1.1	<i>Structural Health Monitoring (SHM)</i> .....	44
4.1.2	<i>Mobile-friendly Dashboard</i> .....	46
4.1.3	<i>System WatchDog</i> .....	48
4.2	ONLINE DASHBOARD .....	49
4.2.1	<i>Overview</i> .....	49
4.2.2	<i>Homepage</i> .....	49
4.2.3	<i>Facility Page</i> .....	50
4.2.4	<i>Geotechnical Tab</i> .....	55
4.2.5	<i>Instrumentation Tab</i> .....	56
4.2.6	<i>Seismic Hazard Tab</i> .....	57
4.2.7	<i>Report Tab</i> .....	59
4.2.8	<i>Data Tab</i> .....	60
4.2.9	<i>Ambient Data Tab</i> .....	61
4.2.10	<i>24 Hours Data Tab</i> .....	62
4.2.11	<i>Sensors Tab</i> .....	63
4.2.12	<i>Data List Tab</i> .....	65
4.2.13	<i>Maintenance Log Tab</i> .....	66
4.2.14	<i>Last Updates Menu Option</i> .....	67
4.2.15	<i>Inbox Menu Option</i> .....	69
4.2.16	<i>Knowledge Base Menu Option</i> .....	70
4.2.17	<i>Contact Menu Option</i> .....	71
4.2.18	<i>Shortcut Toolbar</i> .....	71
4.3	RAPID ASSESSMENT FOR ENGINEERING RESPONSE REPORT .....	72
4.4	GALENA CREEK BRIDGE TRIGGER THRESHOLD VALUES .....	74
<b>CHAPTER 5.</b>	<b>CONTROL FEA MODEL DEVELOPMENT</b> .....	<b>76</b>
5.1	BACKGROUND .....	76

5.2 LAYOUT TAB .....	77
5.3 COMPONENTS TAB .....	78
5.3.1 Materials .....	79
5.3.2 Frame Properties .....	80
5.3.3 Link Properties .....	82
5.3.4 Deck Sections .....	82
5.3.5 Diaphragms .....	85
5.3.6 Parametric Variations .....	85
5.3.7 Bearings .....	86
5.3.8 Foundations .....	87
5.3.9 Abutments .....	87
5.3.10 Bents .....	88
5.4 LOADS TAB .....	88
5.5 BRIDGE TAB .....	89
5.5.1 Bridge Object Data .....	89
5.5.2 Spans .....	90
5.5.3 Abutments .....	92
5.5.4 Bents .....	93
5.5.5 Hinges .....	94
5.5.6 Diaphragms .....	94
5.5.7 Prestressing Tendons .....	95
5.5.8 Update .....	97
5.6 ADVANCED TAB .....	98
5.7 ANALYSIS TAB .....	101
5.7.1 Introduction .....	101
5.7.2 Dead Load Analysis .....	102
5.7.3 Modal Analysis .....	103
5.7.4 Time-history Analysis .....	104
<b>CHAPTER 6. PARAMETRIC MODELING .....</b>	<b>107</b>
6.1 SUPERSTRUCTURE MATERIAL .....	109
6.1.1 Modal Analysis – Superstructure Material .....	109
6.1.2 Time History Analysis – Superstructure Material .....	111

6.2 STRUCTURAL DAMPING .....	115
6.2.1 <i>Modal Analysis – Structural Damping</i> .....	116
6.2.2 <i>Time-history Analysis – Structural Damping</i> .....	116
6.3 ELASTOMERIC BEARING STIFFNESS.....	120
6.3.1 <i>Modal Analysis – Elastomeric Bearing Stiffness</i> .....	123
6.3.2 <i>Time-history Analysis – Elastomeric Bearing Stiffness</i> .....	126
6.4 EFFECTIVE MOMENT OF INERTIA OF SUBSTRUCTURE.....	129
6.4.1 <i>Modal Analysis – Effective Column Moment of Inertia</i> .....	130
6.4.2 <i>Time-history Analysis – Effective Column Moment of Inertia</i> .....	134
6.5 LINK SLAB.....	137
6.5.1 <i>Modal Analysis – Link Slab</i> .....	139
6.5.2 <i>Time-history Analysis – Link Slab</i> .....	140
6.6 SUPERSTRUCTURE MODELING APPROACH.....	144
6.6.1 <i>Modal Analysis</i> .....	146
6.6.2 <i>Time-History Analysis</i> .....	148
6.7 BARRIER RAIL MODELING.....	153
6.7.1 <i>Modal Analysis – Barrier Rail Modelled as Frame Elements</i> .....	155
6.7.2 <i>Time-history Analysis – Barrier Rail Modelled using Frame Elements</i> .....	157
<b>CHAPTER 7. REFINED FINAL MODEL.....</b>	<b>164</b>
7.1 TRIVIAL SOLUTIONS.....	164
7.2 STRUCTURAL DAMPING .....	165
7.3 EFFECTIVE MOMENT OF INERTIA OF SUBSTRUCTURE ELEMENTS .....	166
7.4 MATERIAL STIFFNESS.....	167
7.5 FINAL PROPOSED MODAL ANALYSIS .....	168
7.6 FINAL PROPOSED MODEL TIME-HISTORY ANALYSIS.....	170
<b>CHAPTER 8. CONCLUSIONS AND FUTURE WORK .....</b>	<b>174</b>
8.1 CONCLUSIONS.....	174
8.2 RECOMMENDATIONS.....	175
<b>BIBLIOGRAPHY .....</b>	<b>179</b>
<b>APPENDIX A: EXAMPLE RAPID ASSESSMENT FOR ENGINEERING RESPONSE REPORT.....</b>	<b>B</b>
<b>APPENDIX B: MANUFACTURER SPECIFICATION SHEETS FOR THE INSTALLED SENSORS.....</b>	<b>C</b>
<b>APPENDIX C: CALCULATIONS .....</b>	<b>D</b>

# LIST OF FIGURES

FIGURE 1-1: ELEVATION VIEW OF THE GALENA CREEK BRIDGE .....	1
FIGURE 2-1: GALENA CREEK BRIDGE LOCATION ON I-580 SOUTH OF RENO, NV (GOOGLE, 2021) .....	5
FIGURE 2-2: PLAN VIEW OF EAST FACE OF GALENA CREEK BRIDGE NORTHBOUND STRUCTURE .....	6
FIGURE 2-3: TYPICAL CROSS SECTION OF THE TWO-CELL SUPERSTRUCTURE (M) .....	8
FIGURE 2-4: STRENGTHENED CROSS-SECTION AREAS OF BOX GIRDER .....	8
FIGURE 2-5: TYPICAL USE OF 40 MPA CONCRETE OVER PIERS 2 AND 3 (M) .....	8
FIGURE 2-6: BOTTOM SLAB THICKNESS VARIATION LEGEND FOR PIERS .....	9
FIGURE 2-7: BOX GIRDER VARIATION AT INTERSECTION OF SUPERSRUCTURE AND ARCH (M) .....	10
FIGURE 2-8: EXTERIOR PHOTOGRAPH OF ARCH MERGE REGION .....	10
FIGURE 2-9: INTERIOR PHOTOGRAPH OF ARCH MERGE REGION .....	11
FIGURE 2-10: PHOTOGRAPHS OF GALENA CREEK BRIDGE EXPANSION JOINT HINGE .....	12
FIGURE 2-11: EXAMPLE OF GALENA CREEK BRIDGE DIAPHRAGM .....	14
FIGURE 2-12: HINGE DIAPHRAGM ELEVATION VIEW (M) .....	14
FIGURE 2-13: HINGE DIAPHRAGM ELEVATION VIEW (M) .....	15
FIGURE 2-14: THRUST BLOCK SUPPORTING THE BASE OF THE ARCH AND COLUMN .....	17
FIGURE 2-15: LINK BEAM CONNECTING THE NORTHBOUND AND SOUTHBOUND SUPERSTRUCTURES .....	17
FIGURE 2-16: THE SUPERSTRUCTURE (BLUE) AND SUBSTRUCTURE (ORANGE) ACCELEROMETER PLACEMENT .....	21
FIGURE 3-1: PRIMARY SEISMIC SHM SYSTEM UNIAXIAL ACCELEROMETER LOCATIONS ON THE GALENA CREEK BRIDGE .....	26
FIGURE 3-2: SECONDARY EXPLORATORY SHM SYSTEM SENSOR LOCATIONS ON THE GALENA CREEK BRIDGE .....	26
FIGURE 3-3: UTILITY SHED LOCATED SOUTH OF THE SOUTHBOUND STRUCTURE .....	27
FIGURE 3-4: ACCELEROMETER .....	28
FIGURE 3-5: ALUMINUM PLATE FOR MOUNTING ACCELEROMETERS .....	32
FIGURE 3-6: EXAMPLE OF PLATE WITH THREE SENSORS AT BOTTOM OF PIER 4 .....	32
FIGURE 3-7: PVC CONDUITS ALONG THE FACE OF ABUTMENT 1 .....	33
FIGURE 3-8: PVC CONDUIT EXTRUDING THROUGH THE BOTTOM SLAB NEAR ABUTMENT 1 .....	33
FIGURE 3-9: TYPICAL CABLES RUNNING ALONG THE EAST GIRDER OF THE SUPERSTRUCTURE .....	34
FIGURE 3-10: TYPICAL CONNECTION BETWEEN PRIMARY AND SENSOR CABLES VIA TERMINAL BLOCK .....	34
FIGURE 3-11: LINEAR POTENTIOMETER .....	36
FIGURE 3-12: POTENTIOMETER LOCATED AT WEST EDGE OF ABUTMENT 1 OF NORTHBOUND STRUCTURE .....	37

FIGURE 3-13: EXAMPLE OF POTENTIOMETER INSTALLED AT HINGE 1 .....	37
FIGURE 3-14: BIAXIAL INCLINOMETER INSTALLED A SOUTH FACE OF PIER DIAPHRAGM AT PIER 2 .....	38
FIGURE 3-15: TEMPERATURE PROBE LOCATED IN GALENA CREEK BRIDGE .....	39
FIGURE 3-16: ULTRASONIC ANEMOMETER INSTALLED AT UTILITY SHED .....	40
FIGURE 3-17: OBSIDIAN 12X (TOP) AND 36X (BOTTOM) DATA RECORDERS WITH CABLES .....	41
FIGURE 3-18: BULLET TYPE GPS ANTENNAS .....	42
FIGURE 3-19: ETNA 2 ACCELEROGRAPH AND PROTECTIVE CASE .....	43
FIGURE 4-1: OVERVIEW OF THE SHM MONITORING SOFTWARE .....	45
FIGURE 4-2: DASHBOARD VIEWS COMPATIBLE WITH VARIOUS MOBILE DEVICES .....	46
FIGURE 4-3: EXAMPLE VIEW OF DASHBOARD .....	47
FIGURE 4-4: WATCHDOG SYSTEM TO MONITOR SYSTEM STATUS.....	48
FIGURE 4-5: EXAMPLE QUAKEDOG REPORT .....	48
FIGURE 4-6: DASHBOARD HOMEPAGE .....	50
FIGURE 4-7: FACILITY SELECTION USING LEFT MENU.....	51
FIGURE 4-8: FACILITY SELECTION USING SHORTCUT BAR .....	51
FIGURE 4-9: FACILITY SELECTION FROM MAP .....	52
FIGURE 4-10: EXAMPLE ASSET MANAGEMENT PAGE FOR FREE-FIELD SITE .....	53
FIGURE 4-11: EXAMPLE ASSET MANAGEMENT PAGE FOR GALENA CREEK BRIDGE.....	53
FIGURE 4-12: EXAMPLE FACILITY SUMMARY AND CONTACT INFORMATION FOR GALENA CREEK BRIDGE .....	54
FIGURE 4-13: EXAMPLE GEOTECHNICAL TAB FOR GALENA CREEK BRIDGE .....	55
FIGURE 4-14: EXAMPLE INSTRUMENTATION SUMMARY AND SENSOR LAYOUT FOR PRIMARY SEISMIC MONITORING SYSTEM AND SECONDARY SYSTEM INSTALLED AT THE GALENA CREEK BRIDGE PROVIDED UNDER THE INSTRUMENTATION TAB .....	56
FIGURE 4-15: EXAMPLE SENSOR INSTRUMENTATION AT THE FREE-FIELD SITE UNDER THE INSTRUMENTATION TAB.....	57
FIGURE 4-16: EXAMPLE SEISMIC DESIGN MAPS PROVIDED UNDER SEISMIC HAZARD TAB .....	58
FIGURE 4-17: EXAMPLE RESPONSE SPECTRUM PROVIDED UNDER SEISMIC HAZARD TAB.....	58
FIGURE 4-18: EXAMPLE COLLECTION OF HISTORICAL SHM REPORTS FROM THE FREE-FIELD SITE .....	59
FIGURE 4-19: EXAMPLE COLLECTION OF HISTORICAL SHM REPORTS FROM THE BRIDGE.....	60
FIGURE 4-20: EXAMPLE DATA FILES CONTAINED UNDER DATA TAB FROM THE FREE-FIELD SITE .....	60
FIGURE 4-21: EXAMPLE DATA FILES CONTAINED UNDER DATA TAB FROM THE BRIDGE .....	61
FIGURE 4-22: EXAMPLE COLLECTION OF AMBIENT DATA FILES CONTAINED UNDER AMBIENT DATA TAB.....	61
FIGURE 4-23: EXAMPLE OF SEISMIC GRAPHICS PROVIDED UNDER 24 HOUR DATA TAB FOR THE BRIDGE .....	62
FIGURE 4-24: CLOSE-UP VIEW OF SENSOR 1 IN 24-HOUR DATA .....	62
FIGURE 4-25: EXAMPLE OF TILT SENSOR DATA PROVIDED UNDER SENSORS TAB.....	63



FIGURE 4-26: EXAMPLE OF DISPLACEMENT (POTENTIOMETER) DATA PROVIDED UNDER SENSORS TAB.....	64
FIGURE 4-27: EXAMPLE OF TEMPERATURE AND WIND DATA PROVIDED UNDER SENSORS TAB .....	64
FIGURE 4-28: EXAMPLE OF DATA LIST TAB SHOWING RAW DATA FROM THE FREE-FIELD SENSOR.....	65
FIGURE 4-29: EXAMPLE OF DATA LIST TAB SHOWING RAW DATA FROM THE SENSORS IN THE BRIDGE .....	65
FIGURE 4-30: EXAMPLE OF MAINTENANCE LOG TAB SHOWING HISTORICAL SYSTEM MAINTENANCE .....	66
FIGURE 4-31: EXAMPLE OF CHRONOLOGICAL REPORTS FOUND IN THE LAST UPDATES MENU OPTION .....	67
FIGURE 4-32: EXAMPLE RAPID ASSESSMENT FOR ENGINEERING RESPONSE REPORT COVER.....	68
FIGURE 4-33: EXAMPLE INBOX MENU OPTION ENABLING DIRECT COMMUNICATION WITH QUAKELOGIC.....	69
FIGURE 4-34: EXAMPLE LIST OF FREQUENTLY ASKED QUESTIONS IN KNOWLEDGE BASE MENU OPTION.....	70
FIGURE 4-35: CONTACT MENU OPTION FOR ACCESS TO QUAKELOGIC SUPPORT .....	71
FIGURE 4-36: SHORTCUTS TOOLBAR .....	71
FIGURE 5-1: PRELIMINARY CONTROL MODEL .....	76
FIGURE 5-2: HORIZONTAL CURVATURE OF SPAN 1 (SOUTHBOUND SUPERSTRUCTURE) .....	78
FIGURE 5-3: EXAMPLE LAYOUT LINE INPUT FOR CSIBRIDGE (SOUTHBOUND SUPERSTRUCTURE) .....	78
FIGURE 5-4: EXAMPLE OF SECTIONS FOUND IN THE CSIBRIDGE COMPONENTS TAB .....	79
FIGURE 5-5: EXAMPLE SOLID RECTANGULAR SECTION INPUT FOR ARCH DIAGRAM.....	81
FIGURE 5-6: EXAMPLE SECTION DESIGNER TOOL FOR TYPICAL ARCH FRAME .....	82
FIGURE 5-7: CSIBRIDGE TEMPLATE FOR BOX GIRDER INPUTS.....	83
FIGURE 5-8: EXAMPLE OF LINEAR VARIATION INPUT IN CSIBRIDGE (SPAN 5) .....	86
FIGURE 5-9: LOADS TAB AS SEEN IN CSIBRIDGE .....	88
FIGURE 5-10: EXAMPLE OF SUPERSTRUCTURE SPAN VARIATIONS IN CSIBRIDGE.....	91
FIGURE 5-11: EXAMPLE OF DECK SECTION VARIATION IN CSIBRIDGE .....	92
FIGURE 5-12: TYPICAL CSIBRIDGE INPUT FOR ABUTMENTS .....	92
FIGURE 5-13: TYPICAL CSIBRIDGE INPUT OF BENT INFORMATION .....	93
FIGURE 5-14: TYPICAL CSIBRIDGE PRESTRESSING INPUT .....	96
FIGURE 5-15: EXAMPLE OF CSIBRIDGE TENDON PARABOLIC PATH .....	97
FIGURE 5-16: EXAMPLE OF UPDATING BRIDGE OBJECT MODEL IN CSIBRIDGE .....	98
FIGURE 5-17: ARCH MODELED AS FRAME ELEMENTS IN CSIBRIDGE WITH SEGMENT LABELS .....	98
FIGURE 5-18: EXTRUDE VIEW OF CSIBRIDGE MODEL AT BASE OF COLUMN AND PIER .....	100
FIGURE 5-19: ELEVATION VIEW OF THE LINKS CONNECTING THE ARCH AND BOX GIRDER IN CSIBRIDGE .....	100
FIGURE 5-20: DEFINING THE MASS SOURCE FOR CSIBRIDGE .....	101
FIGURE 5-21: CSIBRIDGE INPUT FOR DEAD LOAD CASE .....	102
FIGURE 5-22: CSIBRIDGE INPUT FOR MODAL ANALYSIS CASE.....	103
FIGURE 5-23: MODAL ANALYSIS RESULTS OF CONTROL MODEL .....	104
FIGURE 5-24: EXAMPLE OF AN IMPORTED GROUND MOTION FROM TEXT FILE IN CSIBRIDGE.....	105

FIGURE 5-25: CSIBRIDGE INPUT FOR TIME-HISTORY LOAD CASE SIMULATING AN EARTHQUAKE .....	106
FIGURE 6-1: ENVELOPE OF TRANSVERSE DISPLACEMENT OF NORTHBOUND SUPERSTRUCTURE FOR SUPERSTRUCTURE MATERIAL STIFFNESS VARIANTS.....	113
FIGURE 6-2: MAXIMUM LONGITUDINAL STRESSES IN SUPERSTRUCTURE FOR SUPERSTRUCTURE MATERIAL STIFFNESS VARIANTS .....	114
FIGURE 6-3: ENVELOPE OF TRANSVERSE DISPLACEMENT OF SUPERSTRUCTURE FROM DAMPING ANALYSES .....	118
FIGURE 6-4: MAXIMUM SUPERSTRUCTURE STRESSES FROM DAMPING ANALYSES.....	119
FIGURE 6-5: ALLOWABLE DEGREES OF FREEDOM (LEFT) OF THE BEARING PADS RELATIVE TO CSIBRIDGE GLOBAL AXES.....	121
FIGURE 6-6: UPPER LIMIT ABUTMENT BEARING STIFFNESS INPUT FOR CSIBRIDGE ( $G = 1.38$ MPA) .....	122
FIGURE 6-7: UPPER LIMIT HINGE BEARING STIFFNESS INPUT FOR CSIBRIDGE ( $G = 1.38$ MPA) .....	122
FIGURE 6-8: MAXIMUM LONGITUDINAL DISPLACEMENT OF SUPERSTRUCTURES FROM BEARING ANALYSES .....	128
FIGURE 6-9: EXAMPLE OF MOI REDUCTION FACTOR APPLIED IN CSIBRIDGE .....	130
FIGURE 6-10: MAXIMUM TRANSVERSE DISPLACEMENT OF SUPERSTRUCTURES FOR SUBSTRUCTURE EFFECTIVE MOI ANALYSES.....	135
FIGURE 6-11: MAXIMUM TRANSVERSE DISPLACEMENT AT MIDSPAN OF SPAN 3.....	136
FIGURE 6-12: NORTHBOUND (WHITE) AND SOUTHBOUND (PINK) SUPERSTRUCTURES HIGHLIGHTED BY COLOR .....	138
FIGURE 6-13: SINGLE SHELL ELEMENT (TEAL) CONNECTING NORTHBOUND (WHITE) AND SOUTHBOUND (PINK) STRUCTURES.....	138
FIGURE 6-14: MAXIMUM TRANSVERSE DISPLACEMENT OF SUPERSTRUCTURES FOR LINK SLAB ANALYSES .....	142
FIGURE 6-15: MAXIMUM SUPERSTRUCTURES STRESSES FOR LINK SLAB ANALYSES .....	143
FIGURE 6-16: EXAMPLE OF FRAME SPINE MODEL USING RIGID LINKS THAT EXTEND TO LINK SLAB SHELL .....	145
FIGURE 6-17: FRAME SPINE SUPERSTRUCTURE MODEL TO REPLICATE THE 2013 UNR SAP2000 MODEL.....	145
FIGURE 6-18: ENVELOPE OF LONGITUDINAL DISPLACEMENT OF SUPERSTRUCTURES FOR SHELL VS SOLID SUPERSTRUCTURE ANALYSES (X-AXIS).....	150
FIGURE 6-19: ENVELOPE OF TRANSVERSE DISPLACEMENT OF SUPERSTRUCTURES FOR SHELL VS SOLID SUPERSTRUCTURE ANALYSES (Y-AXIS) .....	151
FIGURE 6-20: ENVELOPE OF VERTICAL DISPLACEMENT OF SUPERSTRUCTURES FOR SHELL VS SOLID SUPERSTRUCTURE ANALYSES (Z-AXIS) .....	152
FIGURE 6-21: SUPERSTRUCTURE OF CONTROL MODEL MADE UP OF SHELL ELEMENTS.....	153
FIGURE 6-22: BARRIER RAIL FRAME ELEMENTS DRAWN ALONG DECK EDGES .....	154
FIGURE 6-23: BARRIER RAIL CROSS SECTION DEFINED USING SECTION DESIGNER IN CSIBRIDGE.....	155

FIGURE 6-24: ENVELOPE OF MAXIMUM VERTICAL DISPLACEMENT OF SUPERSTRUCTURES FOR PARAPET ANALYSES .....	159
FIGURE 6-25: ENVELOPE MAXIMUM TRANSVERSE DISPLACEMENT OF SUPERSTRUCTURES FOR PARAPET ANALYSES .....	160
FIGURE 6-26: ENVELOPE MAXIMUM LONGITUDINAL DISPLACEMENT OF SUPERSTRUCTURES FOR PARAPET ANALYSES.....	161
FIGURE 6-27: ENVELOPE MAXIMUM STRESSES IN SUPERSTRUCTURE FOR PARAPET ANALYSES .....	162
FIGURE 7-1: ENVELOPE OF VERTICAL DISPLACEMENTS OF NORTHBOUND SUPERSTRUCTURE FOR CONTROL VS FINAL MODELS.....	171
FIGURE 7-2: ENVELOPE OF TRANSVERSE DISPLACEMENT OF NORTHBOUND SUPERSTRUCTURE FOR CONTROL VS FINAL MODELS.....	172
FIGURE 7-3: ENVELOPE OF LONGITUDINAL DISPLACEMENT OF NORTHBOUND SUPERSTRUCTURE FOR CONTROL VS FINAL MODELS.....	173

## LIST OF TABLES

TABLE 2-1: CONCRETE CLASSIFICATION ASSIGNMENTS .....	7
TABLE 2-2: BOTTOM SLAB THICKNESS VARIATION LEGEND .....	9
TABLE 2-3: PRESTRESSING DETAILS .....	12
TABLE 2-4: DIAPHRAGM THICKNESSES .....	13
TABLE 2-5: COLUMN HEIGHTS .....	15
TABLE 2-6: INVENTORY VEHICLE LOAD RATING RESULTS.....	23
TABLE 2-7: OPERATING VEHICLE LOAD RATING RESULTS .....	23
TABLE 3-1: ACCELEROMETER LOCATION AND ORIENTATION .....	30
TABLE 4-1: PRELIMINARY GALENA CREEK BRIDGE TRIGGER THRESHOLD VALUES .....	74
TABLE 5-1: INPUTS FOR BOX GIRDER DEFINITION FOR CSIBRIDGE (M).....	84
TABLE 5-2: CALCULATED STIFFNESS VALUES FOR ELASTOMERIC BEARINGS .....	87
TABLE 5-3: GALENA CREEK BRIDGE SPAN LENGTHS AND STATION LOCATIONS .....	90
TABLE 5-4: BENT ELEVATION VALUES ALONG GLOBAL Z-AXIS .....	93
TABLE 5-5: DIAPHRAGM LOCATIONS.....	94
TABLE 5-6: SEGMENT END NODE OFFSET FOR MODELING ARCH .....	98
TABLE 6-1: LIST OF PARAMETERS AND RESPECTIVE VARIATIONS .....	108
TABLE 6-2: TOP FIVE MODES IN THE LONGITUDINAL DIRECTION FOR SUPERSTRUCTURE MATERIAL VARIATION (X-AXIS).....	110
TABLE 6-3: TOP FIVE MODES IN THE TRANSVERSE DIRECTION FOR SUPERSTRUCTURE MATERIAL VARIATION (Y-AXIS).....	110
TABLE 6-4: TOP FIVE MODES IN THE VERTICAL DIRECTION FOR SUPERSTRUCTURE MATERIAL VARIATION (Z-AXIS) .....	111
TABLE 6-5: COMPARISON OF TOP LONGITUDINAL MODES FOR BEARING STIFFNESS VARIATIONS (X-AXIS) .....	124
TABLE 6-6: COMPARISON OF TOP TRANSVERSE MODES FOR BEARING STIFFNESS VARIATIONS (Y-AXIS) .....	124
TABLE 6-7: COMPARISON OF TOP VERTICAL MODES FOR BEARING STIFFNESS VARIATIONS (Z-AXIS) .....	125
TABLE 6-8: COMPARISON OF TOP LONGITUDINAL MODES FOR MOI VARIATION (X-AXIS) .....	131
TABLE 6-9: COMPARISON OF TOP TRANSVERSE MODES FOR MOI VARIATION (Y-AXIS) .....	132
TABLE 6-10: COMPARISON OF TOP VERTICAL MODES FOR MOI VARIATION (Z-AXIS) .....	133
TABLE 6-11: TOP FIVE MODES IN THE LONGITUDINAL DIRECTION MODAL VARIATION (X-AXIS) .....	139
TABLE 6-12: TOP FIVE MODES IN THE TRANSVERSE DIRECTION MODAL VARIATION (Y-AXIS) .....	139
TABLE 6-13: TOP FIVE MODES IN THE VERTICAL DIRECTION MODAL VARIATION (Z-AXIS).....	139
TABLE 6-14: COMPARISON OF TOP LONGITUDINAL MODES FOR SUPERSTRUCTURE MODELING VARIATION (X-AXIS).....	146

TABLE 6-15: COMPARISON OF TOP TRANSVERSE MODES FOR SUPERSTRUCTURE MODELING VARIATION (Y-AXIS).....	147
TABLE 6-16: COMPARISON OF TOP VERTICAL MODES FOR SUPERSTRUCTURE MODELING VARIATION (Z-AXIS).....	148
TABLE 6-17: COMPARISON OF TOP TRANSVERSE MODES: 2013 SAP2000 MODEL VS SPINE FRAME.....	148
TABLE 6-18: COMPARISON OF TOP LONGITUDINAL MODES FOR BARRIER RAIL VARIATION (X-AXIS) .....	156
TABLE 6-19: COMPARISON OF TOP TRANSVERSE MODES FOR BARRIER RAIL VARIATION (Y-AXIS) .....	156
TABLE 6-20: COMPARISON OF TOP VERTICAL MODES FOR BARRIER RAIL VARIATION (Z-AXIS) .....	157
TABLE 7-1: FINAL MODEL CONCRETE MATERIAL PROPETIES .....	167
TABLE 7-2: COMPARISON OF TOP LONGITUDINAL MODES FOR CONTROL VS FINAL MODEL (X-AXIS) .....	168
TABLE 7-3: COMPARISON OF TOP TRANSVERSE MODES FOR CONTROL VS FINAL MODEL (Y-AXIS).....	168
TABLE 7-4: COMPARISON OF TOP VERTICAL MODES FOR CONTROL VS FINAL MODEL (Z-AXIS) .....	169
TABLE 7-5: COMPARISON OF TOP TRANSVERSE MODES FOR CARR & SANDERS VS FINAL MODEL (Y-AXIS) .....	169
TABLE 8-1: FINAL MODEL NODE NUMBERS CORRESPONDING WITH SENSOR LOCATIONS .....	176

## ABSTRACT

An effective structural health monitoring (SHM) system for bridges is much more than just a network of sensors.

As bridges are now designed to serve for more than 100 years, SHM systems, in combination with bridge rating systems, have been specified to provide a rational basis for prioritization of inspections and maintenance on structural components.

Signature bridges in California, including the Golden Gate, Bay, Dumbarton, and San Mateo Bridges, have instrumentation systems installed to monitor their conditions under daily traffic and responses during seismic events.

Galena Creek Bridge, the largest bridge in Nevada, has now the most sophisticated SHM system installed in the United States.

This SHM system is designed to detect short-term (such as seismic action) and long-term (deterioration and degradation) changes that could potentially damage the bridge. The system includes real-time sensor data analysis and periodic sampling of dynamic response measurements, analyzed through statistical methods to evaluate the current state-of-health (SOH) of the structure.

To identify the bridge's SOH, not only to seismic activity but also to routine traffic, thermal expansion and contraction, and windstorms, critical elements and locations were instrumented. The SHM system consists of 33 accelerometers and a triaxial accelerograph, as well as an array of temperature, wind, displacement, and tilt sensors. The two 24-bit data-loggers on-site collect 830 million data points a day.

The SHM system, utilizing **SMARTBRIDGE** software platform, processes gigabytes of new data each day to assess bridge performance. Intelligent data reduction algorithms immediately show the effects of unusual loads and cumulative performance. Short- and long-term behavior, as well as seismic response of the bridge, can be seen from easy-to-read statistical summaries, data analysis reports, and measurement correlations available at a secure and online dashboard.

The SHM system sends immediate alerts in a variety of forms, including text and email message, upon detection of anomalies or earthquakes to notify proper authorities within NDOT for rapid response.

The true value of this SHM system is to highlight more focused inspections, carry out timely maintenance, and provide a more cost-effective asset management program for the NDOT to mitigate risks to the most iconic bridge of Nevada.



# **EXECUTIVE SUMMARY**

## **Summary of Research Need**

Northern Nevada is a seismically active region of the United States. While a strong earthquake could cause significant damage to infrastructure and injuries to the public, structural health monitoring (SHM) can enable a rapid condition assessment to ensure an efficient recovery. In addition, SHM provides numerous benefits when assessing the condition of a structure for long-term degradation or response to an extreme event. The Nevada Department of Transportation (NDOT) was interested in developing an SHM test bed. Previous monitoring had been performed on the Galena Creek Bridge, making it an ideal structure to further explore SHM as a tool for bridge condition assessment. The Galena Creek Bridge carries Interstate 580 and U.S. Route 395 between Reno and Carson City, Nevada and is the largest concrete cathedral arch bridge in the world with a 210-meter arch span. Inspection of such a large bridge is highly time-consuming and expensive in labor cost. Further, traditional visual inspection can be a subjective assessment that is based on the inspector. To enhance the practice of bridge inspections, SHM has received attention as an effective and automated method of real-time structural assessment, leveraging recent advances in sensor technologies and pertinent data analytics. In this regard, the current project aimed to develop and implement a comprehensive SHM system on the Galena Creek Bridge as an improved safety management tool for NDOT as well as the public.

To compliment the SHM systems, a detailed finite element model was developed in CSiBridge to improve the understanding of the Galena Creek Bridge structural response. A parametric study examined how a range of variables influenced the dynamic properties of the structure. Static dead load, modal, and time-history analyses were performed to provide insights on the influence of each parameter. Recommendations are provided to enable future model calibration to the field-measured data from the SHM systems.

## **Research Findings/Conclusion**

The research successfully designed and implemented an integrated structural health monitoring system for building applications for use on the Galena Creek Bridge. Two new, permanent SHM systems were installed on the northbound structure of the Galena Creek Bridge. A primary seismic SHM system was composed of 33 uniaxial accelerometers located at key locations along the superstructure and substructure with a triaxial seismograph at a free-field site, approximately 150 feet away from the bridge. A secondary exploratory SHM system, composed of potentiometers, inclinometers, temperature gauges, and anemometers, served to further expand the capabilities of the primary system by recording displacement, tilt, temperature, and wind conditions. Following the hardware installation, the system software (i.e., **SMARTBRIDGE** SHM by QuakeLogic) was designed and implemented to perform SHM on the bridge. Based on the identified seismic hazard description of the site, trigger threshold values were established. During a trigger event, the system provides real-time alerts and generates a complete report for any critical seismic event. Ultimately, this project provided a functional SHM testbed that contributes to the advancement of NDOT's facility management methods, potentially reducing cost in infrastructure management and enhancing the continued safe operation of critical infrastructure.

## **CHAPTER 1. INTRODUCTION**

The Galena Creek Bridge carries Interstate 580 and U.S. Route 395 over the Galena Creek, between Carson City and Reno, Nevada (NDOT, 2019). The bridge is comprised of two 526.2-meter long, seven-span, two-cell reinforced concrete box girder bridges. Span 3 of the structure has a length of 210 meters and is supported by a reinforced concrete arch, distinguishing the Galena Creek Bridge as the largest cathedral arch bridge in the world (Figure 1-1). Elastomeric bearing hinges located in Spans 2 and 4 divide the structure into three frames. The northbound and southbound units are connected by a link slab along Frame 2 which provides resistance to lateral loads. The deck of each bridge carries three lanes of traffic and experiences an annual daily traffic (ADT) of 18,000 (NDOT, 2019). Construction of the Galena Creek Bridge was completed in August of 2012 (Carr and Sanders, 2013).



**Figure 1-1: Elevation view of the Galena Creek Bridge**

### **1.1 Research Need and Overarching Project Goal**

The Galena Creek Bridge is located within a 1,000 km long geological depression called Walker Lane, which runs along the Nevada-California border (Briggs and Hammond, 2011). Walker Lane is a collection of active faults, a product of interactions between the Pacific and North American tectonic plates. As a result, Walker Lane is subject to frequent, and sometimes severe, seismic activity. Earthquakes, such as the 2019 7.1-magnitude earthquake recorded in Ridgecrest, CA, can pose a significant threat to structures located in the Walker Lane network of faults (Wolterbeek, 2020).

As technology rapidly advances, bridge owners are beginning to explore methods, such as structural health monitoring (SHM), to supplement traditional visual inspections for assessing structural performance. When properly implemented, SHM can serve as an effective tool to identify complex structural issues by collecting real-time data from a structure. Due to the complexities of the Galena Creek Bridge, the Nevada Department of Transportation (NDOT) has had interest in gaining more understanding of the behavior of the structure during seismic events using SHM. Upon completion of the Galena Creek Bridge, an SHM system was installed by researchers at the University of Nevada at Reno (UNR) to better understand the physical and dynamic properties of the structure (Carr and Sanders, 2013). Accelerometers were located throughout the southbound superstructure and baseline data were collected through a series of field tests. A finite element analysis (FEA) model was made of the Galena Creek Bridge to estimate the individual component forces due to the tests (Carr and Sanders, 2013). The field-measured time-history data served as input for the computational model. The UNR SHM system was initially intended to be a permanent fixture; however, it was abandoned after the completion of the 2013 study.

As a result, in 2018 NDOT identified a research need to explore SHM as a tool to augment bridge structure inspection and management through the repair, enhancement, or replacement of the SHM system on the Galena Creek Bridge. Ultimately, the overarching goal of NDOT is for the Galena Creek Bridge to serve as a catalyst for the implementation of future SHM across the NDOT inventory.

## **1.2 Research Objectives**

The objective of this research was to enhance the understanding of the behavior of the Galena Creek Bridge through the development and implementation of two new permanent SHM systems. These systems provide continuous monitoring of the bridge behavior during routine service loads, such as traffic, wind, and thermal expansion, as well as extreme events, such as seismic events. The project has been divided into four primary objectives:

1. Design and install a primary SHM system to capture the structural response during seismic loading, including a free-field station located adjacent to the Galena Creek Bridge.

2. Design and install an exploratory SHM system to extend the capabilities of the proven seismic system to include displacement, tilt, temperature, and wind responses.
3. Install a software system for data communication, analysis, and continued data collection for establishing reliable trigger threshold values for future events for both SHM systems to automatically generate notifications in the form of email and/or text messages to appropriate NDOT personal. Reports will include the response characteristics and inspection priority.
4. Develop an FEA model of the Galena Creek Bridge using CSiBridge and conduct a parametric study to evaluate changes in the structural response relative to a defined set of parameters.

### **1.3 Report Organization**

This report has been organized into eight chapters. Chapter 1 is a general introduction, including the research need, goal, and objectives. Chapter 2 describes relevant background on the Galena Creek Bridge, including design aspects, previous research conducted on the bridge, and available NDOT inspection and load rating reports. Chapter 3 details both SHM systems installed as part of the project, including the sensor types and the locations of installation. Chapter 4 shows example results from the SHM dashboard and describes the output provided during the trigger events. Chapter 5 presents an FEA model created using CSiBridge to estimate the structural response. Chapter 6 provides results from a parametric study of modeling parameters on the dynamic response of the structure. Chapter 7 describes a final proposed FEA model. Chapter 8 includes conclusions and recommendations for future work.

## **CHAPTER 2. BACKGROUND**

The Galena Creek Bridge is the largest concrete cathedral arch bridge in the world with a 210-meter arch span. The bridge consists of two 526.2-meter cast-in-place, conventionally reinforced concrete box-girder structures partially linked together. Completed in 2012, the bridge connects Reno and Carson City, Nevada as part of Interstate 580 and US Route 395.

UNR, in conjunction with NDOT, instrumented and tested the middle frame of the southbound superstructure from 2008 to 2013. The researchers employed field experiments to characterize baseline dynamic properties (Carr and Sanders, 2013). The 2013 instrumentation system was intended to be a permanent seismic SHM installation; however, at the conclusion of the project, the system was not maintained or monitored. NDOT has a renewed interest in establishing a permanent SHM system on the Galena Creek Bridge to monitor its response to seismic events and routine traffic. The following describes the design, previous research, and relevant NDOT reports on the Galena Creek Bridge.

### **2.1 Description of the Galena Creek Bridge**

The Galena Creek Bridge (Figure 1-1) was constructed in Nevada as part of I-580 Freeway Extension Project to connect Reno and Carson City (Figure 2-1). NDOT designed the Galena Creek Bridge in accordance with AASHTO *Standard Specifications for Highway Bridges, 16th Edition*, including the 2000 interims. The live loads for the bridge design included the standard HS-25-44 truck and California P-13 permit vehicle, while the seismic design was based on a 475-year earthquake. The initial design plans consisted of a steel pilot truss arch that would serve as the framework for the cathedral arch; however, disputes regarding wind loads during construction led to delays in development. Ultimately, the steel pilot truss approach was dismissed in favor of conventional falsework. Construction of the bridge began in 2008 and was completed in 2012.

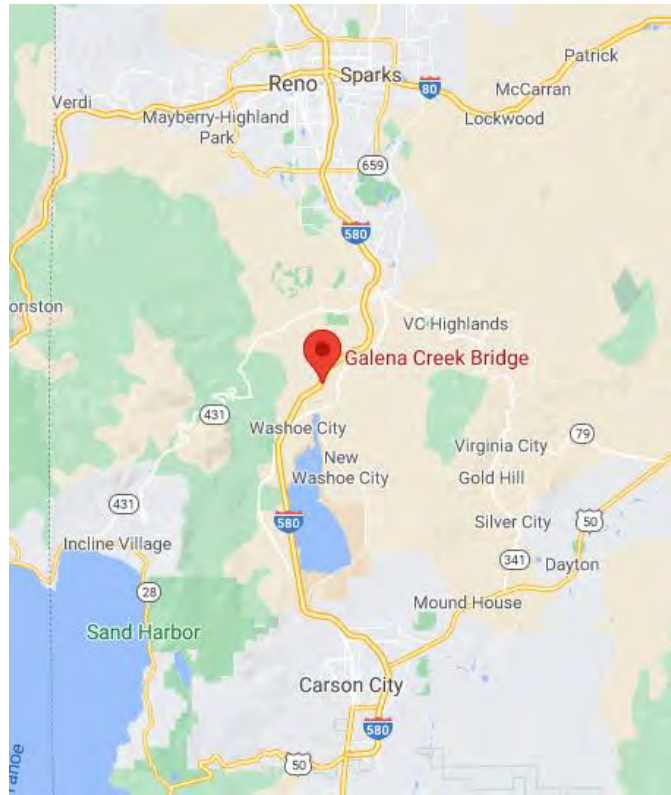


**Figure 2-1: Galena Creek Bridge location on I-580 south of Reno, NV (Google, 2021)**

The Galena Creek Bridge consists of two separate seven-span structures, one carrying northbound traffic and one carrying southbound traffic, tied together laterally by two link beams and a link slab in the arch span. Both the northbound and southbound structures carry three lanes of traffic and experience an average daily traffic of 18,000 vehicles. Longitudinally post-tensioned two-cell box-girders rest on the six sets of single column piers with an integral transversely post-tensioned 0.2 m concrete deck. Each of the 12 piers consists of a single hollow rectangular box column. Span 3 of each structure, measuring 210 m, is supported by a cathedral arch. The bases of the arch and adjacent columns are fixed to a concrete thrust block that is anchored into competent bedrock. The remaining columns are supported by rectangular footings anchored by cast-in-drilled-holes piles of varying depth. Internal expansion joint hinges, located in Spans 2 and 4 near the piers just outside of the arch, divide the structure into three frames and permit longitudinal movement (Figure 2-2). Each frame has a unique prestressing system.



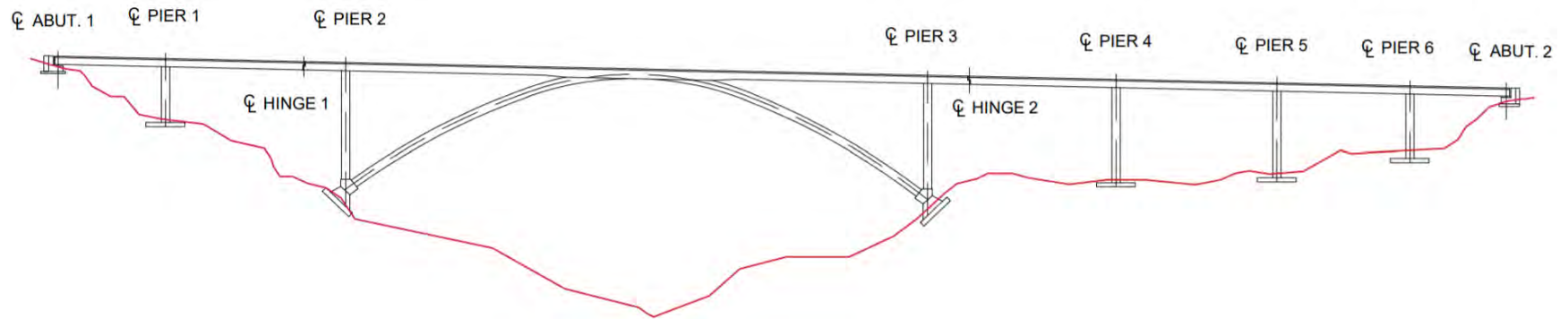


**Figure 2-2: Plan view of east face of Galena Creek Bridge northbound structure**

### 2.1.1 Materials

All reinforcing steel is ASTM A706 Grade 50 and all post-tensioning bars are ASTM A416 Grade 1,860 MPa. Eight classifications of concrete, ranging in strength from 25 MPa to 40 MPa, are used for the different components of the Galena Creek Bridge. Table 2-1 details each classification, strength, and application(s).

**Table 2-1: Concrete classification assignments**

<b>NDOT Concrete Classification</b>	<b>Strength (MPa)</b>	<b>Application(s)</b>
AA	28	Abutments, Wingwalls
AA	28	Thrust blocks, Footings
D	25	Cast-in-drilled-hole piles
DA	28	Pier columns
DA	31	Bottom slab, Diaphragms, Girders
DA	40	Bottom slab, Girders, Diaphragms over Pier 2, and 3
EA	31	Approach slab, Barrier rails
EA	31	Top slab, Hinges

### 2.1.2 Superstructure

The superstructure of each bridge consists of a two-cell reinforced concrete box girder that is primarily composed of 31 MPa concrete. The geometry of the typical box girder section is shown in Figure 2-3. Additional strength over Piers 2 and 3 is provided through the use of 40 MPa concrete for the bottom slab and girders (Figure 2-4). The 40 MPa concrete section begins at each hinge and extends 30.6 m towards the arch (Figure 2-5).

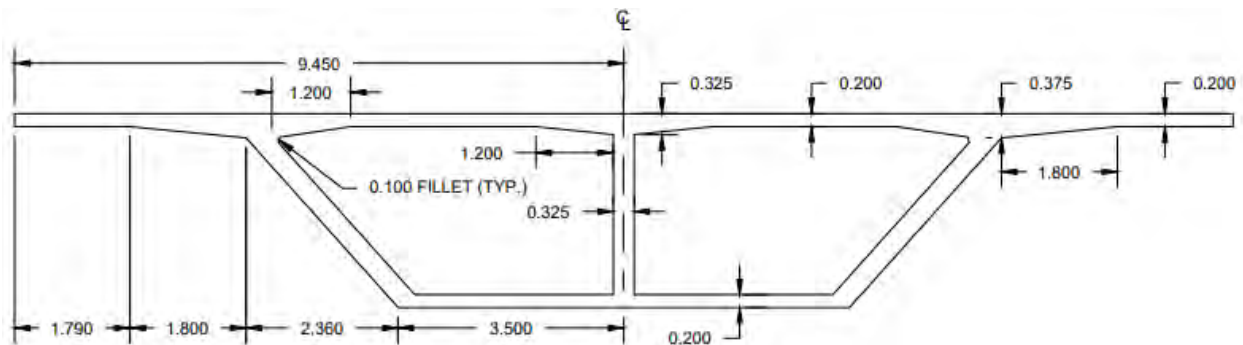


**Figure 2-3: Typical cross section of the two-cell superstructure (m)**

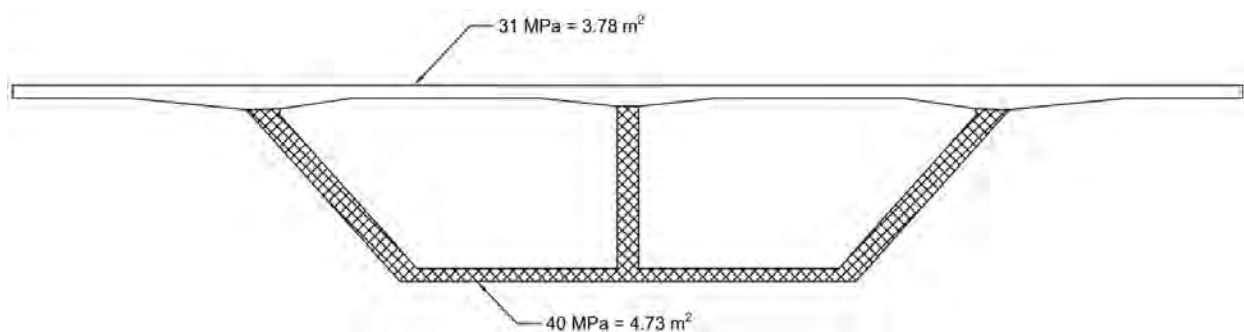


**Figure 2-4: Strengthened cross-section areas of box girder**

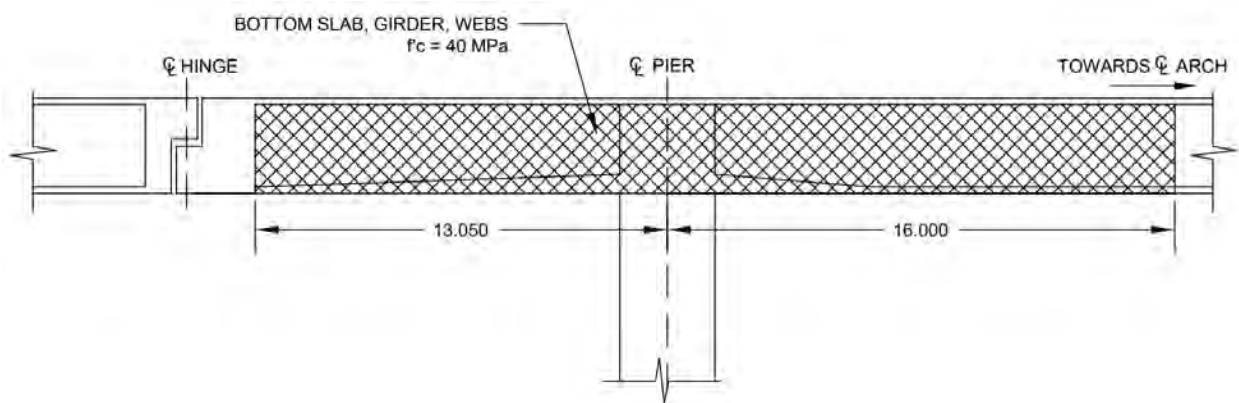


**Figure 2-5: Typical use of 40 MPa concrete over Piers 2 and 3 (m)**

Geometric variations also occurred along the length of the bridge. Specifically, the thickness of the bottom slab transitions linearly from 0.2 m to 0.6 m over Piers 2 and 3 and up to 0.4 m over Piers 1, 4, 5, and 6. At these locations, the thickness of the bottom slab extrudes inwards such that

the total depth of the girder remains constant, as demonstrated in Figure 2-6 and Table 2-2. In addition, the girder depth increases from 3.0 m to 3.6 m over 8.0 m between the fillet diaphragms in Span 3 (Figure 2-7).

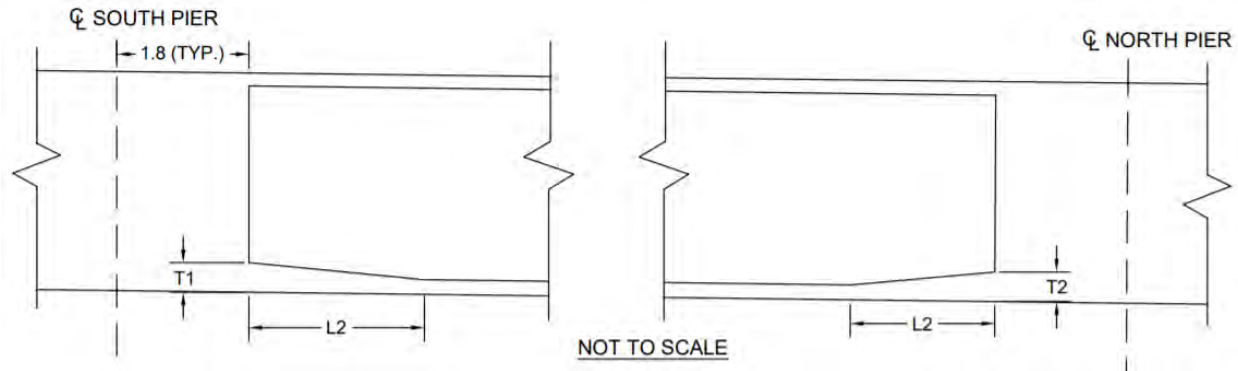


**Figure 2-6: Bottom slab thickness variation legend for piers**

**Table 2-2: Bottom slab thickness variation legend**

Span Number	T1 (mm)	L1 (m)	T2 (mm)	L2 (m)
1	200	N/A	400	2.5
2	400	5.0	600	15.0
3	600	6.0	400	13.2
4	600	13.2	400	5.0
5	400	4.0	400	4.0
6	400	3.0	400	3.0
7	400	2.0	200	N/A

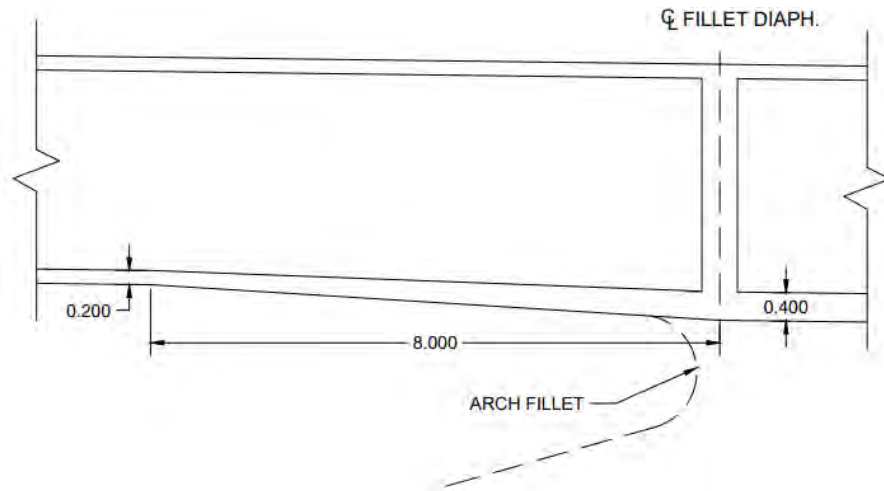


**Figure 2-7: Box girder variation at intersection of supersructure and arch (m)**

Span 3 of each bridge is 210 m long and is supported by a cathedral arch. The crown of the arch coincides with the midspan of Span 3 (Figure 2-8). At this location, the arch extrudes 3.55 m into the box girder (Figure 2-9). A 2.20 m radius fillet is located at the intersection of the bottom slab with the arch to minimize the concentration of stresses. The depth of the box girder and the thickness of the bottom slab increase linearly at the junction of the arch and the superstructure. The girder depth increases to 3.56 m and the soffit thickness increases to 0.40 m. Hatches, located at the columns and the arch crown, allow access between the east and west cells of each box.

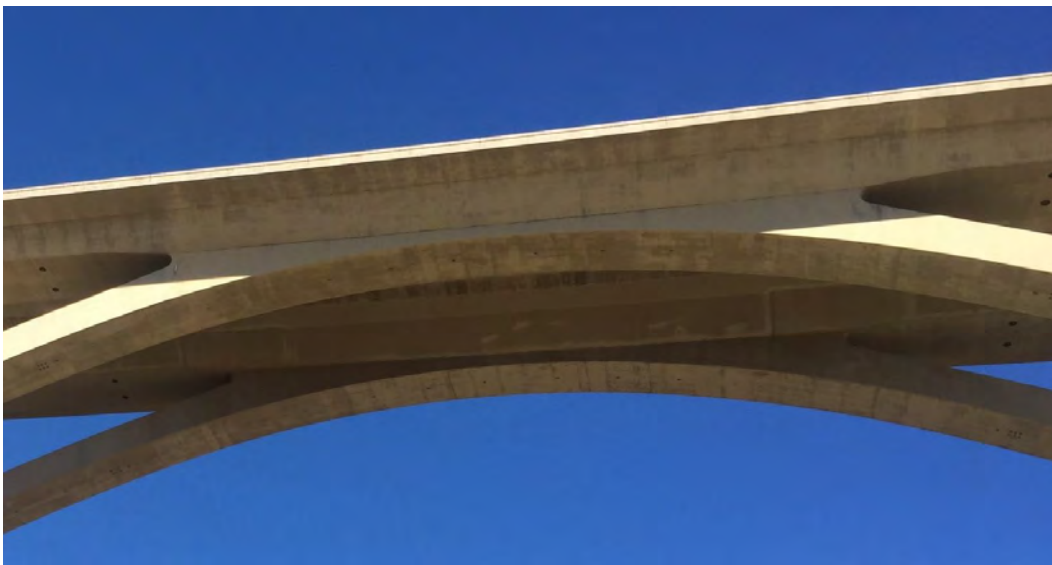


**Figure 2-8: Exterior photograph of arch merge region**



**Figure 2-9: Interior photograph of arch merge region**

Two expansion joint hinges separate each structure into three frames. The hinges are located 15 m from either side of the arch span, measured from the centerline of the hinge to the centerline of the adjacent column. Each hinge consists of an overhang and lower cantilever portion connected by three elastomeric bearing pads (Figure 2-10). The lower cantilevers are elements of Frame 2, and the overhangs are extensions of Frames 1 and 3.



**Figure 2-10: Photographs of Galena Creek Bridge expansion joint hinge**

The traditional longitudinal and transverse reinforcement in the superstructure is #13M and #16M bars spaced at every 0.30 m in the deck and webs and spaced 0.40 m apart in the soffit. In addition, each frame possesses an internal longitudinal post-tensioning system, and both expansion joints are reinforced by external post-tensioning. Longitudinal post-tensioning tendons consist of 27 strands with a diameter of 15.24 mm. Internal longitudinal strands are embedded in the web and walls of the box girder. The deck is transversely post-tensioned at the abutments, hinges, and pier caps. Transverse post-tensioning tendons consist of four 15.24 mm strands. Post-tensioning was conducted once the concrete achieved a compressive strength of 24 MPa. The coefficient of friction,  $U$ , was 0.25 for transverse tendons and 0.20 for longitudinal tendons. All tendons are set in 10 mm deep anchors and have a wobble factor,  $K$ , of 0.00066/m. Table 2-3 provides the tendon quantity, jacking force, and predicted losses for each frame and the deck.

**Table 2-3: Prestressing details**



<b>Location</b>	<b>Number of Tendons</b>	<b>Jacking Force (kN)</b>	<b>Losses (MPa)</b>
Frame 1	9	48,300	179
Frame 2 (Internal)	18	101,300	276
Frame 2 (External)	6	32,600	276
Frame 3	12	64,200	241
Deck (Transverse)	9	812	180

Full-height diaphragms of varying thickness (Table 2-4) provide torsional resistance throughout the interior of the box structure (Figure 2-11). Diaphragms are located at the abutments, piers, fillets, arch crown, midspans, and hinges. Pier diaphragms coincide with the integral pier columns. Intermediate, fillet, and arch crown diaphragms provide additional stiffness. Fillet diaphragms mark where the superstructure connects with the arch. A crown diaphragm is located 6.75 m from the crown of the arch on both sides. A single intermediate diaphragm is located close to the midspan of every span, with the exception of Span 3 that has two intermediate diaphragms located between the fillet diaphragms and the adjacent pier diaphragms. Upper and lower diaphragms are located at both hinges and provide sufficient space for the necessary conventional reinforcement and prestressed tendons in the hinge regions (Figure 2-12).

**Table 2-4: Diaphragm thicknesses**

<b>Diaphragm Type</b>	<b>Thickness (m)</b>	<b>Bridge Sheet</b>
Abutment	1.60	BG-209
Crown	0.30	BG-161
Fillet	0.50	BG-187
Intermediate	0.25	BG-187
Pier	3.60	BG-98
Hinge Upper	2.45	BG-217
Hinge Lower	3.25	BG-212



**Figure 2-11: Example of Galena Creek Bridge diaphragm**

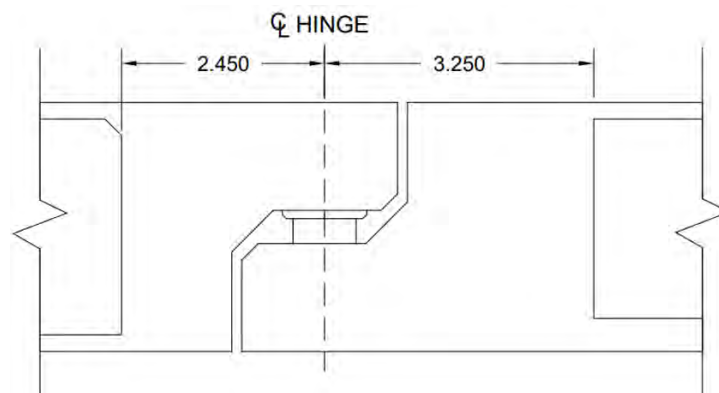


**Figure 2-12: Hinge diaphragm elevation view (m)**

Additional superstructure elements include the link slab and concrete barrier rails. The link slab is 0.20 m thick and connects the northbound and southbound structures between the two hinges (Figure 2-13). The link slab runs the entire length of Frame 2 and is integral with the superstructure. This connection between the twin bridges provides lateral resistance by distributing loads between the two structures. Concrete barrier rails, flush with each end of both decks, were cast after the prestressing was completed. The barrier rail has intermittent expansion joints along the length of the superstructure. Each barrier rail is 1.07 m tall and has a linear weight of 6.503 kN/m.



**Figure 2-13: Hinge diaphragm elevation view (m)**

### *2.1.3 Substructure*

Both the northbound and southbound structures of the Galena Creek Bridge are seven spans and are supported by six single-column piers. Due to site topography, the column height widely varies, resulting in the northbound columns being taller than the southbound columns (Table 2-5). The hollow rectangular piers have exterior dimensions of 6.0 m x 3.0 m, interior dimensions of 4.0 m x 1.8 m, and 0.15 m chamfers in each corner. The columns are oriented with the 6.0 m face (i.e., strong axis), transverse to the centerline of the bridge, to increase resistance to lateral forces. The cross-sectional dimensions of the columns are uniform. Longitudinal reinforcement in the columns consists of #22M bars for Piers 1, 4, 5 and 6 and #29M bars for Piers 2 and 3. Transverse reinforcement includes #16M bars for confinement and #19M bars for shear. A pedestal is located at the bottom of the southbound Pier 4 column. Strong winds knocked over the original reinforcing bars before the concrete was cast during construction, leading to the addition of the pedestal.

**Table 2-5: Column heights**

<b>Pier Number</b>	<b>Northbound Structure (m)</b>	<b>Southbound Structure (m)</b>
1	19.189	16.622
2	38.047	38.049
3	38.769	38.769
4	34.402	19.983
5	31.277	22.158
6	23.935	16.458

Piers located outside of Frame 2, away from the arch, rest on 14.0 m x 13.42 m x 2.75 m pile caps with 12 cast-in-drilled-hole piles having a diameter of 1.22 m. The pile depths vary because each was dug to competent bedrock.

The hollow rectangular cathedral arch supporting Span 3 has exterior dimensions of 6.0 m x 3.6 m and interior dimensions of 5.2 m x 2.8 m with 0.35 m chamfers. The interior of the arch is accessed using a manhole from the box girder. Thrust blocks anchor the bases of the arch to the bottom of the columns at Piers 2 and 3 (Figure 2-14). The footings for Piers 2 and 3 have dimensions of 15.65 m x 12.0 m x 2.0 m and 18.05 m x 12.0 m x 2.0 m, respectively. Footings for both piers are angled at 36°52'12" towards the arch and fixed to the bedrock using 12 steel anchors. The thrust blocks of both piers are connected by a 4.0 m x 6.0 m link beam to further resist lateral loads (Figure 2-15).

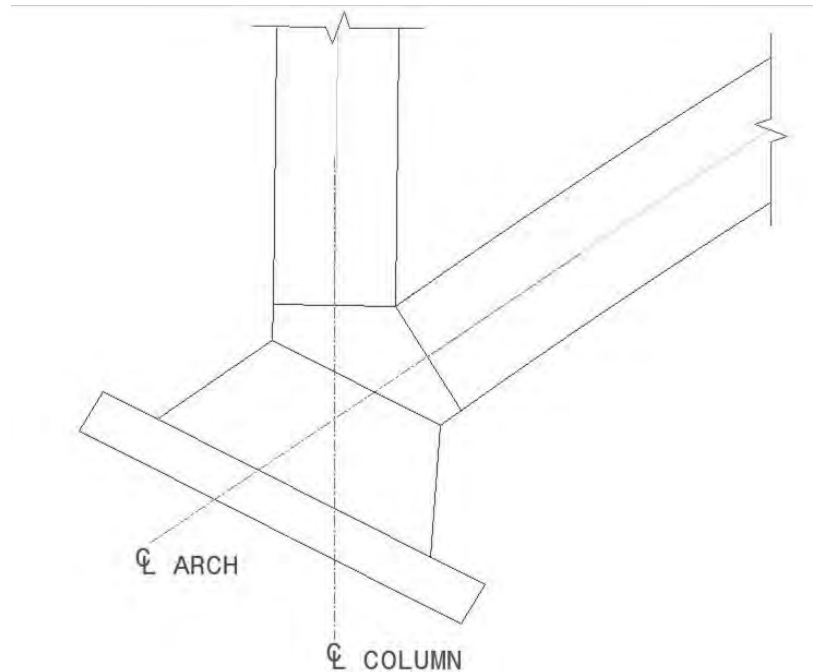


**Figure 2-14: Thrust block supporting the base of the arch and column**



**Figure 2-15: Link beam connecting the northbound and southbound superstructures**

#### *2.1.4 Bearings*

Reinforced elastomeric bearing pads are located at the abutments and expansion joints to permit translation of the superstructure. Each of these locations have three bearing pads spaced at 2.88 m, with the middle bearing aligned with the centerline of the superstructure. All bearings are composed of 60 durometer elastomer and reinforced by alternating layers of elastomer with 2.0 mm thick steel plates. The hinge bearings have a length of 0.71 m, transverse width of 0.76 m,

and a height of 0.29 m. The length, width, and height of the abutment bearings are 0.64 m x 0.64 m x 0.12 m, respectively.

## **2.2 Previous Research on the Galena Creek Bridge**

### *2.2.1 Seismic Time-History Analysis*

During construction of the bridge from 2008 to 2012, NDOT collaborated with UNR to install instrumentation and perform monitoring on the main arch span. The primary purpose of the original study of the Galena Creek Bridge was to gain understanding of the behavior of the structure to seismic loading (Taylor & Sanders, 2008). Nonlinear time-history analysis was performed using SAP2000 v.14 and compared to linear-elastic response spectrum analysis, a more traditional technique used by designers.

Taylor and Sanders developed a finite element model using SAP2000 to predict individual member forces and displacements by considering material and geometric non-linearity (2008). Moment-curvature was used in the computational model to consider the effect of plastic-hinging behavior of the arch and columns on the overall nonlinear behavior of the structure. Shear hinging was neglected as the tall, slender columns of the Galena Creek Bridge are flexure dominant. The moment-rotation response of the substructure components used Takeda hysteresis models to incorporate cyclic loading effects in the model. Gap and hook elements were used at the hinges and abutments to fully capture any nonlinear response.

The basis for the comparison between the two seismic analysis methods was formed by peak structure displacements, moments, and base shears, thereby providing a means to assess the adequacy of the assumptions made in the design process. Elastic response spectrum analysis was performed using the model generated for the non-linear analysis, except that the non-linear elements were replaced with linear elements (Taylor & Sanders, 2008).

The researchers consulted seismologists at UNR to identify acceleration time-history data to be used in the nonlinear analysis. The time histories were selected from earthquake records with similar seismology to that of the nearby strike/slip fault (Taylor & Sanders, 2008). The Federal Emergency Management Agency (FEMA) 356 recommendations were used to scale the

acceleration records. This time-history selection process made the prediction of earthquake loading on the structure more accurate.

The nonlinear time-history analysis was found to have comparable results with elastic response spectrum analysis. The researchers concluded that nonlinear time-history analysis can be effective as an evaluation tool to better understand global structural behavior, as long as the input ground motions are properly selected (Taylor & Sanders, 2008). Using response modification factors, the elastic response spectrum technique can typically estimate member forces and displacements in a structure, as it considers the effects of multiple modes of vibration and combines those effects.

### *2.2.2 Investigation of Load, Time-Dependent, and Temperature-Dependent Effects*

Following the first collaboration between UNR and NDOT, further research on the Galena Creek Bridge focused on installing instrumentation to gain further understanding of various effects on the behavior of the structure. On the southbound structure, strain and temperature data were collected between 2008 and 2010 (Vallejera & Sanders, 2011). Computational models attempted to consider the contribution of load, time, and temperature-dependent effects on the total strain experienced.

The instrumentation system consisted of 108 strain gages and thermistors located at seven arch cross sections and three deck cross sections, as well as five triaxial accelerometers located in the middle frame (Vallejera & Sanders, 2011). Monitoring occurred during construction of the bridge, starting September 2008 and ending December 2010. The strain gages and thermistors were used to measure the contribution of the different effects on total strain. The purpose of the accelerometers was to provide a way to compare the results of the response spectrum analysis from the finite element models to those calculated using experimental field data. The response spectrums for each ground motion were obtained from Seismosignal, a software used to process strong-motion data, then used to determine the Square-Root-of-the-Sum-of-the-Squares (SRSS) response spectrums. Based on 2% probability of exceedance in 50 years, scale factors for each motion were then applied to find the average weighted composite response spectrum.

The models considered the effects of staged construction, the time-dependent behavior of concrete, and temperature change in the structure on the strain measured. The researchers found that the

contribution of temperature was negligible when compared to the contributions of time-dependent effects and load on the total strain (Vallejera & Sanders, 2011). Large error ratios were observed and attributed to strain caused by damage to the instruments or cables during construction, faults in the installation of the system, or frequent power loss to the data collection system. The large error ratios made separating the total strain data collected into strain caused by each effect difficult.

The researchers recommended improved planning and instrumentation protection to minimize the contribution of external variables on the total strain for similar projects in the future (Vallejera & Sanders, 2011). A significant part of the protection of the system was the connections between the data collection system and each instrument, which led Vallejera and Sanders to recommend using durable, simple connectors and hard wiring the cables through field soldering in future field research. Limiting the contribution of any external variables could provide a means to compare the field measured data to the results obtained from the finite element models.

### *2.2.3 Dynamic Characterization and Baseline Testing*

In 2012, NDOT and UNR began another study to characterize the dynamic properties of the completed bridge (Carr & Sanders, 2013). Both existing instrumentation and new installations were employed for the overall monitoring system. To supplement the initial system, accelerometers were installed throughout the southbound main arch span. The purpose of the additional sensors was to make the overall system able to continuously monitor the behavior of the bridge under typical loading, as well as during seismic events. The system was initially intended to be a permanent installation and used for long-term monitoring at the completion of the study; however, no maintenance was provided at the conclusion of the research.

Four biaxial accelerometers, to measure the vertical and transverse responses, and four uniaxial accelerometers, oriented in different directions, were added. The eight new accelerometers were placed every 30 meters between the two expansion joint hinges of the structure (Carr & Sanders, 2013). The new sensor locations were predicted to experience the largest peak modal deflections and accelerations using the modal analysis results from the computational models created in SAP2000. The final instrumentation layout for the study is depicted in Figure 2-16 where the blue stars indicate the superstructure sensors and the orange rhombus mark the substructure sensors.



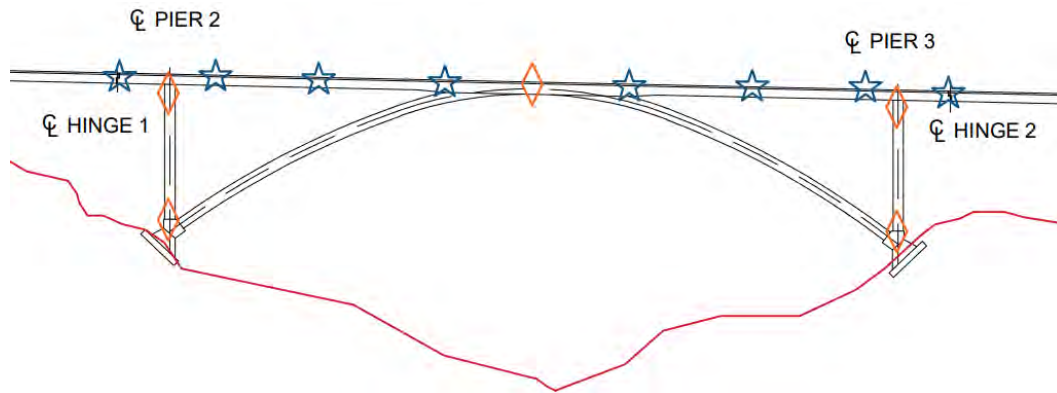


**Figure 2-16: The superstructure (blue) and substructure (orange) accelerometer placement**

During the field experiment, the structure was dynamically excited in the vertical direction using a construction vehicle and in the transverse direction using an eccentric mass shaker. Both tests attempted to validate results of previous models from the NDOT design process (Carr & Sanders, 2013). The finite element models were created in SAP2000 using frame elements, making them spine models. Following the completion of both experiments, the field measured data were compared to the results from the finite element models.

The shaker experiment was used to calculate the transverse damping of the structure. The damping values were found to vary based on the frequency of the vibration, with damping decreasing as frequency increases. For the highest frequencies, an average damping of 3% was reported, which was consistent with the recommended value (Carr & Sanders, 2013). Five out of six natural frequencies were correctly predicted by the model. Gross section properties were found to be more representative of the structure when it was in its initial condition at the time of the experiments. Mode shapes calculated for the experimental frequencies correlated well with the mode shapes from the model.

Following the controlled dynamic testing, traffic loading was monitored for a short duration. The vertical damping of the structure calculated using the field measured data was consistently around 2% across all of the truck experiments, which agreed with the recommended damping value for a structure under working stress (Carr & Sanders, 2013). The researchers experienced difficulties when attempting to model the dynamic effects of the truck loading on the structure. When gross section properties and hinges were modeled to reflect working stresses instead of seismic stresses, the acceleration response in the finite element models agreed more with the experimental data.

Overall, the experimental results agreed with the predicted results from the SAP2000 finite element models (Carr & Sanders, 2013). However, one significant exception was that the models were found to predict lower peak accelerations in the transverse and vertical directions. The researchers concluded that using a single degree-of-freedom (SDOF) system to model the truck would have likely removed some of the inaccuracies in the dynamic load modeling.

## **2.3 Nevada Department of Transportation Reports**

### *2.3.1 Bridge Inspection Report, 2018*

Routine bridge inspections of the Galena Creek Bridge are performed by NDOT personnel every 24 months (CFR §650, 2021). Visual inspections and non-destructive testing are used to evaluate the condition of the bridge elements. Due to the size and location of the bridge, inspections require the use of under-bridge inspection units (UBIT), ladders, and rope access climbing methods. The bridge is situated well-above the Galena Creek; however, the waterway does not impact the footings; as such, degradation measurements are not required. The underground cast-in-place piles were not evaluated during routine inspections. Both the northbound and southbound structures were given a “low risk” rating. Superficial cracking, light efflorescence, minor spalling, and some exposed rebar did not demonstrate notable impact to the structural integrity. The inspection report was reviewed on 08/08/2018 and sealed by an NDOT Professional Engineer on 12/31/2018. Note that although the original bridge design was in metric, inspection reports are documented using imperial (US) units.

The top flange soffit exhibited transverse cracking with efflorescence throughout both bridges. The cracks were generally hairline cracks, expanding up to 3 mm wide. Efflorescence staining was also noted at cracks originating from construction joints. An exposed epoxy coated rebar with minor rusting was noted at the underside of the overhang in Span 2 of the northbound structure. The exterior and interior girders, similarly, had transverse hairline cracking with efflorescence throughout. Diagonal shear cracking up to 1 mm wide was noted at pier and hinge locations. The east exterior girder exhibited more prolific cracking than the west girder, likely due to exposure to ultraviolet light.

Longitudinal cracking was noted throughout the interior of the bridge arches, most notably at the thrust blocks. Arch diaphragms exhibited vertical cracking along the full height of the section. Vertical cracks up to 1 mm wide were noted at the fillet where the arch meets the superstructure. Pier columns showed signs of shrinkage cracking up to 1 mm wide and moderate honeycombing up to 6 mm deep. Hairline cracking was sporadic on both the interior and exterior of the pier columns. Spalls up to 25 mm deep stemmed from construction joints. Piers 5 and 6 had ponding water up to 0.20 m deep, most likely a result of groundwater infiltration. Both abutments displayed isolated hairline cracks along the backwall and wingwalls. Expansion joints, hinges, and drainpipes accumulated typical debris that did not hinder the intended functions.

Although several sprinkler heads appeared slightly depressed, the ice removal system was not tested. Maintenance to be performed before the next inspection included cleaning the deck drains, cleaning the expansion joints, and replacing the preformed joint filler. The hinge crawl space was also to be cleaned and covered to avoid the buildup of further debris. Further suggested maintenance included replacing the chain link fence situated on the concrete barrier, re-applying a protective coating to the substructure, and patching any spalls.

### 2.3.2 Load Rating Report, 09/13/2016

A load rating report of the superstructure was performed by NDOT using SAP2000, WinBDS 5.0.3, and PTRater 4.2 based on the 05/22/2014 bridge inspection report. The live loads used for the analysis were the AASHTO HS20-44 truck, and lane loads as well as California permit vehicles P5, P9, and P13. The rating factors for P7 and P11 trucks were interpolated based on the results of the evaluated California permit vehicles. The results of the load rating analysis, as shown in Table 2-6 and 2-7, state that the bridge has sufficient strength to carry the designated live loads. In addition, it should be noted that the mode of failure for each case was flexure.

**Table 2-6: Inventory Vehicle Load Rating Results**

Vehicle	Rating Factor	Method of Failure
HS20-44	1.37	Flexure

**Table 2-7: Operating Vehicle Load Rating Results**

<b>Vehicle</b>	<b>Rating Factor</b>	<b>Method of Failure</b>
HS20-44	2.29	Flexure
P5	2.88	Flexure
P7	2.28	Flexure
P9	1.67	Flexure
P11	1.45	Flexure
P13	1.23	Flexure

## **CHAPTER 3.     STRUCTURAL HEALTH MONITORING SYSTEM HARDWARE**

As part of the National Strong Motion Project, the United States Geological Survey (USGS) installed an accelerometer-based SHM system at 28 hospitals and two university campuses to monitor the building response to seismic activity. This proven system was adapted for a bridge application and implemented on the Galena Creek Bridge in the current research. A network of uniaxial accelerometers served as the foundation for the primary seismic SHM system. The accelerometers were located throughout the structure, as seen in Figure 3-1, based on modal analyses of the bridge. The selected layout provided a comprehensive image of the dynamic response.

A secondary exploratory SHM system was developed that consisted of four potentiometers, two inclinometers, an anemometer, and two temperature gauges. The sensors were installed on the bridge, as seen in Figure 3-2. The secondary system was designed to be used in conjunction with the accelerometers to provide additional data on the bridge response during seismic events as well as from routine traffic and environmental effects. All sensors for both systems were connected by wires to the data recording systems stored inside a de-icing utility shed located adjacent to the bridge (Figure 3-3). The manufacturer specification sheets for the sensors listed in this chapter are available in Appendix B.

The following sections describe the hardware and sensor installation locations for both systems. Details regarding the control software, online dashboard, data, and reports are described in Chapter 4.

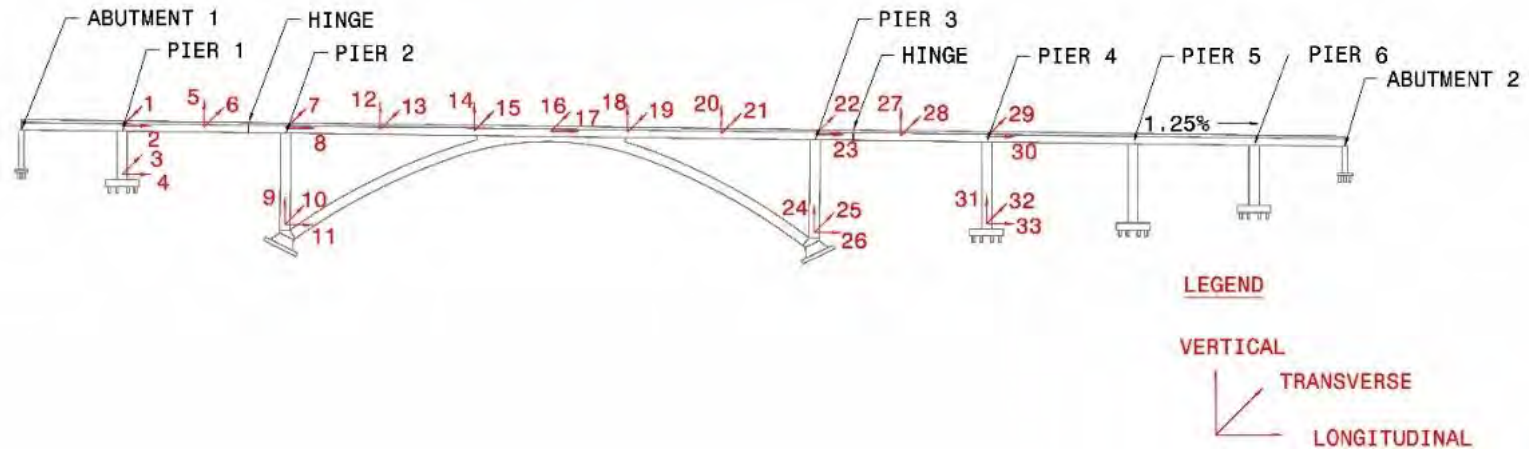


Figure 3-1: Primary seismic SHM system uniaxial accelerometer locations on the Galena Creek Bridge

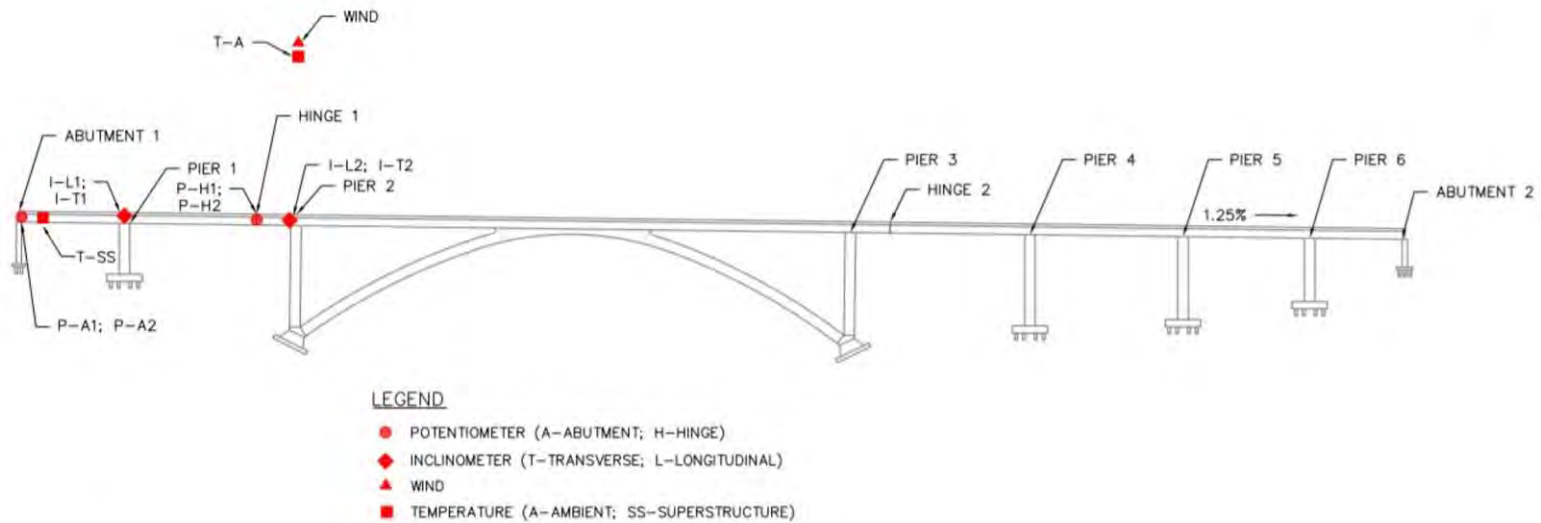


Figure 3-2: Secondary exploratory SHM system sensor locations on the Galena Creek Bridge



**Figure 3-3: Utility shed located south of the southbound structure**

### **3.1 Primary Seismic System Instrumentation**

#### *3.1.1 Accelerometers*

The primary network of sensors consisted of 33 Kinometrics EpiSensor ES-U2 uniaxial accelerometers. Designed to produce low levels of self-noise, the selected accelerometers are intended for SHM applications. The sensors are capable of recording accelerations between  $\pm 0.25g$  and  $\pm 4.00g$  and vibrations ranging from 1 Hz to 200Hz, providing the option to select the limits. Each sensor measures 55 mm x 65 mm x 97 mm and weighs 0.35 kg (Figure 3-4). The ES-U2 were designed for use in rugged conditions, housed in a watertight enclosure and an operating temperature range between  $-20^{\circ}$  and  $70^{\circ}C$ .



**Figure 3-4: Accelerometer**

Previous Galena Creek Bridge research by UNR utilized uniaxial, biaxial, and triaxial accelerometers (Carr and Sanders, 2013). The exclusive use of uniaxial accelerometers was the optimal choice for this project. Uniaxial sensors are more cost effective than their more complex counterparts. In the case of sensor failure, the cost to replace a single unit is significantly lower for a uniaxial accelerometer. Additionally, failure of a triaxial sensor would result in a complete loss of data from that location. Should a uniaxial accelerometer stop functioning, the other sensor(s) at that location would continue to provide feedback, mitigating potential data loss. Finally, most sensor locations did not require acceleration measurements along all three axes; therefore, use of uniaxial accelerometers resulted in the most efficient and flexible system design.

Accelerometers were located throughout the Galena Creek Bridge to capture critical responses during a seismic event (Table 3-1). The number of sensors and orientation (i.e., longitudinal, transverse, and vertical) at each location were optimized to collect relevant data to inform engineers and inspectors of the bridge condition. Sensors were typically located at the top and bottom of piers, arch section, and along the length of the superstructure (Figure 3-1).

Longitudinal sensors were located at the top and bottom of Piers 1 through 4 and the crown of the arch. Frame 1 is supported by Pier 1 with a column height of 19.189 m, marking it as the shortest



column of the bridge. Shorter columns often result in high internal stresses and greater accelerations transferred to the superstructure. Conversely, Piers 2 and 3 are the tallest columns of the structure and are expected to experience the largest displacements.

Vertical sensors were located at the bottom of Piers 2 through 4 as well as at the midspan of Spans 1 and 4, arch-superstructure merge, and halfway between the merges and adjacent piers (Figure 3-1). The locations along the superstructure furthest from the substructure components are most prone to vertical displacements. Discrepancies between the sensors at the bottom of the piers and the free-field site may indicate that the substructure foundations have been compromised.

The Galena Creek Bridge is most vulnerable to lateral forces because the structure is the most flexible in the transverse direction. Therefore, transverse sensors were located at every accelerometer location.

**Table 3-1: Accelerometer location and orientation**

Sensor	Direction	Location
1	Transverse	Top of Pier 1
2	Longitudinal	
3	Transverse	Bottom of Pier 1
4	Longitudinal	
5	Vertical	Midspan of Span 2
6	Transverse	
7	Transverse	Top of Pier 2
8	Longitudinal	
9	Vertical	Bottom of Pier 2
10	Transverse	
11	Longitudinal	
12	Vertical	Midspan between Pier 2 and south merge
13	Transverse	
14	Vertical	South arch/ superstructure merge
15	Transverse	
16	Transverse	Crown of Arch at Span 3
17	Longitudinal	
18	Vertical	North arch/ superstructure merge
19	Transverse	
20	Vertical	Midspan between Pier 3 and north merge
21	Transverse	
22	Transverse	Top of Pier 3
23	Longitudinal	
24	Vertical	Bottom of Pier 3
25	Transverse	
26	Longitudinal	
27	Vertical	Midspan of Span 4
28	Transverse	
29	Transverse	Top of Pier 4
30	Longitudinal	
31	Vertical	Bottom of Pier 4
32	Transverse	
33	Longitudinal	

### *3.1.2 Sensor Installation and Wiring*

Accelerometers were installed at 15 locations along the northbound structure of the Galena Creek Bridge. A 305 mm x 305 mm x 7 mm anodized aluminum plate was fabricated for each of the 15 locations (Figure 3-5). Up to three sensors could be attached to each plate to measure acceleration in all three axes (Figure 3-6). The plates were attached to the interior walls of the structure using concrete anchor screws. The concrete surface was not smooth; therefore, the plate provided a flat surface to mount the accelerometers. In addition, the plate was designed with slotted holes to facilitate leveling to ensure the sensors were accurately aligned in each direction. Each accelerometer was then be mounted to the plate in the desired orientation using hex nut screws. The final step was leveling all sensors to ensure accurate measurements.

The sensors were connected to the data recorder by 15 primary cables (i.e., one to each sensor location throughout the bridge). The cables were routed through PVC conduits that extend from the north wall of the utility shed, along the wingwall and face of Abutment 1 (Figure 3-7), and through the bottom slab of Span 1 (Figure 3-8). The cables were suspended along the length of the structure on L-shaped brackets mounted to the east girder of the box, until the desired sensor location (Figure 3-9). Terminal blocks were used to connect each accelerometer to the primary cable (Figure 3-10). Each primary cable contained wires to connect up to three sensors using the terminal block, although not all sensor locations required three accelerometers.



**Figure 3-5: Aluminum plate for mounting accelerometers**

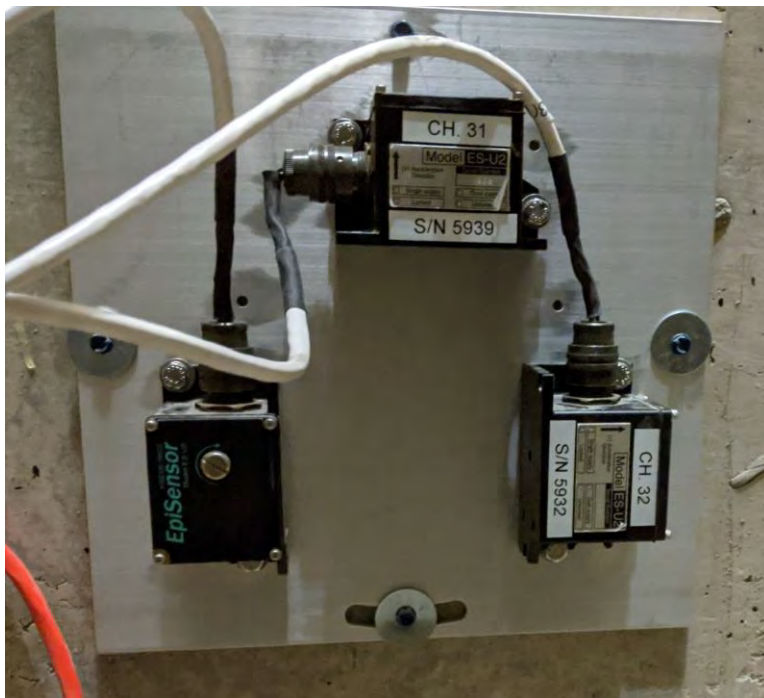


**Figure 3-6: Example of plate with three sensors at bottom of Pier 4**



**Figure 3-7: PVC conduits along the face of Abutment 1**



**Figure 3-8: PVC conduit extruding through the bottom slab near Abutment 1**





**Figure 3-9: Typical cables running along the east girder of the superstructure**

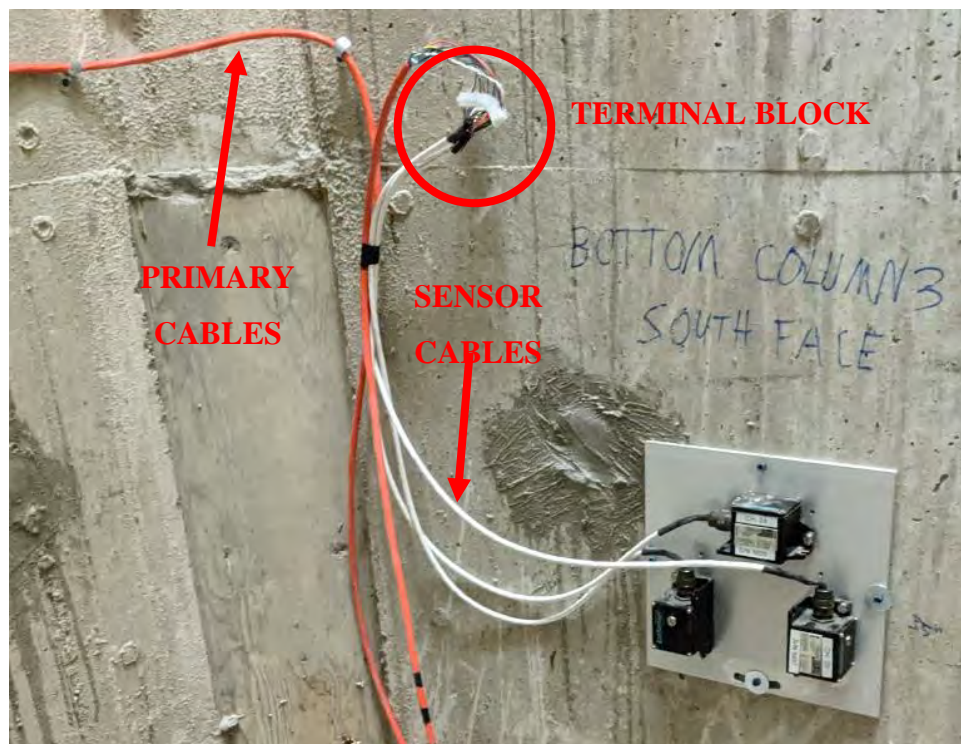


**Figure 3-10: Typical connection between primary and sensor cables via terminal block**

## **3.2 Secondary Exploratory System Instrumentation**

The USGS installed seismic SHM systems at 28 hospitals and two universities as part of the National Strong Motion Project, successfully demonstrating accelerometer-based SHM systems. Development of a secondary exploratory SHM system further expanded the scope of the primary SHM system by adding additional sensor types to measure additional responses. The secondary system consists of displacement, tilt, temperature, and wind sensors.

### *3.2.1 Displacement sensors*

UniMeasure HX-P510 string potentiometers (Figure 3-11) were installed on the Galena Creek Bridge to observe longitudinal displacement between the Frame 1 superstructure and adjacent components during both seismic activity and routine thermal expansion and contraction. Monitoring the expansion joints reveals if the bearings at the hinges and abutments are functioning as intended. The displacement sensor dimensions and weight are 120 mm x 74 mm x 74 mm and 900 g, respectively. Each sensor contains a 0.4 mm diameter string that extends along a single axis up to 2.0 m. The transducer records variations in the extension and retraction of the string with a typical margin of error of  $\pm 0.3\%$ . The HX-series are designed for rugged, field environments. The sensors are made to function within  $-40^{\circ}$  and  $85^{\circ}\text{C}$  and are resistant to water and corrosion.



**Figure 3-11: Linear Potentiometer**

A pair of displacement sensors were attached at the face of Abutment 1 to measure the longitudinal displacement of Frame 1 relative to Abutment 1, as seen in Figure 3-12. The sensors were mounted on the face of the abutment at each side of the bottom slab of the box girder. They were oriented such that the string lay parallel to the superstructure, approximately 0.2 m below the bottom slab. The potentiometer string was attached to a mounting bracket that was installed on the underside of the bottom slab of the bridge.





**Figure 3-12: Potentiometer located at west edge of Abutment 1 of northbound structure**

The second pair of potentiometers were installed at Hinge 1 to monitor the expansion joint and relative movement between Frames 1 and 2. The sensors also provided data regarding the bearing function (Figure 3-13). The first sensor was attached to the east wall of the east cell, while the second sensor was mirrored on the west wall of the west cell. Displacement discrepancies between the potentiometers at each pair indicate irregularities of the structure expansion as related to twist.



**Figure 3-13: Example of potentiometer installed at Hinge 1**

### 3.2.2 Tilt Meter

Reiker Flex Series H6 inclinometers were used to observe rotation at the top of Piers 1 and 2 (Figure 3-14). The biaxial sensors can detect changes in angle up to  $\pm 180^\circ$  about two axes in  $0.05^\circ$  increments with a margin of error up to  $0.2^\circ$ . The inclinometers are designed for field-environments, with a temperature range between  $-40^\circ$  and  $85^\circ\text{C}$  and waterproof housing. The sensor measures 110 mm x 82.8 mm x 45.7 mm and weighs 525 g.

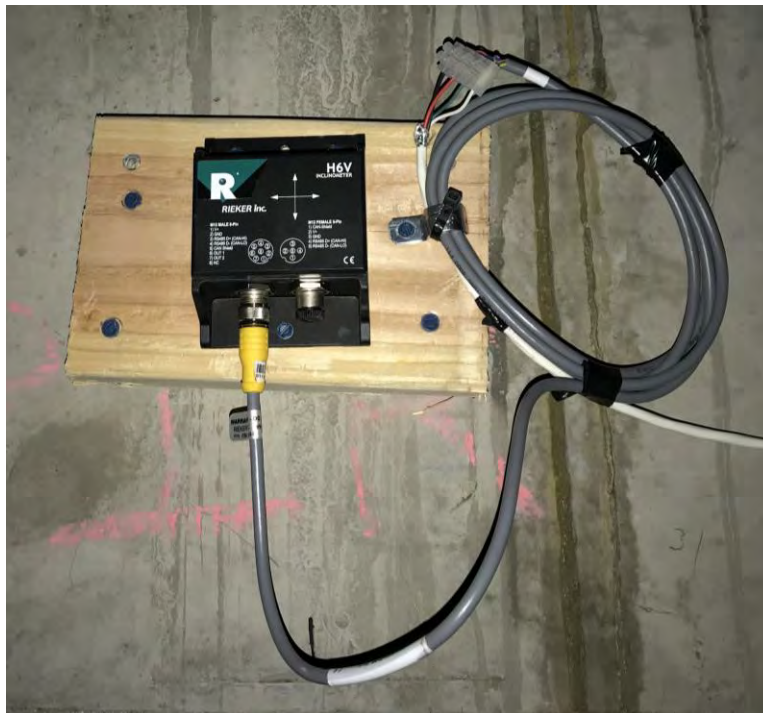


**Figure 3-14: Biaxial inclinometer installed a south face of pier diaphragm at Pier 2**

The tilt meters were installed at the south face of the pier diaphragms at Piers 1 and 2 oriented along the vertical and transverse axes of the bridge. The data collected by the primary system reveals variations in acceleration and displacement between the top and bottom of the columns. The inclusion of inclinometers provides a better representation of column behavior by recording changes in tilt to indicate warping of the columns and superstructure. Inclinometers can also indicate disturbances in the superstructure in the case of foundation displacement due to settlement as well as column tilt due thermal expansion and contraction of the superstructure.

### 3.2.3 Temperature gauges

An R.M. Young Model 41342 Temperature Probe was mounted to record ambient temperature outside the shed. A second probe was located inside the bridge (Figure 3-15). The sensors were installed with multi-plate, aspirated radiation shields which protected the sensor from solar and environmental damage. The temperature gauges had an effective range of  $\pm 50^{\circ}\text{C}$  with an accuracy of  $\pm 0.3^{\circ}\text{C}$ . Temperature measurements are used to correlate between the environmental conditions and the longitudinal displacements of the bridge.



**Figure 3-15: Temperature probe located in Galena Creek Bridge**

The sensor located inside the bridge was installed on the east face of the web, roughly 2.0 m north of the intermediate diaphragm of Span 1. Note that the probe measures the temperature of the surrounding air. Due to the insulation provided by the exterior concrete walls of the box, it is assumed that there is a negligible temperature difference between the air temperature inside the bridge and the concrete superstructure. The second sensor was installed on a mounting bracket on the west wall of the shed (Figure 3-3). The sensor was located 1.0 m above the roof of the shed to mitigate influence from radiation off solid objects.

### 3.2.4 Wind Sensor

An R.M. Young 86000 Ultrasonic Anemometer, developed by Meteorological Instruments, was used to record the magnitude and direction of wind. The sensor transmits and records feedback from ultrasonic pulses emitted by three nodes, thereby accurately measuring wind speed without moving mechanical parts. The elimination of moving components greatly improves the reliability and durability of the anemometer. The wind speed measurement range is between 0 m/s to 75 m/s with changes in velocity in 0.01 m/s increments. The sensor can detect wind direction about the plane perpendicular to the axis about which it is mounted. The wind direction feedback is provided in up to  $0.1^\circ$  and is guaranteed accurate within  $\pm 2^\circ$ . The sensor measures 290 mm in height and 110 mm in diameter. The anemometer was installed on a bracket to the exterior of the shed. To provide the sensor with unobstructed data, the bracket extrudes 1.5 m above the roof of the shed, as seen in Figure 3-3 and Figure 3-16. While it is unlikely that wind conditions would have a significant impact on the health of the structure or the dynamic behavior, the addition of the anemometer demonstrates the effective integration of this sensor into the global SHM system.



**Figure 3-16: Ultrasonic anemometer installed at utility shed**

## 3.3 Data Recorders

Both the seismic and secondary SHM systems had individual data recorders located in the utility shed. The primary SHM system utilized a Kinometrics Obsidian 36X data recorder, while the secondary sensors employed a Kinometrics Obsidian 12X data recorder (Figure 3-17). The Obsidian 36X system has a 36-channel capacity, 33 of which are used for the primary seismic



monitoring system. The Obsidian 12X system has a 12-channel capacity that was fully utilized for the secondary sensors. The Kinemetrics Obsidian hardware was developed for seismic SHM. The hardware was chosen for its capacity to process a significant influx of data and deliver outputs to analysis software. Each unit is preset with several default formats upon which to record and display data. The data recorders are resistant to water and fully operational between temperatures of -20° and 70° C.

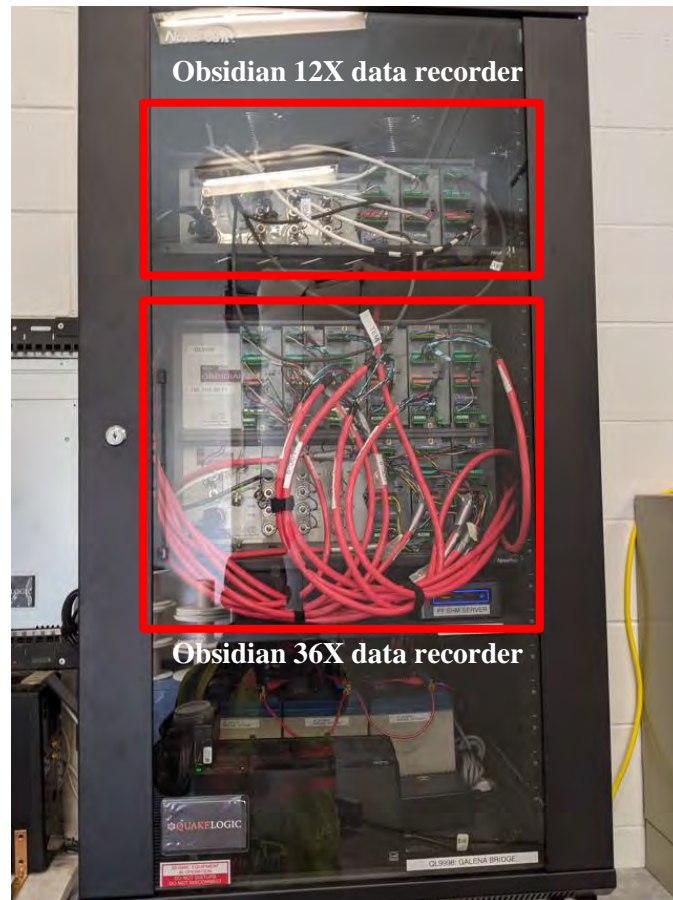


**Figure 3-17: Obsidian 12X (top) and 36X (bottom) data recorders with cables**

Each data recorder is capable of wireless communication through a USB-based Wi-Fi connection. Both data recording systems were wired to separate Bullet III GPS antennas that were mounted on the exterior of the north wall of the utility shed (Figure 3-18). The head of the antenna was 77.5 mm in diameter and measured 66.2 mm tall.



**Figure 3-18: Bullet type GPS antennas**

### **3.4 Free-field Station**

A Kinemetrics ETNA 2 accelerograph was used as a free-field station to record the local ground motions due to seismic activity. The ETNA 2 casing holds a triaxial accelerometer and internal data recording system. The accelerograph is capable of recording ground motions of up to  $\pm 4g$ ; the range is selectable by the user. A built-in GPS allows the system to note the orientation of the ground motions without the need of additional sensors. The internal data recording system has a capacity of 32 GB. The system is compatible with a USB-based Wi-Fi connection or cellular modem. The ETNA 2 measures 150 mm x 150 mm x 75 mm, weighs 1.5 kg, and is operational between temperatures of  $-20^{\circ}$  and  $70^{\circ}$  C. The unit is mounted to the wall of the utility shed and enclosed in a protective case as seen in Figure 3-19.



**Figure 3-19: ETNA 2 accelerograph and protective case**

## CHAPTER 4. CONTROL SOFTWARE, DASHBOARD, AND REPORT

### 4.1 Control Software

The control software, **SMARTBRIDGE** by QuakeLogic, combines the SHM technology together with a warning system to provide the most sophisticated and comprehensive monitoring, alarm, and response system available in the market today. The dynamic **SMARTBRIDGE** solution incorporates:

- Cloud-based technology provides instantaneous, real-time information available to decision-makers and their teams.
- 24/7 monitoring, analysis and reporting on structural health.
- Instant alerts of any damage that may threaten structural integrity, allowing for quick prioritization for safety and recovery activities.
- Detailed SHM assessment reports within two minutes of an alarm-generating event, providing engineering-quality data as a basis for a fully-informed response.
- State-of-the-art integrated earthquake monitoring system allows for rapid action that could potentially save lives following a seismic event.

The **SMARTBRIDGE** integrated technology platform comprises the following systems:

- Structural Health Monitoring
- Mobile-friendly Dashboard
- System Watchdog

#### 4.1.1 *Structural Health Monitoring (SHM)*

The sensors and data logging devices positioned on the bridge are connected to state-of-the-art SHM monitoring software running on the on-site server. This software continuously monitors the integrity of the structure, including its abutment and foundation, and sends real-time event data to the cloud-based mobile-friendly web application in the form of a management dashboard. Figure 4-1 presents an overview of the implemented SHM monitoring software.



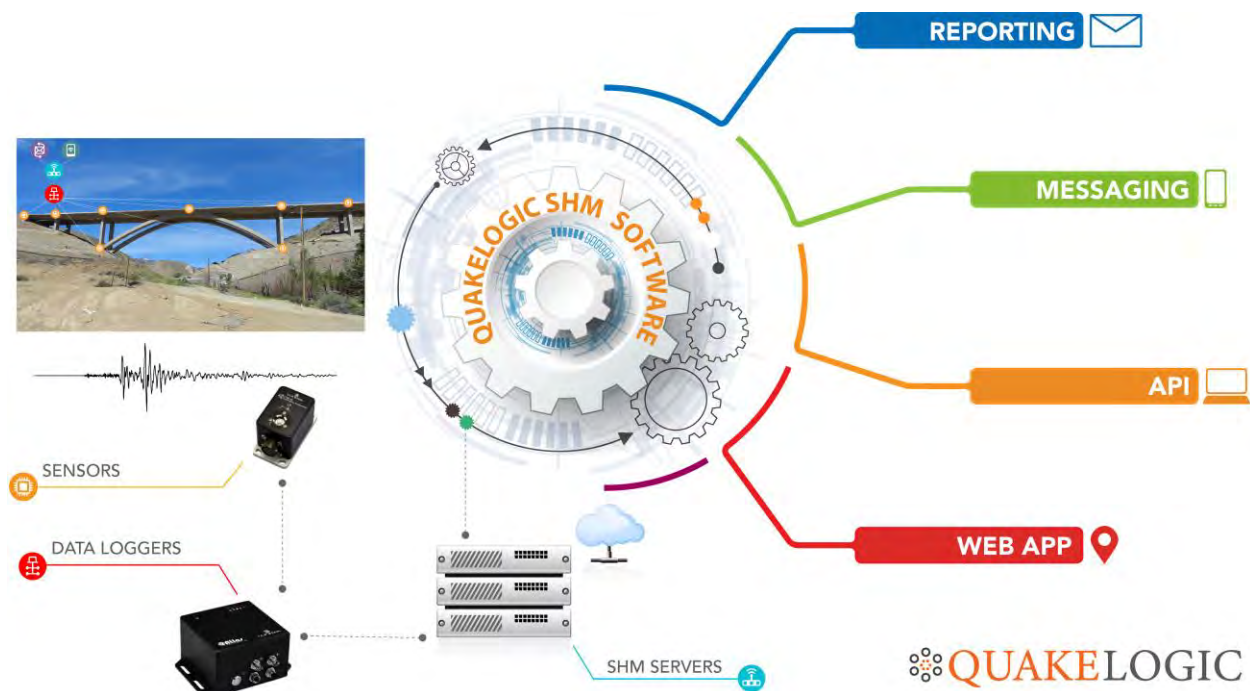


**Figure 4-1: Overview of the SHM monitoring software**

Notifications that are supported by comprehensive reports are sent within seconds of a trigger event, allowing NDOT decision-makers to coordinate emergency responses, prioritize inspections and plan appropriate recovery actions based on accurate, detailed information.

The software offers five major services and features:

- 1) Real-time monitoring is operated by on-site data 24/7 and provides event triggers, offers an easily accessible web application with an effective dashboard display, offers real-time continuous waveform analysis, and includes an Application Programming Interface (API).
- 2) Rapid notification and responses service operates based on set threshold values for response triggers, offers an early warning functionality to decision makers through effective communication means, such as Text (SMS), email, and/or WhatsApp notifications.
- 3) The software also provides comprehensive analysis and reporting features for an advanced understanding of the events by generating ambient data collection, condition analysis, and structural assessment analysis.
- 4) The software has been expanded to cover various data types being collected from the Galena Creek Bridge, and thus offer a broad platform compatibility with accelerometers,

potentiometers (displacement transducers), tilt meters, and weather stations (i.e., temperature and wind).

- 5) Other technical features the software can generate include real-time velocity, displacement and drift computation, acceleration response spectra, spectrograms, frequency response analysis, Fourier amplitude spectra, power spectral density, polarization analysis, and statistical analysis.

#### 4.1.2 Mobile-friendly Dashboard

Real-time information about the health of the bridge is displayed in the form of a management dashboard. The mobile-friendly dashboard is intuitive to use and provides drill-down functionality from the initial single-screen overview through increasingly detailed levels of data and information, as needed. Figure 4-2 presents the developed dashboard views that are compatible with various computer technologies and mobile devices. The dashboard works seamlessly with **SMARTBRIDGE**'s computational platform to organize, store, and display current SHM data and reports. Password security is provided to avoid unauthorized access.



**Figure 4-2: Dashboard views compatible with various mobile devices**

The dashboard (Figure 4-3) includes advanced features, such as sensor display, a map of the most recent earthquakes around the globe, fault maps, etc. It also provides an asset management layout showing all relevant structural, geotechnical, seismic hazard, and other information relevant to the monitored structure.

The further details of the dashboard are provided in the rest of Chapter 4.

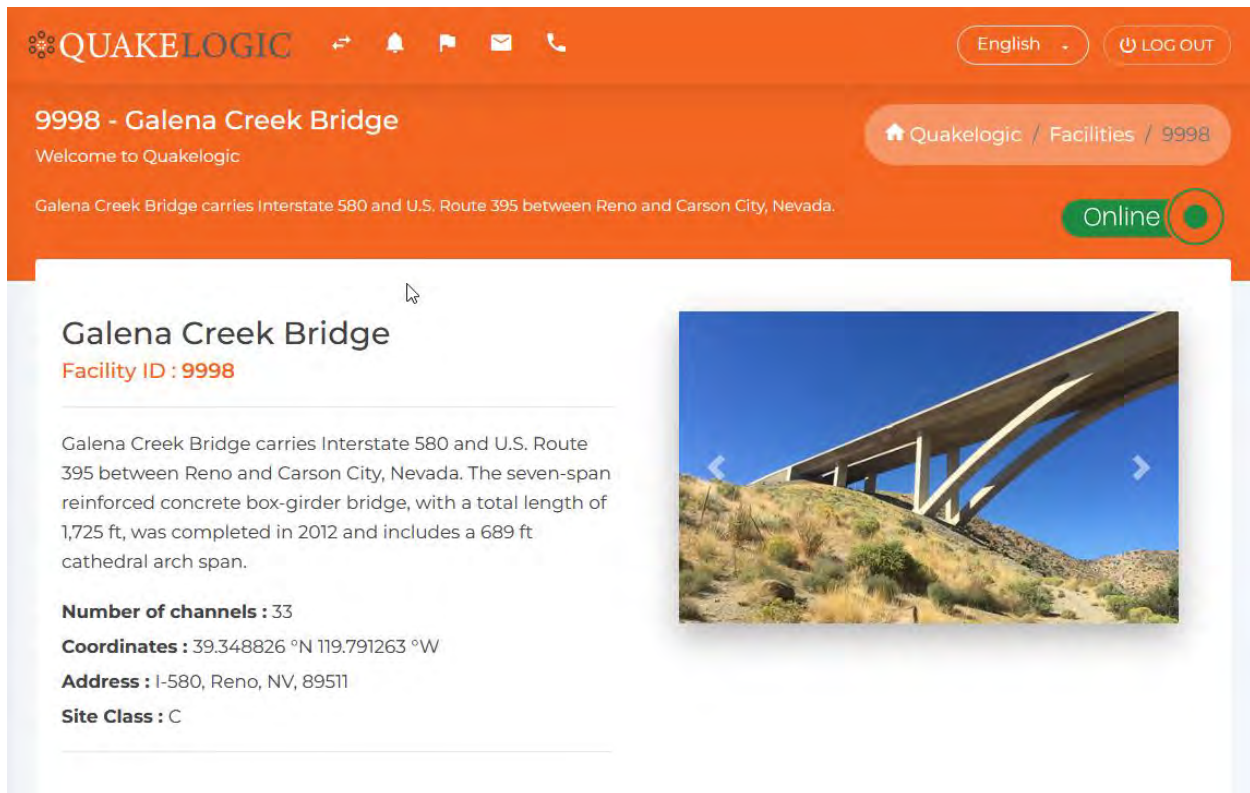


**Figure 4-3: Example view of dashboard**

### 4.1.3 System WatchDog

The watchdog system, **QUAKEDOG**, (Figure 4-4) continuously monitors the entire SHM system platform, including applications, system services, operating systems, network infrastructure and protocols, system metrics and security.



**Figure 4-4: Watchdog system to monitor system status**

QUAKEDOG routinely generates a status report of the structures (Figure 4-5). Any issue affecting the integrity of the SHM system is immediately identified and communicated to QuakeLogic for prompt resolution to ensure uninterrupted system performance.

Host ♦♦	Service ♦♦	Status ♦♦	Last Check ♦♦	Duration ♦♦	Attempt ♦♦	Status Information
GalenaBridge_FF	CPU Performance	OK	04-02-2020 08:20:31	0d 7h 43m 55s	1/3	OK: CPU Idle = 39.03%
	CPU Temperature	OK	04-02-2020 08:23:11	0d 7h 41m 15s	1/3	SENSORS OK
	Current Load	CRITICAL	04-02-2020 08:17:56	5d 22h 50m 30s	3/3	CRITICAL - load average per CPU: 0.70, 0.62, 0.59
	Current Users	OK	04-02-2020 08:14:41	0d 7h 39m 45s	1/3	USERS OK - 0 users currently logged in
	Disk Space	OK	04-02-2020 08:19:03	0d 7h 45m 23s	1/3	DISK OK - free space: / 4155 MB (55.18% inode=72%); /dev/shm 1839 MB (100.00% inode=100%); /home 174201 MB (84.00% inode=95%); /var 1382 MB (73.46% inode=98%); /var/tmp 4155 MB (55.18% inode=72%);
	EW Process	OK	04-02-2020 08:23:48	0d 7h 40m 38s	1/3	PROCS OK: Earthworm process found running: 29
	EW-PDL Process	OK	04-02-2020 08:16:50	0d 7h 47m 36s	1/3	PROCS OK: Earthworm process found running: 8
	Memory Usage	OK	04-02-2020 08:17:36	0d 7h 46m 51s	1/3	OK - 1421 / 3678 MB (38%) Free Memory, Used: 2627 MB, Shared: 68 MB, Buffers: 50 MB, Cached: 370 MB
	NTP Time	OK	04-02-2020 08:21:08	0d 1h 3m 18s	1/3	NTP OK: Offset -0.002327919006 secs
	Ping	OK	04-02-2020 08:15:00	0d 1h 9m 26s	1/3	PING OK - Packet loss = 0%, RTA = 170.82 ms
	SSH	OK	04-02-2020 08:23:43	0d 7h 40m 43s	1/3	SSH OK - OpenSSH_5.3 (protocol 2.0)
	Swap Usage	OK	04-02-2020 08:14:27	0d 7h 39m 59s	1/3	SWAP OK - 90% free (1826 MB out of 2047 MB)
	Total Processes	OK	04-02-2020 08:21:12	0d 7h 43m 14s	1/3	PROCS OK: 234 processes
	Uptime	OK	04-02-2020 08:14:44	0d 7h 39m 42s	1/3	Uptime OK: 43 day(s) 14 hour(s) 14 minute(s)

**Figure 4-5: Example QUAKEDOG report**

## **4.2 Online Dashboard**

### *4.2.1 Overview*

Real-time information about the health of each monitored structure is displayed in the form of a management dashboard. The mobile-friendly dashboard is intuitive to use and provides drill-down functionality from the initial single-screen overview through increasingly detailed levels of data and information as needed. The dashboard stores and displays current SHM data and reports. Encrypted password security is provided to avoid unauthorized access to information. The dashboard includes advanced features, such as a sensor display, a map of most recent earthquakes, a fault map, a list of relevant events, a data and report repository, amongst other features. It also allows manual data entry, on-demand reporting, and on-demand data plotting. All notifications can also be accessed from the dashboard.

### *4.2.2 Homepage*

The homepage of the SHM dashboard shows the location of all monitored structures, and the location and severity of recent earthquakes around the globe (Figure 4-6). The map display can be changed to color, grey or satellite view. Different layers may be selected to show earthquakes and faults.



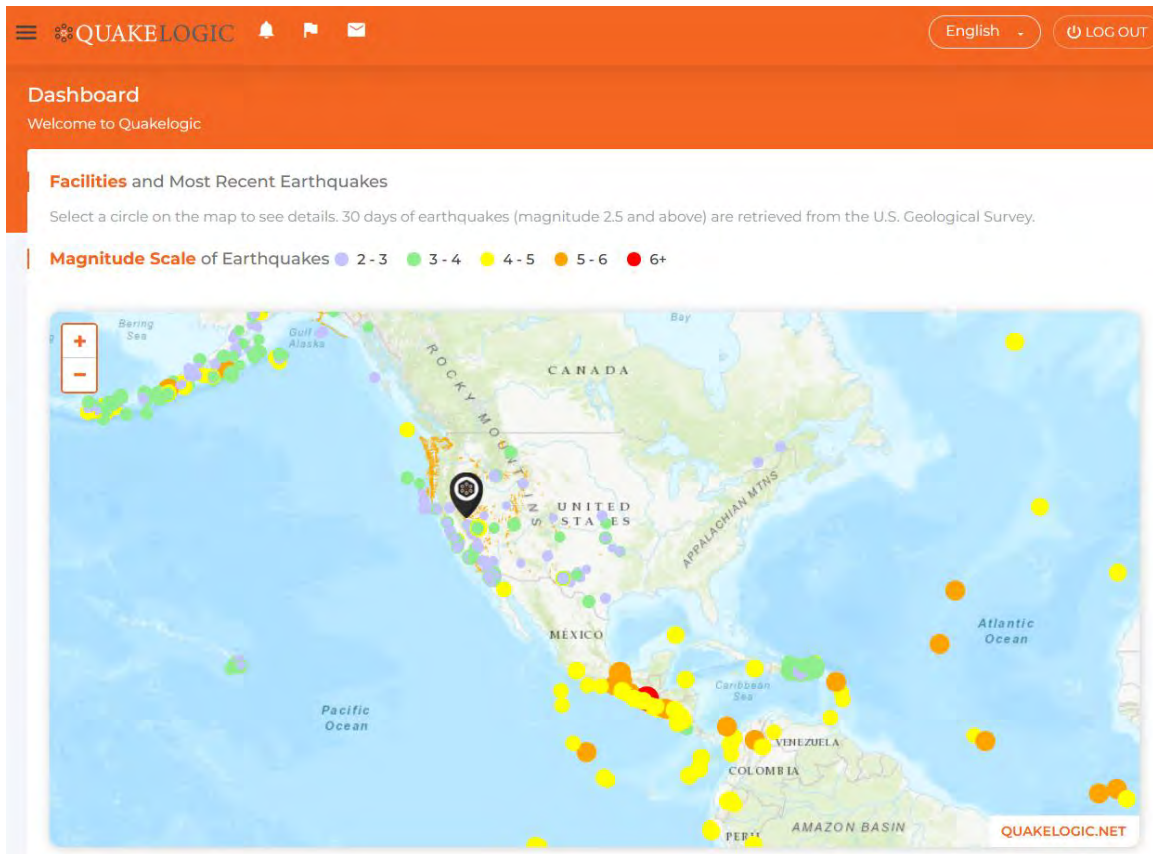


**Figure 4-6: Dashboard homepage**

### 4.2.3 Facility Page

The dashboard allows the user to select the monitored facility using three different methods:

- Menu on the left side (Figure 4-7),
- Facility icon on the shortcut bar (Figure 4-8), or
- From the map (Figure 4-9).

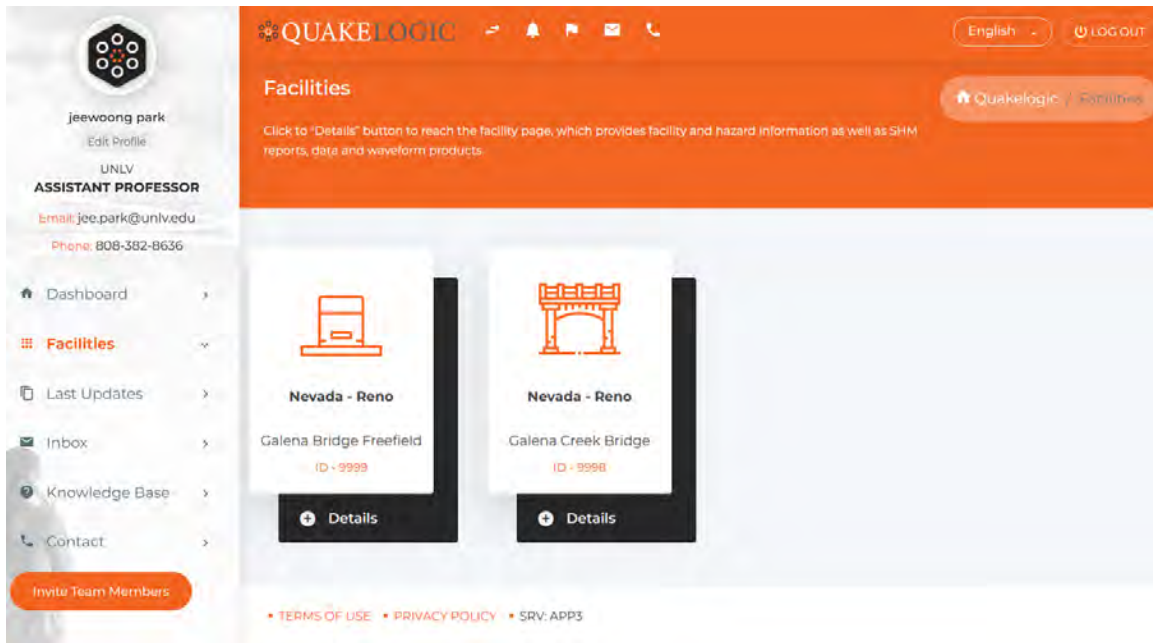


**Figure 4-7: Facility selection using left menu**

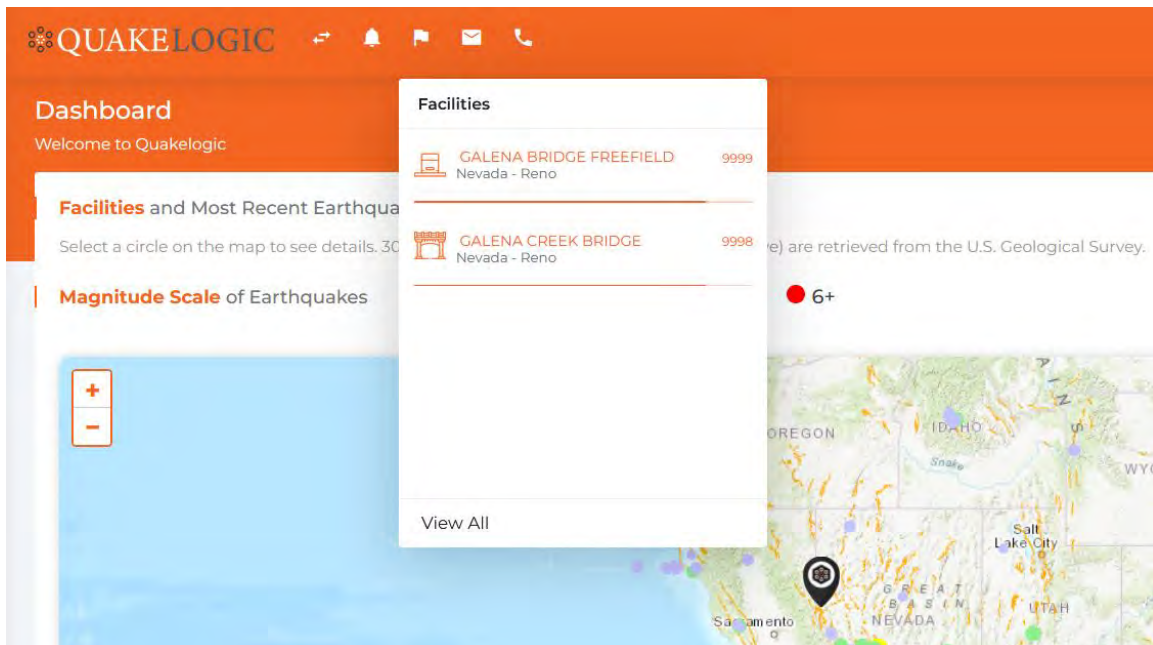


**Figure 4-8: Facility selection using shortcut bar**

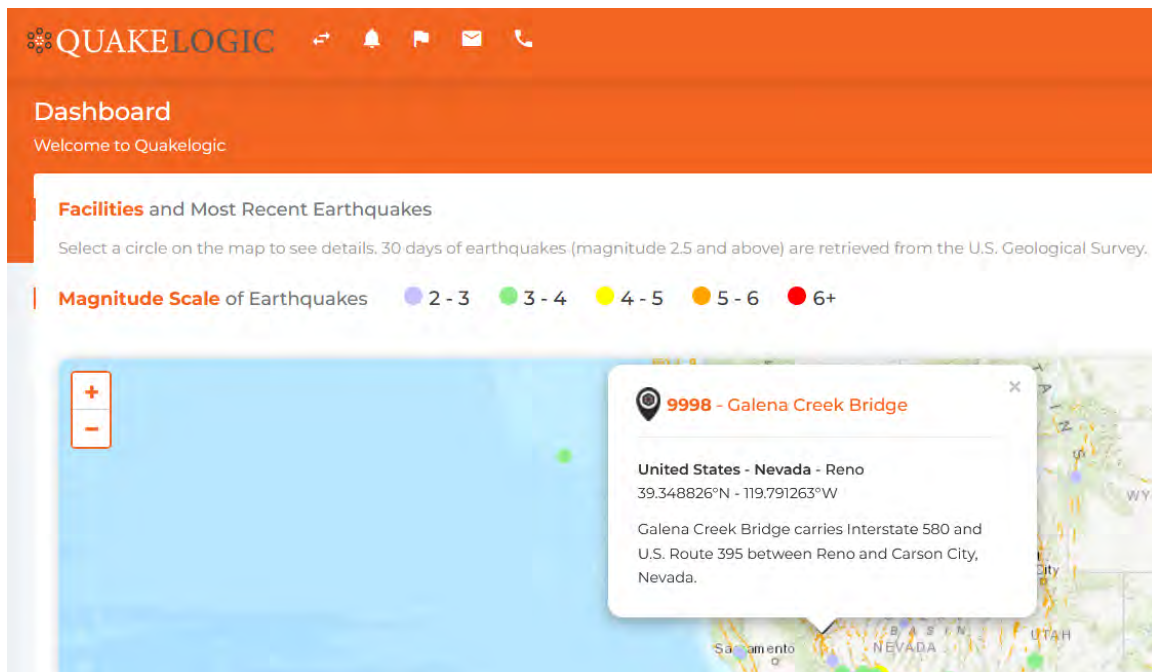


**Figure 4-9: Facility selection from map**

Once the monitored facility is selected from the menu on the left side, the Facility tab (e.g., the free-field facility and the bridge facility) provides an asset management layout showing structural, geotechnical, seismic hazard, and other information relevant to the monitored assets (Figure 4-10 and Figure 4-11). In addition, a facility summary is provided that details general information about the structure, such as type, location, span, etc. as well as contact information for the owner representative (

Figure 4-12). Additional tabs (i.e., menus) are selectable for a variety of features, further detailed in the following sections. Notably, the dashboard has customizable data tables for sensors and tremors, on demand plotting, and manual data entry for sensors if needed.



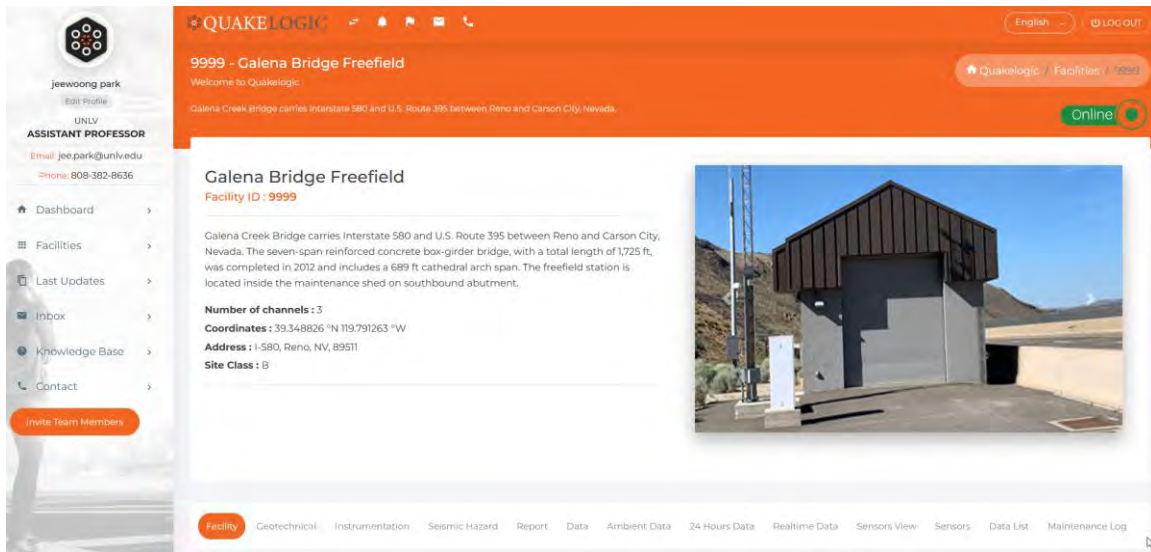


Figure 4-10: Example asset management page for free-field site

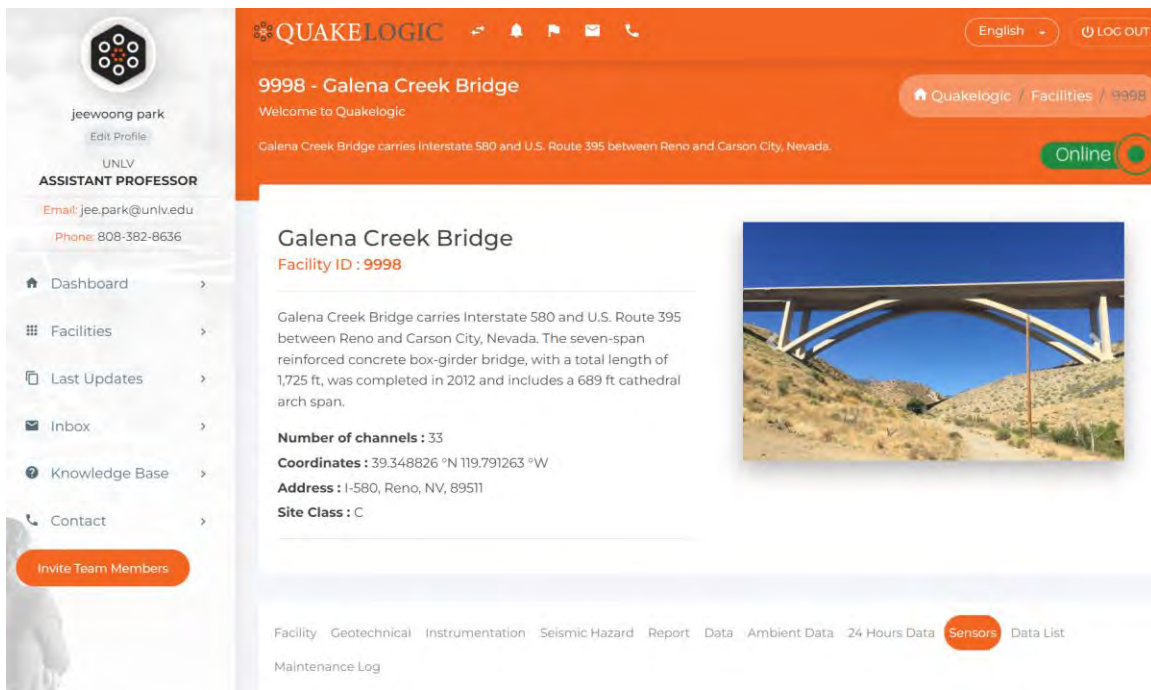


Figure 4-11: Example asset management page for Galena Creek Bridge

- Dashboard
- Facilities
- Last Updates
- Inbox
- Knowledge Base
- Contact
- Invite Team Members

English | LOG OUT

Number of channels : 33  
Coordinates : 39.348826 °N 119.791263 °W  
Address : I-580, Reno, NV, 89511  
Site Class : C

Facility | Geotechnical | Instrumentation | Seismic Hazard | Report | Data | Ambient Data | 24 Hours Data | Sensors | Data List | Maintenance Log

### Facility Summary

The Galena Creek Bridge carries Interstate 580 and U.S. Route 395 between Reno and Carson City, Nevada. The seven-span reinforced concrete box-girder bridge, with a total length of 1,725 ft, was completed in 2012 and includes a 689 ft cathedral arch span. Internal hinges are located near the piers just outside of the arch, allowing for longitudinal movement and forming three separate frames of the structure. The base of the arch is connected to the bottom of the columns at the piers of the middle frame using thrust blocks to transfer load from the arch to the foundation. The longitudinal post-tensioned two cell box-girders rest on the six sets of single column piers. The deck is post-tensioned transversely. The column and arch cross-sections are all hollow rectangular sections. The bridge consists of two separate structures tied together for lateral loading resistance using a link slab between the decks at the crown of the arch and link beams connecting the thrust blocks at the base of the arch. Its freefield station is located on southbound abutment.

### Map Location

### Contact Info

Michael Taylor, P.E.  
775-888-7549  
michaeltaylor@dot.state.nv.us

**Figure 4-12: Example Facility Summary and Contact Information for Galena Creek Bridge**

#### 4.2.4 Geotechnical Tab

The Geotechnical tab (Figure 4-13) provides detailed information about existing knowledge on the behavior of soils under the influence of loading forces and soil-water interactions.

The screenshot displays the QuakeLogic web application interface. On the left is a sidebar for user 'jeewoong park', an UNLV Assistant Professor, with links to Dashboard, Facilities, Last Updates, Inbox, Knowledge Base, and Contact. The main content area is titled '9998 - Galena Creek Bridge' and includes a welcome message and a brief description of the bridge. A large photograph of the bridge is shown on the right. Below the description, a navigation bar highlights the 'Geotechnical' tab, with other options like Instrumentation, Seismic Hazard, Report, Data, Ambient Data, 24 Hours Data, Sensors, Data List, and Maintenance Log. The Geotechnical section contains text about soil sample collection from borings for identification and engineering characterization.

**9998 - Galena Creek Bridge**  
Welcome to QuakeLogic

Galena Creek Bridge carries Interstate 580 and U.S. Route 395 between Reno and Carson City, Nevada.

**Galena Creek Bridge**  
Facility ID : 9998

Galena Creek Bridge carries Interstate 580 and U.S. Route 395 between Reno and Carson City, Nevada. The seven-span reinforced concrete box-girder bridge, with a total length of 1,725 ft, was completed in 2012 and includes a 689 ft cathedral arch span.

**Number of channels :** 33  
**Coordinates :** 39.348826 "N 119.791263 "W  
**Address :** I-580, Reno, NV, 89511  
**Site Class :** C

Facility **Geotechnical** Instrumentation Seismic Hazard Report Data Ambient Data 24 Hours Data Sensors Data List Maintenance Log

Soil samples were collected from the borings for identification, classification, and geotechnical engineering characterization. Disturbed and relatively undisturbed (intact) soil samples were generally collected from the borings at approximately 5-foot intervals to a depth of about 60 ft bgs and at approximately 10-foot intervals thereafter. A total of 63 disturbed and 7 intact soil samples were collected during the field investigation

**Figure 4-13: Example Geotechnical tab for Galena Creek Bridge**

#### 4.2.5 Instrumentation Tab

The Instrumentation tab shows detailed information about the sensors. A summary of the active instrumentation is provided as well as a schematic of the sensor layout for the primary seismic monitoring system and the secondary exploratory system as shown in Figure 4-14 and for the free-field site as shown in Figure 4-15.

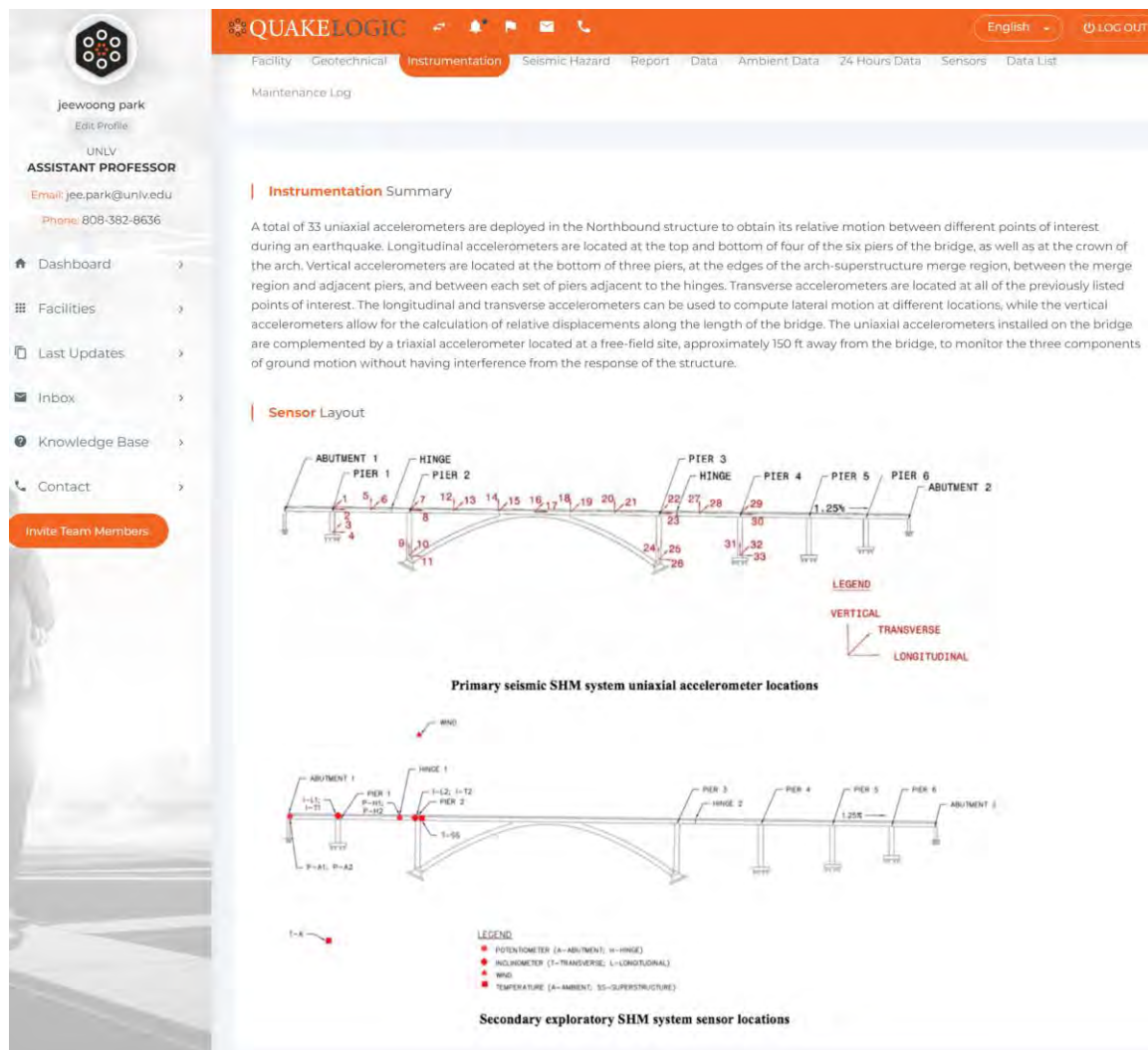


**Figure 4-14: Example instrumentation summary and sensor layout for primary seismic monitoring system and secondary system installed at the Galena Creek Bridge provided under the Instrumentation tab**



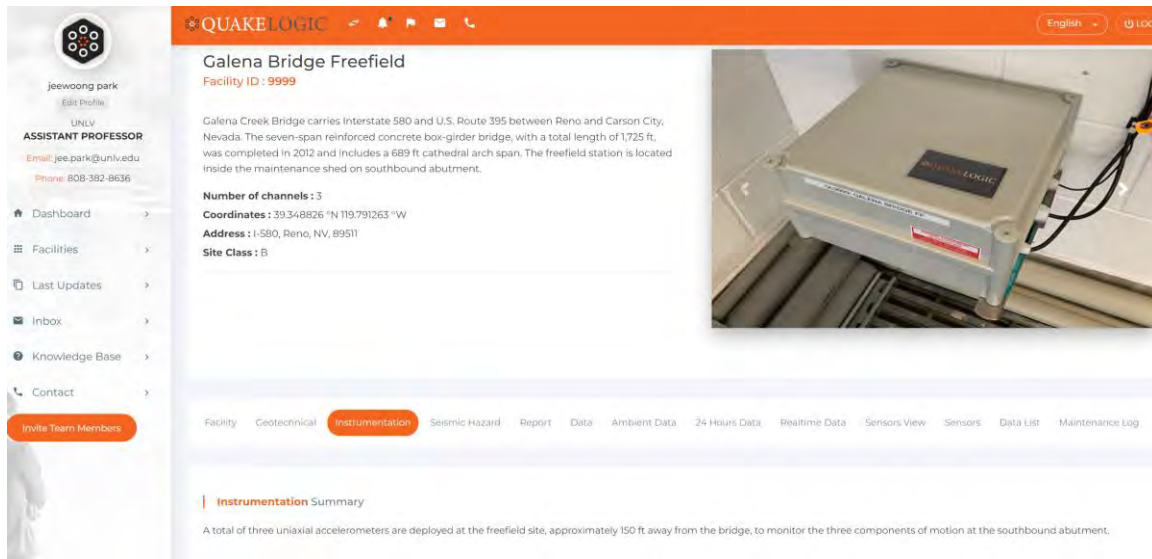


**Figure 4-15: Example sensor instrumentation at the free-field site under the Instrumentation tab**

#### 4.2.6 Seismic Hazard Tab

The Seismic Hazard tab depicts the hazards associated with potential earthquakes in a particular area. Two primary types of data are included: USGS Seismic Design Maps (Figure 4-16) and response spectrum (Figure 4-17). The response spectrum includes plots of the maximum considered earthquake (MCE<sub>R</sub>) Response Spectrum and Design Response Spectrum. The response spectrum was generated based on ASCE/SEI 7-16 guidance. The maps show the peak ground acceleration as well as spectral acceleration at 0.2 and 1.0 seconds for the geographical around the monitored facility. The current trigger values are set based on these hazard map and spectrum data based on the site (see details in the Seismic Hazard Description from a sample report in Appendix A).

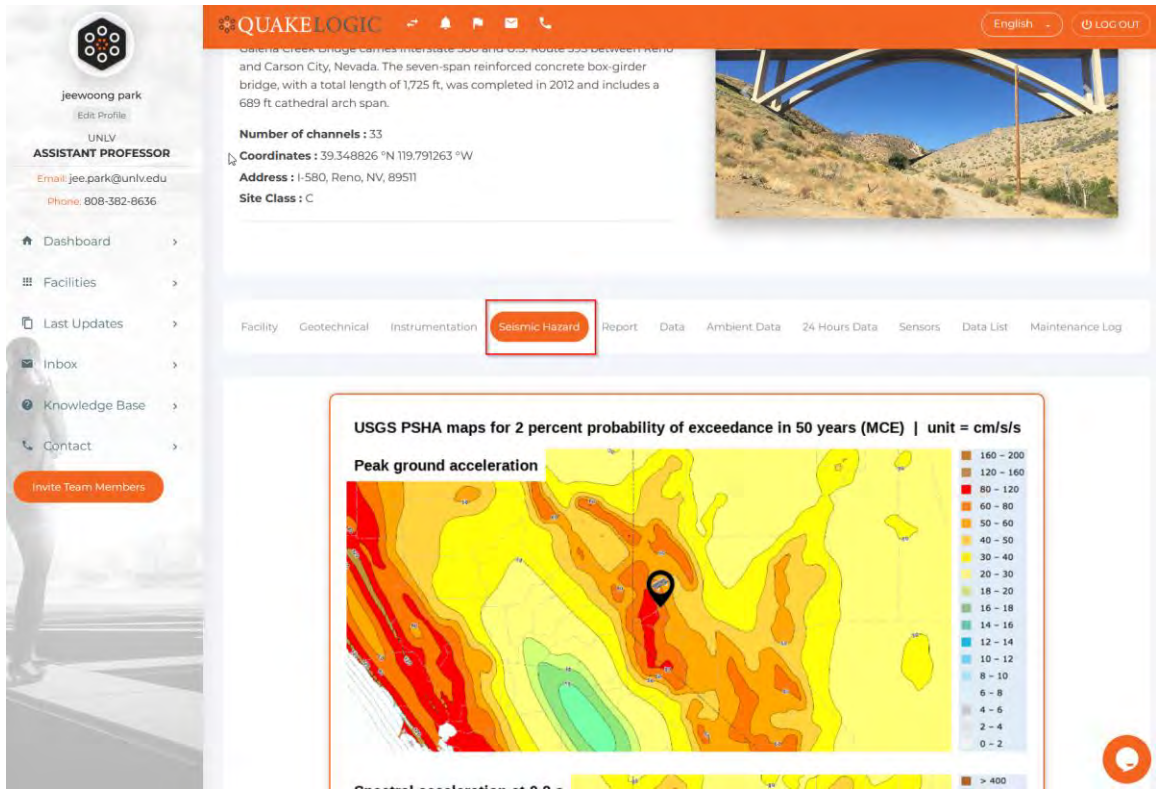


Figure 4-16: Example seismic design maps provided under Seismic Hazard tab

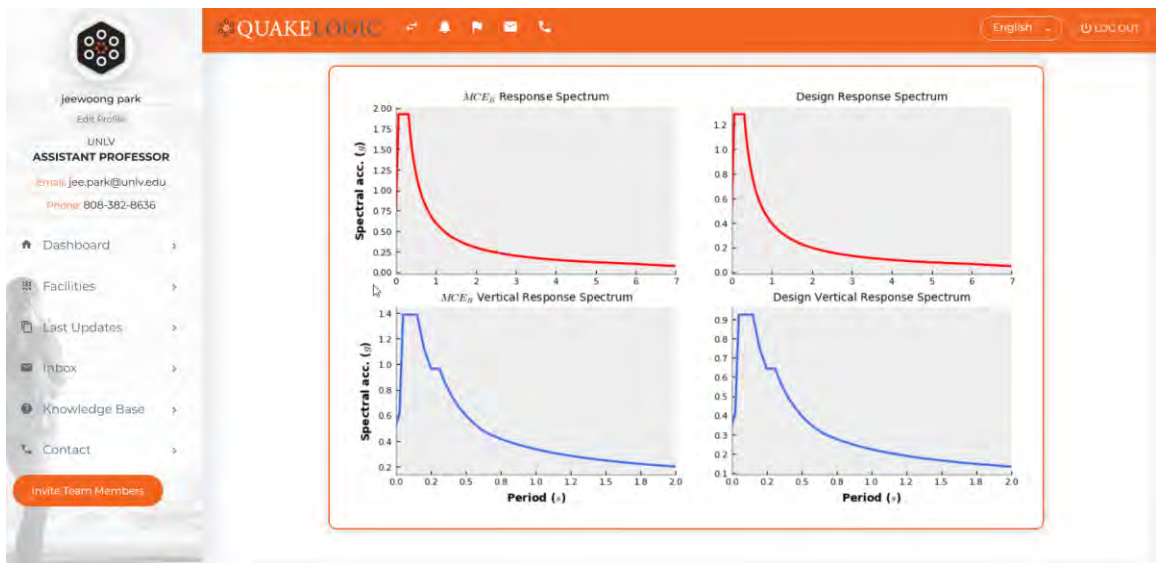
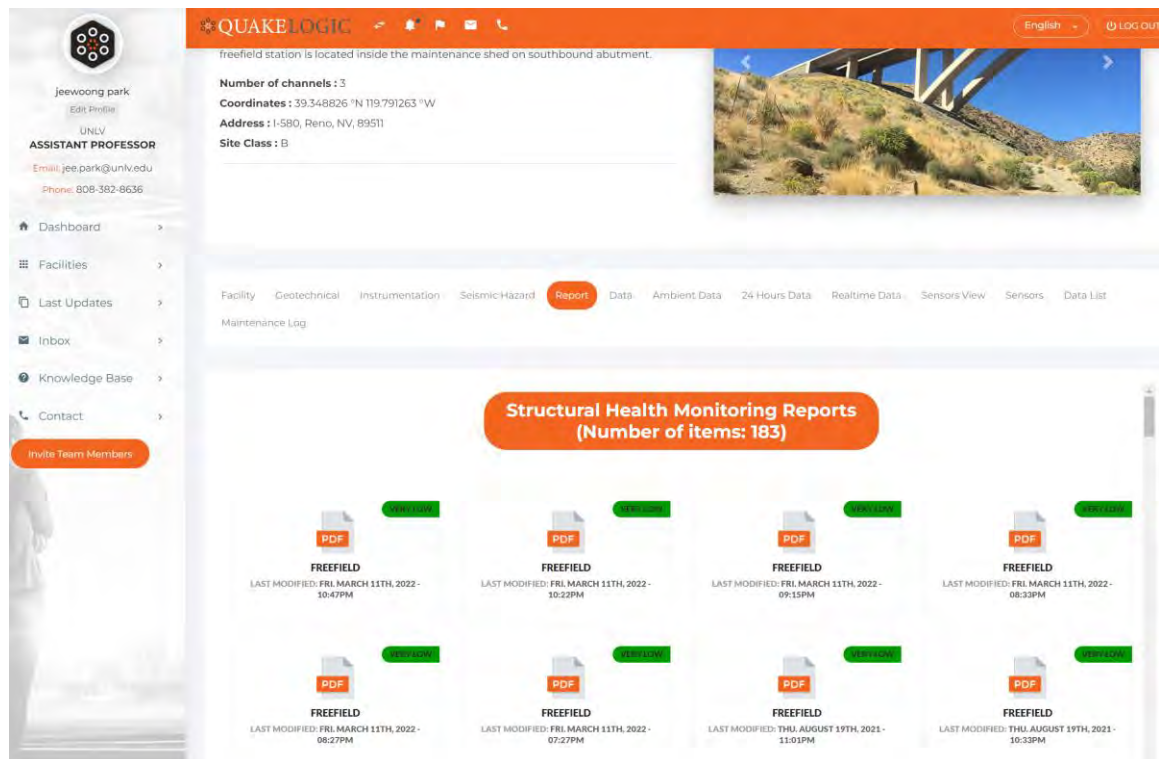


Figure 4-17: Example response spectrum provided under Seismic Hazard tab

#### 4.2.7 Report Tab

The Report tab allows the user to view detailed SHM reports in PDF format. Each report is generated following the trigger of an alarm condition. The reports can be downloaded at any time from this tab. As such, the Report tab provides the opportunity to view historical reports (Figure 4-18 and Figure 4-19). Each PDF file is color coded based on inspection priority (green to red):

- **GREEN:** VERY LOW PRIORITY
- **LIGHT GREEN:** LOW PRIORITY
- **YELLOW:** MEDIUM PRIORITY
- **ORANGE:** HIGH PRIORITY
- **RED:** VERY HIGH PRIORITY



**Figure 4-18: Example collection of historical SHM reports from the free-field site**

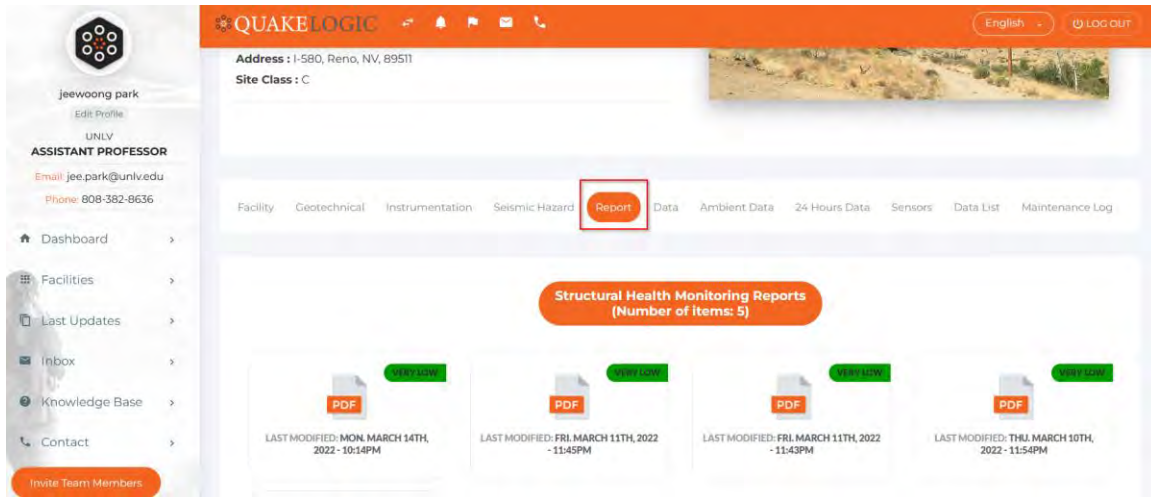


**Figure 4-19: Example collection of historical SHM reports from the bridge**

#### 4.2.8 Data Tab

The Data tab allows the user to download the raw data corresponding to the detected events. Each downloadable file is in ZIP format. This is useful for an expert-level analysis that could help the analyst to conduct a thorough investigation of the event on the structure. Figure 4-20 and Figure 4-21 present example data files for the free-field site and the bridge.

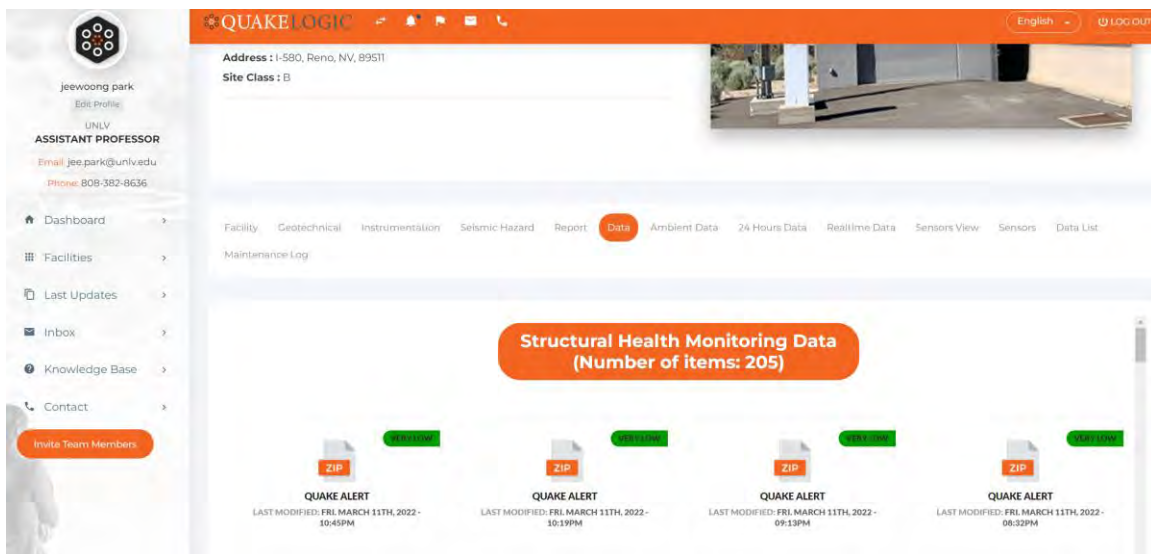


**Figure 4-20: Example data files contained under Data tab from the free-field site**



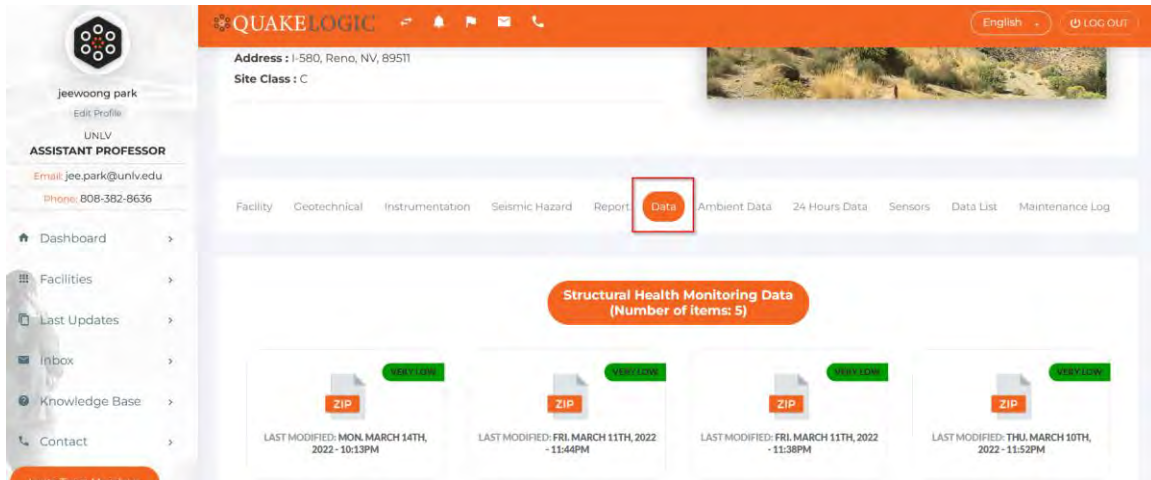


**Figure 4-21: Example data files contained under Data tab from the bridge**

#### 4.2.9 Ambient Data Tab

The Ambient Data tab provides access to zipped data files from ambient data periodically collected from the monitoring location (Figure 4-22). Ambient data is representative of routine daily traffic and is not the result of a trigger event, such as seismic activity. The data helps to access the overall condition of the structure throughout time.

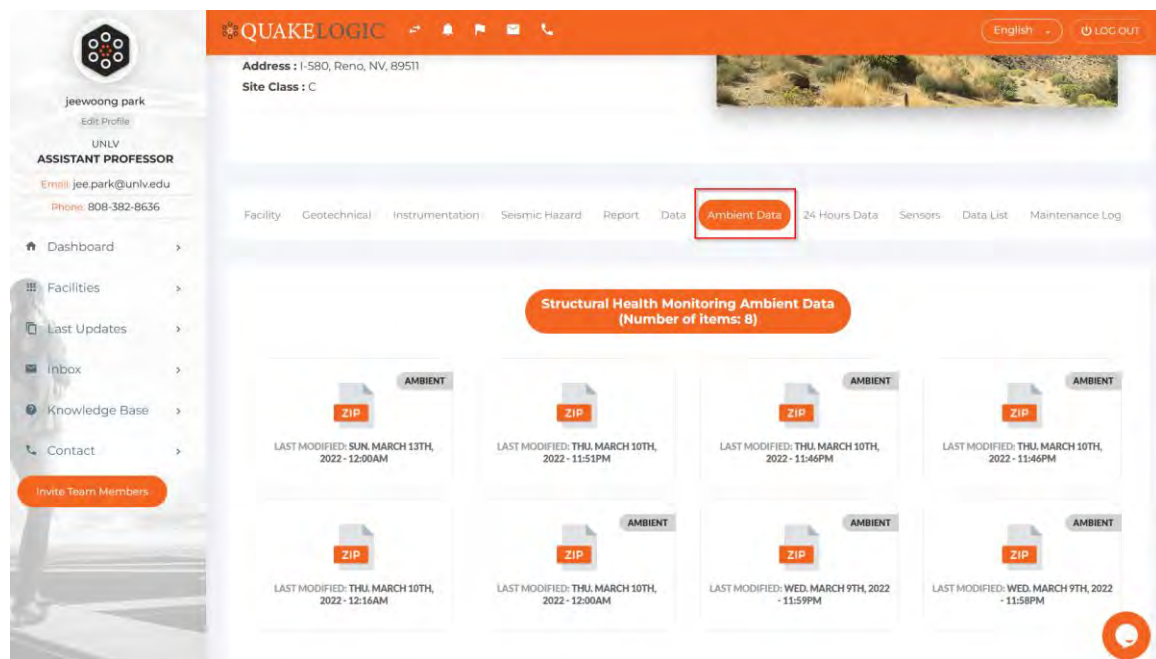


**Figure 4-22: Example collection of ambient data files contained under Ambient Data tab**

#### 4.2.10 24 Hours Data Tab

The 24 Hours Data tab shows the seismic movements of the sensors over the previous 24-hour period. Seismic graphic diagrams for each sensor allow the user to examine the structural response and movements that occurred in the previous 24-hour period (Figure 4-23). This is available both sets of sensors at the free-field site and in the bridge. Figure 4-24 shows a zoom-in view of the data for Sensor 1 corresponding to a portion (up to the seventh hour) of the 24-hour data.

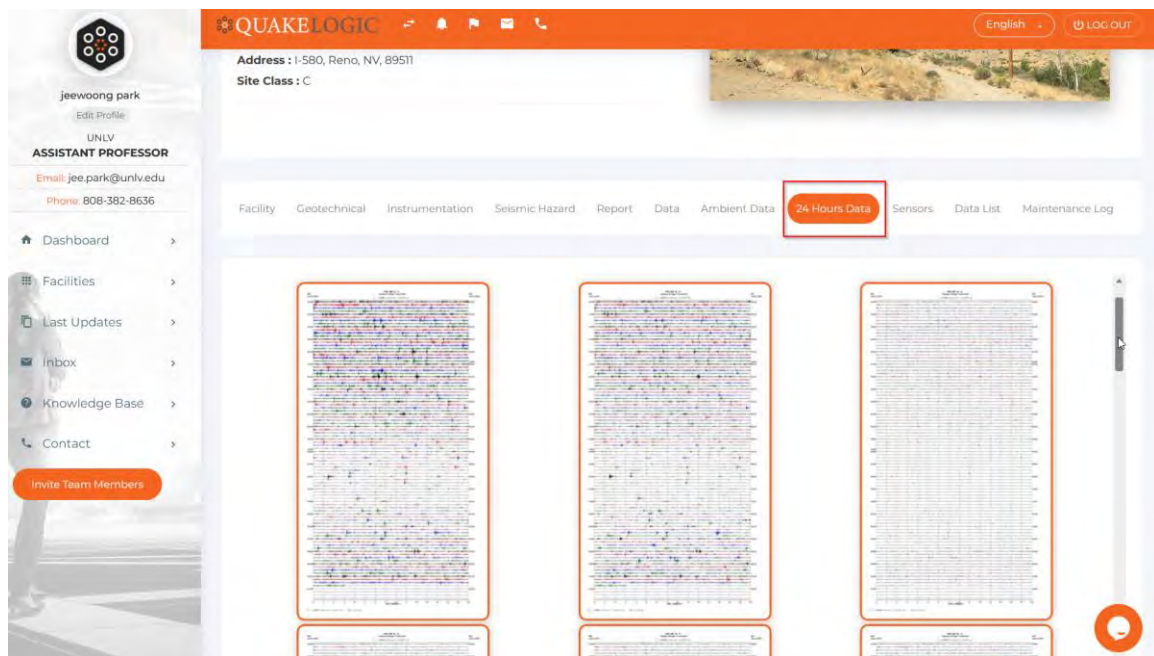


Figure 4-23: Example of seismic graphics provided under 24 Hour Data tab for the bridge

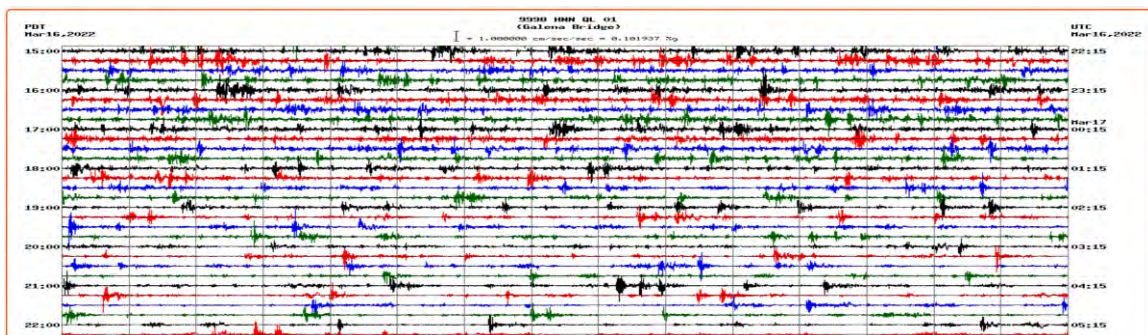
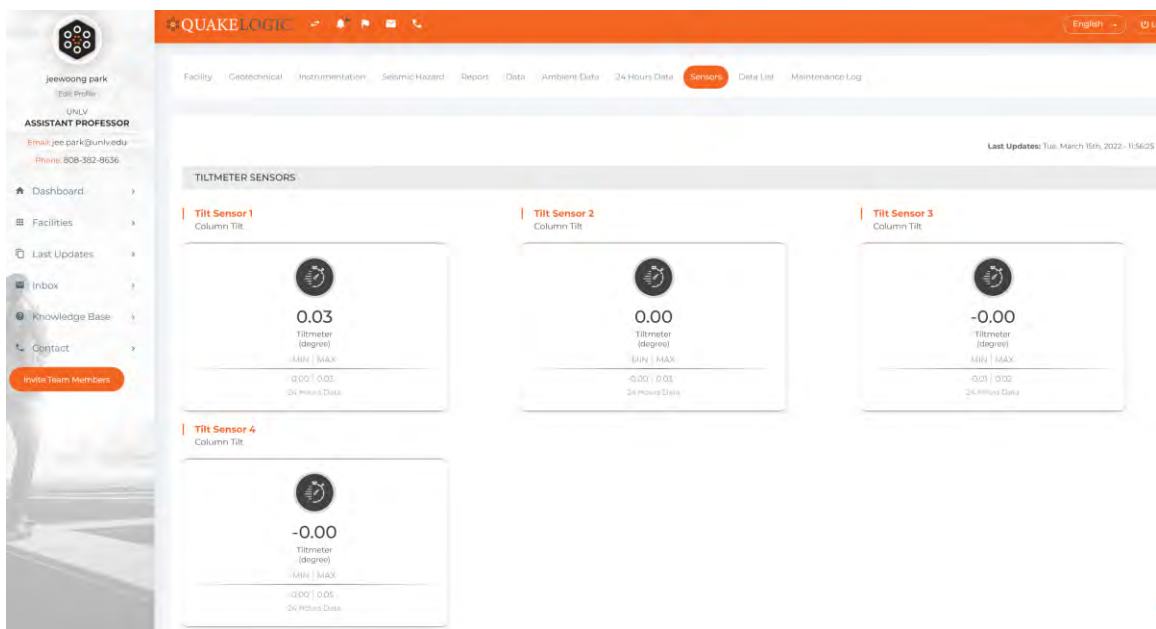


Figure 4-24: Close-up view of Sensor 1 in 24-hour data

#### 4.2.11 Sensors Tab

The Sensors tab from the Galena Creek Bridge facility shows the last updated sensor data from the secondary monitoring system in near real time. Data include the tilt (Figure 4-25), relative displacement (Figure 4-26), and temperature and wind velocity (Figure 4-27) measured by the secondary system sensor components at the designated locations (See Chapter 3.2 for the detailed information about installed locations). These data (tilt and displacement) present responses at critical locations, allowing the user to examine the structural response and movements together with the seismic responses in a comprehensive manner.



**Figure 4-25: Example of tilt sensor data provided under Sensors tab**

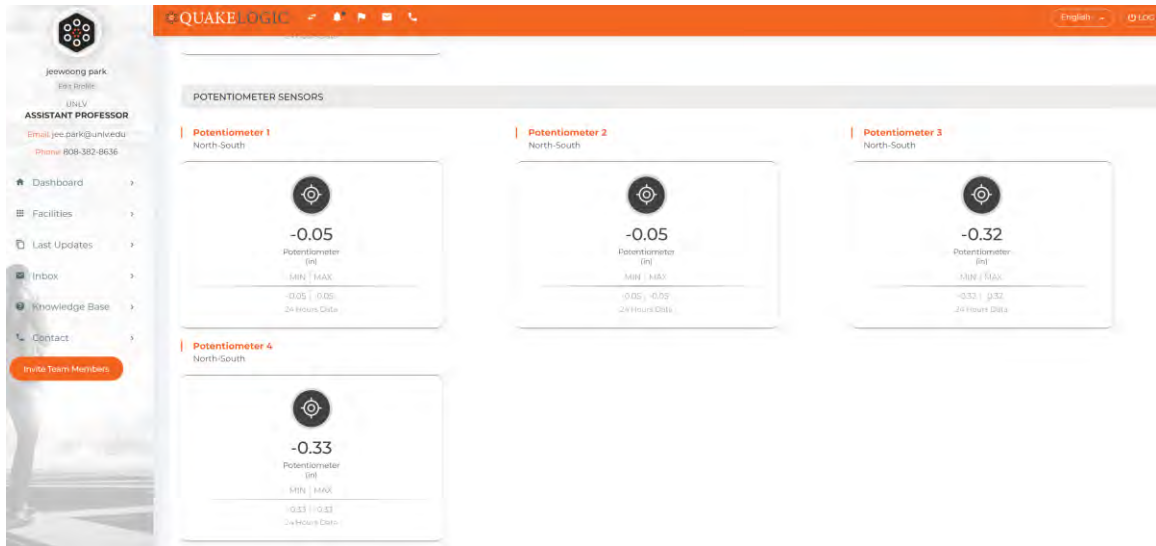


**Figure 4-26: Example of displacement (potentiometer) data provided under Sensors tab**

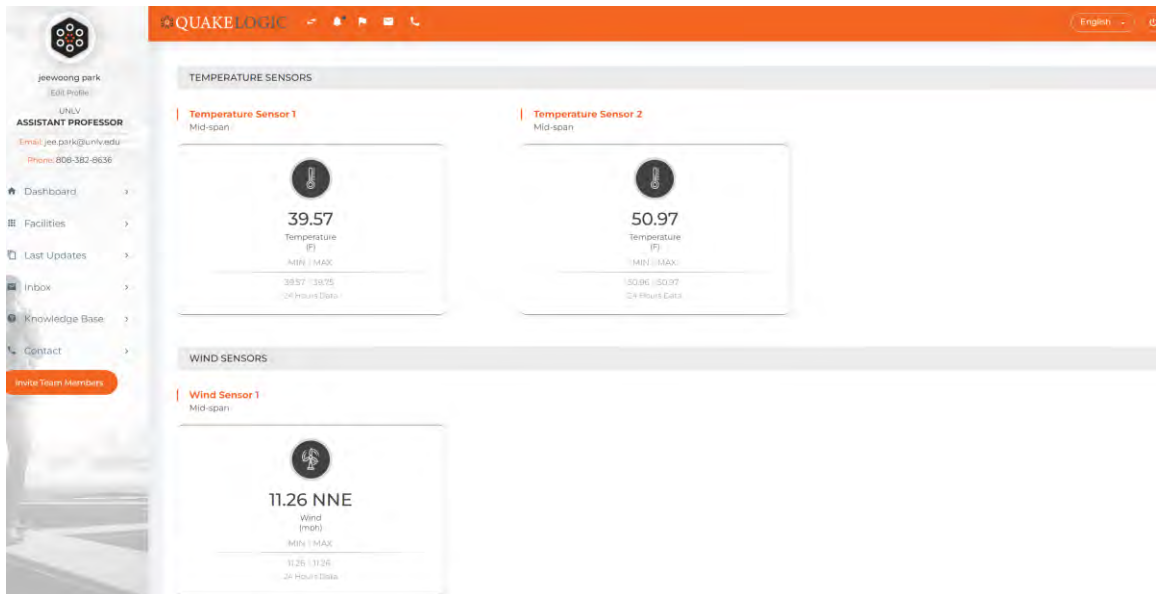


**Figure 4-27: Example of temperature and wind data provided under Sensors tab**



#### 4.2.12 Data List Tab

The Data List tab is available both in the free-field site and the bridge facilities. This allows the users to selectively choose sensors and times of interest and export the corresponding data in either XSL or CSV format. Figure 4-28 and Figure 4-29 show examples from the website.

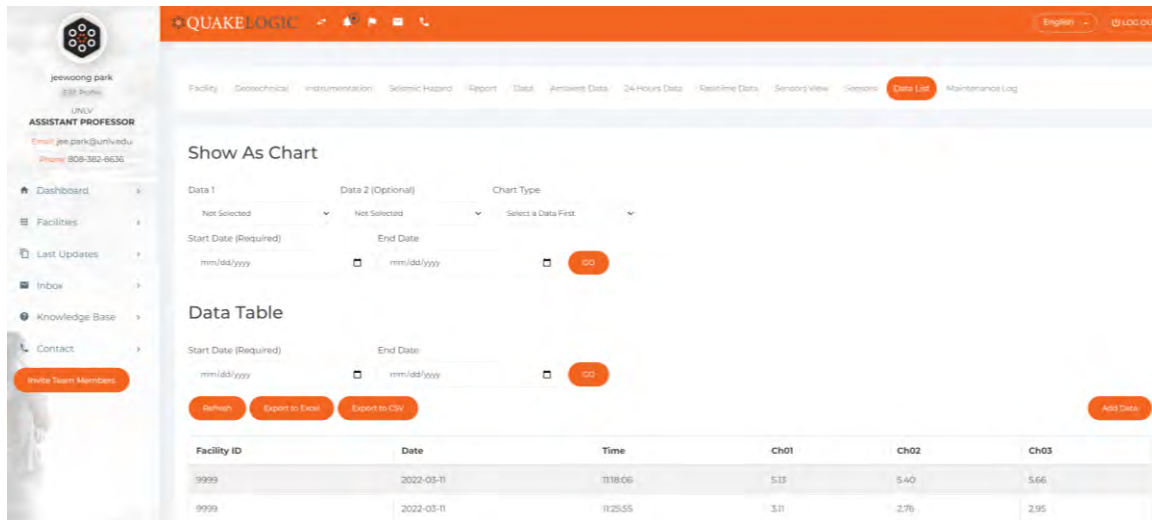


Figure 4-28: Example of Data List tab showing raw data from the free-field sensor

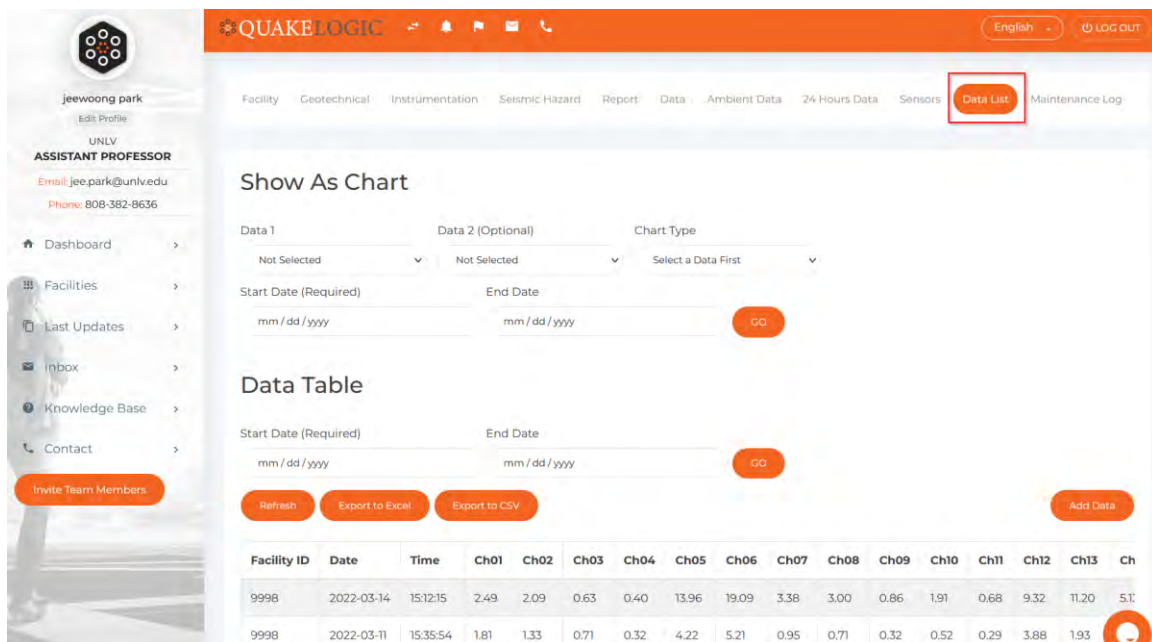


Figure 4-29: Example of Data List tab showing raw data from the sensors in the bridge

### 4.2.13 Maintenance Log Tab

The Maintenance Log tab archives historical data for maintenance performed to the systems (Figure 4-30). The research team added this tab to the system dashboard for convenience in future maintenance.

**QUAKE LOGIC**

Calena Creek Bridge carries Interstate 580 and U.S. Route 395 between Reno and Carson City, Nevada. The seven-span reinforced concrete box-girder bridge, with a total length of 1,725 ft, was completed in 2012 and includes a 689 ft cathedral arch span. The freefield station is located inside the maintenance shed on southbound abutment.

Number of channels : 3  
Coordinates : 39.348826 °N 119.791263 °W  
Address : 1-580, Reno, NV, 89511  
Site Class : B

**Maintenance Log**

Start Date (Required)  End Date

Facility ID	Date	Time	Data	Remind
9999	2022-03-11	11:13:25	The data list tab is added to the dashboard, which shows peak values during alarm conditions with time stamps. The current date and time are based on pacific time only.	
9999	2022-03-11	13:12:30	The real-time data stream tab is opened.	

**Figure 4-30: Example of Maintenance Log tab showing historical system maintenance**

#### 4.2.14 Last Updates Menu Option

The Last Updates menu option on the side menu bar allows the user to view all SHM notifications (Figure 4-31). For easy access, the reports are listed chronologically. The Rapid Assessment for Engineering Response Report can be viewed from this option (Figure 4-32). In addition, the reports can be downloaded as a PDF file. The report contents will be discussed in Section 4.3 and a complete example report is included in Appendix A.

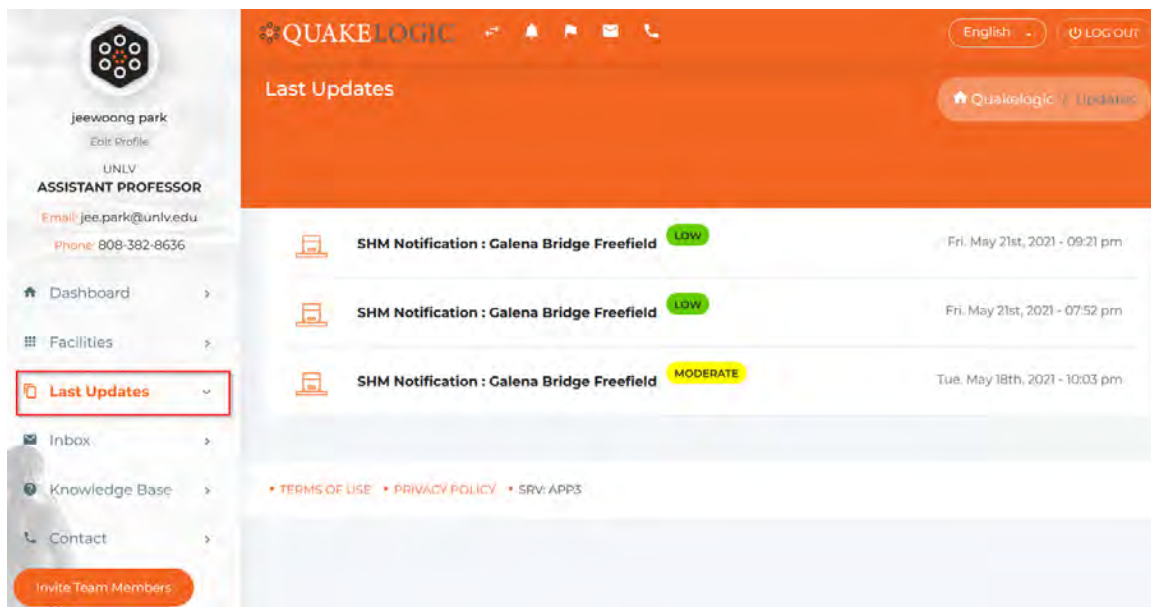


**Figure 4-31: Example of chronological reports found in the Last Updates menu option**

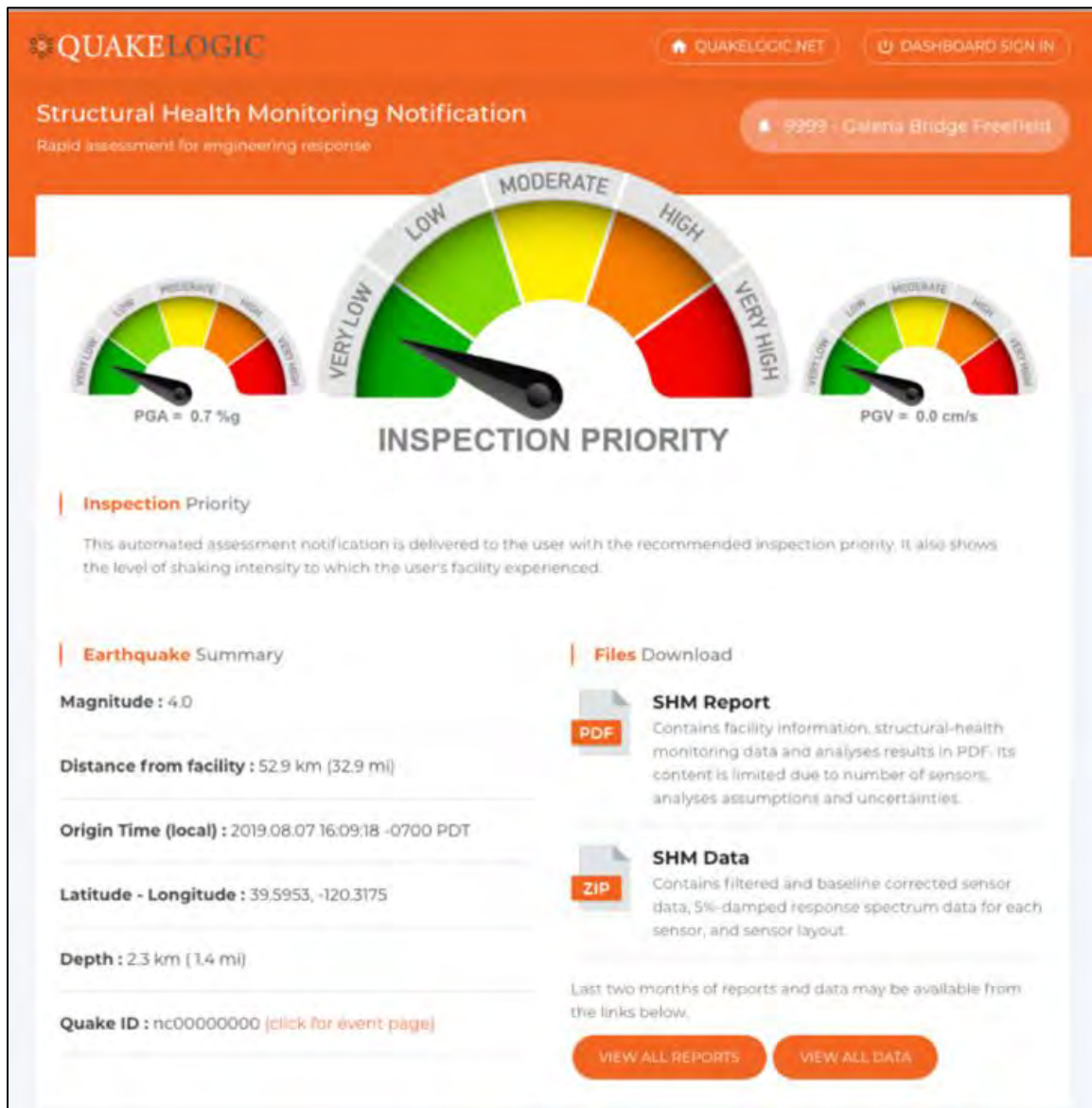
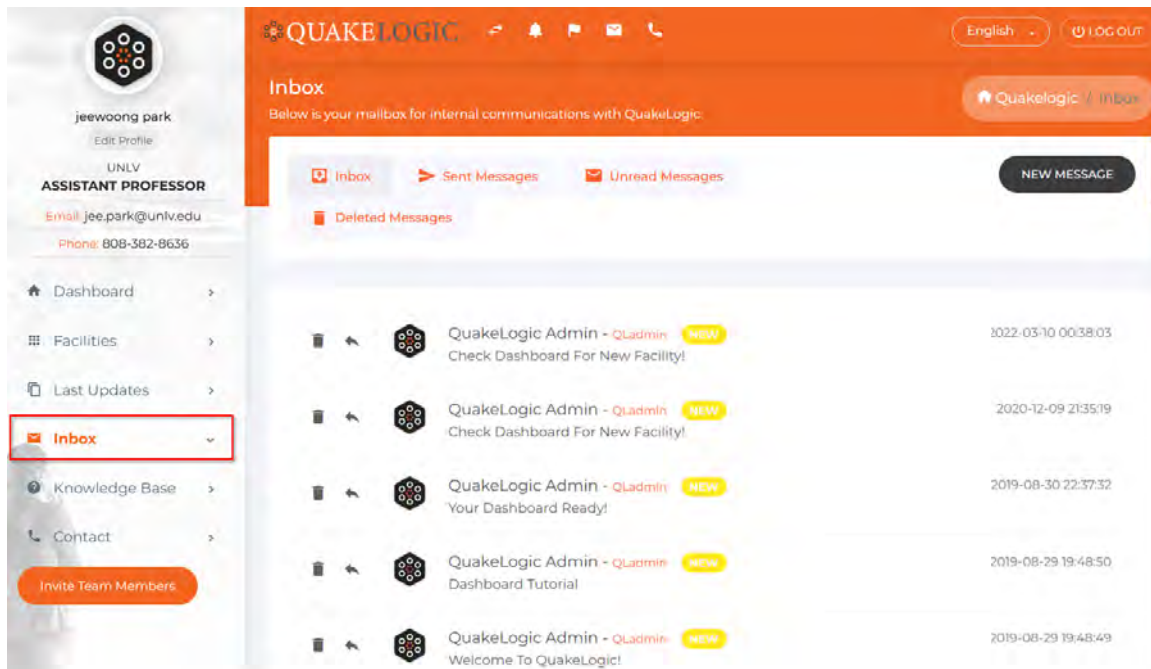


Figure 4-32: Example Rapid Assessment for Engineering Response Report Cover



#### 4.2.15 Inbox Menu Option

The Inbox menu option is a mailbox for internal communications with QuakeLogic (Figure 4-33). Within the Inbox menu option, the user will receive direct messages sent by QuakeLogic. Additionally, the user can contact QuakeLogic directly by using the NEW MESSAGE button in the upper righthand corner. Messages can be deleted or stored for later use by the user.



**Figure 4-33: Example Inbox menu option enabling direct communication with QuakeLogic**

#### 4.2.16 Knowledge Base Menu Option

The Knowledge Base menu option enables the user to review frequently asked questions and prepared responses by QuakeLogic (Figure 4-34). Selecting a question will display detailed responses to commonly encountered questions for a variety of topics, including general information, QuakeLogic SHMapp, Installation, Triggering, Data and Transmission, etc.

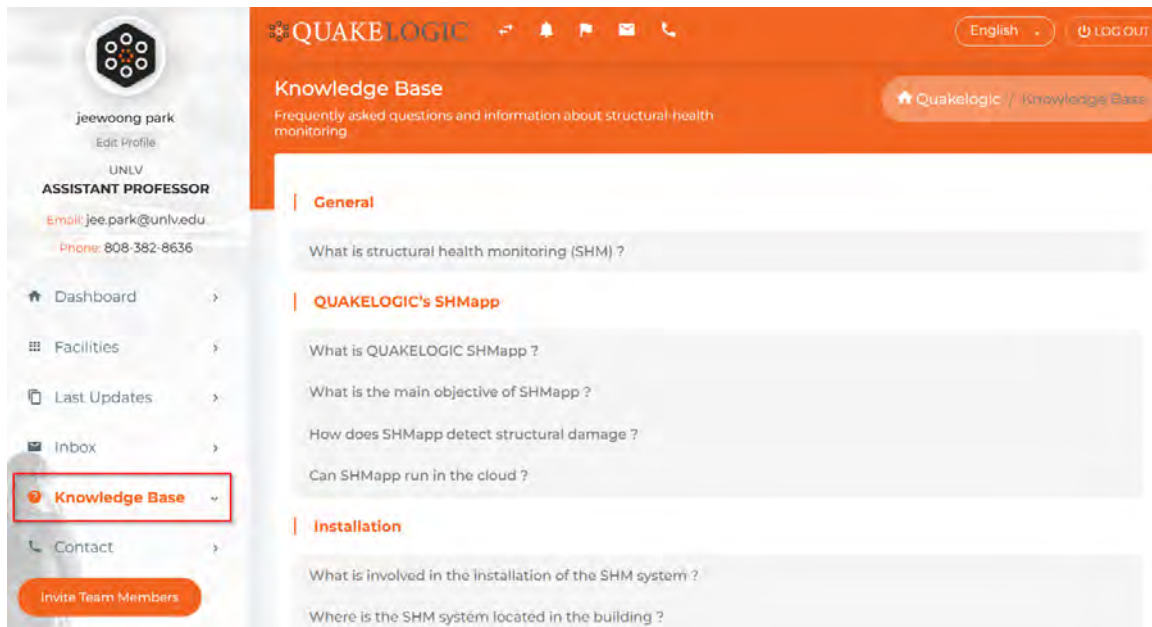


**Figure 4-34: Example list of frequently asked questions in Knowledge Base menu option**

#### 4.2.17 Contact Menu Option

The Contact menu option provides several methods to reach QuakeLogic, including filling out the online form, email, or a Live Chat function in the bottom right of the screen (Figure 4-35). Users are encouraged to not hesitate contacting QuakeLogic if they cannot find the answer to any specific question.

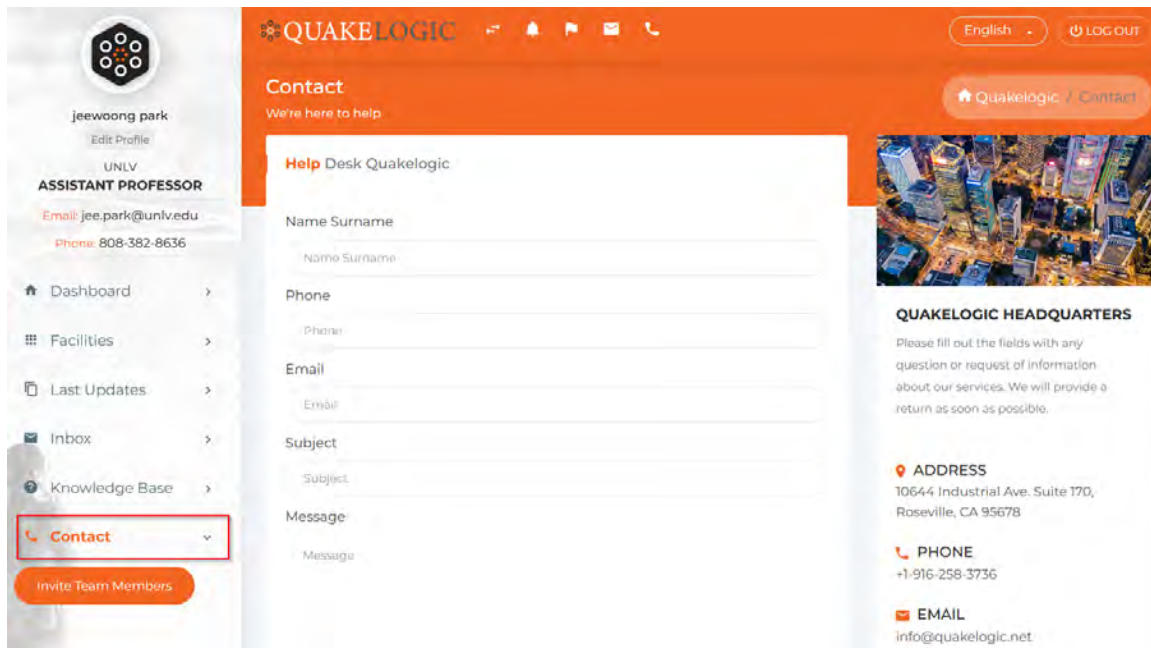


**Figure 4-35: Contact menu option for access to QuakeLogic support**

#### 4.2.18 Shortcut Toolbar

The Shortcuts toolbar includes icons along the top left of the screen (Figure 4-36). The shortcuts provided allow the user to quickly access the notifications (bell icon), check the latest developments (flag icon), check the message box (envelope icon), or contact QuakeLogic by phone (phone icon).

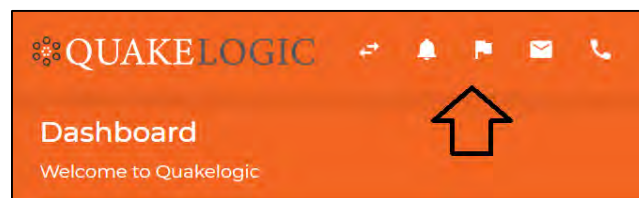


**Figure 4-36: Shortcuts toolbar**

### 4.3 Rapid Assessment for Engineering Response Report

Following a trigger event, a report (Rapid Assessment for Engineering Response Report) is generated to facilitate a rapid assessment of the condition of the structure. The report includes a number of key parameters to help the engineer make actionable decisions on inspection priority and emergency response. A complete example report is provided in Appendix B; however, many of the sections and graphics are duplicated from the online dashboard. The reports are designed to provide detailed descriptions of each parameter, such that a uniformed user could quickly ascertain key information. To summarize, the report is divided into the following sections.

- *Cover Page* – Includes the name of the asset being monitored as well as a photograph. The cover page also provides the inspection priority, rapid assessment, and local time of report origin. Finally, the cover page provides contact information for support.
- *Inspection Priority* – Five levels of inspection priority, ranging from very low to very high, are provided. In addition, the peak ground acceleration (PGA) and peak ground velocity (PGV) are included.
- *Facility Description* – General information about the structure is provided, such as location, age, type of structure, span length, etc. Additionally, any unique features are also provided in this section (e.g., the link slab and beams).
- *Geotechnical Information* – A general description of the geotechnical features of the site is provided in this section. For the Galena Creek Bridge, the geotechnical report was unable to be furnished by NDOT; as such, the description has been left blank.
- *Seismic Hazard Description* – Includes the ASCE/SEI 7-16 risk category, soil classification, seismic design category, and response modification coefficient. In addition, plots of the maximum considered earthquake ( $MCE_R$ ) Response Spectrum and Design Response Spectrum are generated using data from the USGA Seismic Design Maps based on ASCE/SEI 7-16. Finally, this section includes maps of peak ground acceleration as well as spectral acceleration at 0.2 and 1.0 seconds. The maps are based on a two percent probability of exceedance in 50 years.
- *Sensor Description* – A general description of the sensors installed on the structure is provided, including the type and quantity.

- *Sensor Layout* – An engineering schematic of the structure is provided detailing the location of each sensor on the bridge.
- *Sensor Table* – A table of all installed sensors provides the facility ID, network ID, channel ID, and location ID.
- *Peak Relative Acceleration Table* – A table is provided that includes the peak acceleration, ratio of peak acceleration to peak ground acceleration and sensor ID for all three axes.
- *Peak Relative Velocity Table* – A table is provided that includes the peak velocity, ratio of peak velocity to peak ground velocity and sensor ID for all three axes.
- *Acceleration Waveforms* – The acceleration waveforms are plotted for all three axes for each sensor.
- *Velocity Waveforms* – The velocity waveforms are plotted for all three axes for each sensor.
- *Resultant Ground Acceleration, Velocity & Displacement Plots* – To visualize the polarization of the ground motion, hodograph diagrams of the horizontal components are plotted.
- *5%-damped Pseudo-acceleration & Displacement Response Spectra Plots* – Seismic demand is represented in the form of pseudo acceleration response spectrum and acceleration displacement response spectrum (ADRS) with 5% damping. Spectral periods are indicated by red dashed lines in the ADRS plot.
- *Acceleration Waveform & Spectrogram Plots* – A visual representation of the spectrum frequencies of acceleration as varied through time are provided. The plots provide a visual of how the energy level changes during an event.
- *Fourier Amplitude and Power Spectrum Density Plots* – Frequency content of the ground motion are shown in plots of each direction.
- *Horizontal-to-vertical Spectral Ratio Plots* – Plots are provided to identify predominant periods, which are marked with circles in the plot.
- *Spectral Ratio Time Variation* – Time variation of the spectral ratios are plotted for the first three predominant periods identified on normalized Fourier amplitude spectra of differential motions in north-south and east-west directions.

- *Abbreviation List* – Relevant abbreviations throughout the report are provided for convenience.
- *Legal Disclaimer* – The report is provided ‘as-is’ without warranties of any kind. The report does not serve as a replacement for sound engineering judgment of a professional engineer. The information in the report has been generated from a limited number of sensors installed throughout the bridge. As such, the contents are for informational purposes only.
- *Dashboard Sign-in* – A copy of the report and corresponding data are provided at the online dashboard. The sign-in provides a direct link to this information.

#### 4.4 Galena Creek Bridge Trigger Threshold Values

The Galena Creek Bridge SHM systems have predefined trigger thresholds. When exceeded, the systems will record the event, process the data, and send a notification to NDOT personnel. The preliminary trigger thresholds have been set in the systems as defined in Table 4-1. In addition, the systems trigger when a 4.0-magnitude earthquake occurs within a 200 km (124 mi) radius of the site.

**Table 4-1: Preliminary Galena Creek Bridge trigger threshold values**

Parameter Monitored	Location	Threshold Value	Unit
Acceleration North - South	Abutment	0.50%	g
Acceleration East - West	Abutment	0.50%	g
Acceleration Up - Down	Abutment	0.25%	g
Drift	Deck	0.50%	-
Displacement	Joints	2.00	cm
Tilt	Piers	2.50	degree
Acceleration North - South	Bottom of piers	0.50%	g
Acceleration North - South	Bottom of piers	0.50%	g
Acceleration East - West	Bottom of piers	0.25%	g

The trigger threshold values can be easily adapted to meet the specific needs of NDOT. Multiple delays were encountered throughout the project due to a variety of factors, including access limited to entry via the UBIT, scheduling challenges, supplier delays, and COVID restrictions. In addition, controlled load tests using the UBIT and/or loaded dump trucks were not performed because the approach would not have generated the required response to evaluate the system and refine trigger threshold values (i.e., seismic loading versus traffic loading). While the functionality of both the seismic and exploratory systems were confirmed, due to project time lost for the aforementioned reasons, long-term data was unable to be collected. As such, trigger threshold values for the systems were not refined beyond the levels described. Establishing site-dependent as well as structure specific threshold values for a critical seismic event requires sufficient historical data to reliably update/determine the threshold values for the bridge beyond consideration of the seismic hazard description. It is recommended that NDOT continues to collect data until it is found that sufficient data with triggered seismic events is obtained to further refine the threshold values beyond the values set by this research based on the seismic hazard description investigation

## CHAPTER 5. CONTROL FEA MODEL DEVELOPMENT

### 5.1 Background

Computers and Structures, Inc. (CSI) is a California-based software company that produces structural and earthquake engineering software. Their flagship finite element analysis (FEA) software, SAP2000, accommodates a wide range of structural engineering applications, from bridges and buildings to dams and communication towers. The versatility of SAP2000 is due, in part, to the array of tools offered to model structures. Link, shell, frame, and user-defined elements can be assembled in countless ways to suit general structural engineering needs. Although SAP2000 is a capable FEA modeling software for bridge engineering, CSI offers CSiBridge as a more specialized instrument for bridge applications. CSiBridge includes features such as prestressing, hinge and bearing properties, vehicular live loads, and staged construction analysis, thereby making it a suitable choice for the Galena Creek Bridge analysis. Figure 5-1 is an example of the preliminary control FEA model of the Galena Creek Bridge created in CSiBridge v22.1.0.

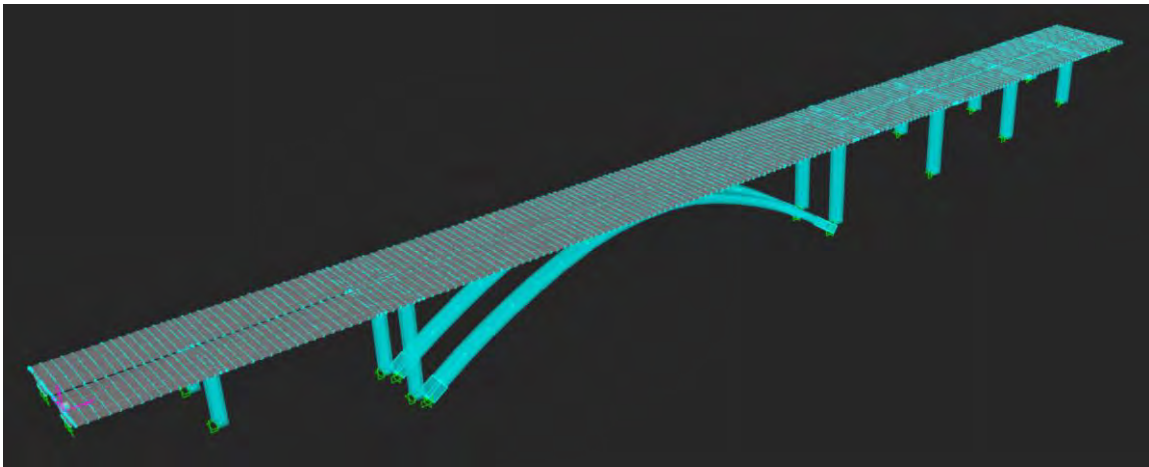


**Figure 5-1: Preliminary control model**

The following sections provide a detailed description of the development of the Galena Creek Bridge control model. Each section is written in the form of a modeling guide to allow future readers the ability to follow the development process and recreate the model. Some structural details for the Galena Creek Bridge will be referenced to the structure description found in Chapter 2 of the report. CSiBridge includes a “Bridge Wizard” feature to guide the user through each input



required to create a functional bridge model. The feature can provide time savings, especially for routine structures. However, the Bridge Wizard was not employed to model the Galena Creek Bridge due to the structure complexity. A manual approach was selected to enable a better understanding of how input parameters influenced the model response and resulting output. Furthermore, the selected approach will more readily facilitate model refinement as field-measured data is collected and used to refine the initial model.

## **5.2 Layout Tab**

The Layout tab is where the global coordinate system is defined, thereby setting the basic orientation of the bridge. The global x-axis was in the longitudinal direction, the y-axis denotes the transverse direction, and the z-axis represents the vertical direction. CSiBridge utilizes a user-defined layout line as the template upon which the bridge is modeled. For live load analyses, vehicle lanes can also be defined in the Layout tab which are then applied as two-dimensional surfaces along the top slab of the bridge.

The primary units for force, length, and temperature are defined in the Layout tab. The Galena Creek Bridge was designed using the metric system; therefore, the model employed units of kilonewtons (kN) for force, meters (m) for length, and Celsius (°C) for temperature.

The first step of the modeling procedure was to define layout lines which serve as the reference upon which the structure is built. For the Galena Creek Bridge, layout lines for both the northbound and southbound structures had an initial bearing of N90E, an initial grade of -1.25% in the longitudinal direction, and an end station of 525 m. Span 1 of the southbound bridge was built on a horizontal curve with a 730 m radius (Figure 5-2). The radius was assumed to be sufficiently large such that it could be ignored for the modeling process; as such, the layout lines for both structures were modeled as completely straight. The centerlines of the northbound and southbound structures are 20.92 m apart for the entire length of the bridge, with the exception of the horizontal curve at Span 1. As such, initial stations for the northbound and southbound structures were defined as (0,0,0) and (0,20.92,0), respectively. Figure 5-3 is an example of the layout line inputs for the southbound bridge. Lanes were not defined during this part of the modeling procedure because live loads were assumed to have a negligible impact on the seismic response of the bridge;

however, lane assignments could be added in the future to evaluate the response of routine traffic loading.

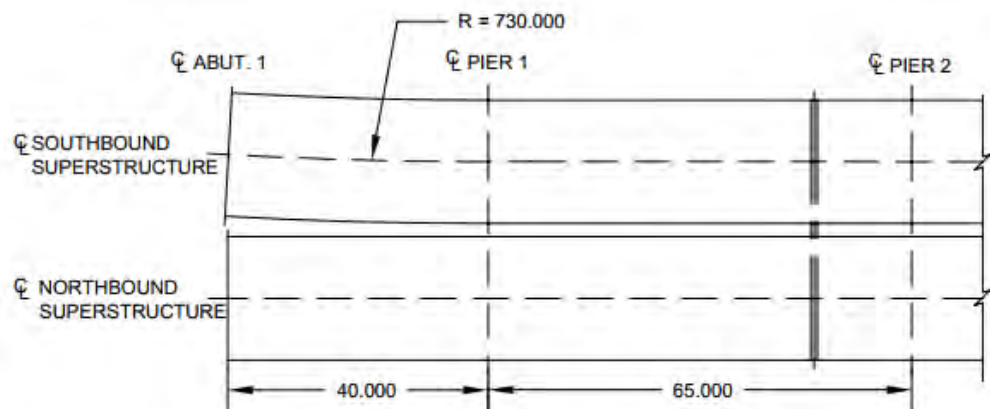


**Figure 5-2: Horizontal curvature of Span 1 (southbound superstructure)**

The screenshot shows the 'Bridge Layout Line Data' dialog box. The 'Bridge Layout Line Name' is 'SB Layout Line'. The 'Coordinate System' is 'GLOBAL'. The 'Units' are 'KN, m, C'. The 'Shift Layout Line' button is 'Modify Layout Line Stations...'. The 'Coordinates of Initial Station' are: Global X: 0., Global Y: 20.92, Global Z: 0. The 'Initial and End Station Data' are: Initial Station (m): 0., Initial Bearing: N900000E, Initial Grade in Percent: -1.25, End Station (m): 525. The 'Horizontal Layout Data' section has buttons 'Define Horizontal Layout Data...' and 'Quick Start...'. The 'Define Layout Data' section has buttons 'Define Vertical Layout Data...' and 'Quick Start...'. The 'OK' and 'Cancel' buttons are at the bottom.

**Figure 5-3: Example layout line input for CSiBridge (southbound superstructure)**

### 5.3 Components Tab

Individual structural components behave in tandem, thereby creating a system-level response. The Components tab in CSiBridge is used to define initial pieces, such as materials, member cross sections, and hinge properties, before being assigned to the global bridge object. The various definitions are organized into three sections and further divided by drop down menus (Figure 5-4). Each menu applicable to the Galena Creek Bridge is discussed in the following subsections. The subsections are organized in the order that they are presented to the user in CSiBridge when inputting initial structure definitions.

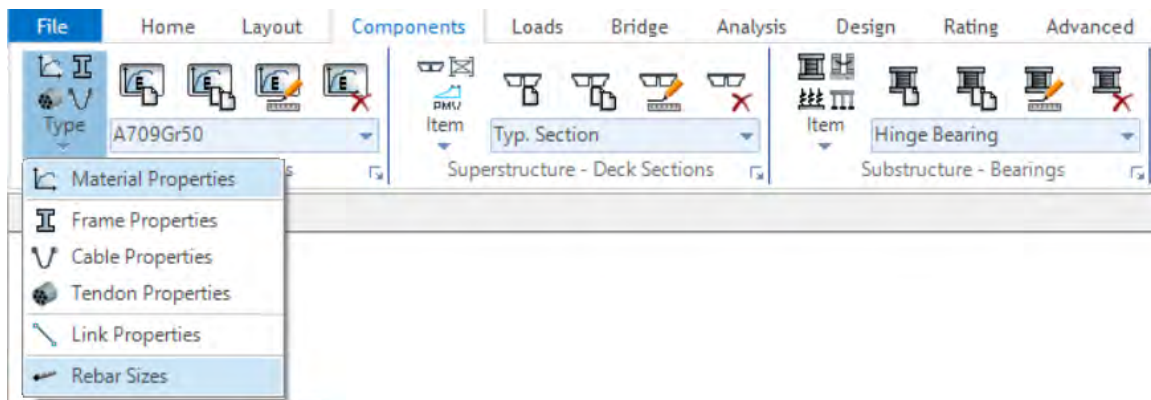


**Figure 5-4: Example of sections found in the CSiBridge Components tab**

### 5.3.1 Materials

Several concrete compressive strengths were used throughout the Galena Creek Bridge, as denoted in the design plans on sheet BG-228. Concrete strengths of 28 MPa, 31 MPa, and 35 MPa were defined for the model. The density for all concrete was defined as 23.56 KN/m<sup>3</sup> (150 lbf/ft<sup>3</sup>), while the modulus of elasticity was calculated using Equation 5.1 from ACI 318-21M Equation 19.2.2.1.b, where  $f'_c$  is in MPa (ACI, 2019).

$$E_c = 4,700 \times \sqrt{f'_c}$$

**Equation 5.1: Modulus of elasticity of concrete (ACI, 2021)**

Some elements of the Galena Creek Bridge were built using a combination of concrete strengths. Specifically, 40 MPa concrete was used in Frame 2 for the bottom slab and webs of the box girder over Piers 2 and 3, while 31 MPa concrete was used for the top slab and pier diaphragms.

CSiBridge does not permit multiple material properties to be assigned to a single superstructure cross section, nor does it allow material properties to vary along the span. Thus, it was conservatively assumed that the superstructure consisted of 31 MPa concrete throughout. As demonstrated by Equation 5.1, the elastic modulus of concrete is a function of the compressive strength, thereby influencing the stiffness and dynamic properties.

The Galena Creek Bridge used A706 Grade 50 steel for the traditional reinforcing bars. While CSiBridge can include reinforcing steel in models, the reinforcing was omitted because it did not influence on the modal properties or dynamic behavior of the structure. Prestressing tendons for the Galena Creek Bridge were A416 Grade 270 steel with a coefficient of friction of 0.2 and a wobble factor of 0.00066/m. The jacking force and projected losses for each set of prestressing tendons are displayed in Table 2-3. Note that the prestressing information was not input during the Components tab portion of the modeling procedure, rather it was later included when defining the bridge object spans.

### *5.3.2 Frame Properties*

Two methods were used to define frame sections. Solid members, such as the link beam and arch diaphragm, were defined using the conventional option of generating a new rectangular concrete section (Figure 5-5). The required input included the member depth, width, and material. Reinforcement details and material property modifiers, while not required, could be included when defining the section. The link beams and arch diaphragms had dimensions of 6.0 m x 4.0 m and 6.0 m x 3.6 m, respectively. The material for the arch diaphragm was 35 MPa concrete and the material for the link beam was 28 MPa concrete.

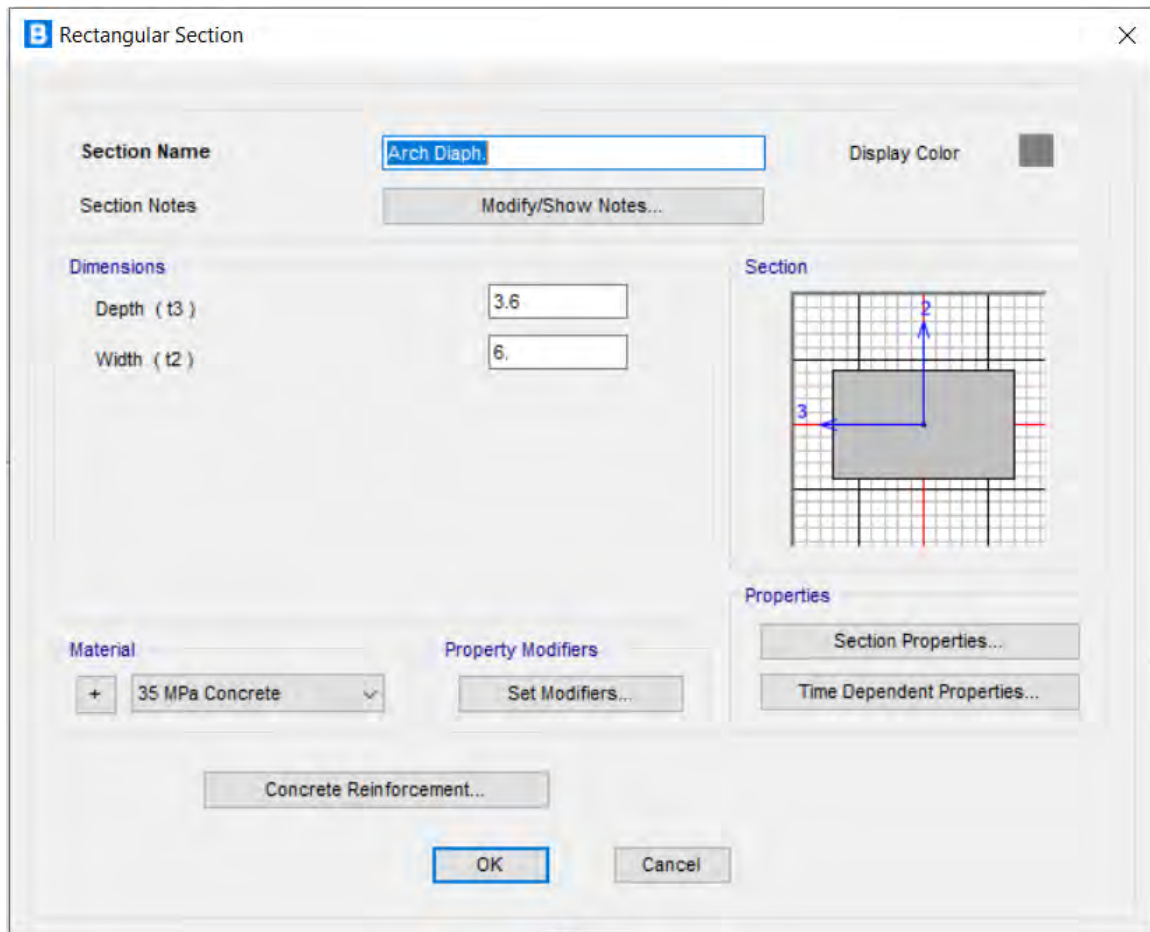


**Figure 5-5: Example solid rectangular section input for arch diagram**

The second approach was to create a unique section using the Section Designer tool (Figure 5-6). The self-weight of the Galena Creek Bridge was manually calculated to verify the total dead load. The hollow pier and arch sections were defined using Section Designer. The perimeters of the pier column and arch sections were drawn using the “draw solid shape” tool, while the interior perimeters were created with the “draw polygon shape” tool. The “resaper” tool was used to define the coordinates for the interior perimeter to incorporate the interior chamfers. Changing the material property of the interior shape to “OPENING” generated the box section void. The outside perimeter was drawn using the “draw solid shape” tool and was assigned the material property of the section.

The material for the arch was 35 MPa concrete and the material for the pier column was 28 MPa concrete. The typical pier column had exterior dimensions of 6.0 m x 3.0 m, interior dimensions of 4.0 m x 1.8 m, and interior chamfers of 0.15 m. The typical arch cross section had exterior

dimensions of 6.0 m x 3.6 m, interior dimensions of 5.2 m x 2.8 m, and interior chamfers of 0.15 m.

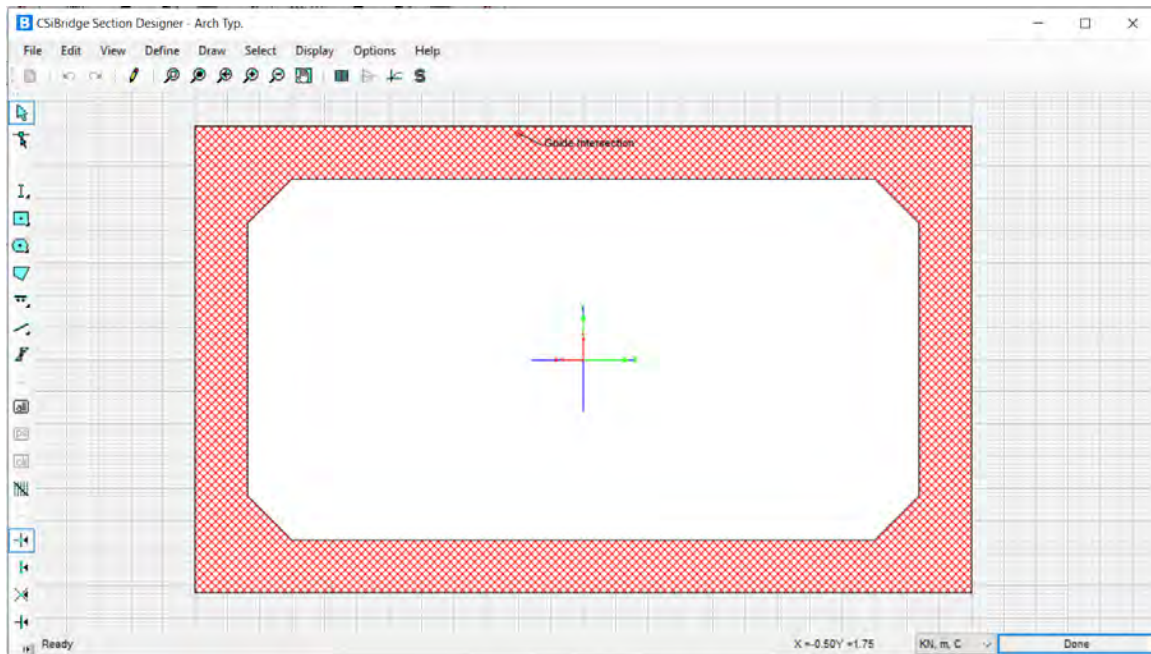


**Figure 5-6: Example Section Designer tool for typical arch frame**

### 5.3.3 Link Properties

Link objects are one-dimensional elements which can be assign specialized properties, such as simulating linear, nonlinear, and even frequency-dependent behavior. Link elements provided a means to connect sections of the Galena Creek Bridge that were difficult to model using frame or shell elements; namely, the fillet merge between the superstructure and the arch. The link elements provided a rigid connection between the two joints without adding additional dead load found in frame elements. The ends were defined as completely fixed and the link was not assigned a mass or force. It should be noted that link elements are a modeling feature and are not to be confused with the link beams, which are part of the Galena Creek Bridge substructure.

### 5.3.4 Deck Sections

CSiBridge offers several preset options for defining the superstructure. The “Ext. Girders Sloped” template was the best selection to model the concrete box girder of the Galena Creek Bridge. The typical superstructure cross section was defined using sheet BG-176 of the design plans (Figure

2-3). The values in Table 5-1 correspond with the inputs required by the CSiBridge diagram (Figure 5-7). The base material of the deck section was set as 31 MPa concrete.

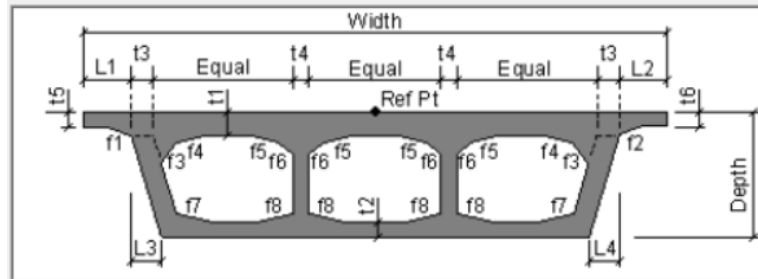


**Figure 5-7: CSiBridge template for box girder inputs**

The weight of the future wearing surface and barrier rails were manually calculated and applied as an area load and line load, respectively, in the Deck Section Definition. The barrier rail line load was calculated as 6.50 kN/m by multiplying the density of concrete ( $23.56 \text{ kN/m}^3$ ) by the barrier cross-sectional area ( $0.28 \text{ m}^2$ ). The FWS area load of  $1.80 \text{ kN/m}^2$  was calculated by assuming an average thickness of 76 mm and a wearing surface density of  $23.56 \text{ kN/m}^3$ . The 2.0% transverse superelevation was assumed to have a negligible impact on the stiffness of the bridge and was not included in the inputs. The bottom slab of the superstructure increases in thickness over the piers. The depth of the girder increases between the fillet diaphragms where the arch meets the superstructure. These variations in deck geometry along the length of the bridge are addressed in the upcoming Parametric Variations section.

**Table 5-1: Inputs for box girder definition for CSiBridge (m)**

Number of Interior Girders	1
Total Width	18.9
Total Depth	3
Left Exterior Girder Bottom Offset (L3)	2.36
Right Exterior Girder Bottom Offset (L4)	2.36
<b>Slab and Girder Thickness</b>	
Top Slab Thickness (t1)	0.2
Bottom Slab Thickness (t2)	0.2
Exterior Girder Thickness (t3)	0.325
Interior Girder Thickness (t4)	0.325
<b>Fillet Horizontal Dimension Data</b>	
f1 Horizontal Dimension	1.8
f2 Horizontal Dimension	1.8
f3 Horizontal Dimension	0.1
f4 Horizontal Dimension	1.2
f5 Horizontal Dimension	1.2
f6 Horizontal Dimension	0
f7 Horizontal Dimension	0
f8 Horizontal Dimension	0
<b>Fillet Vertical Dimension Data</b>	
f1 Vertical Dimension	0.175
f2 Vertical Dimension	0.175
f3 Vertical Dimension	0.1
f4 Vertical Dimension	0.175
f5 Vertical Dimension	0.125
f6 Vertical Dimension	0
f7 Vertical Dimension	0
f8 Vertical Dimension	0
<b>Left Overhang Data</b>	
Left Overhang Length (L1)	3.59
Left Overhang Outer Thickness (t5)	0.2
<b>Right Overhang Data</b>	
Right Overhang Length (L2)	3.59
Right Overhang Outer Thickness (t6)	0.2



### 5.3.5 Diaphragms

Interior diaphragms of varying thicknesses were located throughout the superstructure (Table 2-4). Abutment diaphragms are flush with the ends of the superstructure at Spans 1 and 7. An intermediate diaphragm is located near the midspan of all spans, with the exception of Span 3. Span 3 contains two intermediate diaphragms located 40 m from each pier, providing support between the piers and the crown of the arch. The fillets that merge the arch and box girder are marked by a fillet diaphragm and the crown of the arch has two crown diaphragms spaced 13.5 m apart. All diaphragms were modeled using the 31 MPa concrete material used for the superstructure and considered to be solid along the full depth of the girder, regardless of the access holes.

Hinges, located in Spans 2 and 4, divide the Galena Creek Bridge into three frames. The hinges consist of an overhang and suspended cantilever connected by an elastomeric bearing. The hinge was modeled as a single point at the centerline of the elastomeric bearing, 15 m from the centerline of the nearest pier. The diaphragm thicknesses for each portion of the hinge were measured from the centerline of the bearing to the face of the diaphragm (Figure 2-12).

### 5.3.6 Parametric Variations

The bottom slab thickness increases linearly over the piers and between the fillet diaphragms, where the superstructure connects to the arch. The bottom slab extrudes inwards at the piers so that the total girder depth does not change. The bottom slab variations are defined in Figure 2-6 and Table 2-2. The bottom slab thickness was assumed uniform along the 1.8 m depth of the pier diaphragms.

The girder depth increases from 3.0 m to 3.6 m over 8.0 m between the fillet diaphragms in Span 3 (

Table 2-7). Changes in the deck section were defined in CSiBridge for individual spans. The length of the variations was in relation to the start of the respective span, as seen in Figure 5-8. Span 3 required two separate parametric variations to denote the soffit thickness increase as well as the girder depth change.

**Variation Definition**

Variation Name:  Units:

**Variation Definition**

Point ID	Segment Type and Point Type Segment Is From Point(n - 1) to Point(n)	Distance m	Dim. Change m	Slope m / m
1		0.	0.2	
2	Start of Variation	0.	0.2	
3	Linear	1.8	0.2	
4	Linear	5.8	0.	
5	Linear	52.2	0.	
6	Linear	56.2	0.2	
7	Linear to End of Variation	58.	0.2	

**Variation Sketch** ☐ Use Equal Horizontal And Vertical Scales In Sketch

**Dimension Change Sign**  
Switch Sign of All Dim. Change

Distance:  Dim. Change:  Slope:

OK Cancel

**Figure 5-8: Example of linear variation input in CSiBridge (Span 5)**

### 5.3.7 Bearings

A set of three elastomeric bearings are located at each abutment and hinge of the Galena Creek Bridge. Elastomeric bearings were independently defined for the abutment and hinge (Table 5-2). It was assumed the elastomeric bearings were under large compressive forces; as such, rotation about the longitudinal and transverse axes as well as the translation along the z-axis were negligible. The lateral, vertical, and rotational stiffness properties were calculated as a function of the bearing dimensions using Equations 5.2 – 5.4, respectively (Akogul and Celik, 2008). Bearing dimensions were presented in sheets BG-238 and BG-239 of the design plans.

Bearing property definitions were also required when defining the substructure to superstructure connection. The concrete columns extrude into the girder and act as diaphragms; therefore, it was assumed that the connection between the column and superstructure was rigid. A fully-fixed mock bearing was defined to reflect the integral connection between the piers and the superstructure.

$$K_H: \frac{G * A}{H_r}$$

**Equation 5.2: Elastomeric bearing lateral stiffness**

$$K_V: \frac{E * A}{H_r}$$

**Equation 5.3: Elastomeric bearing vertical stiffness**

$$K_\theta: \frac{E * I}{H_r}$$

**Equation 5.4: Elastomeric bearing rotational stiffness**

**Table 5-2: Calculated stiffness values for elastomeric bearings**

<b>Bearing Location</b>	<b><math>K_H</math> (kN/m)</b>	<b><math>K_V</math> (kN/m)</b>	<b><math>K_\theta</math> (kN×m)</b>
Abutment	4,215	17,500	597.2
Hinge	2,208	9,167	385.1

**5.3.8 Foundations**

Foundations for the Galena Creek Bridge include footings anchored by cast-in-place piles and thrust blocks anchored by steel tiedowns. The footings, located at the base of piers 1, 4, 5, and 6, are each rooted by 12 cast-in-drilled-hole piles. The 1.22 m diameter holes were drilled to bedrock, ranging from 6.1 m to 15.1 m deep. The thrust blocks for Piers 2 and 3 are cast directly into the rock face of the slope below the structure. The base of each thrust block is anchored to the bedrock using 12 tiedowns. Due to the robust connection between the footings and bedrock, it was assumed that the footings were fixed with the ground and not modeled. Fully-fixed foundation springs were assigned at the base of each pier column to represent this assumption.

**5.3.9 Abutments**

The abutments at the end of the Galena Creek Bridge are perpendicular to the centerline of the bridge. The superstructure of the Galena Creek Bridge rests on elastomeric bearings at the abutments with shear keys restricting translation in the transverse direction. As there are no unique

defining properties of the abutments that would influence the dynamic properties of the FEA model, only a single typical abutment was defined. The typical abutment was connected to the bottom of the girder as opposed to being integral, thereby simulating the behavior of the elastomeric bearing pads. The abutments are assigned to the bridge objects later in the modeling procedure.

#### 5.3.10 Bents

The superstructure of the Galena Creek Bridge is supported by 12 pier columns of varying heights (Table 2-5). The columns extend into the structure and act as pier diaphragms. The rectangular columns are oriented to resist transverse bending. Column heights were determined by calculating the difference in elevation between the bottom of the superstructure and the top of the footing at the centerline of each pier. The heights for the northbound and southbound superstructure varied due to local topography, with the northbound structure typically having longer heights. The boundary conditions at both the base and top of the column were defined as fully fixed. The top of each pier column of the Galena Creek Bridge includes a bent; however, a cap beam section was not explicitly modeled because the columns extend into the superstructure, forming a direct connection. This connection was modeled as fully integral with the box girder.

## 5.4 Loads Tab

The Loads tab is used to define the various forces and conditions that is applied to the structure during analyses (Figure 5-9). Live load vehicles, time-history loadings, and response spectrum are some of the loads that can be defined. Vehicle lanes and truck live loads were not defined because routine traffic live loads were assumed to have a negligible impact on the dynamic response of the Galena Creek Bridge.

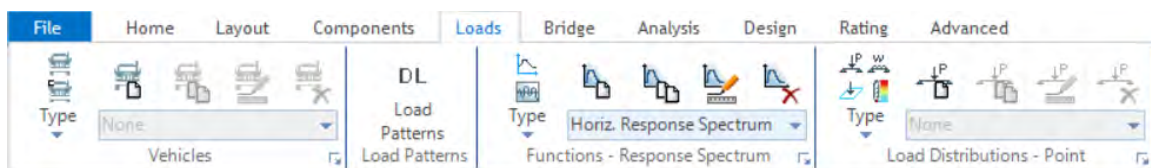


**Figure 5-9: Loads tab as seen in CSiBridge**

Ground motion accelerations were input as time-history loads to CSiBridge by importing two-column .txt files. The left column of the text is the time, in seconds, for each set of data. The right column of text denotes the excitation at the adjacent timestamp. The excitation can be in the form of either a force or an acceleration as long as the units are consistent throughout. Importing time-history data using this method only notes the numerical values for the applied accelerations; units are not assigned until defining the load combinations under the Analysis tab. The primary models were created prior to the complete installation of the SHM system; therefore, the dynamic response of the models was preliminarily evaluated using ground motion accelerations recorded during a magnitude 6.9 earthquake that occurred in El Centro, California in 1940. High intensity ground motions were selected to emulate an extreme event experienced by structures near the area of the Galena Creek Bridge. Ground accelerations in the north-south (global X-axis), east-west (global Y-axis), and vertical (global Z-axis) directions were imported.

It should be noted that the barrier rail and FWS loads were input during the deck section definition. Reviewing the “Loads Distribution” dropdown menu revealed the line loads and area loads for the barrier and FWS, respectively, were automatically populated. The autogenerated inputs were dictated by the deck section values. Manual edits to the auto filled values are reverted when updating the model. This is only applicable to barrier rail and FWS loads, and by proxy, the sidewalk load. CSiBridge does not automatically edit values for additional point, line, or area loads applied outside of the deck definition.

## **5.5 Bridge Tab**

CSiBridge refers to the FEA model under consideration as the “bridge object.” The Bridge tab provides a platform to assign the components defined into a bridge object to be used for analyses. The primary difference between the northbound and southbound bridges was the height of the columns. For modeling efficiency and accuracy, a single superstructure model (i.e., northbound) was generated and copied about the southbound layout line. The southbound structure was then modified by assigning the appropriate pier definitions.

### *5.5.1 Bridge Object Data*

The first step of modeling the bridge object is to define the spans within the length of the structure. Spans can be defined either by station length or span length, which are demonstrated in Table 5-3. As there is no definitive advantage of one method over the other, the spans were input using span length. The spans of the Galena Creek Bridge are defined from south to north; Station 0 coincides with the centerline of the south abutment.

**Table 5-3: Galena Creek Bridge span lengths and station locations**

	<b>Span 1 (m)</b>	<b>Span 2 (m)</b>	<b>Span 3 (m)</b>	<b>Span 4 (m)</b>	<b>Span 5 (m)</b>	<b>Span 6 (m)</b>	<b>Span 7 (m)</b>
Span Length	40	65	210	68	58	48	36
Start Station	0	40	105	315	383	441	489
End Station	40	105	315	383	441	489	525

### 5.5.2 *Spans*

The purpose of the “Spans” definition is to input any parametric variations of the superstructure along a span. The linear variations, previously defined in the Components tab, are applied to the bottom slab thickness, as demonstrated in Figure 5-10. Superstructure variations were assigned to the respective spans, with Span 3 requiring two inputs for the bottom slab and box girder depth. “The Show Section Variation” option was used to visually confirm the correct superstructure variations were assigned at locations with geometric changes (Figure 5-11).

**Bridge Section Variation Definition**

Bridge Object Name: NB Structure  
Span Label: Span 3  
Base Bridge Section Property: Typ. Section

Bridge Section Variation Is Defined By:  
☒ User Definition Define/Show Variations...  
☐ Reference to Another Span

Display Section  
Show Base Section...  
Show Section Variation...

User Defined Variation For Concrete Box Girder - Sloped  
☒ Distance Measured from Start of Span ☐ Distance Measured from Start Abutment

Parameter	Variation
<b>General Data</b>	
Total Width	Constant
Total Depth	Span 3 Depth Change
Left Exterior Girder Bottom Offset (L3)	Constant Girder Slope
Right Exterior Girder Bottom Offset (L4)	Constant Girder Slope
<b>Slab and Girder Thickness</b>	
Top Slab Thickness (t1)	Constant
Bottom Slab Thickness (t2)	Span 3 Bot. Slab Var. ▾
Exterior Girder Thickness (t3)	Constant
Interior Girder Thickness (t4)	Constant
<b>Fillet Horizontal Dimension Data</b>	
f1 Horizontal Dimension	Constant
f2 Horizontal Dimension	Constant
f3 Horizontal Dimension	Constant

OK Cancel

Figure 5-10: Example of superstructure span variations in CSiBridge

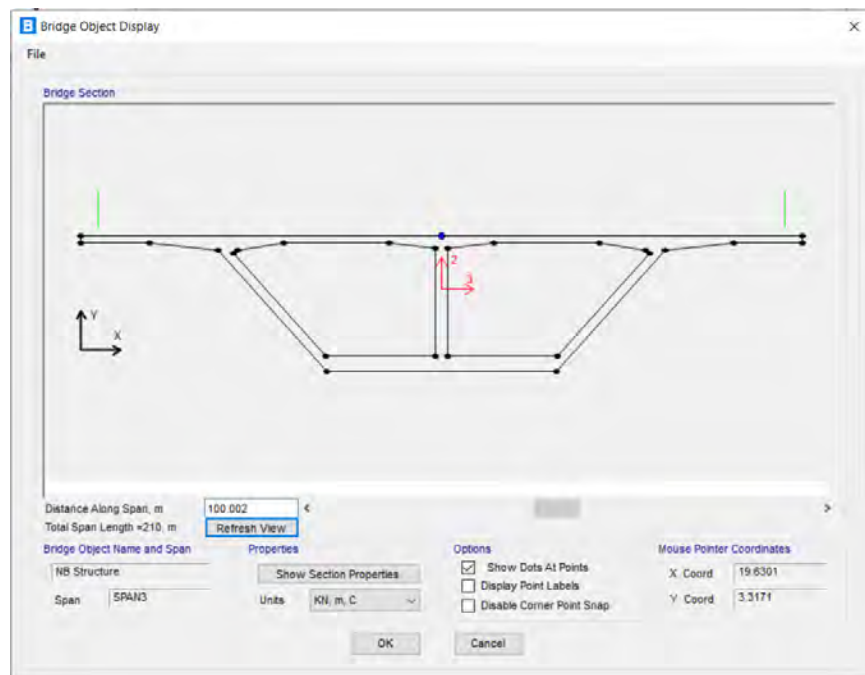


**Figure 5-11: Example of deck section variation in CsiBridge**

### 5.5.3 Abutments

The abutments followed the same numbering system as the spans: the south supports were Abutment 1, and the north supports were labeled as Abutment 2. Abutment diaphragms were denoted as flush with the end of the superstructure. The superstructure was supported at each abutment by three bearings centered about the layout line with a uniform spacing of 2.88 m. As stiffness values were assigned in the Bearing definition, no additional restrainer properties were attached to the bearings when defining the abutments. The 0.15 m joint between the superstructure and abutment seat is connected by a reinforced elastomeric bearing. This was modeled in CSiBridge by locating the abutment and bearings 0.15 m and 0.075 m below the bottom of superstructure, respectively. CSiBridge uses elevation values for the substructure with respect to the global coordinate system; therefore, the elevations had to consider the 1.25% longitudinal grade. Abutment and bearing elevations for the start abutment were -3.15 m and -3.08 m and the elevations at the end abutment were -9.86 m and -9.71 m, respectively.

Bridge Object Abutment Assignments

Bridge Object Name: NB Structure

Units: KN, m, C

Start Abutment: End Abutment

**End Abutment**

**Superstructure Assignment**

Support Name: Span 7

Abutment Direction (Bearing Angle): Default

Diaphragm Property: + Abut. Diaph.

Diaphragm Offset Location: Flush

**Substructure Assignment**

☐ None

☒ Abutment Property: + Abutment Typ.

☐ Bent Property: +

**Substructure Location**

Elevation (Global Z): -9.8625

Horizontal Offset: 0

Note: Horizontal offset is from layout line to midlength of abutment.

**Bearing Assignment**

☐ Girder-by-Girder

☒ General

Bearing Property: + Abutment Bearing

Restrainer Property at Bearing: + None

Elevation at Layout Line (Global Z): -9.7125

Rotation Angle from Bridge Default: 0

Number of Bearings for Bridge Section: 3

Uniform Spacing: 2.875

Offset from Section Ref. Point to Bearing Center: 0

**Bearing-by-Bearing Overwrites for End Abutment**

Modify/Show Overwrites... No Overwrites Exist

OK Cancel

**Figure 5-12: Typical CSiBridge input for abutments**



### 5.5.4 Bents

The pier column information, previously defined in the Components tab, was assigned at the ends of Span 1 – 6. Pier diaphragms were assigned at each bent location as well as the “mock” fixed bearing. Like the end abutment, the elevation values were based off the global z-axis (Table 5-4). Values were calculated based on the station location, accounting for the -1.25% longitudinal grade. Bent elevations were input as flush with the bottom of the 3 m deep box girder (Figure 5-13).

**Table 5-4: Bent elevation values along global z-axis**

	Pier 1 (m)	Pier 2 (m)	Pier 3 (m)	Pier 4 (m)	Pier 5 (m)	Pier 6 (m)
Bent Elevation	-3.5	-4.3125	-6.9375	-7.7875	-8.5125	-9.1125

**Figure 5-13: Typical CSiBridge input of bent information**

### 5.5.5 Hinges

Hinges divide the structure into three frames, defined based on the distance from the start of their respective span: Hinge 1 is 50 m from the start of Span 2 and Hinge 2 is 15 m from the start of Span 4. The hinges were assumed to be at half the depth of the girder (1.5 m) with global elevations of -2.63 m and -5.63 m for Hinges 1 and 2, respectively. Each hinge consists of an upper and lower cantilever connected by three elastomeric bearings (**Error! Reference source not found.**). The lower cantilever portions of the hinges are attached to Frame 2. The overhang cantilever portions are parts of Frames 1 and 3. These considerations were incorporated when assigning diaphragm definitions to either side of the hinge.

### 5.5.6 Diaphragms

Only the intermediate, fillet, and crown diaphragms were explicitly modeled. Diaphragms at the abutments, piers, and hinges were assigned during the definition of each respective component. Diaphragm locations were assigned from the start of each span, as shown in Table 5-5.

**Table 5-5: Diaphragm locations**

Location	Diaphragm Type	Distance from Start of Span (m)
Span 1	Intermediate	17.60
Span 2	Intermediate	29.00
Span 3	Intermediate	40.00
	Fillet	74.25
	Crown	98.40
	Crown	111.90
	Fillet	135.75
	Intermediate	170.00
Span 4	Intermediate	36.60
Span 5	Intermediate	29.00
Span 6	Intermediate	24.20

Span 7	Intermediate	21.00
--------	--------------	-------

### 5.5.7 Prestressing Tendons

Five sets of prestressing tendons were used to counter tensile stresses in the structure, as detailed in Table 2-3. All three frames have an internal prestressing system anchored at either the hinge diaphragm or abutment diaphragm. Additionally, Frame 2 also has external prestressing tendons at the hinge diaphragms. The effect of prestressing was assigned to the model as a force. The A416 Grade 270 steel used for the tendons was a preset material option from CSiBridge. The center of gravity of the prestressing force follows a series of parabolic curves, as denoted on sheet BG-225 of the bridge design plans. An example of a typical input for prestressing data in the model is demonstrated in Figure 5-14.

Modeling the tendons in CSiBridge was done by defining a series of nodes that follow the path of the prestressing force. Once the initial starting station was assigned, nodes alternated between “Parabola Intermediate Point” and “Parabola End Point” to define the path of the strand center of gravity. Peaks and valleys marked intermediate points, while inflection points marked parabola end nodes (Figure 5-15). The vertical offset input for each node was based on the local axis of the layout line as opposed to the global axis; therefore, the -1.25% longitudinal grade was not considered when assigning the tendon locations.

The transverse location of the prestressing force can be edited in CSiBridge. It was assumed that adjusting the horizontal layout of the strands did not have an impact on the dynamic properties of the model; thus, no modifications were performed. Similarly, transverse prestressing in the integral deck over each pier was assumed to have a negligible effect on structural behavior and was not included in the model.



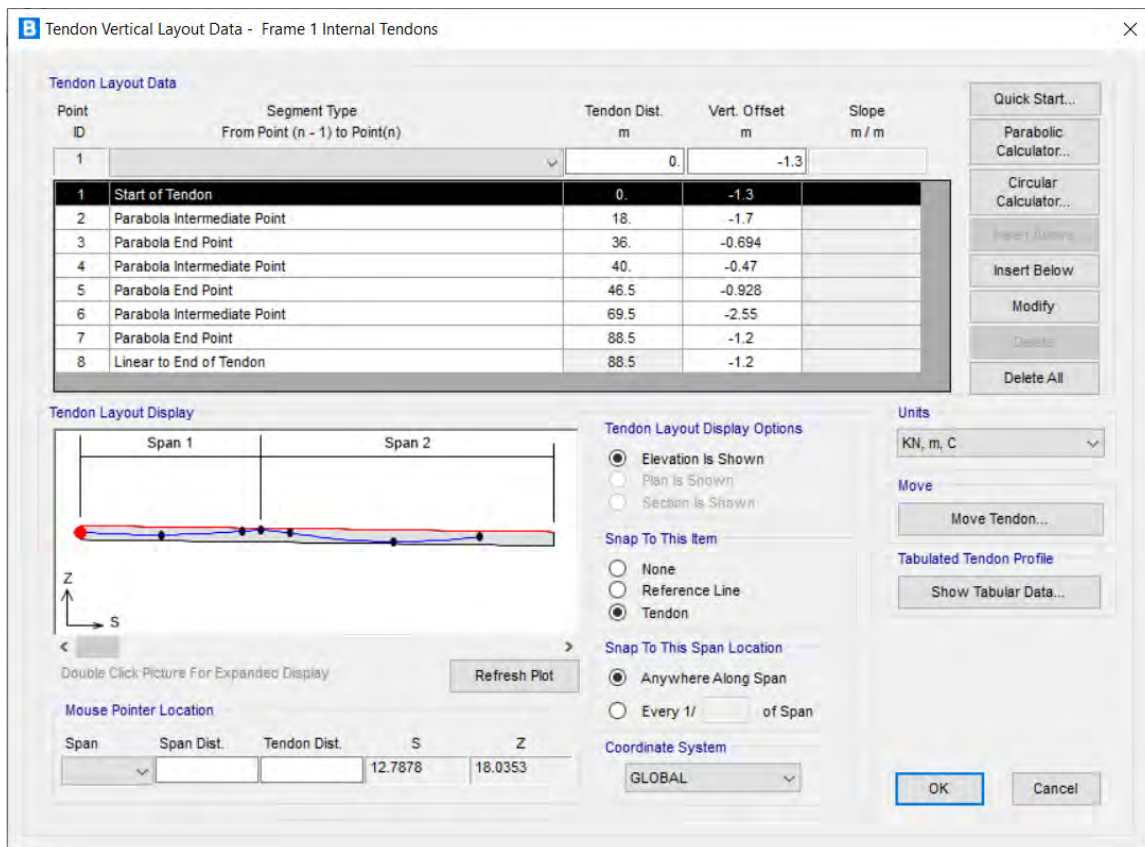


**Figure 5-15: Example of CSiBridge tendon parabolic path**

### 5.5.8 Update

Inputting components into a bridge object model does not automatically incorporate the changes. The Update feature refreshes the model and incorporates changes made to the selected bridge object. This feature is intended to reduce loading times and improve processing speed by allowing the user to dictate the refresh rate of any changes made to the bridge object. It should be noted that the Update feature only incorporates edits made to the bridge object model components and does not refresh additional modeling performed using the tools in the Advanced tab.

The Update feature offers the option to model the superstructure as either as frame, shell, or solid elements. The northbound and southbound structures of the Galena Creek Bridge were updated individually as Area Object Models to model the superstructure as a collection of 3D shell elements, as seen in Figure 5-16. Although modeling the structure as a solid object may better simulate the physical behavior than a shell model, the additional computational time did not warrant the relatively minor change in analysis results.

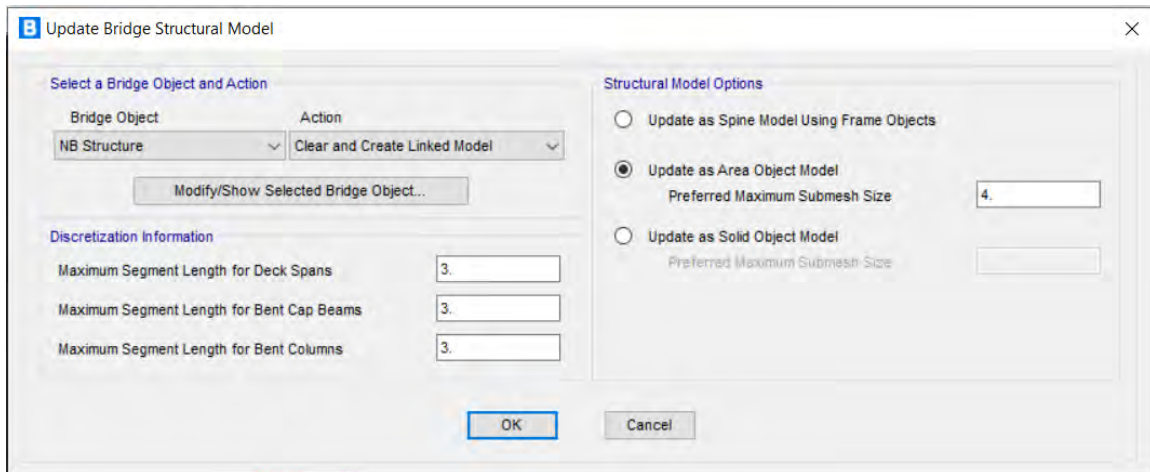


**Figure 5-16: Example of updating bridge object model in CSiBridge**

## 5.6 Advanced Tab

The Advanced tab provides an array of tools to add or edit properties not defined by the presets available in the Components tab. The bridge arch was modeled as a series of 19 frame elements following the segment geometry defined on sheets BG-10 and BG-142 of the design plans, as seen in Figure 5-17 (NDOT, 2006). The segments are labeled from south to north, starting with Segment 0. Segments north of the crown of the arch, Segment 9, continue in descending order with the additional suffix of “A” (Figure 5-17). In the model, 19 segment ends were defined by generating nodes offset along the global x- and z-axis, as shown in Table 5-6. After the template for the arch had been positioned, the joints were connected using frame elements. All of the frame elements are box sections, with the exception of Segments 0 and 0A which are solid shapes to denote the arch diaphragm (Figure 5-18).

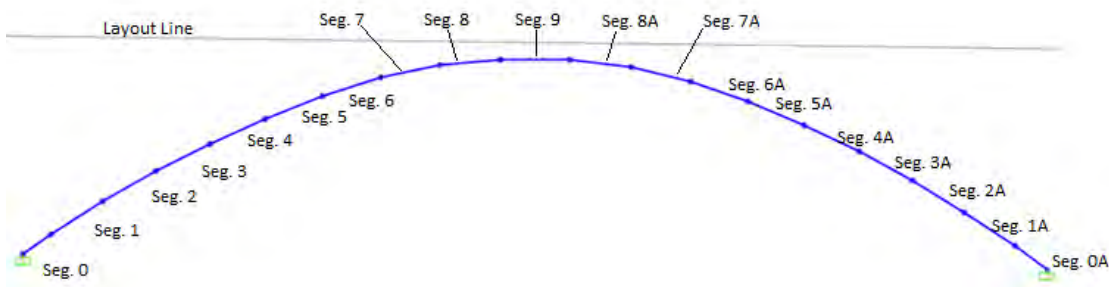


**Figure 5-17: Arch modeled as frame elements in CSiBridge with segment labels**

**Table 5-6: Segment end node offset for modeling arch**

<b>Segment Number</b>	<b>X-axis offset (m)</b>	<b>Z-axis offset (m)</b>
0	5.539	3.829
1	10.203	6.502
2	10.507	6.000
3	10.784	5.485
4	11.037	4.957
5	11.263	4.416
6	11.517	3.695
7	11.838	2.480
8	12.033	1.212
9	13.814	-0.183
8A	11.997	-1.532
7A	11.767	-2.794
6A	11.416	-4.000
5A	11.142	-4.715
4A	10.901	-5.248
3A	10.635	-5.770
2A	10.342	-6.277
1A	10.027	-6.771
0A	6.313	-4.639

As was the case for Piers 2 and 3, the arch was assumed to be fully-fixed at the connection to the thrust block. The rectangular box section of the arch is oriented to provide lateral resistance. To verify that the frame elements were correctly oriented, the arch was observed from several angles using a 3D view of the extruded members (Figure 5-18). Each frame element was visually inspected to confirm that the longer face of the rectangular section was oriented along the global y-axis.



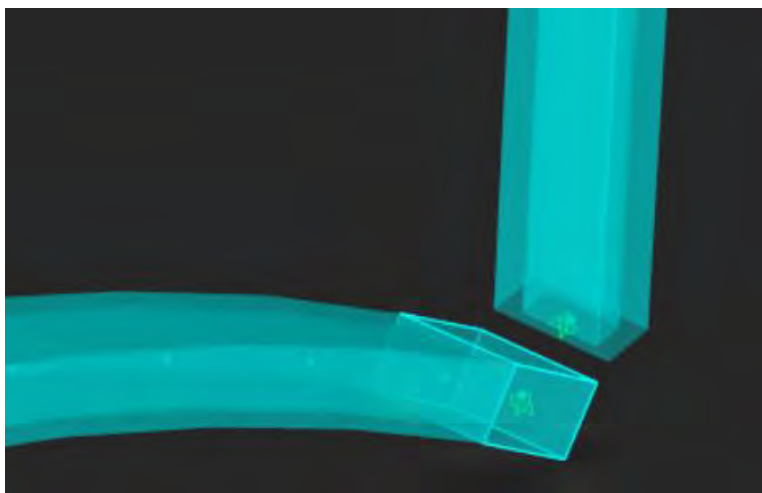


**Figure 5-18: Extrude view of CSiBridge model at base of column and pier**

The arch crown extends into the superstructure where the superstructure box girder increases in depth. CSiBridge does not have a function to join components in this manner; therefore, the merge was modeled by connecting rigid link elements from the bottom of the box girder to nodes along the arch frame elements. Figure 5-19 shows the elevation view of the arch crown where the two components merge. The three middle link elements connecting the arch to the bottom of the superstructure are not explicitly visible in the figure because they are relatively small compared to the scale of the image. The exterior-most link elements extend down from the fillet diaphragms to the arch. Modeling additional link elements had a negligible impact on the response of the structure. Increasing the number of link elements to 13 decreased modal participation factors by less than 0.2% and transverse displacement less than 0.7 mm.

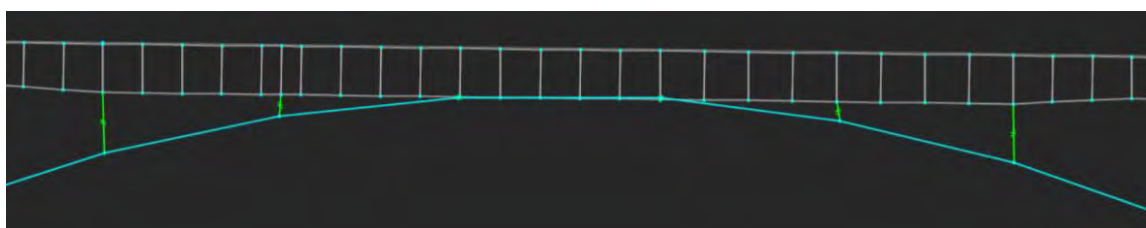


**Figure 5-19: Elevation view of the links connecting the arch and box girder in CSiBridge**

The final step before running an analysis was to define the Mass Source. The mass source specifies the elements and loads considered as a mass for modal analyses. As the linear time-history analyses use the modal results to calculate dynamic response, accurately defining the mass source is critical to achieving accurate results. The default setting for the mass source only considers the self-weight

of elements. The FWS area and barrier rail load patterns were included as masses, demonstrated in Figure 5-20, to better represent the actual mass of the bridge when performing analyses.

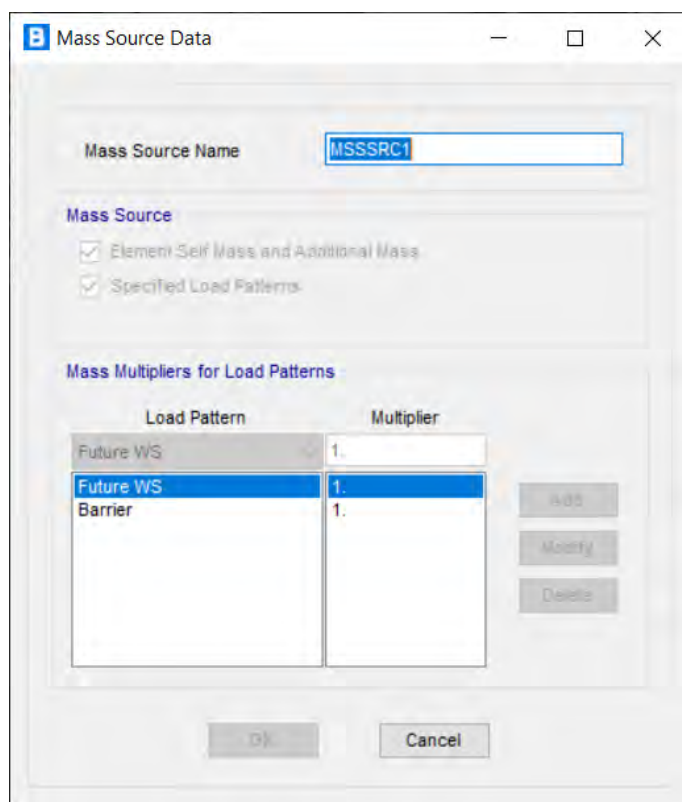


**Figure 5-20: Defining the Mass Source for CSiBridge**

## 5.7 Analysis Tab

### 5.7.1 Introduction

The results from three load cases were considered when developing the CSiBridge model. All model variants, including the control model, were subjected to a dead load, modal, and time-history analysis. The dead load case was a basic method to confirm consistency between the models. Although many factors influence the modal properties of the FEA model, the gravity loads from the structure remained constant. Excessive variations in the dead load implied a flaw in the modeling process, aiding in debugging the model and identifying errors. Modal analysis provides the dynamic properties of the bridge, based on the physical properties and layout of the structure. Comparing changes, such as modal periods and participation ratios, revealed how variations to the model influence the physical properties and subsequent dynamic behavior. The linear time-history

analysis, simulating an earthquake, shows the accelerations, displacements, and stresses experienced by the structure during an extreme event, providing a brief window into the physical response of the bridge as it is subjected to ground motions.

### 5.7.2 Dead Load Analysis

CSiBridge determines the self-weight of the structure by summing the vertical forces at all the base nodes. The dead load combination included the physical self-weight of the modeling elements, barrier rail line loads, and FWS area loads (Figure 5-21). Manual calculations for the structure dead load can be found in the Appendix C

The dead load of the structure calculated by CSiBridge was 504.2 MN. Manual calculations determined the self-weight of the Galena Creek Bridge to be 505.9 MN, a difference of 0.34%. Previous research of the Galena Creek Bridge calculated the self-weight of the structure as 499.0 MN, which yields a difference of 0.99%. The difference between both calculated values of the self-weight and the CSiBridge dead load are less than 1.0%; therefore, it is likely that all the component inputs for the Galena Creek Bridge object had been modeled sufficiently.

**Load Case Data - Linear Static**

Load Case Name:  Set Def Name Modify/Show...

Load Case Type: Static Design...

Stiffness to Use:  
☒ Zero Initial Conditions - Unstressed State  
☐ Stiffness at End of Nonlinear Case

Important Note: Loads from the Nonlinear Case are NOT included in the current case.

Analysis Type:  
☒ Linear  
☐ Nonlinear

Mass Source:

Load Type	Load Name	Scale Factor
Load Pattern	DEAD	1.
Load Pattern	Barrier	1.
Load Pattern	Future WS	1.

Add Modify Delete

OK Cancel

**Figure 5-21: CSiBridge input for Dead Load Case**

### 5.7.3 Modal Analysis

The modal response of a structure is a function of the physical properties. After a modal analysis, CSiBridge provides information on modal periods, frequencies, participation factors, and more. Changes to these parameters reveal how modifying independent variables of the model influences the physical and modal properties. Furthermore, comparing the results of the control model to previous research served as a benchmark for dynamic properties. Due to the computational efficiency of using a shell bridge object to conduct the modal analysis, up to 100 modes were reported (Figure 5-22). The initial results of the modal analysis are demonstrated in Figure 5-23.

**Load Case Data - Modal**

**Load Case Name:** MODAL **Set Def Name** **Notes** **Modify/Show...**

**Load Case Type:** Modal **Design...**

**Stiffness to Use:**  
☒ Zero Initial Conditions - Unstressed State  
☐ Stiffness at End of Nonlinear Case  
Important Note: Loads from the Nonlinear Case are NOT included in the current case

**Type of Modes:**  
☒ Eigen Vectors  
☐ Ritz Vectors

**Mass Source:** MSSSRC1

**Number of Modes:**  
Maximum Number of Modes: 100  
Minimum Number of Modes: 1

**Loads Applied:**  
☐ Show Advanced Load Parameters

**Other Parameters:**  
Frequency Shift (Center): 0.  
Cutoff Frequency (Radius): 0.  
Convergence Tolerance: 1.000E-09  
☒ Allow Automatic Frequency Shifting

**OK** **Cancel**

**Figure 5-22: CSiBridge input for modal analysis case**

	OutputCase	StepType	StepNum	Period	UX	UY	UZ	SumUX	SumUY	SumUZ	RX
		Text	Unitless	Sec	Unitless	Unitless	Unitless	Unitless	Unitless	Unitless	Unitless
▶	MODAL	Mode	1	1.739789	3.757E-07	0.52418	9.697E-08	3.757E-07	0.52418	9.697E-08	0.05456
	MODAL	Mode	2	1.342364	0.12342	3.581E-08	5.607E-05	0.12342	0.52418	5.616E-05	3.713E-09
	MODAL	Mode	3	1.214145	7.518E-06	0.00575	1.143E-07	0.12343	0.52993	5.628E-05	0.00015
	MODAL	Mode	4	1.027973	5.757E-06	0.03387	2.211E-08	0.12343	0.5638	5.63E-05	0.00996
	MODAL	Mode	5	0.976535	0.15056	1.183E-07	5.633E-05	0.274	0.5638	0.00011	3.872E-05
	MODAL	Mode	6	0.788076	2.346E-05	0.03675	1.722E-06	0.27402	0.60055	0.00011	0.02237
	MODAL	Mode	7	0.761587	0.06197	0.00047	0.00212	0.33598	0.60102	0.00223	0.00037
	MODAL	Mode	8	0.743692	0.00108	0.00047	0.00011	0.33706	0.60149	0.00234	0.005
	MODAL	Mode	9	0.717267	0.00014	0.0424	0.00145	0.33721	0.6439	0.00379	0.00015
	MODAL	Mode	10	0.711639	0.00121	0.00051	0.06836	0.33842	0.64441	0.07215	8.301E-05
	MODAL	Mode	11	0.69448	0.00039	0.02225	3.184E-06	0.33881	0.66666	0.07216	0.02321
	MODAL	Mode	12	0.669667	0.09256	2.602E-05	0.0202	0.43137	0.66669	0.09235	0.00373
	MODAL	Mode	13	0.657849	0.01171	0.00728	0.0035	0.44308	0.67397	0.09586	0.01805
	MODAL	Mode	14	0.635307	0.01183	0.00017	0.00576	0.45491	0.67414	0.10162	0.03364
	MODAL	Mode	15	0.621209	0.09588	0.00042	0.02641	0.55079	0.67455	0.12802	0.00818

**Figure 5-23: Modal analysis results of control model**

#### 5.7.4 Time-history Analysis

To evaluate the dynamic response of the CSiBridge model, it was subjected to ground motion accelerations along all three degrees of freedom. Ground motions of the 1940 magnitude 6.9 El Centro earthquake were selected to represent extreme condition for the Galena Creek Bridge. Ground motions along the longitudinal, vertical, and transverse axes were imported in the form of two-column .txt files. The left column of the file is the timestamp (sec) of the datapoint and the right column is the corresponding acceleration (g). The imported .txt file is conveyed as a function graph, as seen in Figure 5-24.

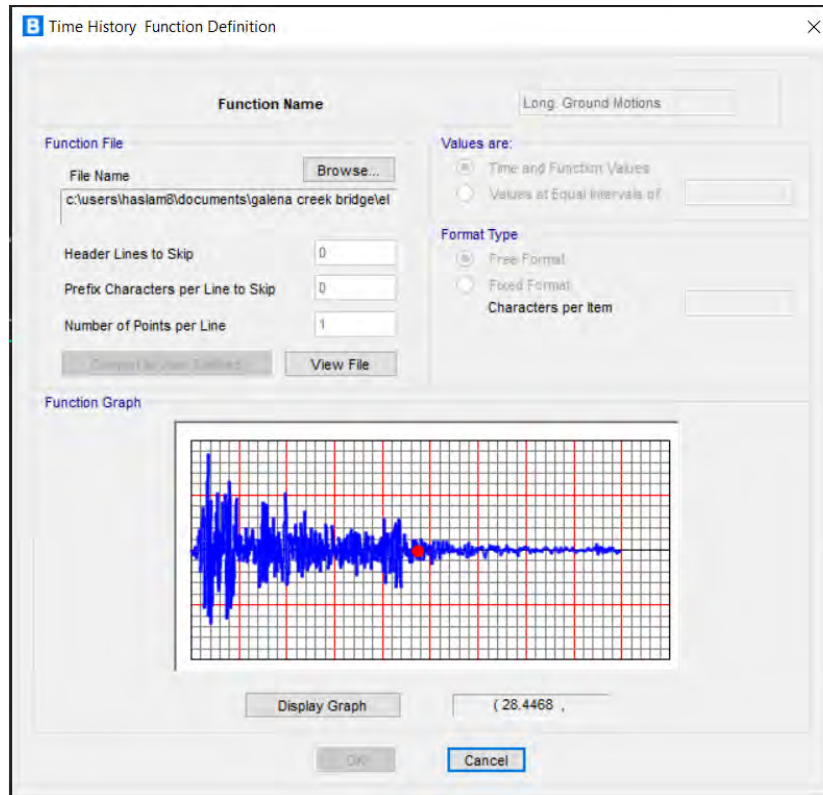


**Figure 5-24: Example of an imported ground motion from text file in CSiBridge**

The base unit for distance used for the CSiBridge model was meters; therefore, the ground motions were subject to a scale factor of 9.81 to convert from gravitation acceleration to  $\text{m/s}^2$  (Figure 5-25). Previous research on the Galena Creek Bridge emphasized the significance of using appropriate ground motions, specifically those reflective of the structure geographical location (Taylor and Sanders, 2008). While the sample ground motions used for the preliminary analyses are not directly from Walker Lane, the study aids in understanding the bridge response to extreme events. Additional information from the SHM system is needed to further refine the model to reflect the physical behavior.



**B** Load Case Data - Linear Modal History

Load Case Name: Linear Earthquake Analysis [Set Def Name] [Modify/Show...]

Initial Conditions:

- ☒ Zero Initial Conditions - Start from Unstressed State
- ☐ Continue from State at End of Modal History

Important Note: Loads from this previous case are included in the current case

Modal Load Case:

Use Modes from Case: MODAL

Loads Applied:

Load Type	Load Name	Function	Scale Factor
Accel	U1	Long. Ground	9.81
Accel	U1	Long. Ground M	9.81
Accel	U2	Trans. Ground M	9.81
Accel	U3	Vert. Ground Mo	9.81

[Add] [Modify] [Delete]

☐ Show Advanced Load Parameters

Time Step Data:

Number of Output Time Steps: 18001

Output Time Step Size: 5.000E-03

Other Parameters:

Modal Damping: None [Modify/Show...]

Load Case Type: Time History [Design...]

Analysis Type:

- ☒ Linear
- ☐ Nonlinear

History Type:

- ☒ Transient
- ☐ Periodic

Solution Type:

- ☒ Modal
- ☐ Direct Integration
- ☐ Frequency Domain

Mass Source: Previous (MSSSRC1)

[OK] [Cancel]

**Figure 5-25: CSiBridge input for time-history load case simulating an earthquake**



## **CHAPTER 6.     PARAMETRIC MODELING**

A parametric analysis was conducted to understand the behavior of the Galena Creek Bridge to variations in select parameters that are believed to influence the dynamic response. This investigation evaluated seven parameters (Table 6-1): superstructure material, material damping, elastomeric bearing stiffness, column effective moment of inertia, superstructure modeling method, link slab modeling method, and barrier rail modeling technique. Each parameter was further defined by a range of variables used to assess the influence of the given parameter. In total, 23 analyses were conducted as part of the study and a final recommended model is detailed in Chapter 7. Ultimately, the results of the parametric study will be used to validate the final model with the field-measured data from the SHM system and will be used to make any necessary model refinements.

Dead load, modal, and time-history analyses were performed on each model variant to assess changes in the structural response. Initially, the dead load analysis was used to verify that any modifications to the control model did not result in anomalous variations. Consistency of the calculated weight served as a preliminary quality control check before the results from either the modal analysis or the time-history analysis were considered. Following the dead load verification, a modal analysis was conducted to determine the natural frequencies. The top five modes about all three degrees of freedom, in terms of participation factor, were recorded and used during the subsequent analyses. Finally, a time-history analysis of each model was performed, applying the ground motion accelerations from the 6.9-magnitude El Centro earthquake. The accelerations, which were 53 seconds in duration in increments of 0.02 seconds, were applied along all three degrees of freedom. The selected seismic event was intended to represent an extreme loading case for the Galena Creek Bridge. The resulting response of both the superstructure and substructure elements were considered. Variations in displacement and internal stresses provided feedback on how each parametric variation influenced dynamic behavior.

**Table 6-1: List of parameters and respective variations**

Parameter	Superstructure Material (MPa)	Material Damping (%)	Elastomeric Bearing Stiffness, $G$ (MPa)	Column Effective Moment of Inertia, $E$	Superstructure Modeling Method	Link Slab Modeling Method	Barrier Rail Modeling Technique
Control	31	2	Pinned	$1.00I_g$	Shell	6 m max.	Line Load
Variations	36	5	0.9	$0.95I_g$	Frame Spine	3 m max.	Frame
	40	7	1.38	$0.90I_g$	Solid	12 m max.	
			Fixed	$0.85I_g$			
				$0.80I_g$			
				$0.75I_g$			
				$0.70I_g$			
				$0.65I_g$			
				$0.60I_g$			
				$0.55I_g$			
				$0.50I_g$			

## 6.1 Superstructure Material

A range of concrete strengths were used for the construction of the Galena Creek Bridge, as discussed in Chapters 2 and 5. Most components, such as the arch and the pier columns, were comprised of a single type of concrete. However, the box girder superstructure was primarily 31 MPa concrete with some sections constructed of 40 MPa concrete. Higher strength concrete was used in areas where additional strength and stiffness were required: bottom slab, web, and exterior girders of the box girder over Piers 2 and 3. The higher strength area extends 13.05 m from the centerline of the pier to the hinge diaphragm, and 16.0 meters toward the center of the arch, demonstrated by Figure 2-5. CSiBridge does not permit the user to incorporate material changes to the superstructure along the length of the bridge, nor does it provide a means to compose a composite box girder from multiple materials. As demonstrated in Equation 5.1, the Modulus of Elasticity of the concrete is calculated as a function of the compressive strength. Therefore, defining the superstructure of the control model as 31 MPa concrete would likely result in a more flexible response than the actual bridge due to the reduced stiffness.

Two model variants were created to account for the additional superstructure stiffness at these locations. The variants considered higher strength concrete for the superstructure over the entirety of Spans 2 through 4. The first variant used a weighted average approach to determine the superstructure material strength. The deck, 31 MPa material, has a cross-sectional area of 3.78 m<sup>2</sup>. The remaining box girder, including the bottom slab, web, and girders, was comprised of 40 MPa concrete and has a cross section of 4.73 m<sup>2</sup> (Figure 2-4). The weighted average approach approximates the material strength of the composite sections as 36 MPa. The second variant, considered an overstrength model, applied 40 MPa concrete to the entirety of Spans 2 through 4. The overstrength approach was intended to serve as an upper limit on the response due to increased stiffness between the design and as-built concrete strengths.

### 6.1.1 Modal Analysis – Superstructure Material

It was expected that increasing the compressive strength, and subsequently  $E$ , would yield an increase in structure stiffness. This expectation was confirmed by the result of the modal and time-history analyses.

Table 6-2 through Table 6-4 provides a comparison of the resulting periods and modal participation factors for the top five modes about all three degrees of freedom. The variant models composed of higher strength concrete demonstrated increased participation ratios and frequencies across most modes in the vertical and transverse directions. Mode 1, the primary transverse mode, was an outlier as the participation factor increased marginally from 55.0% to 55.6%, while the modal period decreased.

In contrast, the 36 MPa and 40 MPa models demonstrated higher modal participation factors about the longitudinal direction. The stiffer superstructures resisted deflections about the vertical and transverse axes. However, the increase in stiffness attracted larger stresses which were transferred to the substructure components. The rectangular box columns and arches are oriented to resist transverse loading; as such, the additional stresses carried by the substructure resulted in increased displacement about the column weak axis (i.e., longitudinal direction).

**Table 6-2: Top five modes in the longitudinal direction for superstructure material variation (X-axis)**

31 MPa Superstructure (Control Model)			36 MPa Superstructure				40 MPa Superstructure			
Mode	Period, $T_{control}$ (s)	Modal Part. Factor (%)	Mode	Period, $T$ (s)	Modal Part. Factor (%)	$T/T_{control}$	Mode	Period, $T$ (s)	Modal Part. Factor (%)	$T/T_{control}$
2	1.342	12.3	2	1.318	12.4	0.982	2	1.305	12.5	0.972
4	0.976	15.1	4	0.976	11.0	1.000	4	0.975	15.1	0.999
9	0.671	9.2	9	0.661	12.4	0.985	9	0.655	11.9	0.976
11	0.627	9.8	11	0.619	16.8	0.987	11	0.613	9.0	0.978
39	0.284	9.3	40	0.279	16.8	0.982	40	0.277	17.1	0.975

**Table 6-3: Top five modes in the transverse direction for superstructure material variation (Y-axis)**

31 MPa Superstructure (Control Model)			36 MPa Superstructure				40 MPa Superstructure			
Mode	Period, $T_{control}$ (s)	Modal Part. Factor (%)	Mode	Period, $T$ (s)	Modal Part. Factor (%)	$T/T_{control}$	Mode	Period, $T$ (s)	Modal Part. Factor (%)	$T/T_{control}$

1	1.688	55.0	1	1.669	55.4	0.989	1	1.657	55.6	0.982
5	0.819	9.5	5	0.815	9.2	0.995	5	0.812	9.0	0.991
17	0.513	7.0	17	0.511	6.6	0.997	17	0.509	4.0	0.993
24	0.386	1.9	25	0.377	1.5	0.976	16	0.515	3.7	1.333
51	0.240	1.2	36	0.3	1.2	1.250	25	0.373	1.9	1.554

**Table 6-4: Top five modes in the vertical direction for superstructure material variation (Z-axis)**

31 MPa Superstructure (Control Model)			36 MPa Superstructure				40 MPa Superstructure			
Mode	Period, $T_{control}$ (s)	Modal Part. Factor (%)	Mode	Period, $T$ (s)	Modal Part. Factor (%)	$T/T_{control}$	Mode	Period, $T$ (s)	Modal Part. Factor (%)	$T/T_{control}$
7	0.713	5.8	7	0.699	5.2	0.981	7	0.691	4.9	0.970
15	0.560	3.9	18	0.495	4.0	0.884	18	0.488	3.6	0.871
18	0.506	4.1	20	0.457	3.9	0.904	20	0.449	3.8	0.888
20	0.469	3.9	21	0.448	3.8	0.954	21	0.44	4.1	0.937
44	0.263	6.1	44	0.257	4.4	0.976	43	0.254	4.7	0.965

### 6.1.2 Time History Analysis – Superstructure Material

Displacements and internal stresses were both considered when examining the results of the time-history analysis from the El Centro earthquake ground motions. The data collected were evaluated using an envelope approach. The envelope approach considers the status of the bridge at every step of the time-history analysis and consolidates the most extreme response at each location along the length of the structure. Figure 6-1 displays the maximum absolute displacements of the superstructure in the transverse direction for the control model (31 MPa) in contrast to the 40 MPa superstructure model. The length along the structure (y-axis in the graph) is measured from Abutment 1 to Abutment 2. Figure 6-2 displays extreme longitudinal stresses experienced along the length of the superstructure.

As seen in Figure 6-1, the 40 MPa superstructure demonstrated a reduced curvature of deformation along Spans 2 through 4, suggesting that the spans modeled using stiffer materials had reduced

second-order effects. As a result, other sections of the superstructure experience increased first-order deformations. This phenomenon is best observed along the negative displacements of Spans 5 through 7 in Figure 6-1. As expected, the stiffer superstructure resulted in larger internal stresses. The midspan of Span 2 and adjacent half of Span 3 both showed up to a 26.7% increase in stress, supporting the data shown in Figure 6-1 (i.e., the internal stresses increase as the superstructure resists second-order deformations).

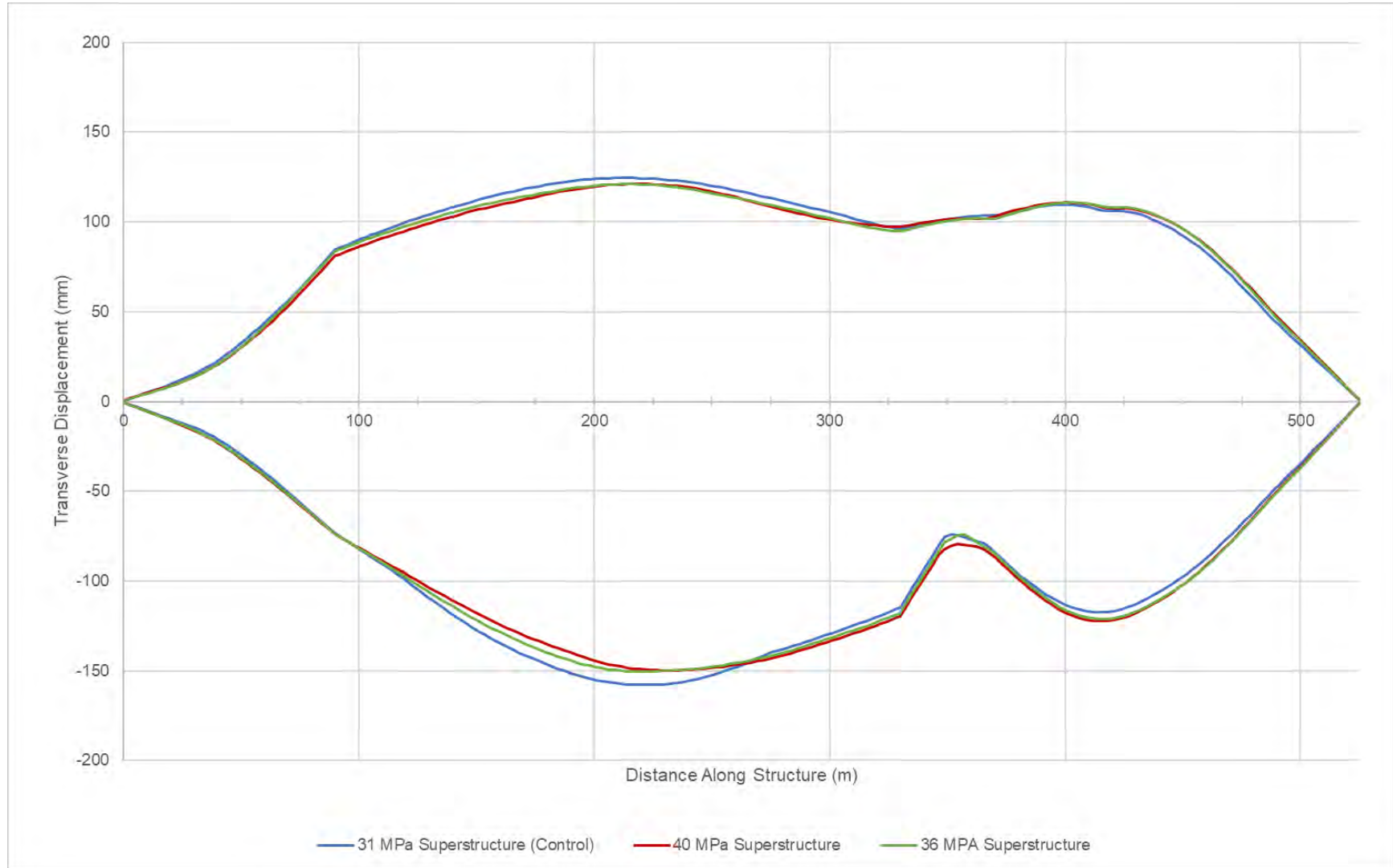


**Figure 6-1: Envelope of transverse displacement of northbound superstructure for superstructure material stiffness variants**

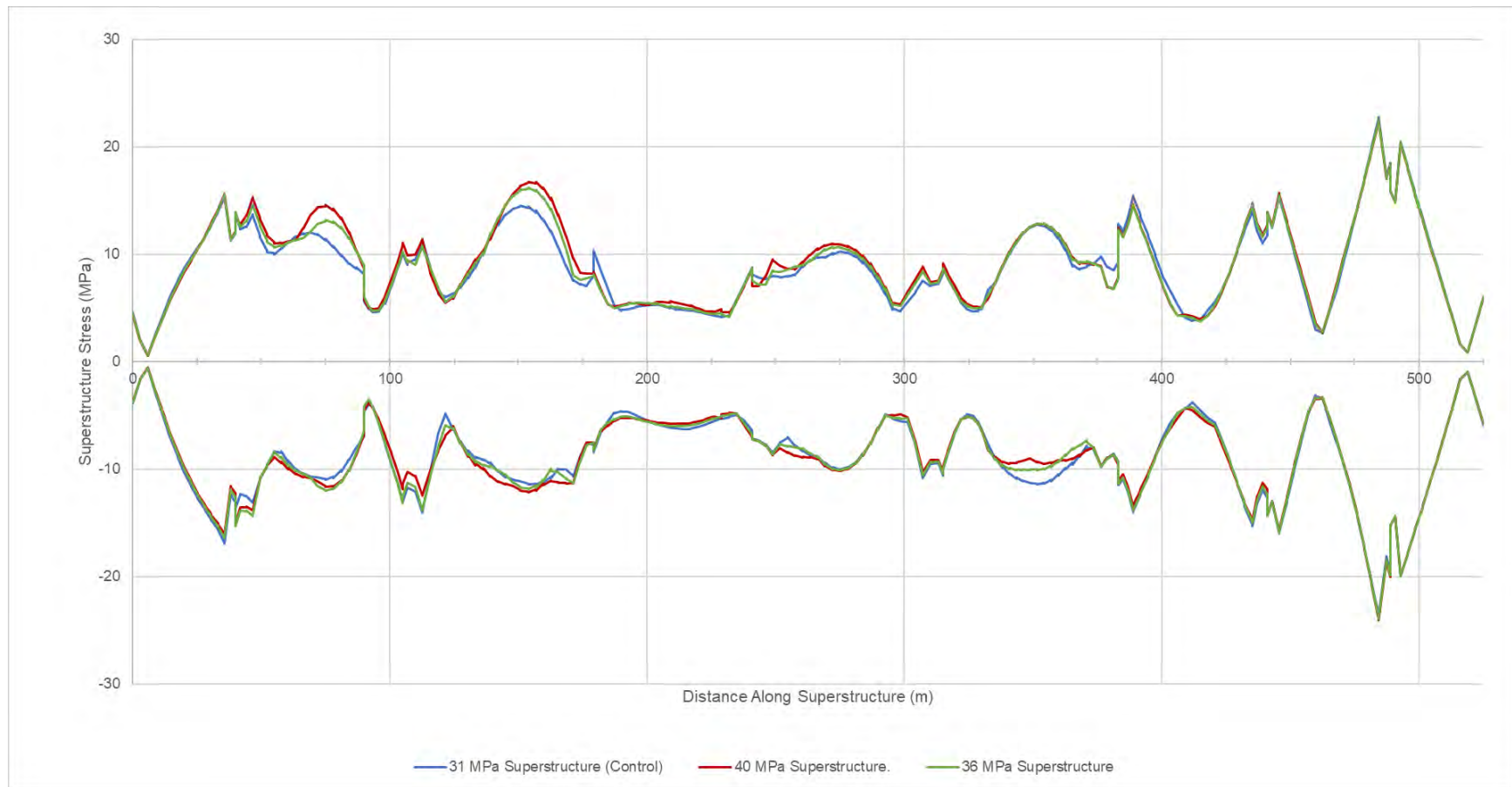


**Figure 6-2: Maximum longitudinal stresses in superstructure for superstructure material stiffness variants**



The evaluation of superstructure material stiffness has several limitations that must be considered. As previously mentioned, the material change was applied to the full length of Spans 2 through 4 due to modeling limitations of CSiBridge. In reality, only portions of the box girder over select areas of Piers 2 and 3 were comprised of higher strength concrete. As a result, it is likely that the changes in second-order effects between model variants were more dramatic than those exhibited by the existing structure. Future research into the stiffened superstructure sections could consider assigning property modifiers to the designated areas using tools in the Advanced tab of CSiBridge.

As previously mentioned, the material strengths specified in the design plans are minimum requirements. Therefore, it is likely that the actual concrete strength and stiffness of the Galena Creek Bridge is higher than the control model. This same logic would apply to all concrete components of the entire bridge (i.e., not solely the superstructure sections that use 40 MPa concrete). The accuracy of the model could be further improved by examining cylinder test results sampled from the concrete used during construction; however, an average value would need to be employed for the composite superstructure sections. Determining the actual effective strength of the concrete may improve the calibration of the model to the existing structure.

## **6.2 Structural Damping**

Damping is a structural property which quantifies the dissipation of kinetic energy (Chopra, 2017). A structure swaying in free vibration with no material damping would oscillate with the same amplitude and frequency indefinitely. The amplitude of vibration is reduced over time as a function of damping. In a 2013 study, the Galena Creek Bridge was subject to vertical and lateral excitation to determine baseline values for the physical properties (Carr and Sanders, 2013). A vertical excitation was induced by driving a 16,400 kg truck off of a 0.15 m tall ramp, while lateral excitation was induced using an eccentric mass shaker mounted to the link slab.

The damping values from the vertical loading experiments ranged from 1.3% to 2.2%, with an average of 1.85%. The bridge reliably demonstrated an average damping of 3.0% during the higher frequencies generated by the mass shaker. These results are consistent with the 2% – 3% damping typical for reinforced concrete structures with negligible cracking (Chopra, 2017). The most recent bridge inspection noted cracking throughout the columns and arches up to 0.8 mm wide and minor

spalls up to 12.7 mm deep (NDOT, 2018). The damage recorded from this bridge inspection was assumed to have an insignificant impact on the modal properties of the Galena Creek Bridge. Based on the results of the field tests and the corroborating values from established sources, the initial material damping for the concrete definitions in CSiBridge were set as 2.0%.

To evaluate the influence of the structure damping ratio on the response of the model to ground motions, two additional model variants were created. Reinforced concrete exhibiting minor hairline cracking developed throughout the service life is typically representative of 5% damping (Chopra, 2012). Conversely, material damping of 7% is more indicative of concrete members that display significant cracking that occurs before the yielding of the reinforcing steel. For each case, the damping ratio of interest was assigned to every type of concrete definition in that model.

#### *6.2.1 Modal Analysis – Structural Damping*

All CSiBridge models were considered to be classically damped systems where the modal properties are not dependent on the damping ratio, and the modes for an undamped model would be the same as those of a model with any material damping value. As such, the modal information for this series of tests is identical with those of the control model and modal analyses were not performed for this variable.

#### *6.2.2 Time-history Analysis – Structural Damping*

Comparing the transverse displacements between the models in Figure 6-3 shows consistent and expected patterns; specifically, as the damping value increases the displacement of the superstructure decreases. At the crown of the arch, the control model has a maximum transverse displacement of 15.7 cm. The 5% damping model exhibits a 10.1% decrease in displacement (14.0 cm) at the same location. The crown of the arch of the 7% damping model only displaces 13.4 cm, a 14.7% decrease from the control model. Further, the limited data suggests that continual increases in material damping yields diminishing changes in the displacement of the superstructure.

Similarly, increasing the damping reduces the internal stresses of the superstructure, with the same pattern of diminishing returns observed. Figure 6-4 reveals that increasing the damping from 2% to 5% reduced the stresses up to 19.8%. However, the plots for 5% and 7% damping are nearly

congruent. Although the 7% damping model displayed reduced stresses across the entire length of the bridge, the superstructure only noted an average decrease of 0.8 MPa. In contrast, the 5% damping model experienced an average reduction of 2.0 MPa compared to the 2% damping control model.

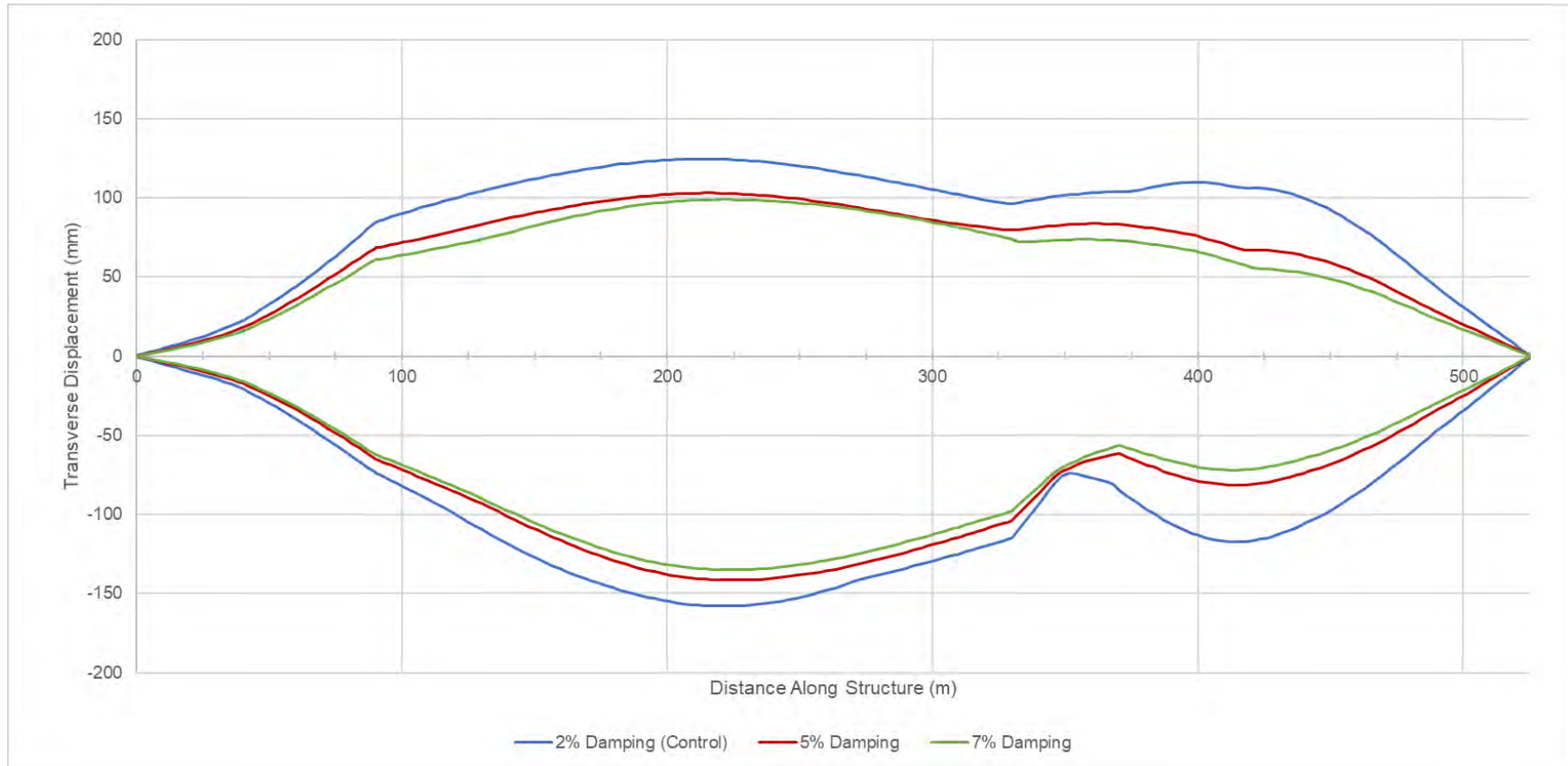


**Figure 6-3: Envelope of transverse displacement of superstructure from damping analyses**

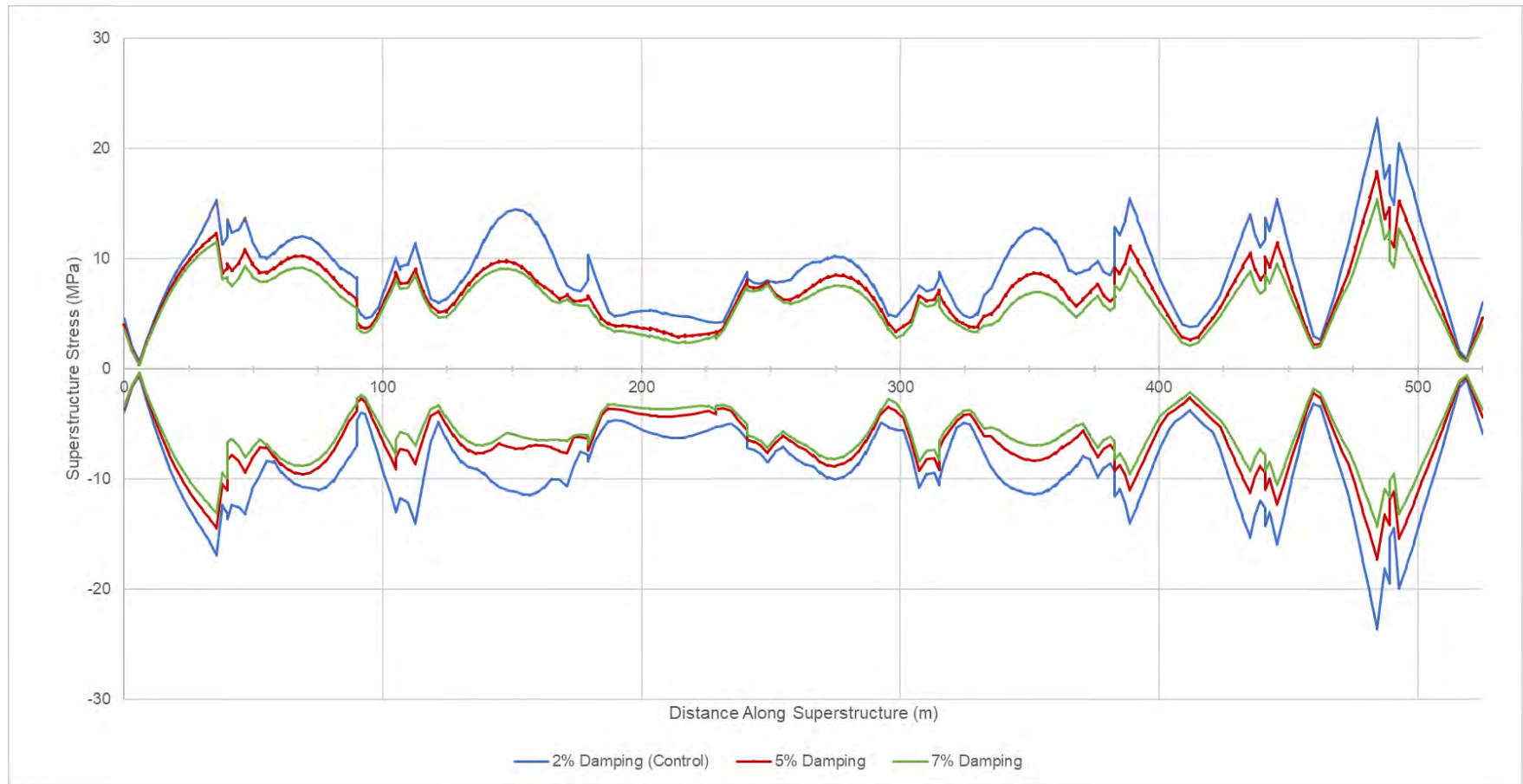


**Figure 6-4: Maximum superstructure stresses from damping analyses**

The results from the time-history analyses show that damping has a significant influence on the displacement and stresses experienced by the structure. Verification of the current damping of the Galena Creek Bridge would be conducted by comparing the dynamic response of the structure to the FEA model. The damping of concrete structures is directly dependent on the structural integrity of the concrete; therefore, as cracks initiate and propagate in bridge components, the material damping value changes as well. This parametric evaluation assumed the same material damping throughout all concrete components of the model. As the Galena Creek Bridge continues to develop cracking throughout the service life, appropriate damping ratios would need to be applied to deteriorating components to continuously reflect the true behavior.

### **6.3 Elastomeric Bearing Stiffness**

The elastomeric bearings of the Galena Creek Bridge permit mild translation and rotation of the superstructure at the expansion joints and abutments. These components can be effective in reducing the stresses within the superstructure by allowing limited and controlled deflection. Properly replicating bearing behavior is key to simulating the interactions between the frames of the existing structure.

CSiBridge has bearing stiffness inputs for both translation and rotation about the three degrees of freedom in the bearing definition. Restrainer properties can also be attached to bearings as a means to add advanced properties, such as limitations on allowable rotation and translation. Although both methods of assigning physical properties to bearings in CSiBridge are viable, the calculated stiffness values were input in the initial bearing definitions to simplify the editing procedure and to facilitate model updates. Typically, restrainer properties would be used to model complex elements, such as seismic retrofitting steel cables. The 2018 bridge inspection performed by NDOT did not note excessive or unusual displacements at the abutments and hinges (NDOT, 2018). As such, additional restrainer inputs were not deemed necessary.

CSiBridge requires the user to explicitly define the number of bearings used when defining the substructure elements, such as the abutments or bents. However, the input for hinges only permits a single bearing component to be assigned. The orientation of the bearings at the hinges are congruent; therefore, it was assumed that the three bearings at the hinges behaved in tandem. The

physical properties of the single hinge bearing defined in CSiBridge were the summation of the stiffnesses of the three elastomeric bearings in the actual structure. Figure 6-5 demonstrates the allowable rotations and translations assigned to the bearing definitions with respect to the global axis definition in CSiBridge. The idealized models of reinforced elastomeric bearings conservatively assumed no rotation about the longitudinal or transverse axis.

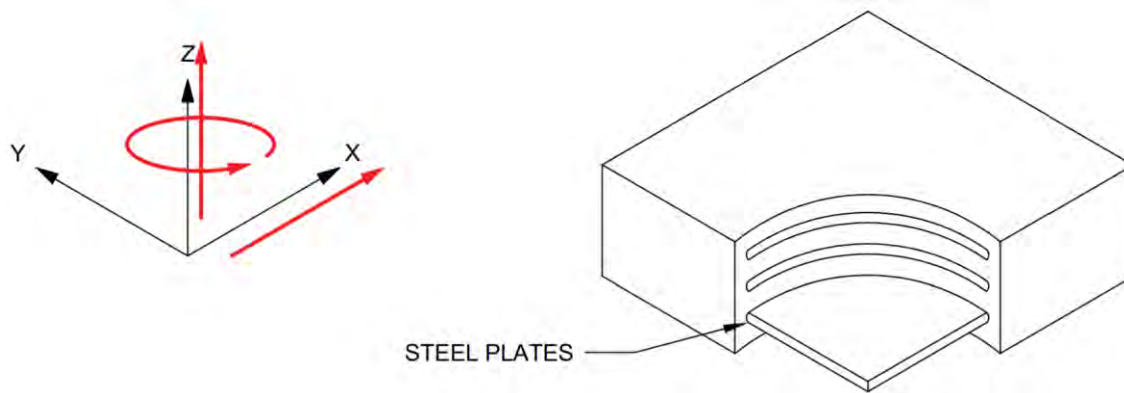


**Figure 6-5: Allowable degrees of freedom (left) of the bearing pads relative to CSiBridge global axes**

Equations 5.2 – 5.4 were used to calculate the stiffness of the bearing pads (Akogul, 2008). Table 14.7.6.2-1 of the AASHTO LRFD Specifications suggests the allowable shear modulus ( $G$ ) range for 60 durometer elastomers is from 0.90 MPa to 1.38 MPa at 22.8° C (AASHTO, 2020). The control model assumed  $G = 0.90$  MPa to allow the initial structure to have decreased stiffness. Evaluation of bearing stiffness involved assigning the maximum recommended shear modulus ( $G = 1.38$  MPa). This approach was used to determine the probable range that the bearing stiffnesses would influence the dynamic properties of the FEA model. The calculated values for the hinge and abutment bearings using  $G = 1.38$  MPa are displayed in Figure 6-6 and Figure 6-7.

**Bridge Bearing Data** [X]

**Bridge Bearing Name** Abutment Bearing **Units** KN, m, C

**Bridge Bearing Is Defined By:**

☐ Link/Support Property ☐ User Definition

**User Bearing Properties**

DOF/Direction	Release Type	Stiffness
Translation Vertical (U1)	Partial Fixity	3451091.
Translation Normal to Layout Line (U2)	Fixed	
Translation Along Layout Line (U3)	Partial Fixity	5483.675
Rotation About Vertical (R1)	Partial Fixity	748.704
Rotation About Normal to Layout Line (R2)	Fixed	
Rotation About Layout Line (R3)	Fixed	

OK Cancel

Figure 6-6: Upper limit abutment bearing stiffness input for CSiBridge ( $G = 1.38$  MPa)

**Bridge Bearing Data** [X]

**Bridge Bearing Name** Hinge Bearing **Units** KN, m, C

**Bridge Bearing Is Defined By:**

☐ Link/Support Property ☐ User Definition

**User Bearing Properties**

DOF/Direction	Release Type	Stiffness
Translation Vertical (U1)	Partial Fixity	7441561.
Translation Normal to Layout Line (U2)	Fixed	
Translation Along Layout Line (U3)	Partial Fixity	8618.713
Rotation About Vertical (R1)	Partial Fixity	1659.39
Rotation About Normal to Layout Line (R2)	Fixed	
Rotation About Layout Line (R3)	Fixed	

OK Cancel

Figure 6-7: Upper limit hinge bearing stiffness input for CSiBridge ( $G = 1.38$  MPa)



Two additional bearing conditions were considered to suggest the probable limit of influence that bearings have on the dynamic properties of the structure. Removing the stiffness values would assume that the bearings allowed free translation and rotation about the desired degrees of freedom. This modeling condition would result in a decrease in stiffness and likely increase in displacements. Conversely, modeling all bearings as fully fixed would simulate the maximum stiffness bearing conditions would produce.

#### *6.3.1 Modal Analysis – Elastomeric Bearing Stiffness*

Increasing the shear modulus of the elastomers from 0.90 MPa to 1.38 MPa marginally increased the stiffness of the structure. Although Table 6-6 shows that there were no noticeable changes to the transverse modes, the longitudinal modes demonstrated the greatest dependence on this parameter. The bearings at both the hinges and abutments were restricted in the transverse direction by shear keys; as such, increasing the bearing stiffness resulted in the frequencies of the top transverse modes changing less than 1.0%. Likewise, the top vertical modes experienced inconsequential changes (under 0.5%). The high vertical stiffness of the elastomer resulted in the bearings acting similar to being fully constrained in translation along the vertical axis. In contrast, the top longitudinal modes experienced period and participation factor reductions of up to 2.7% and 14.3%, respectively (Table 6-5).

The fully-fixed bearing variant restricted translation and rotation about all three degrees of freedom. As expected, the periods for most modes decreased to reflect the increased stiffness of the model. Note that several of the top transverse modes demonstrated significant increase in periods, likely a result of restricting rotation about the vertical axis. Conversely, 14 of the 15 modes observed of the free bearing model showed an incremental increase in periods. It should be noted that Table 6.7 reveals the change in vertical modes was almost negligible, with the average increase being less than 0.2%. This further confirms that the high calculated vertical stiffness of the elastomeric bearings acts similar to a bearing that completely restricts vertical translation.

**Table 6-5: Comparison of top longitudinal modes for bearing stiffness variations (X-axis)**

G = 0.90 MPa Bearings (Control Model)			G = 1.38 MPa Bearings				Fully-Fixed Bearings				Free Bearings			
Mode	Period, $T_{control}$ (s)	Modal Part. Factor (%)	Mode	Period, $T$ (s)	Modal Part. Factor (%)	$T/T_{control}$	Mode	Period, $T$ (s)	Modal Part. Factor (%)	$T/T_{control}$	Mode	Period, $T$ (s)	Modal Part. Factor (%)	$T/T_{control}$
2	1.342	12.3	2	1.332	13.0	0.992	3	0.919	5.4	0.685	2	1.366	10.8	1.017
4	0.976	15.1	4	0.952	14.9	0.975	11	0.550	3.3	0.564	4	1.027	15.6	1.052
9	0.671	9.2	9	0.666	8.5	0.993	17	0.454	11.1	0.677	9	0.684	9.7	1.019
11	0.627	9.8	11	0.623	9.9	0.994	36	0.277	27.1	0.442	11	0.633	9.4	1.011
39	0.284	9.3	40	0.283	10.6	0.996	37	0.272	14.2	0.957	39	0.285	15.7	1.002

**Table 6-6: Comparison of top transverse modes for bearing stiffness variations (Y-axis)**

G = 0.90 MPa Bearings (Control Model)			G = 1.38 MPa Bearings				Fully-Fixed Bearings				Free Bearings			
Mode	Period, $T_{control}$ (s)	Modal Part. Factor (%)	Mode	Period, $T$ (s)	Modal Part. Factor (%)	$T/T_{control}$	Mode	Period, $T$ (s)	Modal Part. Factor (%)	$T/T_{control}$	Mode	Period, $T$ (s)	Modal Part. Factor (%)	$T/T_{control}$
1	1.688	55.0	1	1.688	55.0	1.000	1	1.595	56.2	0.945	1	1.689	55.0	1.000
5	0.819	9.5	5	0.819	9.5	1.000	4	0.731	7.8	0.893	5	0.819	9.5	1.000
17	0.513	7.0	17	0.513	7.1	1.000	13	0.500	2.7	0.976	17	0.513	7.0	1.000
24	0.386	1.9	24	0.386	1.9	1.000	15	0.482	1.4	1.249	24	0.386	1.9	1.000
51	0.240	1.2	50	0.240	1.2	1.000	20	0.382	2.3	1.594	50	0.240	1.2	0.998

**Table 6-7: Comparison of top vertical modes for bearing stiffness variations (Z-axis)**

<b>G = 0.90 MPa Bearings (Control Model)</b>			<b>G = 1.38 MPa Bearings</b>				<b>Fully-Fixed Bearings</b>				<b>Free Bearings</b>			
<b>Mode</b>	<b>Period, <math>T_{control}</math> (s)</b>	<b>Modal Part. Factor (%)</b>	<b>Mode</b>	<b>Period, <math>T</math> (s)</b>	<b>Modal Part. Factor (%)</b>	<b><math>T/T_{control}</math></b>	<b>Mode</b>	<b>Period, <math>T</math> (s)</b>	<b>Modal Part. Factor (%)</b>	<b><math>T/T_{control}</math></b>	<b>Mode</b>	<b>Period, <math>T</math> (s)</b>	<b>Modal Part. Factor (%)</b>	<b><math>T/T_{control}</math></b>
7	0.713	5.8	8	0.704	3.2	0.988	5	0.708	9.7	0.994	7	0.720	4.2	1.010
15	0.560	3.9	18	0.505	3.9	0.902	10	0.565	8.8	1.009	15	0.561	4.8	1.001
18	0.506	4.1	20	0.469	4.0	0.927	13	0.500	5.5	0.990	18	0.506	4.3	1.000
20	0.469	3.9	21	0.458	3.4	0.976	14	0.499	8.1	1.062	20	0.469	4.0	1.000
44	0.263	6.1	44	0.263	6.3	1.000	39	0.262	5.9	0.996	44	0.263	6.4	1.000

### 6.3.2 Time-history Analysis – Elastomeric Bearing Stiffness

The time-history analysis results verify the conclusions from the modal analysis. The vertical and transverse displacements from the ground motions were nearly identical. This is because lateral translation for both the hinge and abutment bearings was fully restricted. It was assumed that the shear keys at both locations were effectively preventing lateral translation.

Superstructure displacements along the longitudinal axis demonstrated noticeable changes because of editing the bearing stiffnesses (Figure 6-8). Specifically, Frame 3 of the  $G = 1.38$  MPa variant experienced an average 8.3% decrease in longitudinal displacement. Increasing the stiffness of the bearings increased the interactions between the frames of the Galena Creek Bridge. As the bearing stiffness increased, the high stiffness of Frame 2 would limit the displacements of Frames 1 and 3.

Note that Frame 2 demonstrates nearly identical behavior among all the cases considered for this variable. The maximum lateral displacements of Frame 2 diverge the most from those of the other analyses near Hinge 1. This is likely a result of the fixed Abutment 1 located only 90 m from Hinge 1. Although the envelope longitudinal displacements of Frames 1 and 3 show greater discrepancies between the models than Frame 2, the results are inconclusive. The free bearing model variant showed increased longitudinal displacements throughout Frame 1. However, the maximum positive longitudinal displacement along Frame 3 was an average of 15.1% lower than the two models with bearing stiffnesses assigned. This is likely a consequence of the specific ground motion. Further research on the influence of bearing properties could consider various ground motions to develop more substantial correlations. Another option could be to apply symmetrical ground motions, such as a sine wave, about both directions of the desired axes.

The results suggest that the bearing boundary conditions limiting translation and rotation are more important than the actual calculated stiffness values. Although increasing the bearing stiffness from  $G = 0.90$  MPa to 1.38 MPa increased the stiffness of the model, the difference in the modal analyses and time-history responses was negligible. The more significant changes to the modal behavior and dynamic response resulted from adding fixities to the bearing definitions to model them as rigid. These conclusions mirror those found in previous research conducted at the Georgia Institute of Technology (Wang, 2010). Wang found that the stiffness values assigned to elastomeric bearings did not influence the load bearing capacity of the bridges.

This page intentionally left blank.

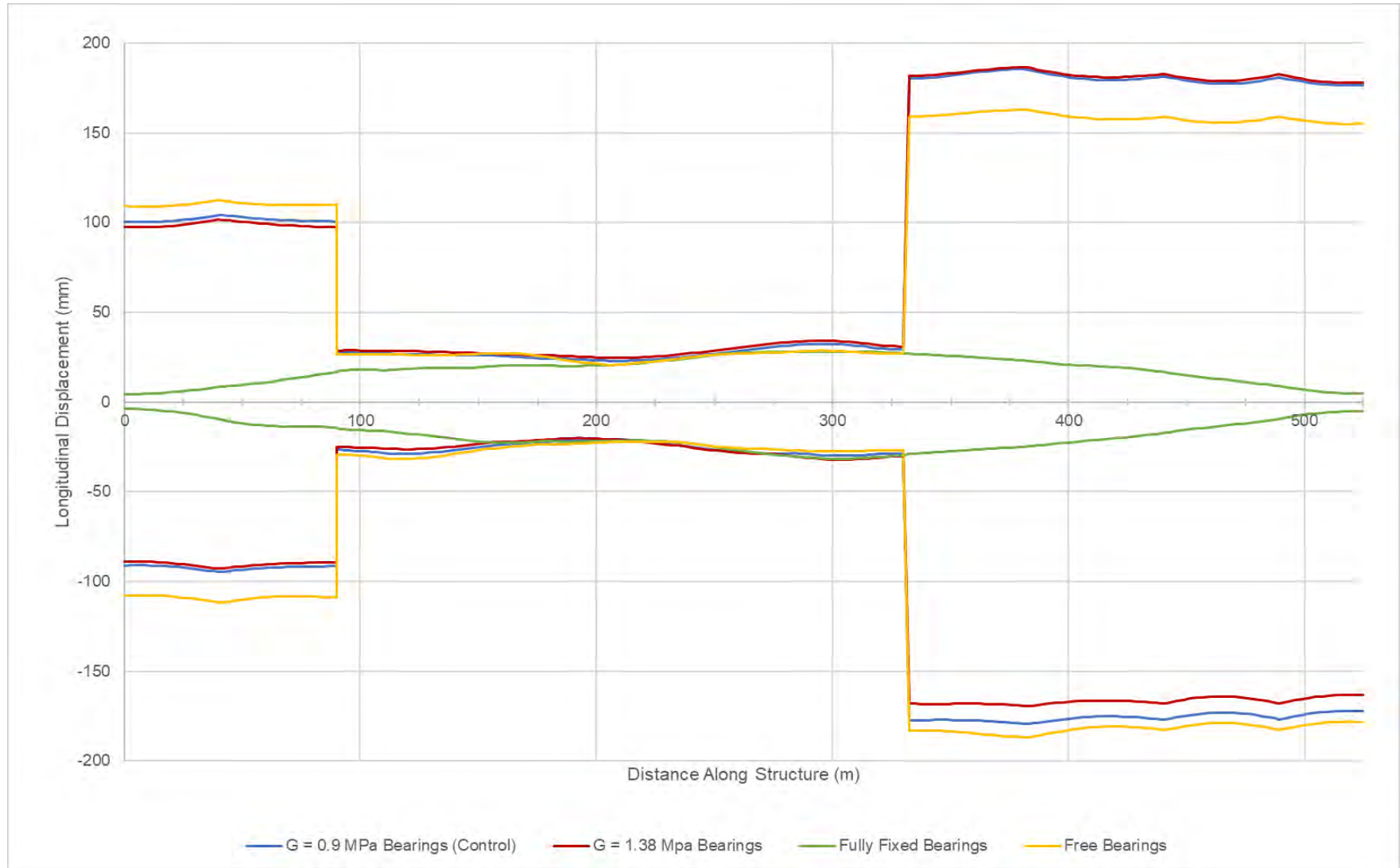


**Figure 6-8: Maximum longitudinal displacement of superstructures from bearing analyses**

## 6.4 Effective Moment of Inertia of Substructure

As cracks propagate, reinforced concrete elements suffer from a reduction in flexural rigidity. ACI suggests that when performing linear-elastic analyses, concrete cracking can be accounted for by applying a reduction factor to the moment of inertia (MOI) of the concrete member, specifically reducing the MOI of a column to 70% to provide conservative estimates during the design process. Note that the gross cross-sectional area does not need additional factors when using this method. While conservative assumptions aid in the safe design of structures, they do not typically represent the physical in-service behavior. To better understand how variations in the moment of inertia influence the model, scaling factors for the moment of inertia were investigated between 100% and 50% in 5% increments.

A typical rectangular box column section of the Galena Creek Bridge has a gross MOI of  $11.59 \text{ m}^4$  about the transverse axis and  $44.57 \text{ m}^4$  about the longitudinal axis. The typical arch section has gross MOIs of  $14.22 \text{ m}^4$  and  $33.50 \text{ m}^4$  about the transverse and longitudinal axes, respectively. The MOI scaling factor was applied to the elements in CSiBridge by accessing the section properties of the arch and column cross sections under the Components tab, as can be seen in Figure 6-9. For these set of trials, the same constant was applied to both the Pier Column and the Arch Typical. sections.

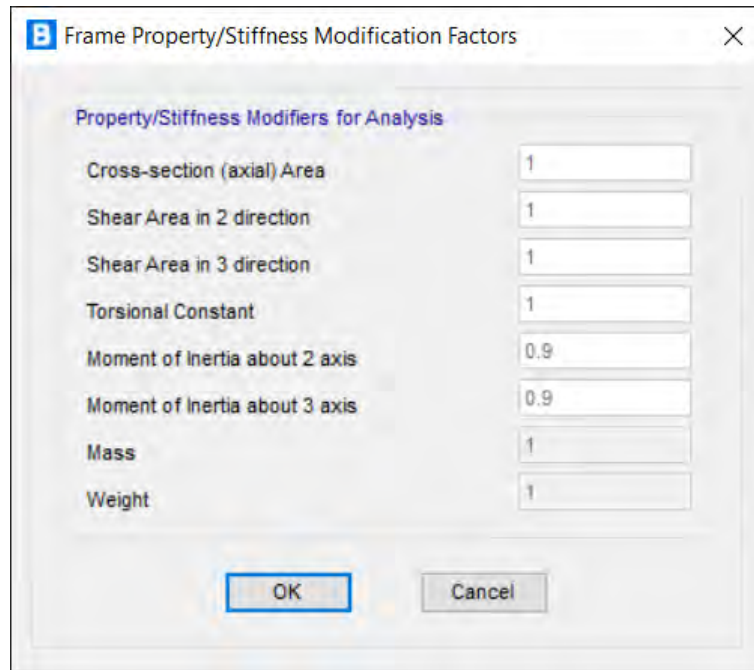


**Figure 6-9: Example of MOI reduction factor applied in CSiBridge**

#### 6.4.1 Modal Analysis – Effective Column Moment of Inertia

A total of 10 variant models were analyzed, excluding the control model. Tables 6.8 to 6.10 display the partial results from performing modal analyses; they show 10% increments as opposed to 5% for the purposes of presenting the findings in a clear format. The side-by-side comparison of the changes in period and participation factors reveal an inverse correlation between effective MOI and modal periods. The periods for the longitudinal and transverse modes considered increased as the effective MOI of the substructure elements decreased: the longitudinal modes increased up to 33.2% and the transverse modes increased up to 24.3%. This validates the assumption that increasing the flexibility would decrease the natural frequencies. The vertical modal data only exhibited minor changes between the analyses, suggesting that the substructure flexibility has minimal influence on the vertical behavior of the bridge.



**Table 6-8: Comparison of top longitudinal modes for MOI variation (X-axis)**

100% MOI (Control Model)				90% MOI				80% MOI			
Mode	Period, $T_{control}$ (s)	Modal Part. Factor (%)		Mode	Period, $T$ (s)	Modal Part. Factor (%)	$T/T_{control}$	Mode	Period, $T$ (s)	Modal Part. Factor (%)	$T/T_{control}$
2	1.342	12.3		2	1.391	12.4	1.037	2	1.411	12.5	1.051
5	0.976	15.1		5	1.007	15	1.032	5	1.043	14.9	1.069
12	0.669	9.2		12	0.682	10.2	1.019	12	0.696	11.9	1.040
15	0.621	9.6		15	0.635	9.5	1.023	15	0.649	8.2	1.045
42	0.284	10.3		42	0.286	13.7	1.007	43	0.286	13.8	1.007
70% MOI				60% MOI				50% MOI			
Mode	Period, $T$ (s)	Modal Part. Factor (%)	$T/T_{control}$	Mode	Period, $T$ (s)	Modal Part. Factor (%)	$T/T_{control}$	Mode	Period, $T$ (s)	Modal Part. Factor (%)	$T/T_{control}$
2	1.452	12.7	1.082	2	1.501	12.9	1.118	2	1.559	13.3	1.162
5	1.086	14.9	1.113	5	1.139	14.7	1.167	5	1.206	14.5	1.236
7	0.824	6.7	1.232	7	0.854	6.9	1.277	6	0.891	6.5	1.332
12	0.713	13.7	1.148	12	0.735	16.3	1.184	12	0.765	19.6	1.232
43	0.288	16.3	1.014	44	0.29	18.1	1.021	44	0.293	19.2	1.032

**Table 6-9: Comparison of top transverse modes for MOI variation (Y-axis)**

100% MOI (Control Model)				90% MOI				80% MOI			
Mode	Period, $T_{control}$ (s)	Modal Part. Factor (%)		Mode	Period, $T$ (s)	Modal Part. Factor (%)	$T/T_{control}$	Mode	Period, $T$ (s)	Modal Part. Factor (%)	$T/T_{control}$
1	1.739	52.4		1	1.804	52.9	1.037	1	1.865	53.6	1.072
4	1.027	3.3		4	1.057	3.5	1.029	4	1.089	3.6	1.060
6	0.788	3.6		6	0.801	3.7	1.016	6	0.816	3.8	1.036
9	0.717	4.2		9	0.735	4.3	1.025	9	0.755	4.1	1.053
21	0.504	7.2		21	0.523	7.2	1.038	20	0.546	6.8	1.083
70% MOI				60% MOI				50% MOI			
Mode	Period, $T$ (s)	Modal Part. Factor (%)	$T/T_{control}$	Mode	Period, $T$ (s)	Modal Part. Factor (%)	$T/T_{control}$	Mode	Period, $T$ (s)	Modal Part. Factor (%)	$T/T_{control}$
1	1.945	54.3	1.118	1	2.041	55.1	1.174	1	2.162	56.1	1.243
4	1.128	3.8	1.098	4	1.173	3.9	1.142	4	1.23	3.9	1.198
6	0.835	3.9	1.060	6	0.859	4.0	1.090	7	0.889	4.0	1.128
9	0.776	3.6	1.082	9	0.8	3.0	1.116	9	0.827	5.3	1.153
20	0.571	6.7	1.133	20	0.601	6.3	1.192	18	0.64	3.8	1.270

**Table 6-10: Comparison of top vertical modes for MOI variation (Z-axis)**

100% MOI (Control Model)				90% MOI				80% MOI			
Mode	Period, $T_{control}$ (s)	Modal Part. Factor (%)		Mode	Period, $T$ (s)	Modal Part. Factor (%)	$T/T_{control}$	Mode	Period, $T$ (s)	Modal Part. Factor (%)	$T/T_{control}$
10	0.711	6.8		10	0.723	6.5	1.017	10	0.733	5.5	1.031
19	0.559	3.8		22	0.509	5.8	0.911	22	0.514	6.3	0.919
22	0.502	5.6		24	0.474	4.2	0.944	24	0.479	4.1	0.954
24	0.468	4.4		25	0.464	3.4	0.991	25	0.470	3.6	1.004
48	0.263	5.8		47	0.268	6.6	1.019	47	0.270	5.1	1.027
70% MOI				60% MOI				50% MOI			
Mode	Period, $T$ (s)	Modal Part. Factor (%)	$T/T_{control}$	Mode	Period, $T$ (s)	Modal Part. Factor (%)	$T/T_{control}$	Mode	Period, $T$ (s)	Modal Part. Factor (%)	$T/T_{control}$
10	0.748	4.6	1.052	16	0.627	3.7	0.882	13	0.741	5.3	1.042
22	0.522	6	0.934	22	0.532	4	0.952	22	0.545	3.7	0.975
24	0.480	4.2	0.956	24	0.493	4.8	0.982	24	0.503	6.1	1.002
25	0.477	3.9	1.019	25	0.485	3.9	1.036	45	0.288	3.7	0.615
46	0.275	7.9	1.046	46	0.28	9.3	1.065	46	0.284	6.3	1.080

#### 6.4.2 Time-history Analysis – Effective Column Moment of Inertia

The results from the time-history analyses corroborate the data from the modal analyses; decreasing the effective MOI of the substructure elements increases the deflection across the superstructure. Figure 6-10 shows that the structure experiences the greatest changes in deflection at Span 3 as the abutments restrict transverse displacement. To better view the influence of the effective MOI on maximum displacement, Figure 6-11 plots the envelope transverse displacement at the midspan of Span 3. The graph clearly shows that the increments between model variants increase as the effective MOI decreases. Reducing the factor from 100% to 90% results in a 11 mm increase in displacement at this location; however, reducing the factor from 70% to 60% resulted in an increase of up to 121 mm at the crown of the arch.

It was noted in Figure 6-10 that the transverse displacements of Spans 6 and 7 did not follow the typical pattern exhibited by the rest of the structure. For Spans 1 through 5, decreasing the effective MOI of the substructure elements would increase the transverse displacement, as expected. Spans 6 and 7 demonstrate relatively congruent behavior between 100% and 70% effective MOI. Additionally, the 60% MOI analysis demonstrated less displacement than the control model between 425 m and 525 m along the structure. This is likely due to extreme deflections at Span 3 and the abutment boundary condition. The inverse curvature of Frame 3 of the structure is a result of connecting the displacements at Hinge 2 to Abutment 2, which restricts transverse translation. It is also likely that the atypical behavior might be a result of the specific ground motion applied. Performing further time-history analyses using various ground motions would reveal whether the behavior by Spans 6 and 7 is typical of the FEA model.

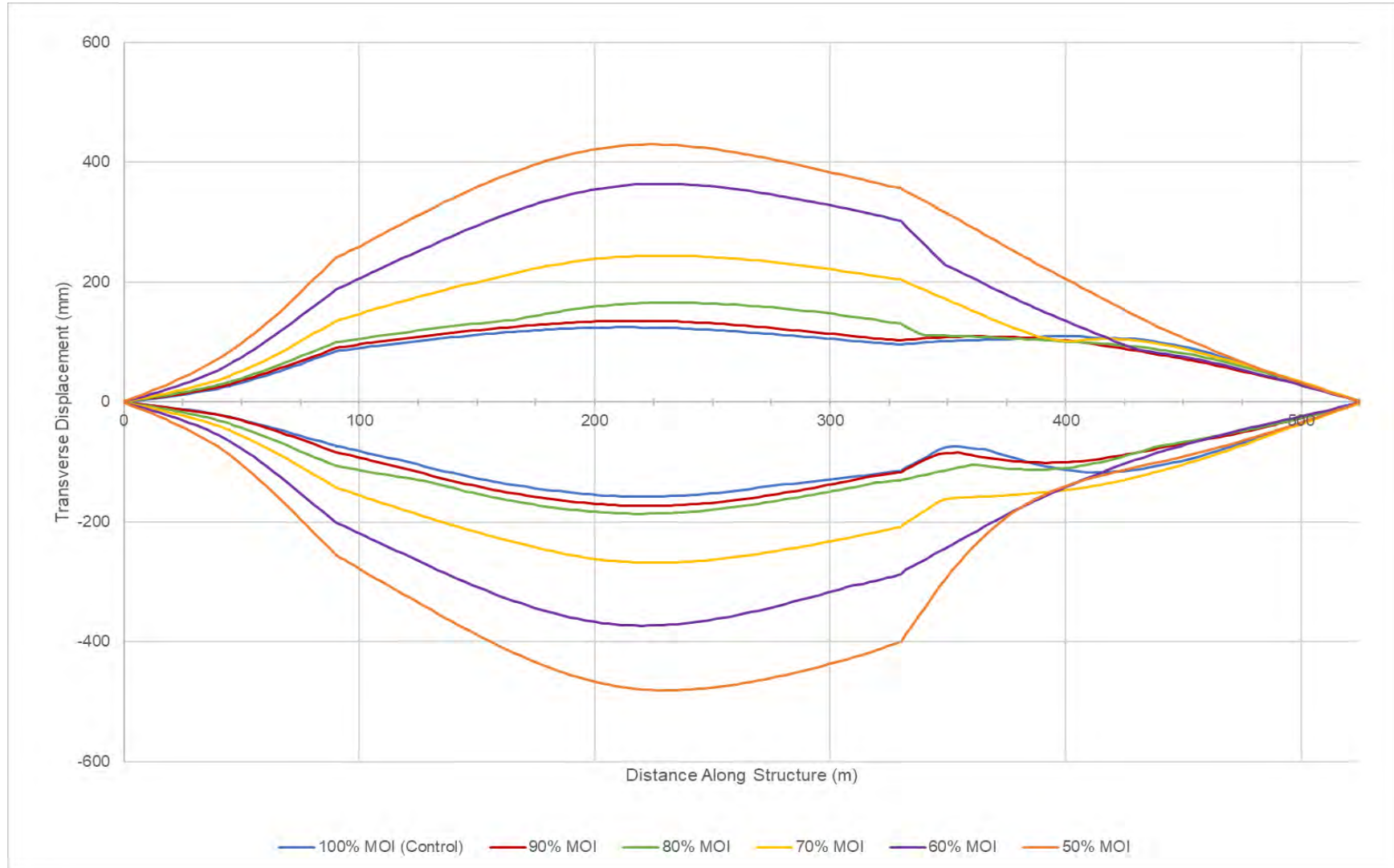


**Figure 6-10: Maximum transverse displacement of superstructures for substructure effective MOI analyses**

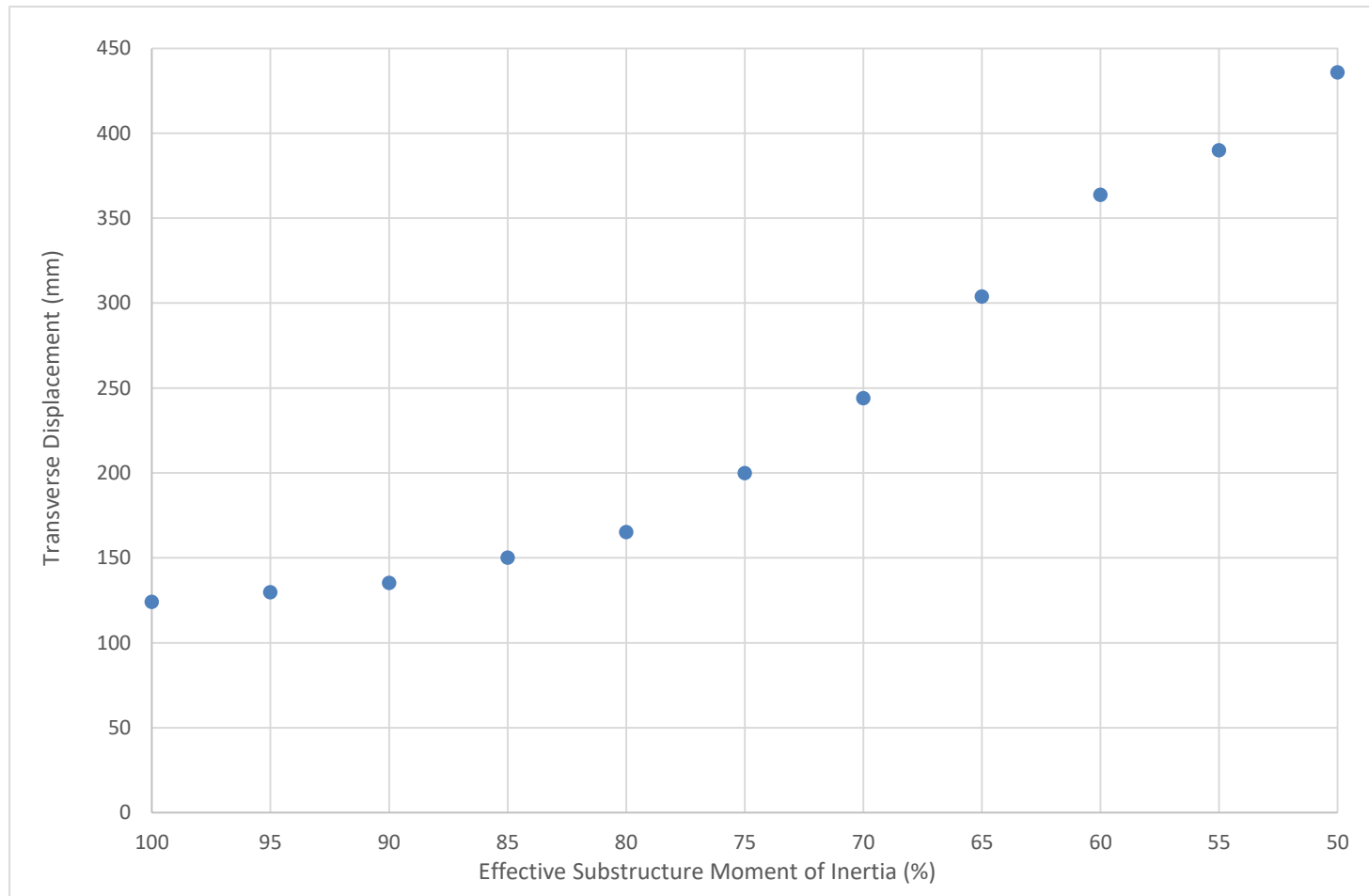


**Figure 6-11: Maximum transverse displacement at midspan of Span 3**

Applying a universal MOI reduction factor is not a practical representation of the Galena Creek Bridge. The time-history analysis of the control model reveals that the columns of the bridge experience different internal stresses and deformations. Substructure components that attract larger forces, such as Pier 1, develop deeper cracks than members that are not subject to as severe bending moments, resulting in different effective MOI factors. To further pursue this avenue of research would require tracking the moments in individual substructure elements. From there, the applied MOI reduction factor for each column would increase proportionally to the bending moments experienced based on reasonably assumed crack lengths. Finally, this parametric study only performed linear time-history analyses. Excessive reduction in the effective MOI of the substructure would likely result in the element failing before reaching the displacements noted in this evaluation.

## **6.5 Link Slab**

A 0.2 m thick link slab connects the northbound and southbound structures along the length of Frame 2. As the primary component connecting the northbound and southbound superstructures, the link slab provides significant resistance to lateral loads. The link slab is considered to be integral with the adjacent bridge decks due to the sufficient steel reinforcing between the aforementioned components. As the Galena Creek Bridge is most vulnerable to lateral loads, accurately modeling the link slab is crucial to calibrating the FEA model to in-service behavior.

The bridge object superstructure is comprised of shell elements that are up to 3 m in length, as set by the user through the Update feature in CSiBridge. The nodes used to define the rectangular link slab shells for the control model are attached to every other node of the superstructure; as such, the link slab shell elements are up to 6 m long. Two additional modeling methods were considered for simulating the link slab. The first variant considered decreasing the interval size of the link slab elements. All boundary conditions remain fixed and the maximum length for the link slab shell elements was reduced to 3 m. The second approach was to use a single shell element to connect Frame 2 of the northbound and southbound bridges. CSiBridge permits users to define nodes for a 2D shell element about a single plane. As the deck of both superstructures follow the same - 1.25% grade, a single shell element was modeled by using each node at the ends of the bridge deck. The singular shell, comprising of 176 edge nodes, was used to mitigate interactions between

numerous shell elements. A color coordinated representation is demonstrated by Figure 6-12 with the northbound and southbound superstructures highlighted in white and pink, respectively. Figure 6-13 demonstrates the single shell element, highlighted in teal, used to connect the northbound and southbound structures.

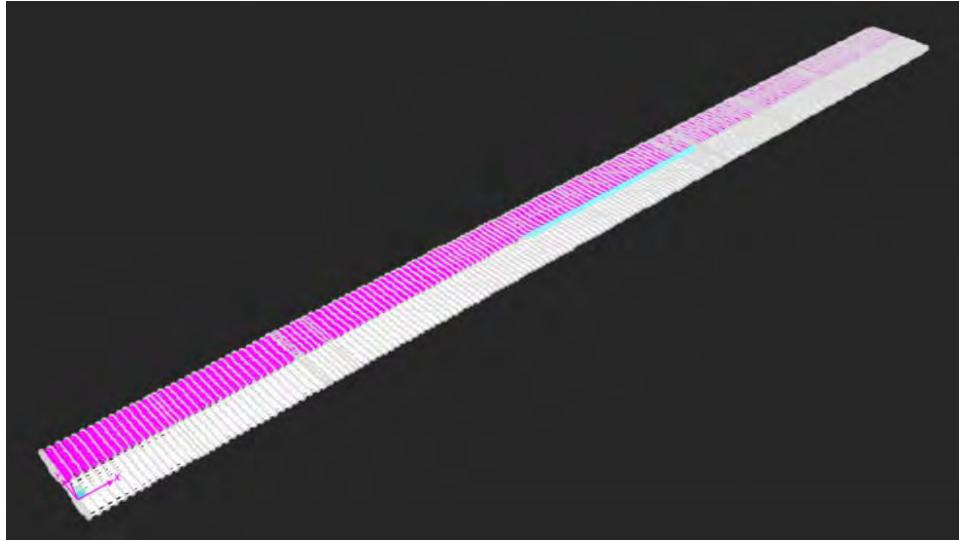


**Figure 6-12: Northbound (white) and southbound (pink) superstructures highlighted by color**

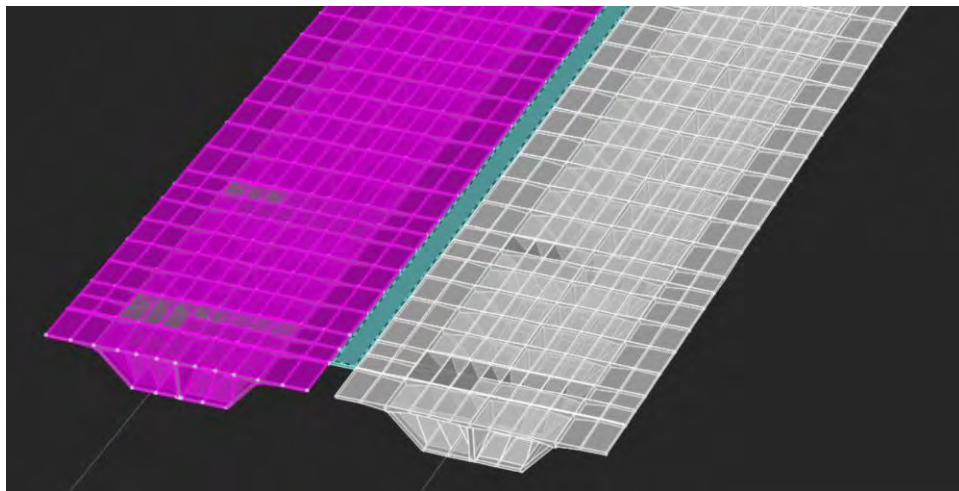


**Figure 6-13: Single shell element (teal) connecting northbound (white) and southbound (pink) structures**



### 6.5.1 Modal Analysis – Link Slab

The results of the modal analyses of the control model and both link slab variants are displayed in Tables 6.11 – 6.13 the modal periods between the three FEA models compared are nearly identical. As the link slab is intended to be a component that resists lateral loadings, it was expected that the transverse modes would demonstrate the greatest variation between models. However, all changes between subsequent model were less than 0.5%.

**Table 6-11: Top five modes in the longitudinal direction modal variation (X-axis)**

6 m Link Slab Intervals (Control Model)			3 m Link Slab Intervals				Single Link Slab Shell Element			
Mode	Period, $T_{control}$ (s)	Modal Part. Factor (%)	Mode	Period, $T$ (s)	Modal Part. Factor (%)	$T/T_{control}$	Mode	Period, $T$ (s)	Modal Part. Factor (%)	$T/T_{control}$
2	1.342	12.3	2	1.342	12.3	1.000	2	1.342	12.3	1.000
4	0.976	15.1	4	0.977	15.1	1.001	4	0.977	15.1	1.001
9	0.671	9.2	9	0.671	9.3	1.000	9	0.671	9.2	1.000
11	0.627	9.8	11	0.627	9.8	1.000	11	0.627	9.8	1.000
39	0.284	9.3	39	0.284	9.5	1.000	39	0.284	9.1	1.000

**Table 6-12: Top five modes in the transverse direction modal variation (Y-axis)**

6 m Link Slab Intervals (Control Model)			3 m Link Slab Intervals				Single Link Slab Shell Element			
Mode	Period, $T_{control}$ (s)	Modal Part. Factor (%)	Mode	Period, $T$ (s)	Modal Part. Factor (%)	$T/T_{control}$	Mode	Period, $T$ (s)	Modal Part. Factor (%)	$T/T_{control}$
1	1.688	55	1	1.688	55	1.000	1	1.688	55	1.000
5	0.819	9.5	5	0.819	9.5	1.000	5	0.819	9.5	1.000
17	0.513	7	17	0.513	7	1.000	17	0.513	7	1.000
24	0.386	1.9	24	0.387	1.9	1.003	24	0.387	1.9	1.003
51	0.24	1.2	51	0.24	1.1	1.000	51	0.24	1.1	1.000

**Table 6-13: Top five modes in the vertical direction modal variation (Z-axis)**

6 m Link Slab Intervals (Control Model)			3 m Link Slab Intervals				Single Link Slab Shell Element			
Mode	Period, $T_{control}$ (s)	Modal Part. Factor (%)	Mode	Period, $T$ (s)	Modal Part. Factor (%)	$T/T_{control}$	Mode	Period, $T$ (s)	Modal Part. Factor (%)	$T/T_{control}$
7	0.721	5.8	7	0.712	5.8	0.998	7	0.712	5.8	0.988
15	0.56	3.9	15	0.56	3.9	1.000	15	0.56	3.9	1.000
18	0.505	4.1	18	0.506	4.1	1.002	18	0.506	4	1.002
20	0.469	3.9	20	0.469	4	1.000	20	0.469	4	1.000
44	0.263	6.1	44	0.263	6	1.000	44	0.263	6	1.000

### 6.5.2 Time-history Analysis – Link Slab

The results of the time-history analyses confirm the data presented by the modal analyses. Both the stresses and the displacements of the superstructure are congruent, with variations of less than 0.1%. The variations in results are minimal such that Figure 6-14 and Figure 6-15 appear to display results from a single analysis. The analyses suggest that the number of elements and nodes when modeling the link slab for a linear analysis does not impact the dynamic behavior of the model as long as the boundary conditions for the shell elements are consistent.

Although the results between the control model and the additional link slab modeling variants suggest that shell interval size is irrelevant, note that the scope of this study focused on linear time-history analyses. Linear analysis assumes a direct correlation between applied forces and resulting displacements and stresses. A nonlinear time-history analysis would account for material nonlinearity as the concrete cracks and the steel yields. Increasing the number of intervals and elements in a nonlinear analysis typically provides more accurate results.

The design plans intended for the link slab to be integral with the deck. This initial assumption is a crucial factor when calibrating the FEA model to actual dynamic behavior. The 2018 Bridge Inspection Report did not note any significant cracking in the link slab, likely confirming that the components are behaving as intended (NDOT, 2018). Damage from routine service loads or extreme seismic activity could result in the inefficient transfer of forces between the link slab and

bridge decks. To replicate such behavior, shell boundary conditions at locations of interest would have to be released accordingly.

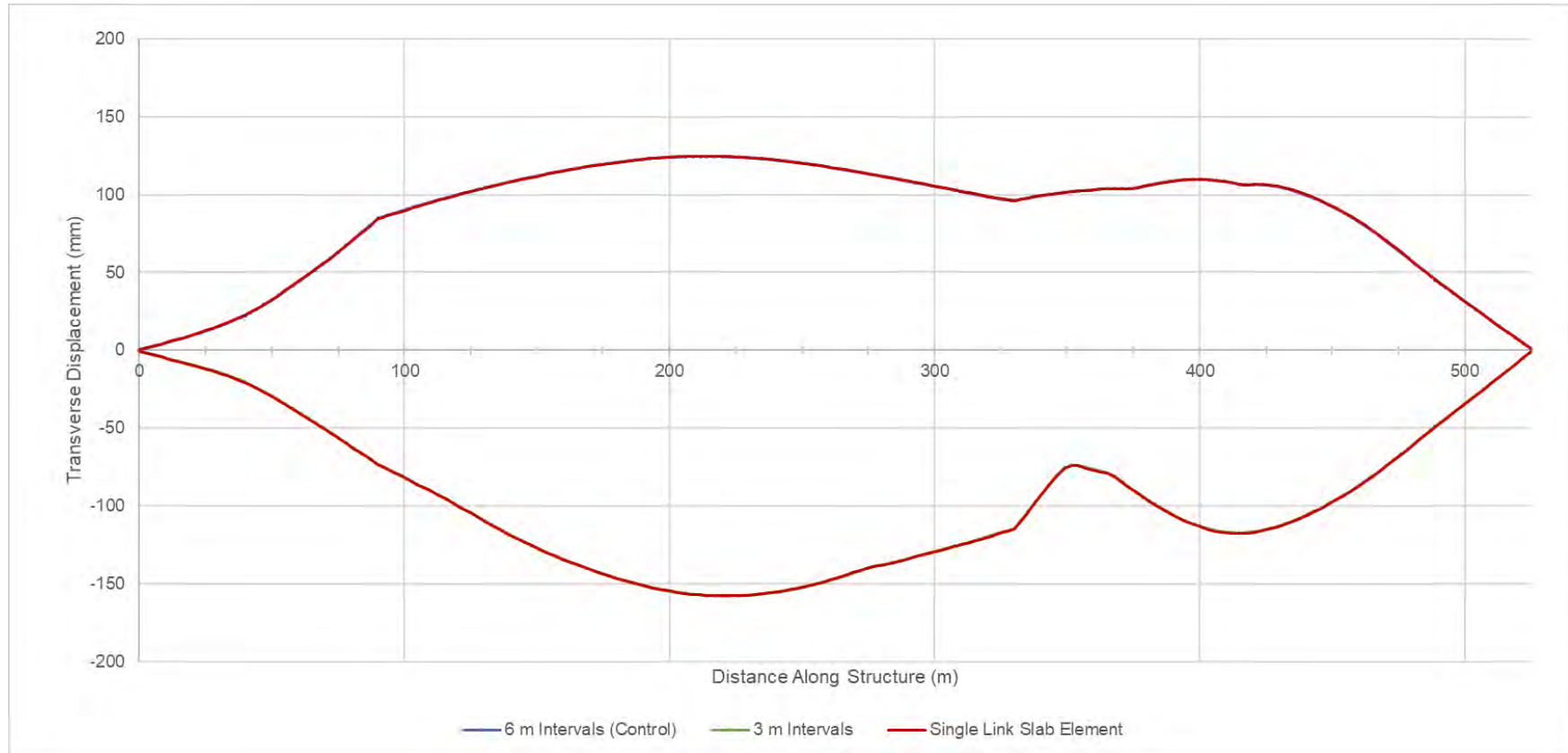


**Figure 6-14: Maximum transverse displacement of superstructures for link slab analyses**

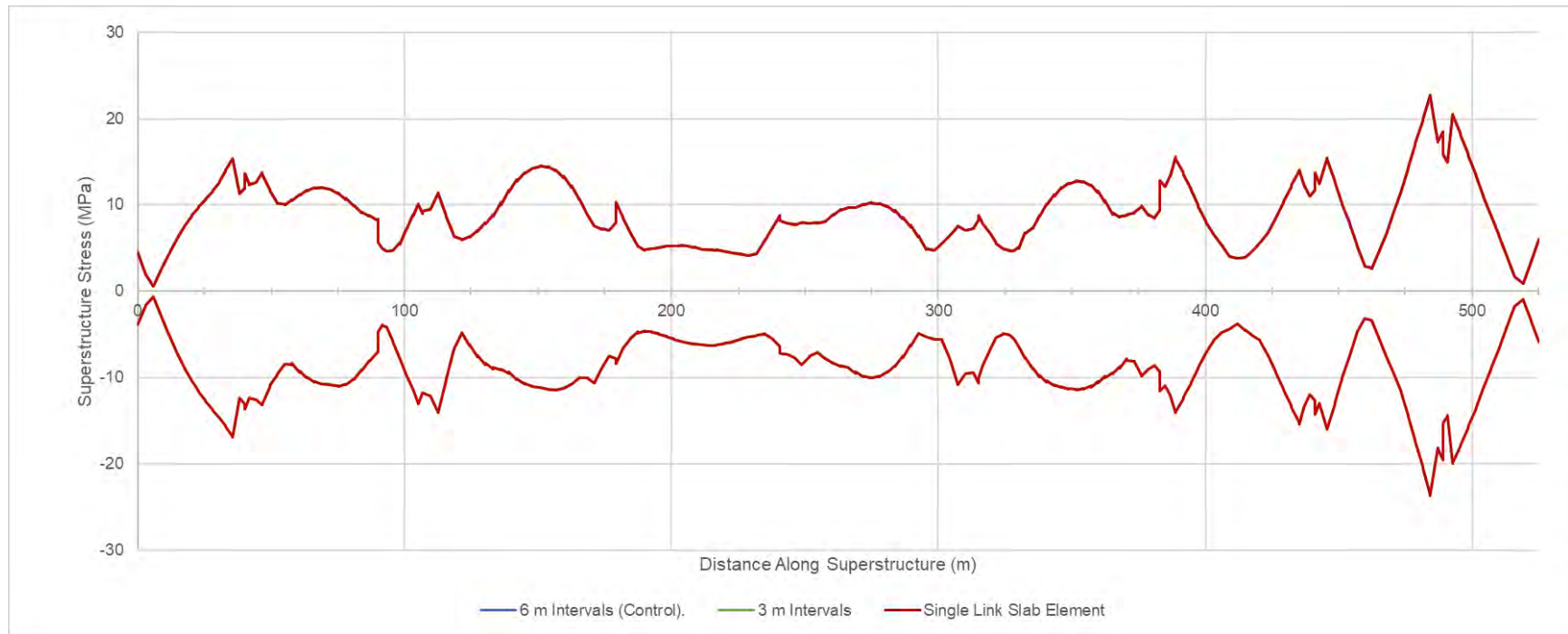


**Figure 6-15: Maximum superstructures stresses for link slab analyses**

## 6.6 Superstructure Modeling Approach

The control model defined the superstructure as an assembly of shell elements. The shell approach was selected to be computationally efficient yet produce reasonable results. Specifically, modeling the superstructure as shell elements would provide more accurate results than a spine frame structure. Further, the approach would yield similar results to a solid model at faster computational times. This study investigated these assumptions by defining the superstructure as using each modeling approach.

In addition to comparing the results to the control model, the spine frame model analyses results were compared to the 2013 study on the Galena Creek Bridge. The work performed by Carr and Sanders developed a SAP2000 FEA model to estimate modal properties. SAP2000 was limited to defining the superstructure as a series of frame elements. When using frame elements, the 3D representation of the model exists solely for visual purposes; as such, nodes are not generated at the edge of the deck (i.e., where the link slab connects to the box girder superstructure). The previous study simulated the connection between the northbound and southbound structures, which are spaced 20.92 m apart, using a combination of rigid links and shell elements. The rigid link elements extend from the superstructure spine, marking the centerline of the box girder, 9.45 m towards the adjacent structure, leaving a 2.02 m gap between the end nodes. The link slab shell elements then connect on either side to the rigid links, as can be seen in Figure 6-16. It should be noted that the spacing of the rigid links is not uniform, as can be seen in Figure 6-17. Based on a comparison of the model to the bridge plans, it is assumed this approach was taken to account for the additional reinforcing bars used at key locations in the structure (e.g., the arch-superstructure merge region and the hinge and pier diaphragms).

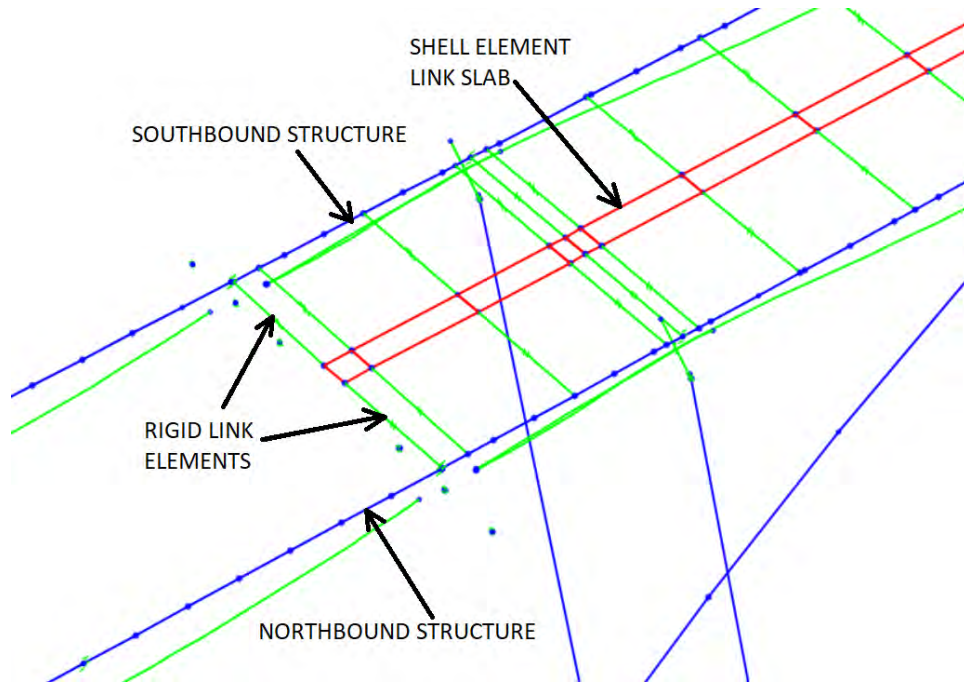


**Figure 6-16: Example of frame spine model using rigid links that extend to link slab shell**

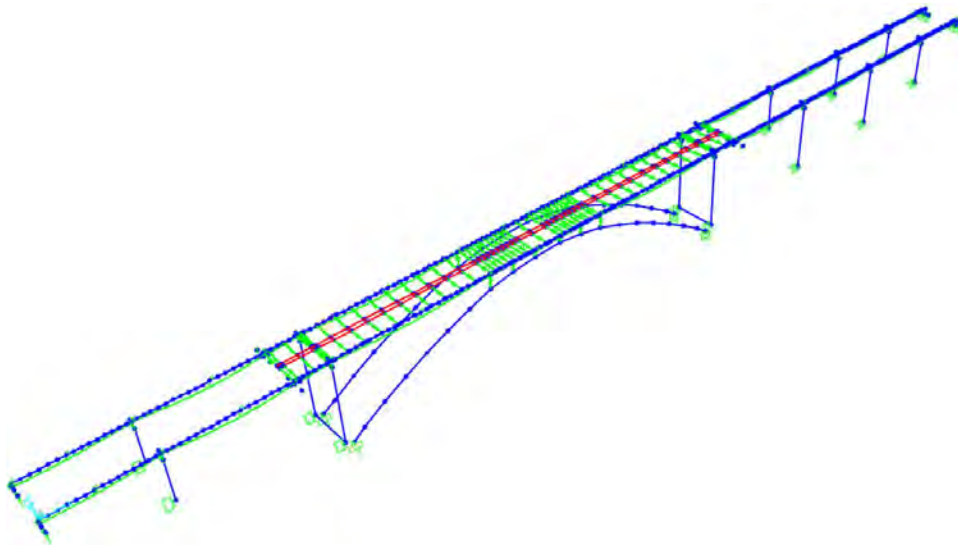


**Figure 6-17: Frame spine superstructure model to replicate the 2013 UNR SAP2000 model**

This evaluation also considered defining the superstructure using solid elements. In FEA, solid elements are a direct 3D representation of the component being modeled. Analyses are performed by modeling the desired material between the defined nodes of the 3D component. In contrast, shell elements are a 2D representation of 3D elements. When 3D features are simplified into 2D

elements, the analysis is also subsequently simplified. Shell elements were initially used to define the control model to reduce computational times for the various variant models analyzed. A superstructure consisting of solid elements was expected to be a more accurate representation of the Galena Creek Bridge.

As stated in Section 5.5.8, Update feature under the Bridge tab controls the modeling method used to develop the bridge object superstructure. Note that redefining the bridge using the Update feature only accounts for definitions from the Components tab. After generating the spine frame model, the connection between the superstructure and arch had to be redefined. Like the control model, six vertical rigid link elements were used between the fillet diaphragms to simulate the merge between the arch and the superstructure

#### *6.6.1 Modal Analysis*

The use of rigid link elements to simulate the bridge deck resulted in additional stiffness when compared to the control model. Most of the modes considered in Table 6-14 – 6.16 exhibited decreased periods in relation to the control model. The most notable difference was the 20% decrease in modal period of primary transverse mode (Mode 1). It was noted that several of the modes considered in the transverse and vertical directions demonstrated increases compared to those of the control model. This is likely a result of the non-uniform spacing of the link elements along the length of the structure. The less stiff areas of Frame 2, such as between the arch crown and Pier 2, would be prone to higher distortions under loading.

In contrast, the modal analyses of the solid superstructure model remained relatively like that of the control model. The top five modes about all three degrees of freedom experienced an average variation of 1.5%. The most significant increase was a 36% increase (0.086 seconds) in Mode 51, suggesting that the shell model slightly underpredicted the lateral excitation of the bridge system.

**Table 6-14: Comparison of top longitudinal modes for superstructure modeling variation (X-axis)**



Shell Element Superstructure (Control Model)			Spine Frame Superstructure				Solid Element Superstructure			
Mode	Period, $T_{control}$ (s)	Modal Part. Factor (%)	Mode	Period, $T$ (s)	Modal Part. Factor (%)	$T/T_{control}$	Mode	Period, $T$ (s)	Modal Part. Factor (%)	$T/T_{control}$
2	1.342	12.3	2	1.315	12.3	0.979	2	1.343	12.4	1.001
4	0.976	15.1	3	0.932	14.8	0.954	4	0.999	14.7	1.023
9	0.671	9.2	9	0.613	9.5	0.913	10	0.667	11.3	0.994
11	0.627	9.8	10	0.590	7.7	0.942	12	0.631	10.0	1.008
39	0.284	9.3	32	0.274	16.1	0.966	39	0.283	16.6	0.995

**Table 6-15: Comparison of top transverse modes for superstructure modeling variation (Y-axis)**

Shell Element Superstructure (Control Model)			Spine Frame Superstructure				Solid Element Superstructure			
Mode	Period, $T_{control}$ (s)	Modal Part. Factor (%)	Mode	Period, $T$ (s)	Modal Part. Factor (%)	$T/T_{control}$	Mode	Period, $T$ (s)	Modal Part. Factor (%)	$T/T_{control}$
1	1.688	55.0	1	1.349	52.2	0.799	1	1.678	31.5	0.994
5	0.819	9.5	5	0.784	8.6	0.958	5	0.808	5.8	0.987
17	0.513	7.0	8	0.621	3.1	1.210	18	0.502	4.0	0.979
24	0.386	1.9	13	0.500	8.8	1.293	22	0.427	0.6	1.106
51	0.240	1.2	33	0.272	2.2	1.134	34	0.326	1.0	1.359

**Table 6-16: Comparison of top vertical modes for superstructure modeling variation (Z-axis)**

Shell Element Superstructure (Control Model)			Spine Frame Superstructure				Solid Element Superstructure			
Mode	Period, $T_{control}$ (s)	Modal Part. Factor (%)	Mode	Period, $T$ (s)	Modal Part. Factor (%)	$T/T_{control}$	Mode	Period, $T$ (s)	Modal Part. Factor (%)	$T/T_{control}$
7	0.721	5.8	7	0.657	8.2	0.922	9	0.709	0.2	0.995
15	0.56	3.9	10	0.590	5.2	1.054	15	0.562	0.3	1.004
18	0.505	4.1	14	0.475	7.9	0.939	17	0.508	0.3	1.004
20	0.469	3.9	16	0.433	7.6	0.923	20	0.469	0.2	0.999
44	0.263	6.1	38	0.242	8.0	0.918	43	0.261	0.4	0.990

The modal analysis of the spine frame model was dissimilar to the modal information documented from the 2013 study performed by Carr and Sanders. As seen in Table 6-17, the spine frame variant was considerably stiffer than the 2013 SAP2000 model, with the modal periods of the top transverse modes of the spine frame model an average of 23.3% lower than those of the SAP2000 model. These discrepancies can be explained by the fact the SAP2000 model assumed a decreased cracked MOI for the columns whereas the CSiBridge models were defined using the gross MOI.

**Table 6-17: Comparison of top transverse modes: 2013 SAP2000 model vs spine frame**

2013 SAP2000 Model (Carr and Sanders)			Frame Spine Superstructure			
Mode	Period, $T_{control}$ (s)	Modal Part. Factor (%)	Mode	Period, $T$ (s)	Modal Part. Factor (%)	$T/T_{control}$
1	1.650	38.9	1	1.349	52.2	0.817
5	0.990	4.1	5	0.784	8.6	0.792
10	0.720	5.5	8	0.621	3.1	0.862
11	0.670	0.9	13	0.500	8.8	0.746
32	0.320	1.1	33	0.272	2.2	0.851

### 6.6.2 Time-History Analysis

The results of the time-history analysis revealed that the spine frame model demonstrated increased transverse displacement at Frames 1 and 2 of the model, but significantly decreased displacements at Frame 3 (Figure 6-19). The midspan of the arch experienced the greatest increase in transverse displacement of up to 60%. In contrast, Span 4 of the frame spine model experienced up to 22% less transverse displacement than the control model. As the most significant changes in transverse deflection were at Frame 2, it is likely that the variations are a result of the means of modeling the link slab as opposed to the superstructure itself. It was noted in Section 6.5 that the shell intervals for modeling the link slab was not a factor on the modal properties of the FEA model. The continuous fixed connection between the edges of the link slab and superstructure shell elements provided a fluid transfer of stresses between the adjacent elements, regardless of the number of shell segments used. When the link slab is supported by an intermittent series of rigid links, it behaves similar to a one-way slab and loses stiffness. This loss of stiffness resulted in the sharp increase in deformations in Frame 2 of the variant model.

It is likely that decreasing the interval size between rigid links would not yield more reliable results. The rigid links attached to the resulted in a sharp decrease in the modal periods of the top transverse modes. The inclusion of additional link elements would further decrease the modal periods without realistically simulating the flow of stresses between the superstructure and link slab. Unfortunately, redefining the superstructure as a spine frame inevitably changes the modeling method for the link slab, meaning this modeling method cannot be tested as an independent variable. Although the influence of a spine frame model is inconclusive, these results show that the rigid link element approach was not an appropriate method of modeling the connection between the northbound and southbound structures.

The results of subjecting the solid superstructure model to the El Centro earthquake ground motions corroborate the information from the modal analyses. Figure 6-18 –Figure 6-20 show that the envelope displacements about all three axes are nearly identical. As noted in previous section, the most notable change was an increase in transverse participation factor of Mode 51. Spans 6 and 7 reflect this change in modal behavior by exhibiting a slight increase in maximum lateral displacement of up to 5 mm from the control model.

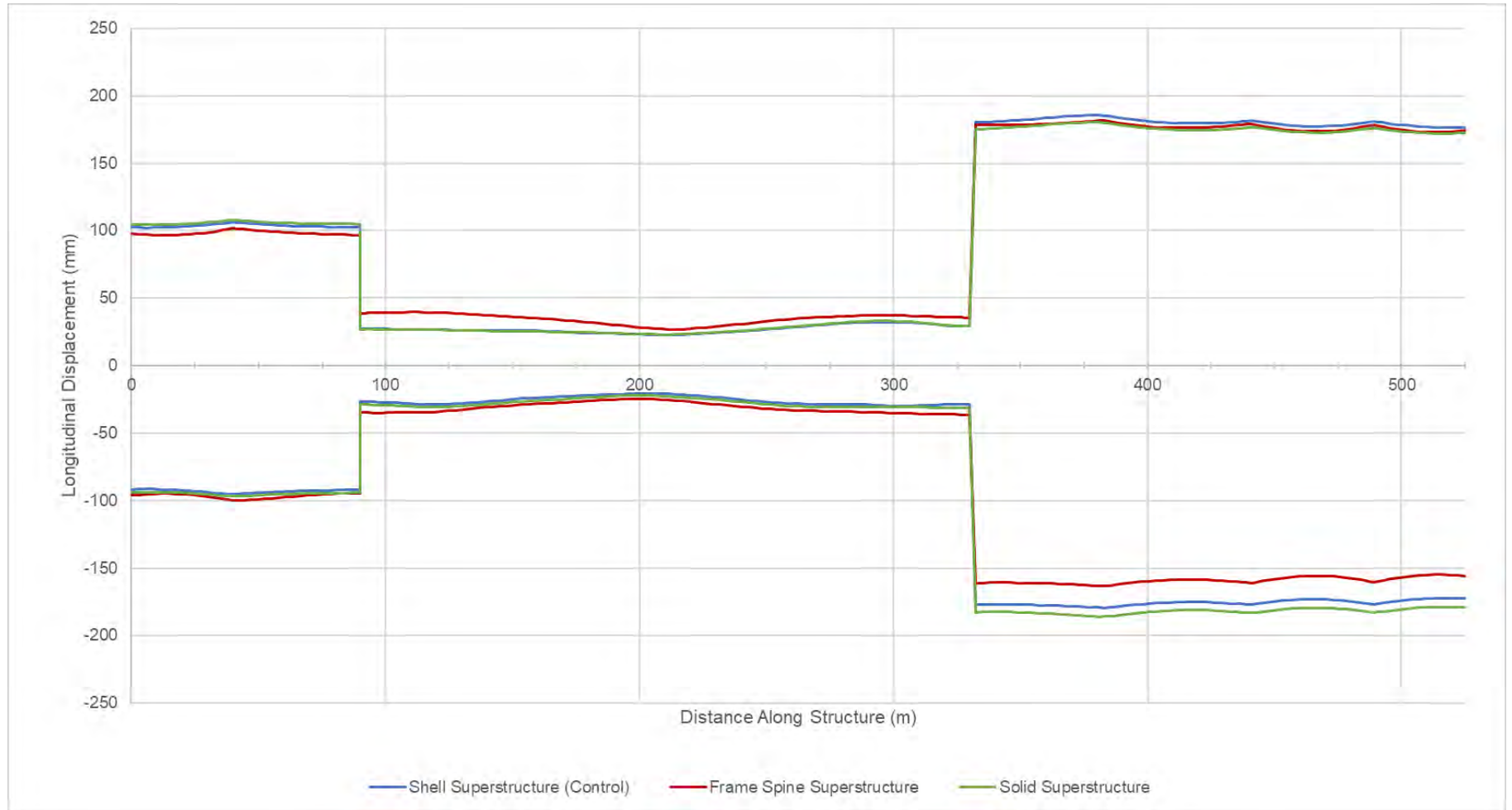


**Figure 6-18: Envelope of longitudinal displacement of superstructures for shell vs solid superstructure analyses (X-axis)**

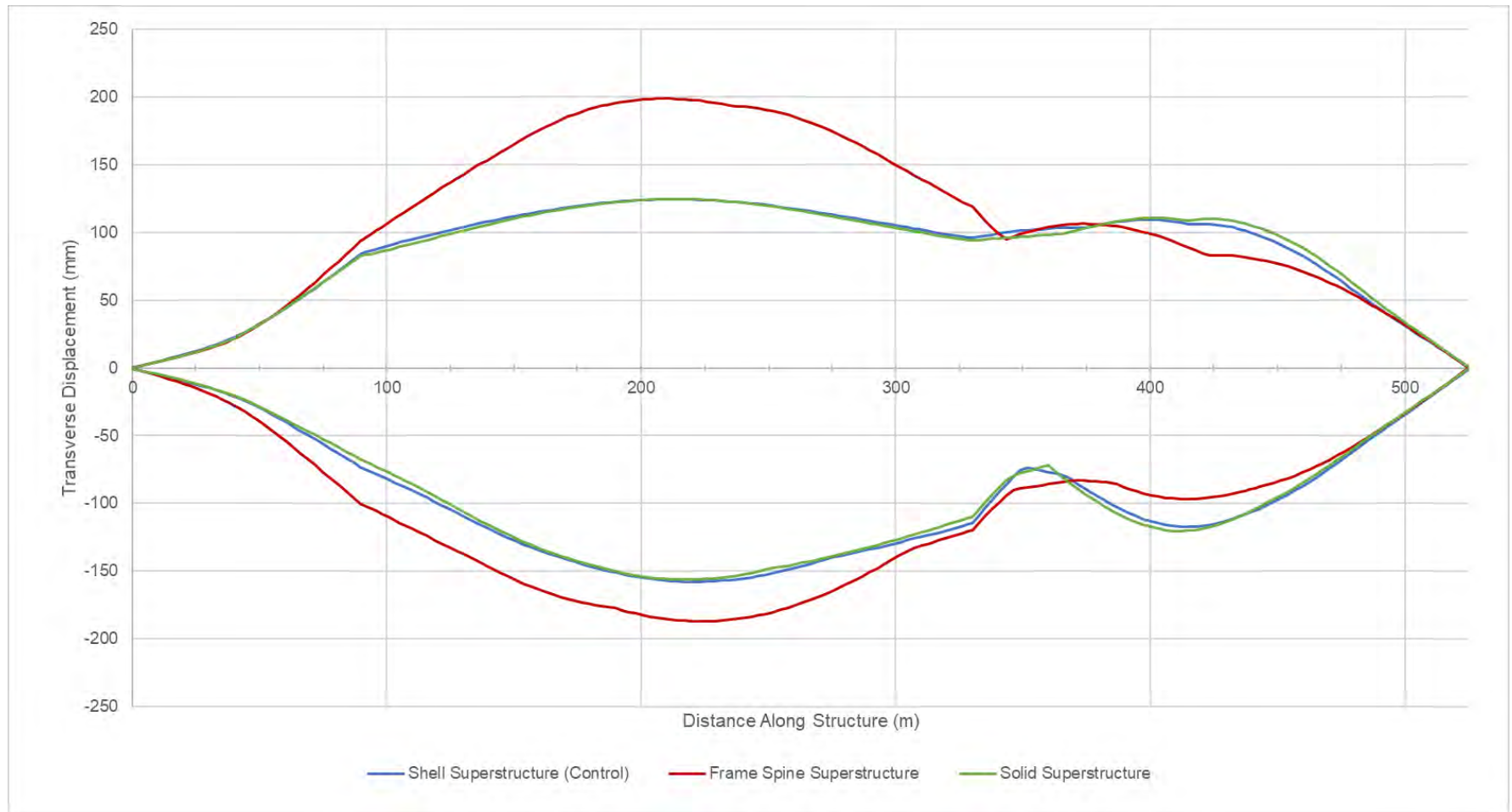


**Figure 6-19: Envelope of transverse displacement of superstructures for shell vs solid superstructure analyses (Y-axis)**

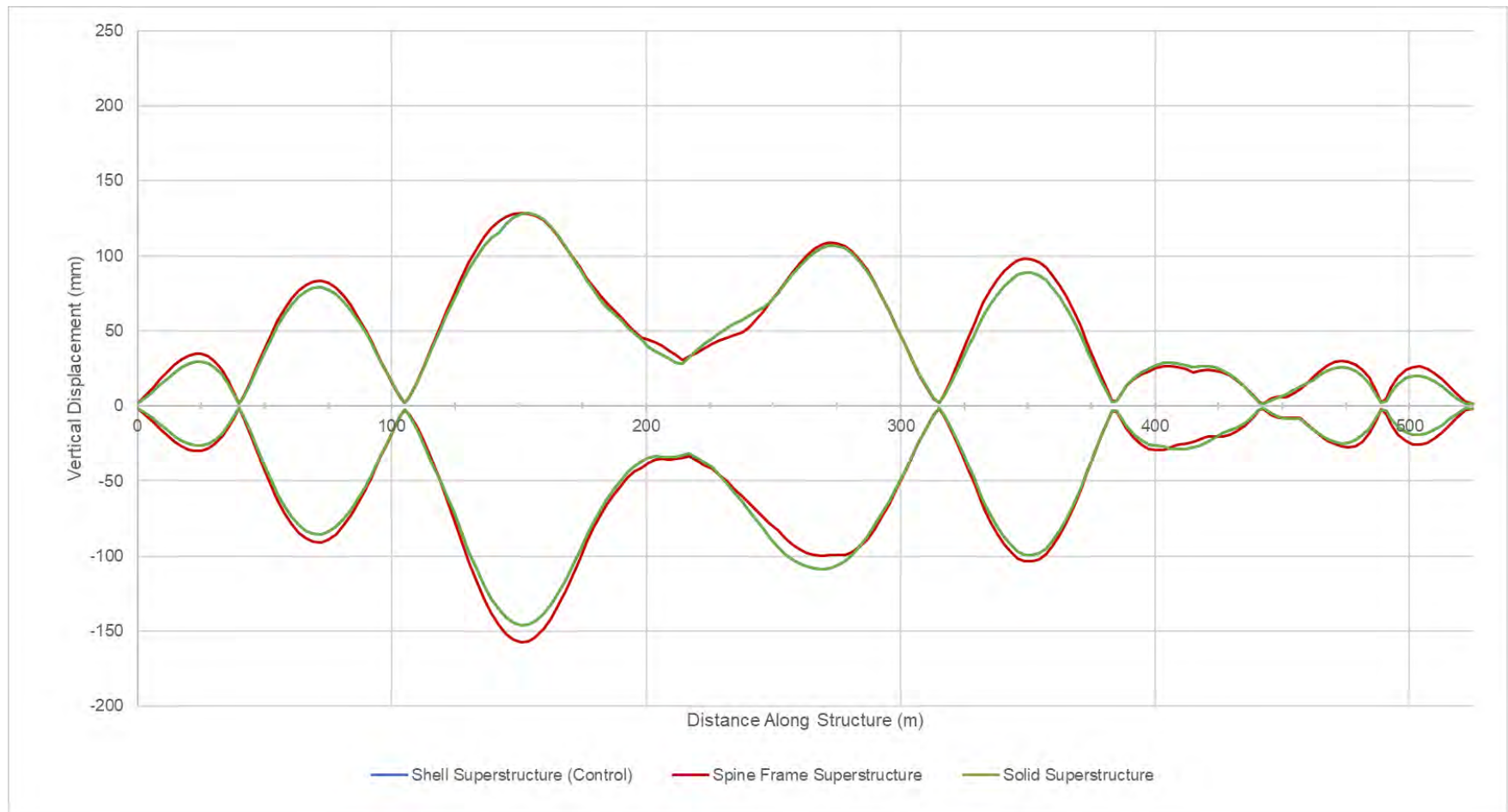


**Figure 6-20: Envelope of vertical displacement of superstructures for shell vs solid superstructure analyses (Z-axis)**

The conclusion drawn from performing the modal and time-history analyses suggests that the shell superstructure used in the control model definitions was an effective approach to modeling. As previously mentioned, shell elements are a means to simplify 3D structures using a 2D model. From a visual standpoint, the concrete box girder is a compilation of simple, thin geometric shapes. The geometric shapes range from a thickness of 0.2 – 0.6 m. As such, these relatively thin components allowed for shell elements to be an effective means of modeling the superstructure, as seen in Figure 6-21. The trivial discrepancies are likely a result of the increased number of mesh intervals used for analyzing solid elements as compared to shell elements.

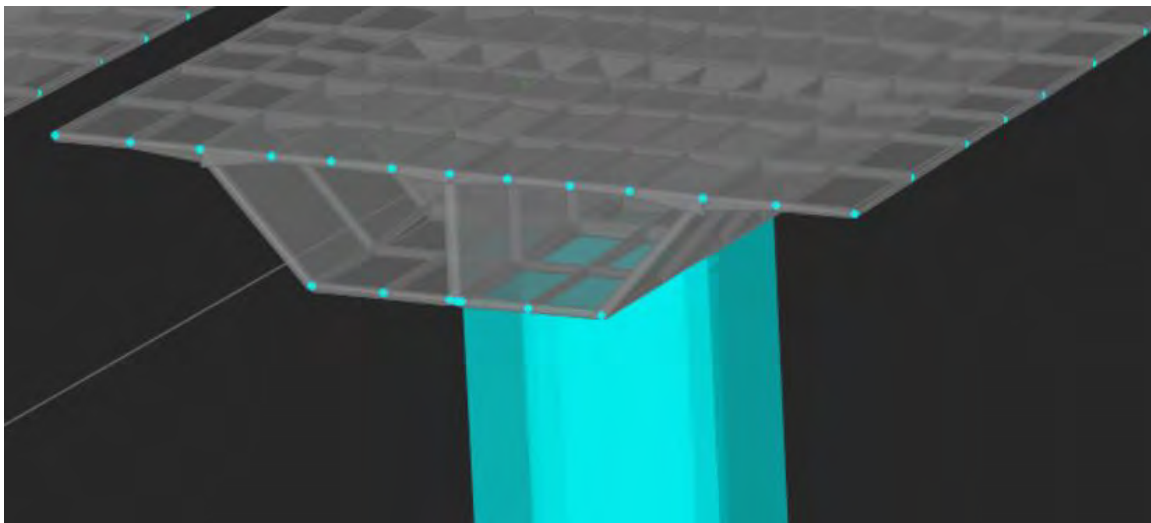


**Figure 6-21: Superstructure of control model made up of shell elements**

## **6.7 Barrier Rail Modeling**

Parapets are not typically considered structural elements for bridge design. While this leads to conservative calculations for load bearing capacity, it does not accurately reflect the stiffness and dynamic properties of in-service structures. The control model considers the weight of the barrier rail as a line load applied at the edges of the bridge deck. The line loads are defined as a mass for modal analyses and, subsequently, time-history analyses. To determine the possible influence of the secondary structural elements, a custom frame element was defined and modeled along the edge of the deck to represent the barrier rail (i.e., the lighter teal colored element at edge of deck in Figure 6-22). For this modeling approach, the barrier rail line load was removed from the deck definition portion of the Components tab and from the mass source definition of the Advanced tab.

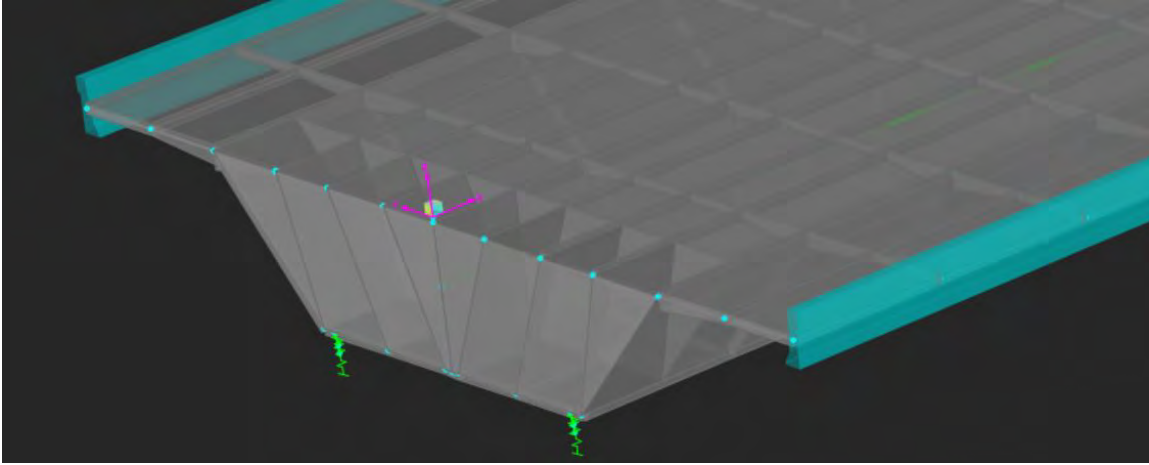


**Figure 6-22: Barrier rail frame elements drawn along deck edges**

The barrier rail frame was a user defined component created in the Section Designer tool under the Components tab, as seen in Figure 6-23. The barrier rails were modeled along the edge of the 2D bridge deck shell elements using the Draw Frame tool under the Advanced tab. It was assumed that the 20 mm chamfers used to blunt the top edges of the barrier had negligible impact on the stiffness and dead load of the superstructure and were not modeled when defining the parapet shape. Note that linear frame elements model the component around the center of gravity of the cross section, which was automatically defined by the Section Designer tool, as can be seen in Figure 6-23. Adding the barrier rail as additional frame elements would not model them as perfectly integral with the deck. To best simulate this connection, the frame elements were drawn along every node of the superstructure deck shell elements. The existing barrier rail of the Galena Creek Bridge has expansion joints intermittently located along the length of the structure. The initial modeling approach assumed a continuous parapet with no expansion joints; therefore, all the connections between the elements were modeled as rigid joints. This method was applied to provide an upper limit on the additional stiffness a barrier could provide, while the control model represented the designed condition of no additional stiffness from the barrier.



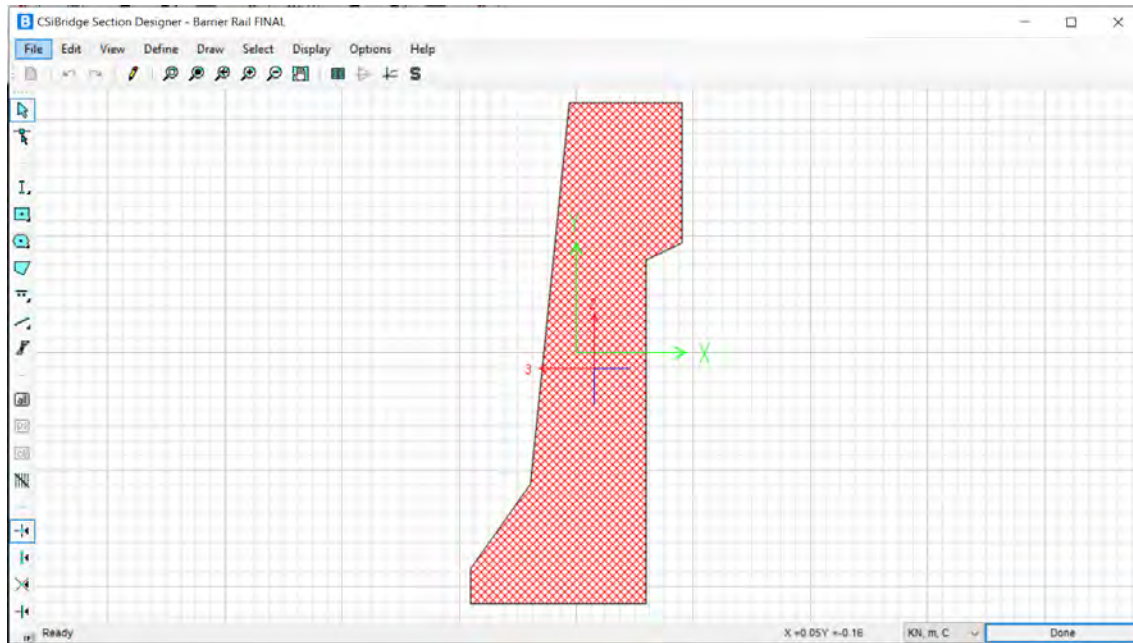


**Figure 6-23: Barrier rail cross section defined using Section Designer in CSiBridge**

#### 6.7.1 Modal Analysis – Barrier Rail Modelled as Frame Elements

The inclusion of the barrier rail as a frame element to the model was expected to increase the superstructure stiffness and reduce deflection, specifically in the vertical and transverse axes. It was anticipated that the barrier rail frame elements would act similar to flanges when resisting moments about the vertical axis and subsequently decrease translation. Additionally, the vertical orientation of the barrier rails would resist moments about the global y-axis and reduce vertical displacements. The general increase in stiffness to the superstructure from the frame elements was expected to reduce the modal periods about all three degrees of freedom.

The modal analyses suggested that modeling the barrier rail as a frame element had a negligible impact on the dynamic properties of the FEA model. Although 13 of the 15 modes considered in Tables 6.18 – 6.20 decreased in modal periods, the average reduction was incremental (less than 0.7%). Typically, the influence of barrier rails on load bearing capacity of a bridge diminished as the size and complexity of the structure increases (Akinci, Liu and Bowman, 2008). The 525 m long, seven span, cathedral arch Galena Creek Bridge is far larger and more complex than any of those considered in the literature. As such, it is logical to assume that the impact of from the barrier rail on the dynamic properties is negligible.

**Table 6-18: Comparison of top longitudinal modes for barrier rail variation (X-axis)**

Barrier Rail Line Load (Control Model)			Barrier Rail as Frame Element			
Mode	Period, $T_{control}$ (s)	Modal Part. Factor (%)	Mode	Period, $T$ (s)	Modal Part. Factor (%)	$T/T_{control}$
2	1.342	12.3%	2	1.335	12.3%	0.995
4	0.977	15.1%	4	0.977	15.1%	1.001
9	0.671	9.4%	9	0.669	9.3%	0.997
11	0.627	9.8%	11	0.625	10.3%	0.997
39	0.284	9.7%	39	0.283	12.3%	0.997

**Table 6-19: Comparison of top transverse modes for barrier rail variation (Y-axis)**

Barrier Rail Line Load (Control Model)			Barrier Rail as Frame Element			
Mode	Period, $T_{control}$ (s)	Modal Part. Factor (%)	Mode	Period, $T$ (s)	Modal Part. Factor (%)	$T/T_{control}$
1	1.688	55.0%	1	1.665	55.7%	0.986
5	0.819	9.5%	5	0.802	9.3%	0.979
17	0.513	7.0%	17	0.509	6.5%	0.992
24	0.386	1.9%	24	0.386	2.0%	0.999
51	0.240	1.2%	51	0.242	1.8%	1.008

**Table 6-20: Comparison of top vertical modes for barrier rail variation (Z-axis)**

Barrier Rail Line Load (Control Model)			Barrier Rail as Frame Element			
Mode	Period, $T_{control}$ (s)	Modal Part. Factor (%)	Mode	Period, $T$ (s)	Modal Part. Factor (%)	$T/T_{control}$
7	0.713	5.8%	7	0.709	7.0%	0.995
15	0.560	3.9%	15	0.557	3.8%	0.995
18	0.506	4.1%	18	0.502	4.1%	0.992
20	0.469	3.9%	20	0.466	4.2%	0.993
44	0.263	6.1%	44	0.262	5.3%	0.997

### 6.7.2 Time-history Analysis – Barrier Rail Modelled using Frame Elements

The results from the time-history analyses corroborate the results of the modal analyses; incorporating barrier rails as frame elements did not decrease superstructure displacements and stresses as expected. Prior sections have revealed that the longitudinal behavior is controlled by the substructure and bearings. This behavior is further confirmed by Figure 6-26 which shows that modeling barrier rails had no notable impact on the longitudinal displacements. Rather than provide resistance to vertical displacements, several locations along the structure actually experienced greater displacements. Figure 6-24 shows that the superstructure of the variant model experienced up to 11 mm more vertical displacement at Span 3 and up to 14 mm at Span 1 than the control model. The transverse displacement of the superstructure, shown in Figure 6-25, reveals up to an 8 mm reduction in offset along Frame 2. However, this behavior is not consistent along the length of the structure as displacements at both Span 1 and Span 4 of the variant model are greater than that of the control model by up to 14 mm.

Previous research on the influence of barrier rails as secondary structural elements observed changes in girder moment distribution factors, and thus internal stresses, as opposed to displacement. Figure 6-27 compares the stresses in the superstructure between the control model and the barrier rail variant. Rather than the expected decrease in internal stresses, the variant model showed identical internal stresses to the control model. At several sections of Frames 1 and 3, the variant model experienced marginally greater stresses of up to 2.5 MPa. Frames 1 and 3 of the

bridge are supported by shorter columns than Frame 2 and, as a result, are stiffer. It is likely that this approach to modeling the barrier rail caused a greater increase in stresses at locations of the superstructure that were already relatively stiff. This behavior contradicts the expected decrease in girder stresses when modeling the barrier rail.

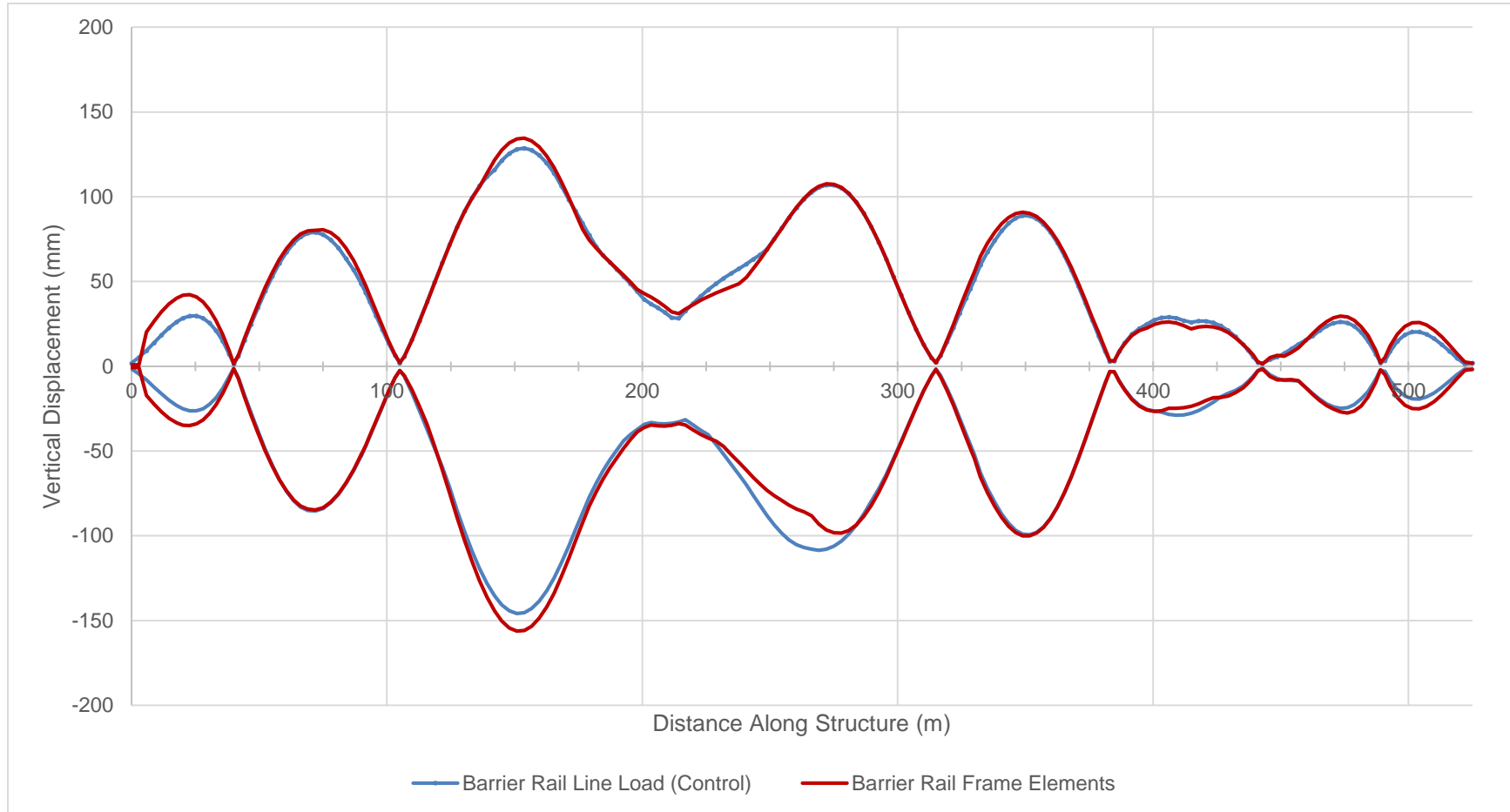


**Figure 6-24: Envelope of maximum vertical displacement of superstructures for parapet analyses**

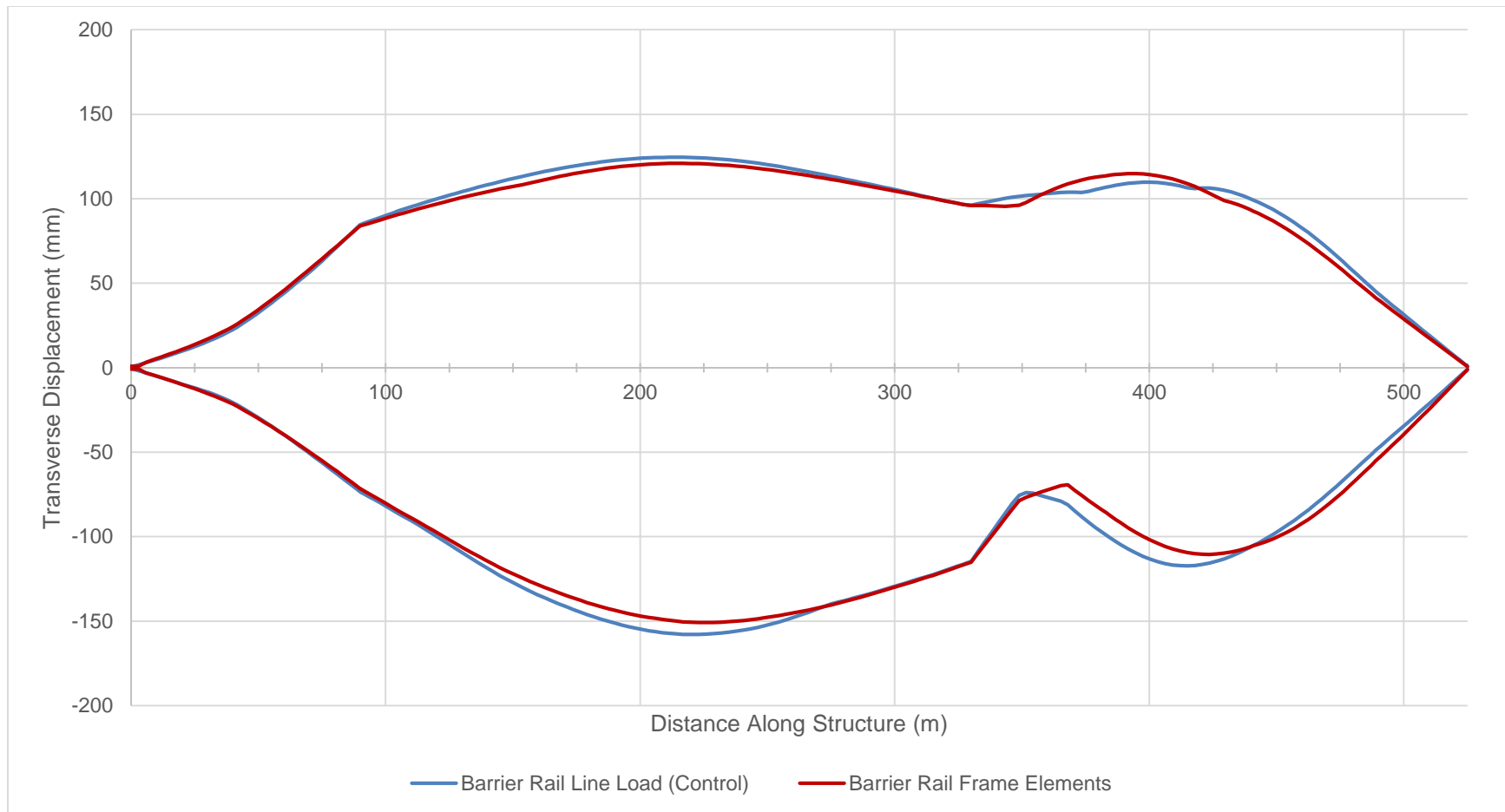


**Figure 6-25: Envelope maximum transverse displacement of superstructures for parapet analyses**

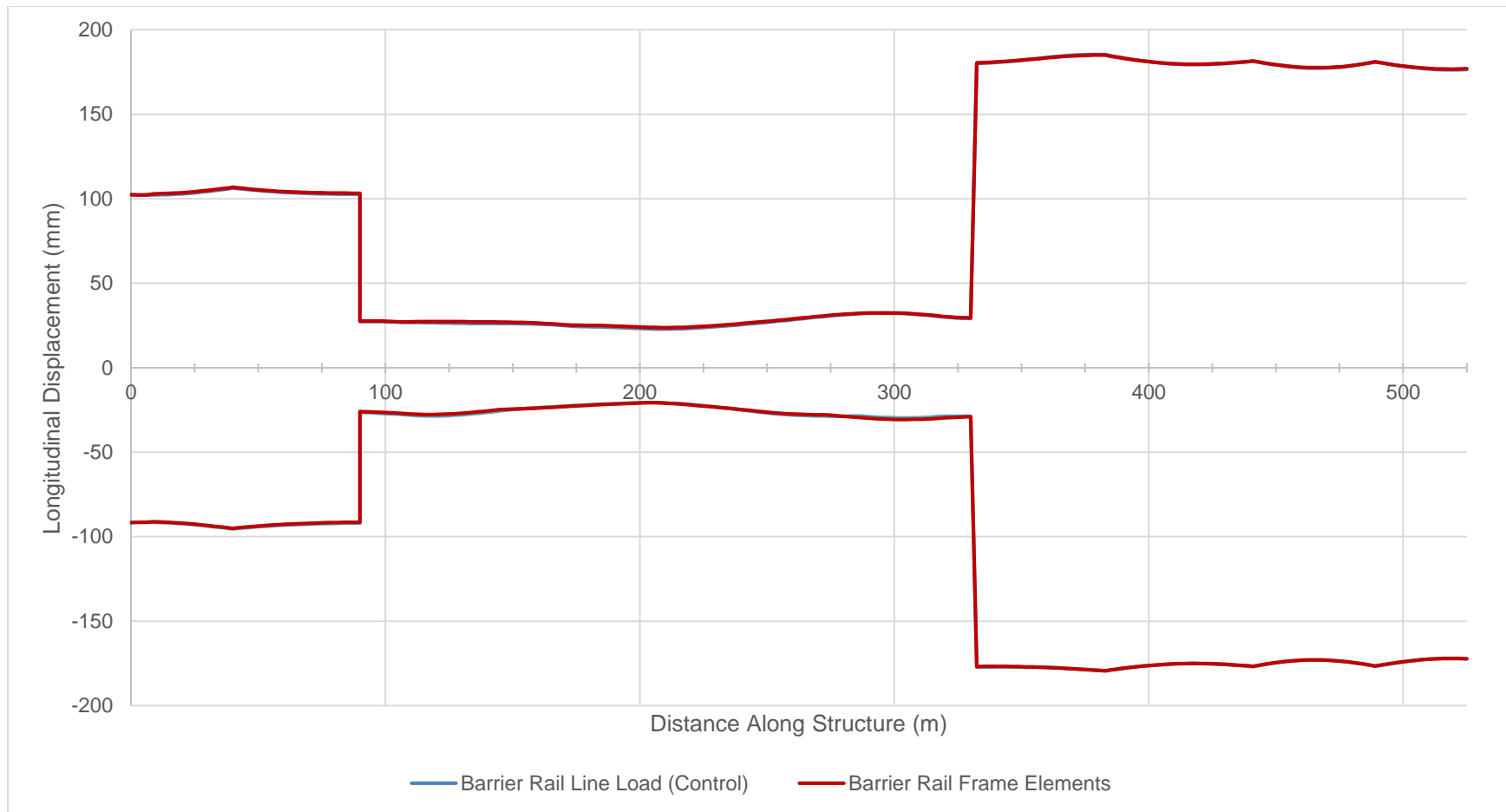


**Figure 6-26: Envelope maximum longitudinal displacement of superstructures for parapet analyses**

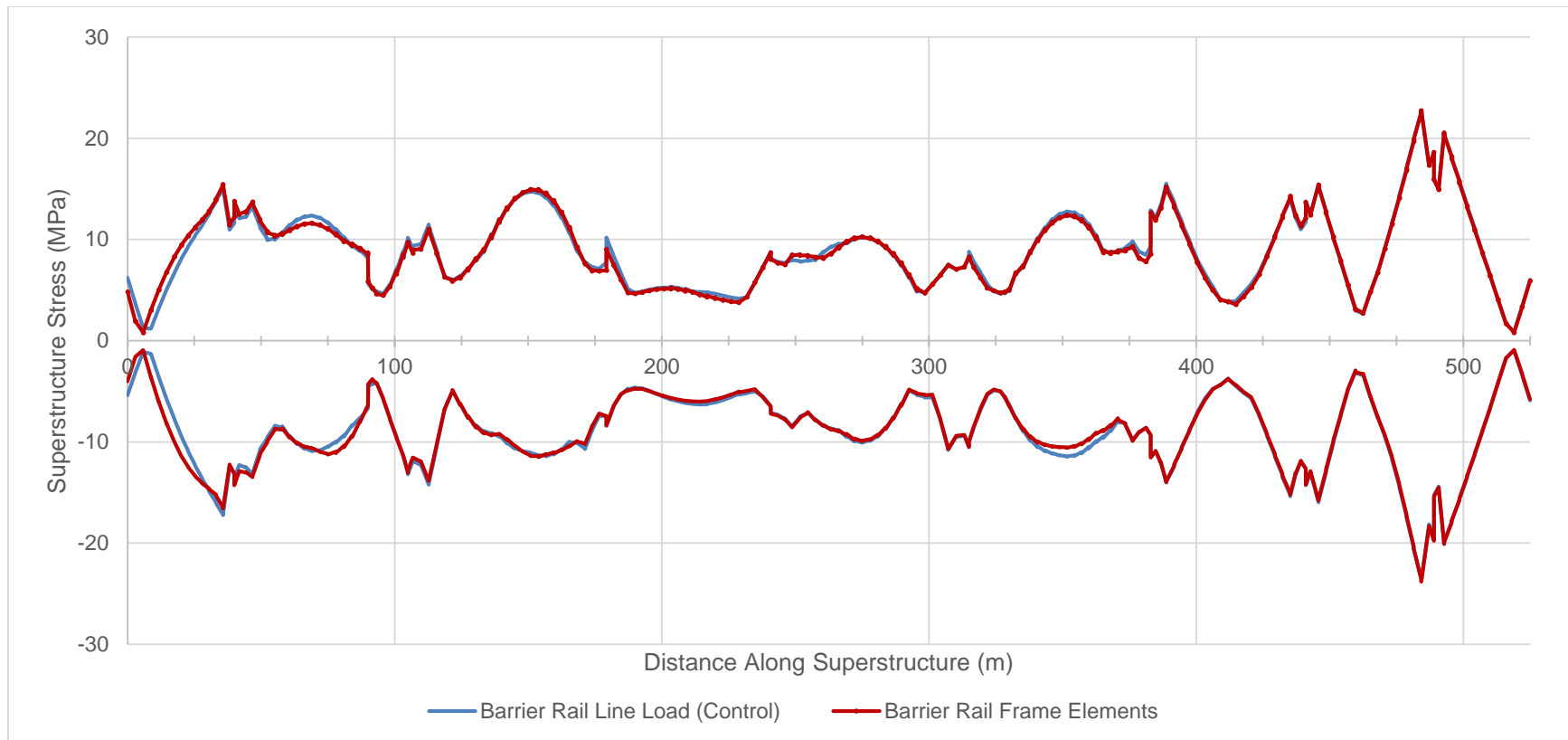


**Figure 6-27: Envelope maximum stresses in superstructure for parapet analyses**



Modeling the barrier rail as frame elements did not produce the expected results typical of their influence as secondary structural elements. One of the primary assumptions for this modeling approach was the transfer of shear flow between the parapet and the deck due to the substantial transverse reinforcing connecting the elements. It appears likely that modeling them in intervals along the nodes of the superstructure did not replicate the behavior of a continuous connection, in spite of their common degrees of freedoms at the nodes.

Additionally, previous research indicates that discontinuities in the barrier rail resulted in stress concentrations in both areas of positive and negative moment (Akinci, 2008). Further examination of the influence of barrier rails on the Galena Creek Bridge would require replicating the expansion joints and discontinuities in the barrier rail along the length of the bridge. Leaving gaps between the frame elements at joint locations would simulate this behavior. Another option would be to simply release the rotational boundary constraints of the 2D frame elements at joint locations. Note that most barrier rail segments measured between 11.7 m and 18.4 m between expansion joints. As the continuous barrier rail addition had a nominal impact on the dynamic properties of the Galena Creek Bridge FEA model, it is assumed that incorporating the expansion joints, rather than resulting in stress concentrations, would further mitigate the impact of this method of modeling the barrier rail.

## CHAPTER 7. REFINED FINAL MODEL

A refined CSiBridge model was developed using the results from the parametric study. The final model is intended to be a platform upon which to further calibrate, based on field-measured data. As noted in the 2013 study performed by Carr and Sanders, using generic ground motion data for time-history analyses is an effective means to estimate dynamic response; however, appropriate ground motions recorded from the local area are required to accurately calibrate the model to the actual response. In the absence of the measured data, several modifications were incorporated to the control model in preparation for final tuning with measured data.

Several of the variables examined through the parametric study resulted in trivial solutions, meaning the influence of these factors on the dynamic properties of the bridge were negligible. Specifically, the link slab shell intervals, bearing stiffness, and superstructure modeling techniques were found to be adequate in the control model. However, the structural damping, substructure effective moment of inertia, and material stiffness parameters were found to need additional refinement for the proposed model. The following sections detail the trivial solutions and refined parameters.

### 7.1 Trivial Solutions

The link slab of the control model used shell element increments of up to 6.0 m long to simulate connection between the northbound and southbound structures. The parametric study evaluated the best way of modeling the connection between the two bridges by editing the length of the shell element intervals. Neither increasing the number of intervals nor replacing the intervals with a single element resulted in noticeable changes, typically under 0.5%. Unless a nonlinear time-history analyses is required to accurately capture the measured response, it was recommended that the approach to modeling the link slab remain consistent to that of the control model.

The shear modulus ( $G$ ) of the elastomer influences the stiffness of the bearing pads. The control model uses the lowest value for  $G = 0.90$  MPa, as recommended by AASHTO. A model variant using the highest recommended value ( $G = 1.38$  MPa) resulted in a maximum longitudinal displacement reduction of 9 mm. Further, the vertical and transverse displacement data between

the control model and stiff bearing variant were identical. As such, it was concluded that the bearing stiffness did not have a significant impact on the dynamic response of the bridge; therefore, the bearing stiffness values remained based on  $G = 0.90$  MPa.

Several modeling techniques were also considered for defining the superstructure. The control model employs shell elements to generate the superstructure, whereas the variant models considered the superstructure as a spine frame and solid elements. The modal results between the control model and solid element superstructure variant had minor discrepancies in lower modes, and the results from the time-history analyses were generally parallel. The vertical and longitudinal modes considered exhibited less than a 0.8% difference between the control model and the solid superstructure model. Performing a linear-time history analysis indicated that lateral excitation of the solid superstructure model demonstrated an average difference of 1.1% from the control model.

Results from the modal and time-history analyses for the spine frame model were not analogous to any of the other models. Due to the complexities of modeling the link slab with frame element superstructures, this approach to modeling the Galena Creek Bridge was determined to be unsuitable. Based on the agreement between the shell and solid elements, as well as computational efficiency of the shell element approach, it is recommended to model the superstructure using shell elements.

## **7.2 Structural Damping**

The 2018 bridge inspection report (NDOT, 2018) noted minor cracking on the observable area of the bridge, likely as a result of thermal expansion and contraction. Literature on damping properties of pristine concrete structures suggests that the damping likely ranges from 2% – 3% (Chopra, 2012). As the concrete elements sustain more damage, the damping ratio increases. Therefore, the initial assumption of 2% damping applied uniformly throughout the CSiBridge model may not be an accurate representation of the in-service structure.

Previous research on the Galena Creek Bridge performed vertical and lateral excitation tests (Carr and Sanders, 2013). It was noted during these experiments that the calculated damping for the horizontal and vertical tests were different. When applying lateral excitation using an eccentric mass shaker, damping ratios between 2.6% and 3.4% were recorded. Alternatively, applying

vertical excitation using a large construction vehicle resulted in damping ratios between 1.8% and 2.5%. As such, using different damping ratios for various material definitions would result in a more accurate model. As previously noted, the development of minor cracking suggests that the assigned values should be higher than the idealized 2% – 3% from literature. For the recommended model, the upper limits of the damping recorded during the 2013 study were considered: 3.4% damping would be applied to transverse and longitudinal directions and 2.5% damping would be applied in the vertical direction.

For this approach, different vertical and lateral damping ratios were applied. The results of the time-history analyses conducted during the parametric study proposed that the substructure components were the controlling elements for longitudinal and transverse behavior. This was best demonstrated in the relatively large changes in transverse displacement noted during the effective moment of inertia study. Conversely, the superstructure definition was the primary factor in vertical excitation, best exemplified in the study of various strength concretes for Spans 2 through 4. The conclusion was that applying one damping ratio to the substructure materials and another damping ratio to the superstructure and link slab materials would be the best approach to simulate the structural behavior. The box girder, barrier rails, and link slab are composed of 31 MPa concrete, with 40 MPa material used at select sections. The pier columns and arches are made of 28 MPa and 35 MPa concrete, respectively. The final model was updated by assigning damping values of 2.5% to the 31 MPa material and 3.4% to the 35 MPa and 28 MPa materials.

### **7.3 Effective Moment of Inertia of Substructure Elements**

As cracks propagate and grow, reinforced concrete elements suffer from a reduction in flexural rigidity. ACI suggests that when performing linear-elastic analyses, concrete cracking can be accounted for by applying a reduction factor to the moment of inertia (MOI) of the concrete member. ACI recommends reducing the MOI of a column to 70% to provide conservative estimates during the design process. While this conservative assumption aids in the safe design of structures, it does not represent the physical behavior of in-service structures.

Scaling factors were applied to the MOI of the substructure elements of the FEA model to better understand how substructure stiffness influenced the dynamic response. MOI scaling factors

between 100% and 50% were investigated in 5% increments, where 100% MOI defined the control model. Once a range of behavior had been established, the next step was to determine the extent of damage to the substructure of the existing bridge. The 2018 NDOT bridge inspection report noted the columns and arches typically demonstrated minor hairline cracking characteristic of routine service loads, with cracks up to 8 mm wide and spalling up to 27 mm deep. Cracking, however minor, adversely effects the effective MOI of the substructure components. The effective MOI of the arch and column frame elements was reduced to 95% to account for the minor cracking that was documented while providing a more realistic value than the conservative assumption of 70% proposed by ACI.

#### 7.4 Material Stiffness

The modulus of elasticity of the various elements of the Galena Creek Bridge were calculated as a function of the compressive strength of each material, with higher strength concretes having increased stiffness. Although CSiBridge currently does not offer means for the user to assign multiple material properties to a concrete box girder definition, the various models analyzed showed the influence of material stiffness on the dynamic response of the structure. As previously mentioned, the concrete strengths specified in the design plans are minimum requirements and it is highly likely that the actual material strengths of the Galena Creek Bridge are higher. To account for the compressive strength above the design value, the compressive strength and modulus of elasticity of the concrete materials used for the CSiBridge model were increased by a factor of 10%, as seen in Table 7-1. Note that this is an estimated value based typical data. Confirmation of this assumption would require access to the 28-day cylinder compression tests performed during the construction of the Galena Creek Bridge.

**Table 7-1: Final model concrete material propeties**

<b>Concrete Design Strength (MPa)</b>	<b>Factored Strength (MPa)</b>	<b>Factored Modulus of Elasticity (MPa)</b>
28	30.8	27,357
31	34.1	28,785
35	38.5	30,586

## 7.5 Final Proposed Modal Analysis

Classical damping was assumed for the CSiBridge model. As such, edits to the damping ratios would not impact the modal analysis. The material stiffness and substructure moment of inertia controlled the changes in modal results between the control model and final proposed model. The parametric study noted that decreasing the effective MOI of the substructure frame elements would predominantly result in an increase in transverse modal periods and participation factors. The longitudinal and vertical excitations were also influenced, but to a nominal degree (i.e., less than 1% among the top modes). Conversely, increasing the material stiffness of both the superstructure and substructure elements would result in lower modal periods about all three degrees of freedom. Comparing the top five modes about each axis in Tables 7.2 – 7.4 confirms these assumptions. The modal periods of the final model decreased along all three axes, with the exception of a single transverse mode, likely a result of decreasing the effective MOI of the substructure frame elements.

**Table 7-2: Comparison of top longitudinal modes for control vs final model (X-axis)**

Control Model			Final Model			
Mode	Period, $T_{control}$ (s)	Modal Part. Factor (%)	Mode	Period, $T$ (s)	Modal Part. Factor (%)	$T/T_{control}$
2	1.342	12.3	2	1.300	12.3	0.969
4	0.976	15.1	4	0.950	15.1	0.973
9	0.671	9.2	9	0.647	10.4	0.964
11	0.627	9.8	11	0.604	9.8	0.963
39	0.284	9.3	39	0.272	10.0	0.957

**Table 7-3: Comparison of top transverse modes for control vs final model (Y-axis)**

Control Model			Final Model			
Mode	Period, $T_{control}$ (s)	Modal Part. Factor (%)	Mode	Period, $T$ (s)	Modal Part. Factor (%)	$T/T_{control}$
1	1.688	55.0	1	1.635	55.3	0.969
5	0.819	9.5	5	0.794	9.4	0.970

17	0.513	7.0	17	0.498	7.0	0.971
24	0.386	1.9	24	0.372	2.0	0.962
51	0.24	1.2	36	0.293	1.1	1.222

**Table 7-4: Comparison of top vertical modes for control vs final model (Z-axis)**

Control Model			Final Model			
Mode	Period, $T_{control}$ (s)	Modal Part. Factor (%)	Mode	Period, $T$ (s)	Modal Part. Factor (%)	$T/T_{control}$
7	0.721	5.8	7	0.685	5.1	0.950
15	0.56	3.9	18	0.486	4.2	0.869
18	0.505	4.1	20	0.450	4.0	0.891
20	0.469	3.9	21	0.441	3.6	0.940
44	0.263	6.1	44	0.253	6.1	0.962

The modal analyses from the final model were also compared to the 2013 Carr and Sanders study (Table 7-5). As the Galena Creek Bridge is most vulnerable to lateral forces, the top transverse modes were used as the benchmark to compare the model. The final model demonstrated marginally lower modal periods than those resulting from the lateral excitation experiments, likely because the Carr and Sanders study was performed within months of the completion of the bridge construction. The concrete of the Galena Creek Bridge has had almost an additional decade to cure; therefore, additional strength and stiffness gains would be expected. Further, despite being in service for eight years, the 2018 NDOT bridge inspection report did not note substantial deterioration that would result in significant loss of stiffness.

**Table 7-5: Comparison of top transverse modes for Carr & Sanders vs final model (Y-axis)**

Carr and Sanders Model			Final Model			
Mode	Period, $T_{control}$ (s)	Modal Part. Factor (%)	Mode	Period, $T$ (s)	Modal Part. Factor (%)	$T/T_{control}$
1	1.650	38.9	1	1.635	55.3	0.991

5	0.990	4.1	5	0.794	9.4	0.802
10	0.720	5.5	17	0.498	7.0	0.692
11	0.670	0.9	24	0.372	2.0	0.554
32	0.320	1.1	36	0.293	1.1	0.916

## 7.6 Final Proposed Model Time-History Analysis

The envelope displacements from the time-history analysis are analogous to the results from the modal analysis. The final model demonstrated more moderate envelope displacements than the control model from the same ground motions. Interestingly, the decreases in superstructure vertical displacements (Figure 7-1) are greater in areas with long unbraced lengths, such as between Pier 2 and the arch crown. Conversely, shorter spans such as Spans 1 and 3, show greater vertical displacements than those of the control model.

Notably in Figure 7-2, increasing the material stiffness reduced the maximum transverse displacement along the entire length of the structure. However, decreasing the effective MOI of the substructure increases the curvature of the envelope displacement curves, as seen in Figure 6-10. This behavior exhibited again in Figure 7-2; decreasing the substructure stiffness to 95% increased the curvature of the graph despite the additional material stiffness. Figure 7-3 shows that the modifications made for the final model decreased the longitudinal displacements of Frame 1 by an average of 8.8 mm and Frame 3 by 19.5 mm, whereas Frame 2 experienced almost no net change.



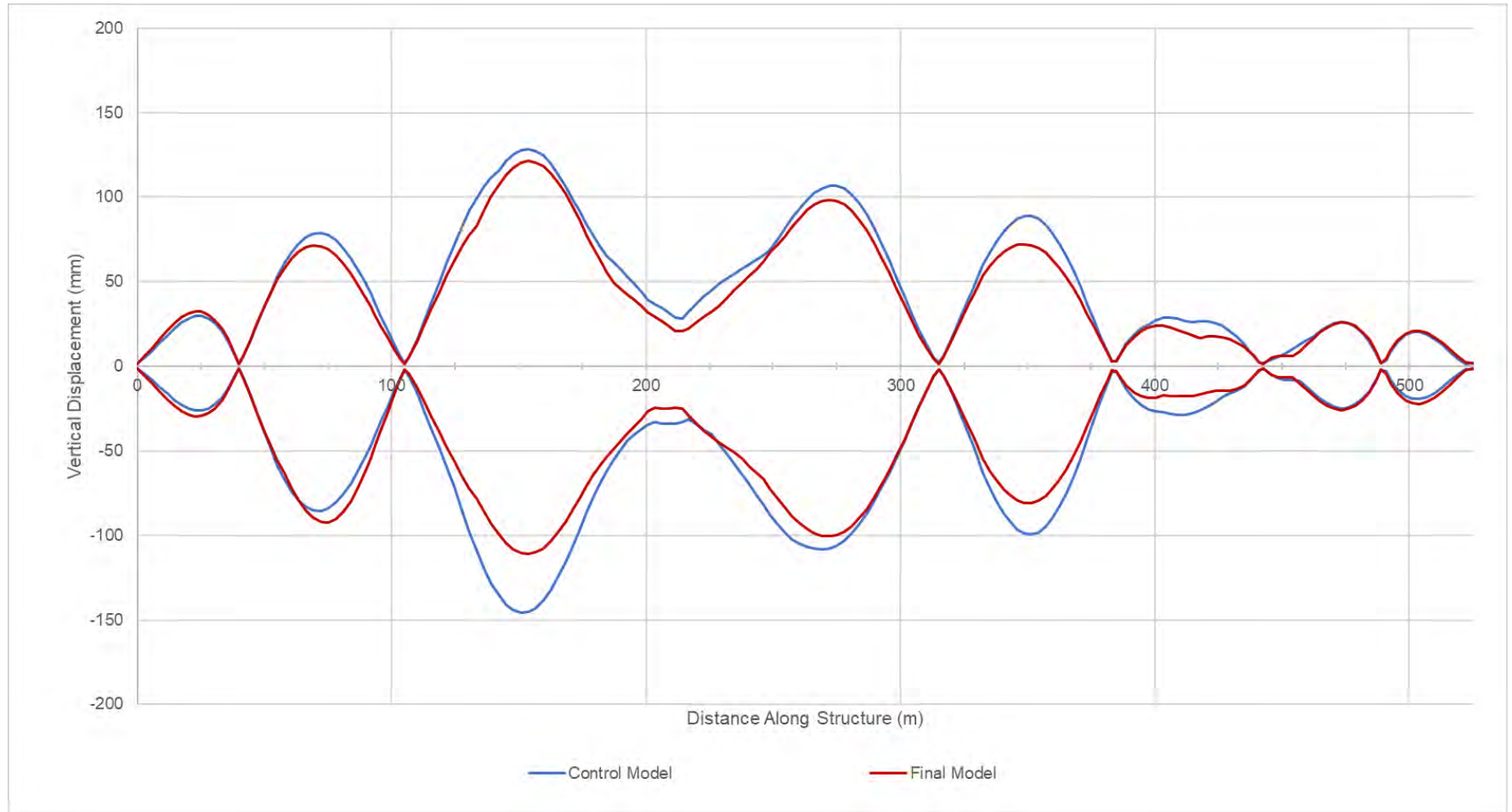


**Figure 7-1: Envelope of vertical displacements of northbound superstructure for control vs final models**

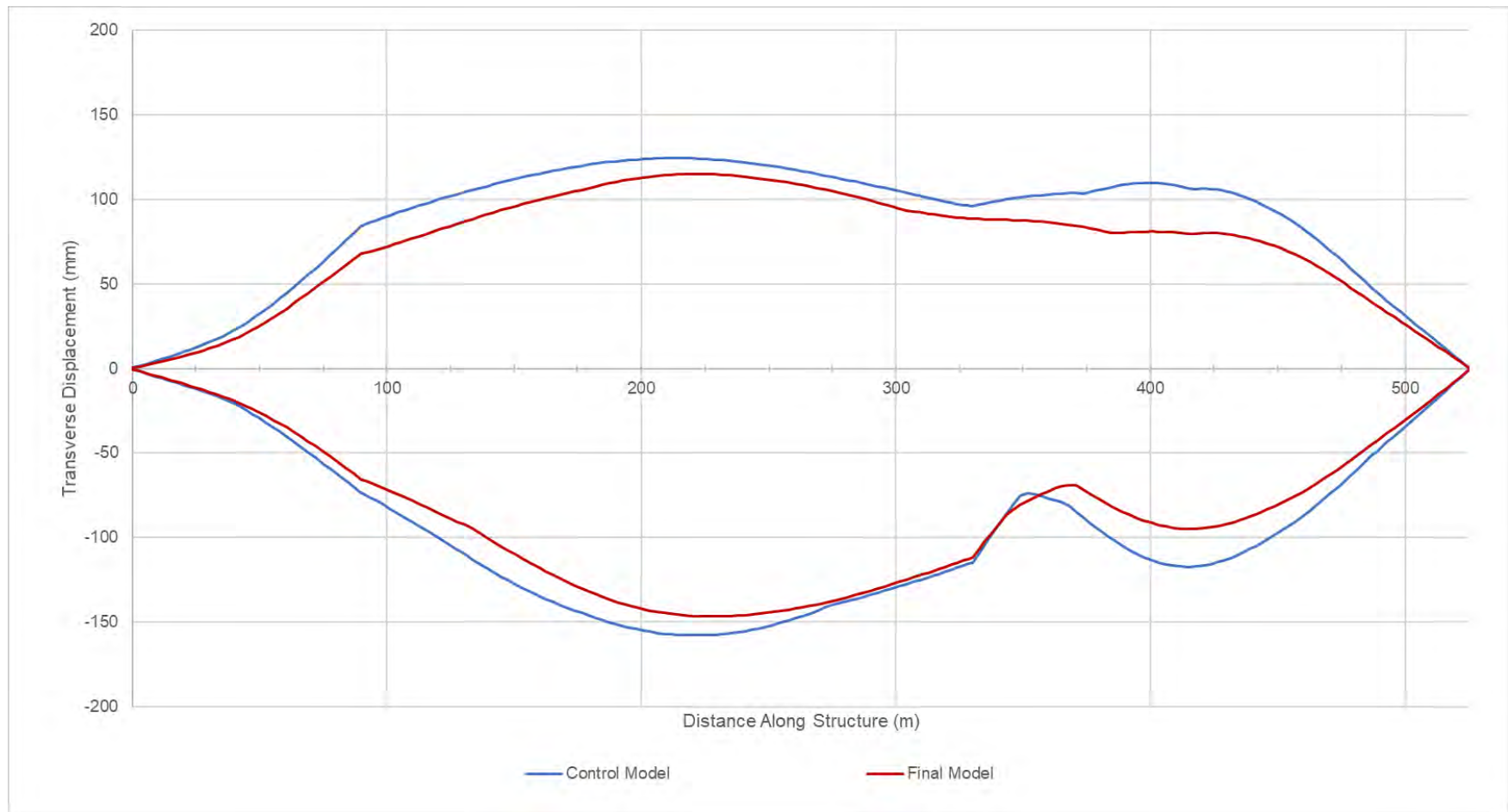


**Figure 7-2: Envelope of transverse displacement of northbound superstructure for control vs final models**

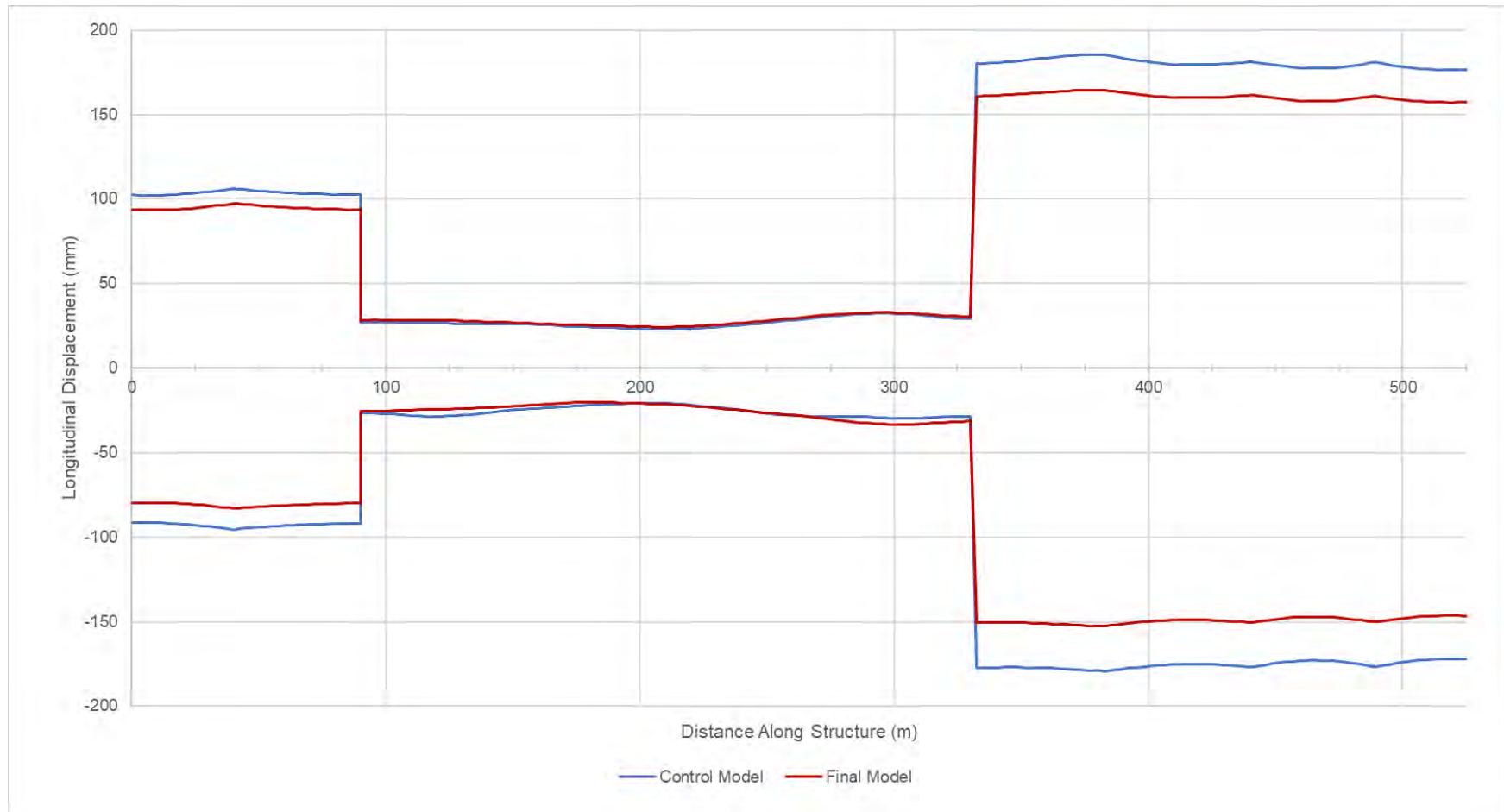


**Figure 7-3: Envelope of longitudinal displacement of northbound superstructure for control vs final models**

## CHAPTER 8. CONCLUSIONS AND FUTURE WORK

### 8.1 Conclusions

As the largest cathedral arch bridge in the United States, the Galena Creek Bridge was the focus of a study to adapt a structural health monitoring system previously employed for building applications for use on bridges. Two new, permanent SHM systems were installed on the northbound structure of the Galena Creek Bridge to enhance the understanding of the dynamic and in-service response of the bridge. A primary seismic SHM system was composed of 33 uniaxial accelerometers located at key locations along the superstructure and substructure with a triaxial seismograph at a free-field site, approximately 150 feet away from the bridge.

A secondary exploratory SHM system, composed of potentiometers, inclinometers, temperature gauges, and anemometers, served to further expand the capabilities of the primary system by recording displacement, tilt, temperature, and wind conditions. The inclusion of additional sensors for this study could help to adapt the seismic system for the bridge and to gather data on additional response characteristics. The two SHM systems continuously monitor the Galena Creek Bridge behavior during routine service loads, such as traffic, wind, and thermal expansion, as well as extreme events, such as seismic events.

After completing the hardware installation, the system software, **SMARTBRIDGE** SHM by QuakeLogic, was designed and implemented to perform SHM of the Galena Creek Bridge. Based on the identified seismic hazard description of the site, trigger threshold values were established. During a trigger event, the system provides real-time alerts and generates a complete engineering assessment report for any critical seismic event. Further, the system is designed to enable a user to selectively extract and monitor specific sensor components and the corresponding behavior of the bridge for a detailed expert-level analysis. Ultimately, this project provided a functional SHM testbed that contributes to the advancement of NDOT's facility management methods, potentially reducing the cost in infrastructure management and enhancing the safety and continued operation of critical infrastructure.

In addition to the SHM systems installed on the structure, an FEA model of the Galena Creek Bridge was developed using CSiBridge. A parametric study was conducted to evaluate changes in the structural response relative to a defined set of parameters. The parametric study concluded that the methods of modeling the superstructure, barrier rail, link slab, and expansion joint bearings for the control model were sufficient. Additional variables considered in the study, such as the effective moment of inertia of the substructure elements, structural damping ratios, and material stiffnesses, were modified to reflect the behavior of bridge more accurately. Data recorded by the SHM systems can be used in future studies to further calibrate the results of time-history analyses of the analytical model to the field-measured dynamic response of the bridge.

At the submission of this document, no significant ground motions were recorded. Multiple delays were encountered throughout the project due to a variety of factors, including bridge access limited to the UBIT, scheduling challenges, supplier delays, and Covid restrictions. In addition, controlled load tests using the UBIT and/or loaded dump trucks were not performed because the approach would not have generated the required response to evaluate the system (i.e., seismic loading versus traffic loading). To properly evaluate the capabilities of the SHM systems, a seismic loading that exceeds typical noise from routine service loads is required. While the functionality of both the seismic and exploratory systems were confirmed, due to project time lost for the aforementioned reasons, long-term data were unable to be collected. As such, trigger threshold values for the systems were not refined beyond the levels previously described. Further, the CSiBridge model was unable to be calibrated to the in-service response. Once the FEA model of the Galena Creek Bridge is tuned, it can be used as an additional means to evaluate the structural integrity of the bridge. Furthermore, the CSiBridge model could be used to predict the response and potential damage of the bridge to more extreme seismic excitation.

## **8.2 Recommendations**

One of the key factors in the dynamic response is the reliable behavior of the abutments and expansion joints. Predictable behavior between the frames of the bridge is crucial for the longevity of the structure. As such, additional string potentiometers added at Hinge 2 and Abutment 2 would ensure any irregularities in Frame 3 are captured. As Frame 1 has the shortest columns, both the superstructure and substructure experience the greatest internal stresses. Conversely, Frame 2 has

the tallest columns and longest spans, resulting in the greatest vertical and transverse displacements. The addition of displacement sensors at the elastomeric bearing locations bookending Frame 3 would confirm the intended longitudinal translation between Frames 2 and 3.

Although the instrumentation locations were selected with the explicit intent of providing an understanding of dynamic behavior, the connection between the northbound and southbound structures remains an underexplored area of study. The expansion joint boundary conditions control the longitudinal behavior of the bridge. Likewise, the connection between the northbound and southbound structures are a defining characteristic of the transverse behavior. Instrumentation to monitor the integrity and condition of the link slab could provide valuable insights on the bridge performance. The addition of weather-resistant strain gages along the length of the link slab would provide information on the component response as well as signify potential damage as it occurs.

The ultimate goal of the FEA model was to conduct a calibration to the physical dynamic response of the Galena Creek Bridge. The parametric study explored several variables that influence the modal and dynamic behavior of the model. Although the results of the parametric evaluation led to the development of a final proposed FEA model, the dynamic response of the model has yet to be verified by comparing to field-measured data. Calibration of the model can be conducted by comparing the excitation experienced by nodes of the model to the sensors at each of the 15 locations. Table 8-1 lists each of the sensor locations with the corresponding node designation to aid with future calibration attempts.

**Table 8-1: Final model node numbers corresponding with sensor locations**

<b>Sensor Location</b>	<b>CSiBridge Node Number</b>
Top of Pier 1	4200
Bottom of Pier 1	4199
Midspan of Span 2	775
Top of Pier 2	4202
Bottom of Pier 2	4201
Midspan between Pier 2 and south merge	1415
South arch/superstructure merge	1574

Crown of Arch at Span 3	1795
North arch/superstructure merge	2014
Midspan between Pier 3 and north merge	2175
Top of Pier 3	4204
Bottom of Pier 3	4203
Midspan of Span 4	2874
Top of Pier 4	4206
Bottom of Pier 4	4205

There are several other factors that must be considered when calibrating the FEA model to in-service behavior. One of the initial assumptions was that live loads did not influence the dynamic response. Additionally, the bearings were assumed to only permit rotation about the vertical direction. Further research can consider releasing the rotational fixities of the elastomeric bearing about the horizontal axes. The scope of this study was limited to linear time-history analyses. The bridge will likely exhibit linear behavior for a majority of minor ground motions; however, the influence of an extreme seismic activity may require a nonlinear time-history analyses. This more complex method of analysis will also require reevaluating the approach to modeling components, such as the columns and link slab. Evaluating these advanced parameters will yield a FEA model that will consistently predict the dynamic response of the Galena Creek Bridge to seismic activity. The complete model would then serve alongside the seismic and exploratory SHM systems to monitor the integrity of the structure throughout the service life.

Establishing site-dependent as well as structure specific threshold values for a critical seismic event requires sufficient historical data to reliably update/determine the threshold values for the bridge beyond consideration of the seismic hazard description. With the detailed data provided by the implemented SHM system upon future seismic events, this research suggests NDOT continues to collect data until it is found that NDOT obtained sufficient data with triggered seismic events. The structural responses, which can be understood with the SHM system, coupled with the triggered events should then be investigated to further refine the threshold values beyond the values set by this research based on the seismic hazard description investigation.

Finally, for the installed SHM systems to provide NDOT with the greatest benefits, routine monitoring and maintenance is required. Currently, the systems use a cellular modem connection for communication that is owned and maintained by the contractor. Installing a wired data connection would greatly enhance the speed and reliability of the system notifications, thereby enabling the most functionality of the system. Further, like all software packages, the **SMARTBRIDGE** SHM software is continually being enhanced with new features and improvements are being released regularly. To maintain peak system functionality, a service agreement with QuakeLogic could be beneficial for NDOT.



## BIBLIOGRAPHY

- AASHTO. (2020) *AASHTO LRFD Bridge Design Specifications, 9<sup>th</sup> Edition*. American Association of State Highway and Transportation Officials.
- ACI. (2019) *ACI CODE-318-19: Building Code Requirements for Structural Concrete and Commentary*. American Concrete Institute.
- Akinci, N. O., Liu, J. and Bowman, M. D. (2008) ‘Parapet Strength and Contribution to Live-Load Response for Superload Passages’, *Journal of Bridge Engineering*, 13(1), pp. 55–63. doi: 10.1061/(asce)1084-0702(2008)13:1(55).
- Akogul, C. and Celik, O. (2008) ‘Effect of Elastomeric Bearing Modeling Parameters on the Seismic Design of RC Highway Bridges with Precast Concrete Girders’, *The 14th World Conference on Earthquake Engineering*.
- Briggs, R. W. and Hammond, W. C. (2011) *Evaluation of Geodetic and Geologic Datasets in the Northern Walker Lane*.
- Carr, T. M. and Sanders, D. H. (2013) *Instrumentation and Dynamic Characterization of the Galena Creek Bridge*. University of Nevada, Reno.
- Chopra, A. (2017) *Dynamics of Structures, 5<sup>th</sup> Edition*. Pearson
- FHWA. (2013) *Post-Tensioning Tendon Installation and Grouting Manual*, p. 184.
- FHWA. (2016) *Post-Tensioned Box Girder Design Manual*. Washington, DC: Federal Highway Administration, p. 389.
- NDOT (2019) *Galena Creek Bridge Northbound Routine Inspection Report*.
- Taylor, M. S. and Sanders, D. H. (2008) *Seismic Time History Analysis and Instrumentation of the Galena Creek Bridge*. University of Nevada, Reno. doi: 10.1017/CBO9781107415324.004.
- Vallejera, J. M. and Sanders, D. H. (2011). *Instrumentation and monitoring of the Galena Creek Bridge*. Center for Civil Engineering Earthquake Research at University of Nevada, Reno, Report No. 11-03.
- Wang, N. (2010) *Reliability-Based Condition Assessment of Existing Highway Bridges*. Georgia Institute of Technology.
- Wolterbeek, M. (2020) *How the burgeoning Walker Lane may split the American West*. University of Nevada at Reno.

**APPENDIX A:**  
**EXAMPLE RAPID ASSESSMENT FOR ENGINEERING RESPONSE**  
**REPORT**

**Galena Bridge**

| **Rapid Assessment:** Very low level motion detected. No action required.

| **Report Origin Local Time:** 2022.03.11 15:44:09 -0800 PST



This is a computer-generated structural health monitoring (SHM) report and has not yet been reviewed by an Engineer. Its content is limited due to number of sensors, analyses assumptions and uncertainties. Inspection prioritization notifications will be sent shortly if the SHM system determines shaking occurred at user's facility.

**Questions? Contact us**

**Email:** [support@quakelogic.net](mailto:support@quakelogic.net)

**Phone:** +1-916-258-3736

[www.quakelogic.net](http://www.quakelogic.net)

### **| Facility Description**

The Galena Creek Bridge carries Interstate 580 and U.S. Route 395 between Reno and Carson City, Nevada. The seven-span reinforced concrete box-girder bridge, with a total length of 1,725 ft, was completed in 2012 and includes a 689 ft cathedral arch span. Internal hinges are located near the piers just outside of the arch, allowing for longitudinal movement and forming three separate frames of the structure. The base of the arch is connected to the bottom of the columns at the piers of the middle frame using thrust blocks to transfer load from the arch to the foundation. The longitudinal post-tensioned two cell box-girders rest on the six sets of single column piers. The deck is post-tensioned transversely. The column and arch cross-sections are all hollow rectangular sections. The bridge consists of two separate structures tied together for lateral loading resistance using a link slab between the decks at the crown of the arch and link beams connecting the thrust blocks at the base of the arch. Its freefield station is located on southbound abutment.

### **| Geotechnical Description**

N/A

## | Seismic Hazard Description

Standard = ASCE/SEI 7-16

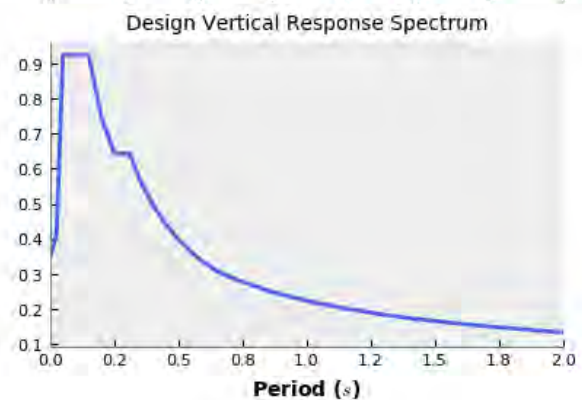
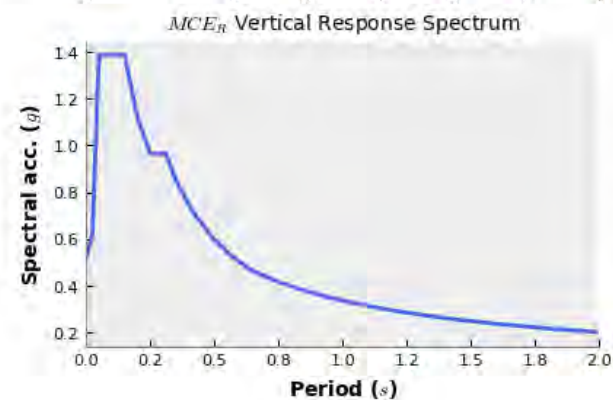
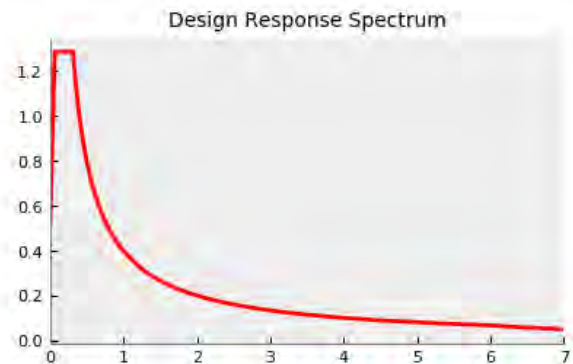
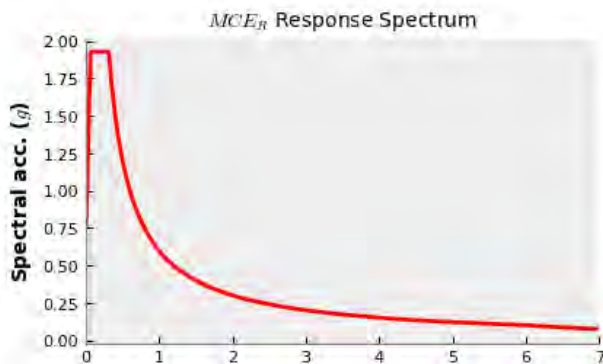
Risk category = IV

Soil class = B

Seismic design category = D

Response modification coefficient = 8

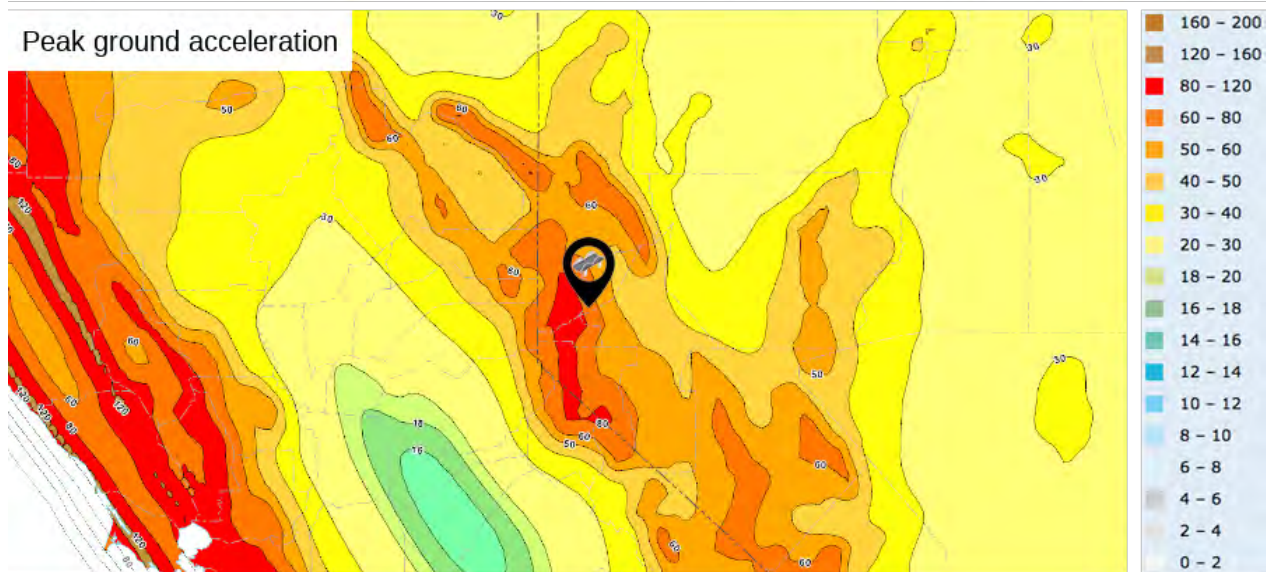
MCE_R ground motion (0.2 s), $S_s = 2.142$	Seismic design value (1.0 s), $S_{D1} = 0.398$
MCE_R ground motion (1.0 s), $S_1 = 0.746$	Long-period transition period, $T_L = 6$
Site amplification factor (0.2 s), $F_a = 0.9$	MCE_G peak ground acceleration, $PGA = 0.926$
Site amplification factor (1.0 s), $F_v = 0.8$	Site modified PGA, $PGA_M = 0.834$
Site-modified spec. acc. (0.2 s), $S_{MS} = 1.928$	Site amplification factor at PGA, $F_{PGA} = 0.9$
Site-modified spec. acc. (1.0 s), $S_{M1} = 0.597$	Importance factor, $I_e = 1.5$
Seismic design value (0.2 s), $S_{DS} = 1.285$	Vertical coefficient, $C_v = 0.9$



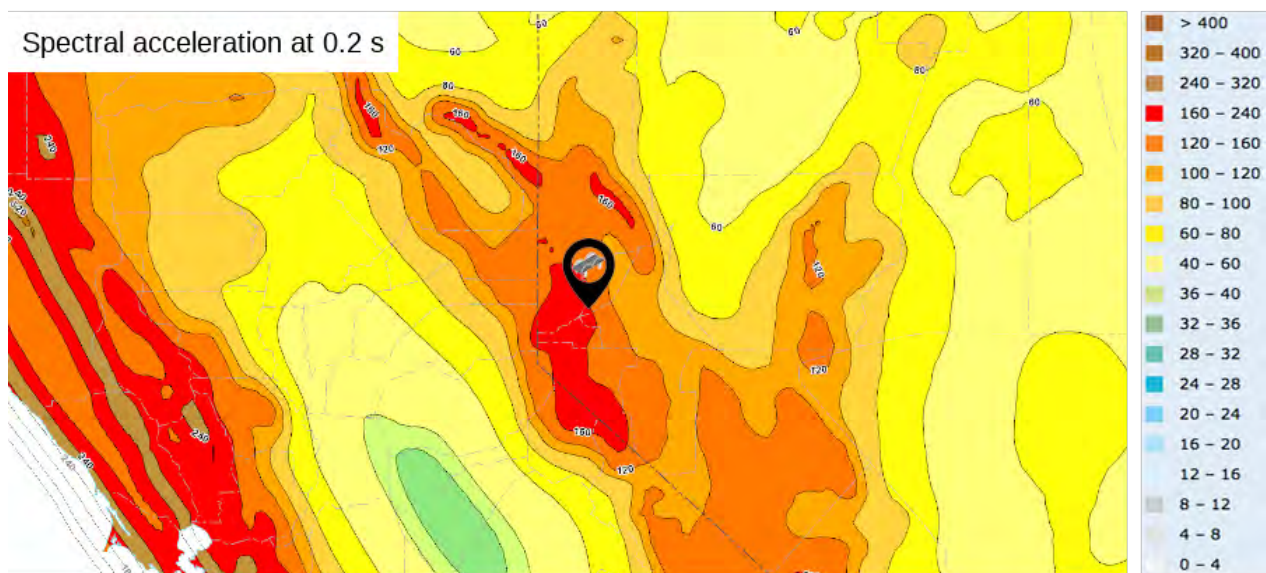
Data source is USGS Seismic Design Maps based on ASCE/SEI 7-16 and ASCE/SEI 7-16 Table 1.5-2. Additional data for site-specific ground motion procedures in accordance with ASCE/SEI 7-16 Ch. 21 are available from USGS.



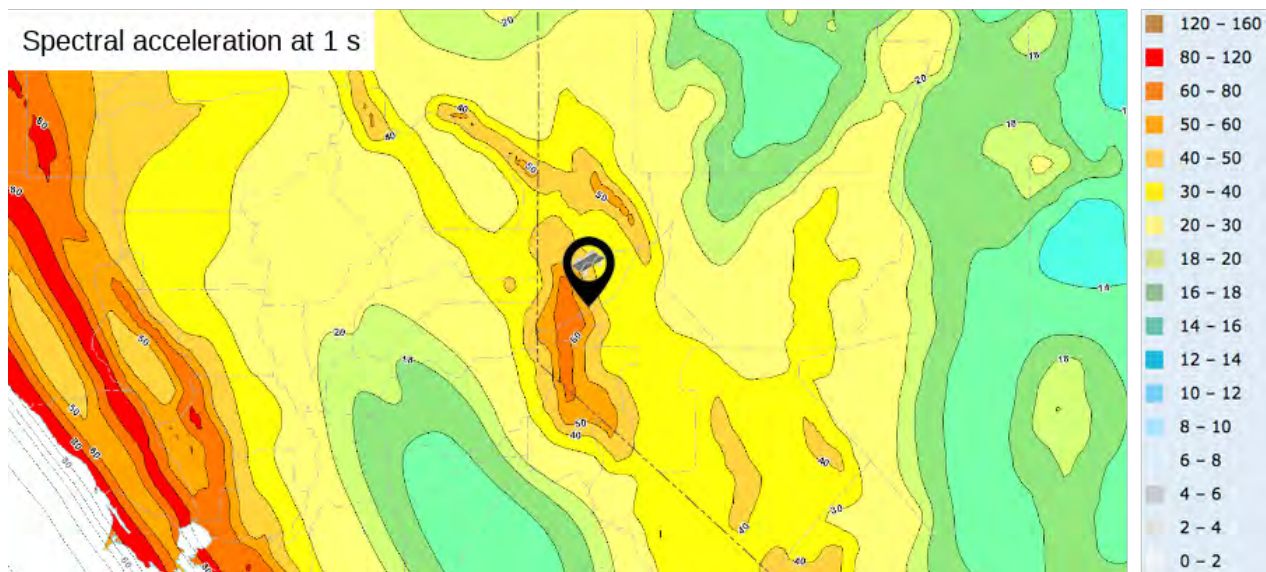
Peak ground acceleration



Spectral acceleration at 0.2 s



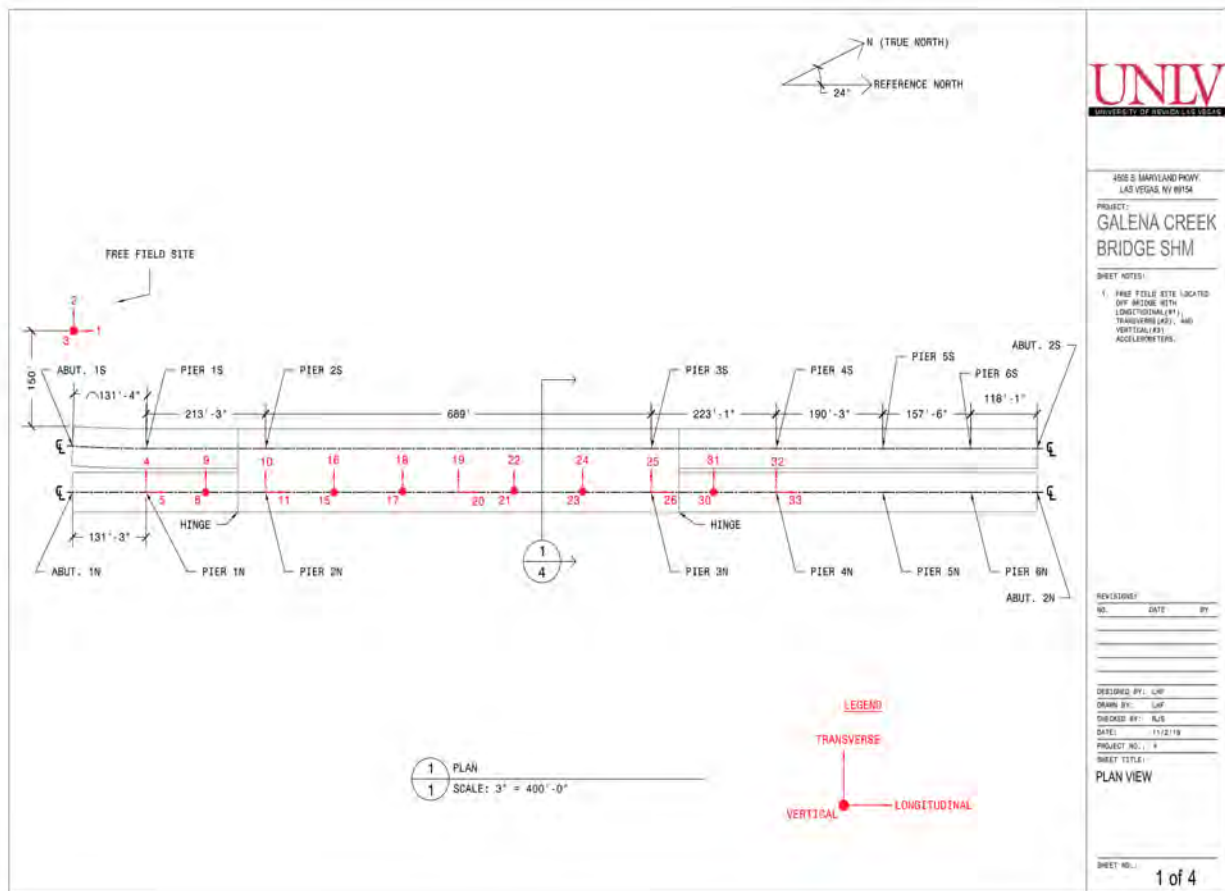
Spectral acceleration at 1 s



## | Sensor Description

A total of 33 uniaxial accelerometers are deployed in the Northbound structure to obtain its relative motion between different points of interest during an earthquake. Longitudinal accelerometers are located at the top and bottom of four of the six piers of the bridge, as well as at the crown of the arch. Vertical accelerometers are located at the bottom of three piers, at the edges of the arch-superstructure merge region, between the merge region and adjacent piers, and between each set of piers adjacent to the hinges. Transverse accelerometers are located at all of the previously listed points of interest. The longitudinal and transverse accelerometers can be used to compute lateral motion at different locations, while the vertical accelerometers allow for the calculation of relative displacements along the length of the bridge. The uniaxial accelerometers installed on the bridge are complemented by a triaxial accelerometer located at a free-field site, approximately 150 ft away from the bridge, to monitor the three components of ground motion without having interference from the response of the structure.

## Sensor Layout



## Sensor Table (Acceleration)

Network ID	Facility ID	Channel ID	Location ID
QL	9998	HNN	01
QL	9998	HNE	02
QL	9998	HNZ	03
QL	9998	HNN	04
QL	9998	HNE	05
QL	9998	HNZ	06
QL	9998	HNN	07
QL	9998	HNE	08
QL	9998	HNZ	09
QL	9998	HNN	10
QL	9998	HNE	11
QL	9998	HNZ	12
QL	9998	HNN	13



QL	9998	HNE	14
QL	9998	HNZ	15
QL	9998	HNN	16
QL	9998	HNE	17
QL	9998	HNZ	18
QL	9998	HNN	19
QL	9998	HNE	20
QL	9998	HNZ	21
QL	9998	HNN	22
QL	9998	HNE	23
QL	9998	HNZ	24
QL	9998	HNN	25
QL	9998	HNE	26
QL	9998	HNZ	27
QL	9998	HNN	28
QL	9998	HNE	29
QL	9998	HNZ	30
QL	9998	HNN	31
QL	9998	HNE	32
QL	9998	HNZ	33

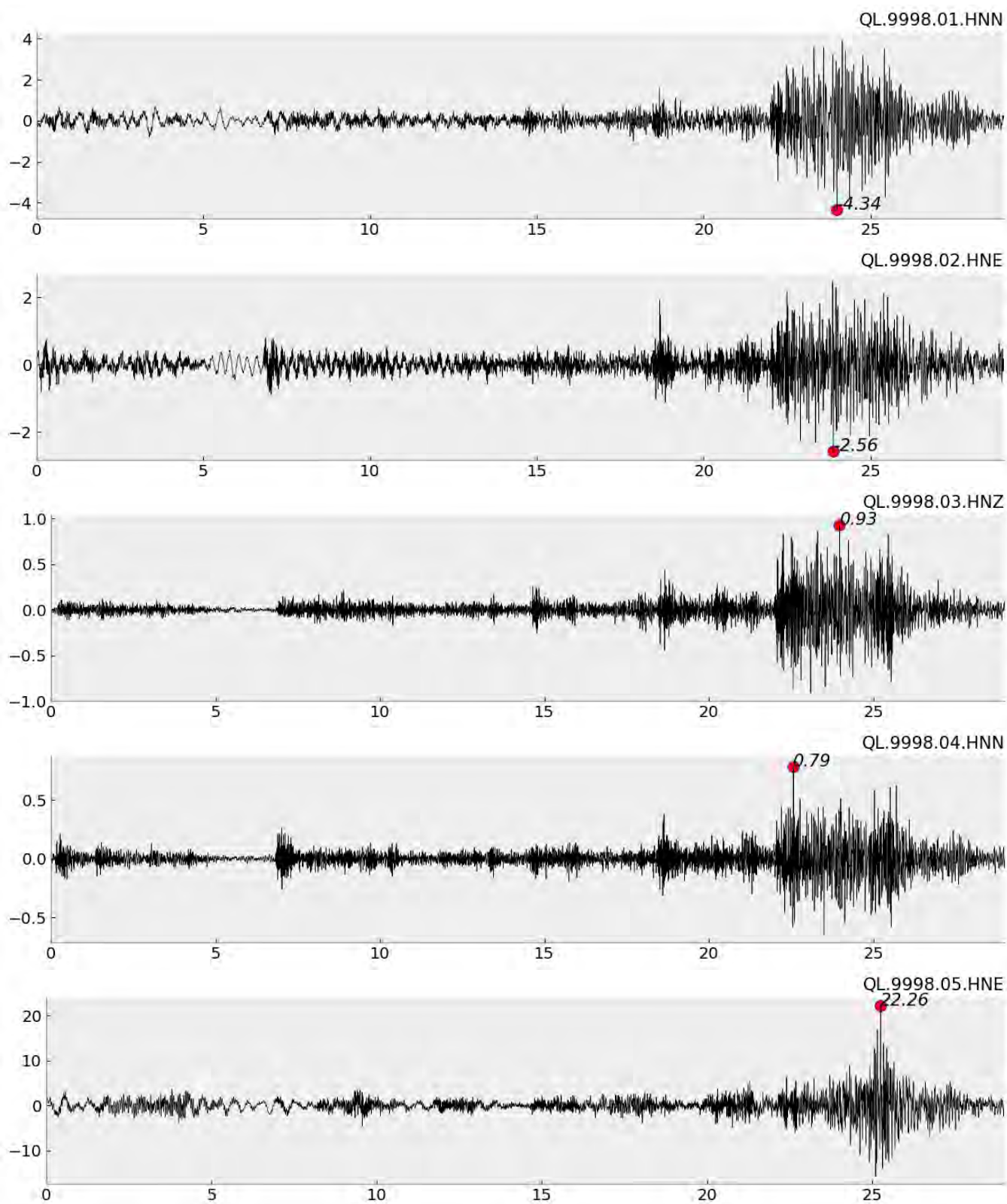
## | Sensor Peak Values Table

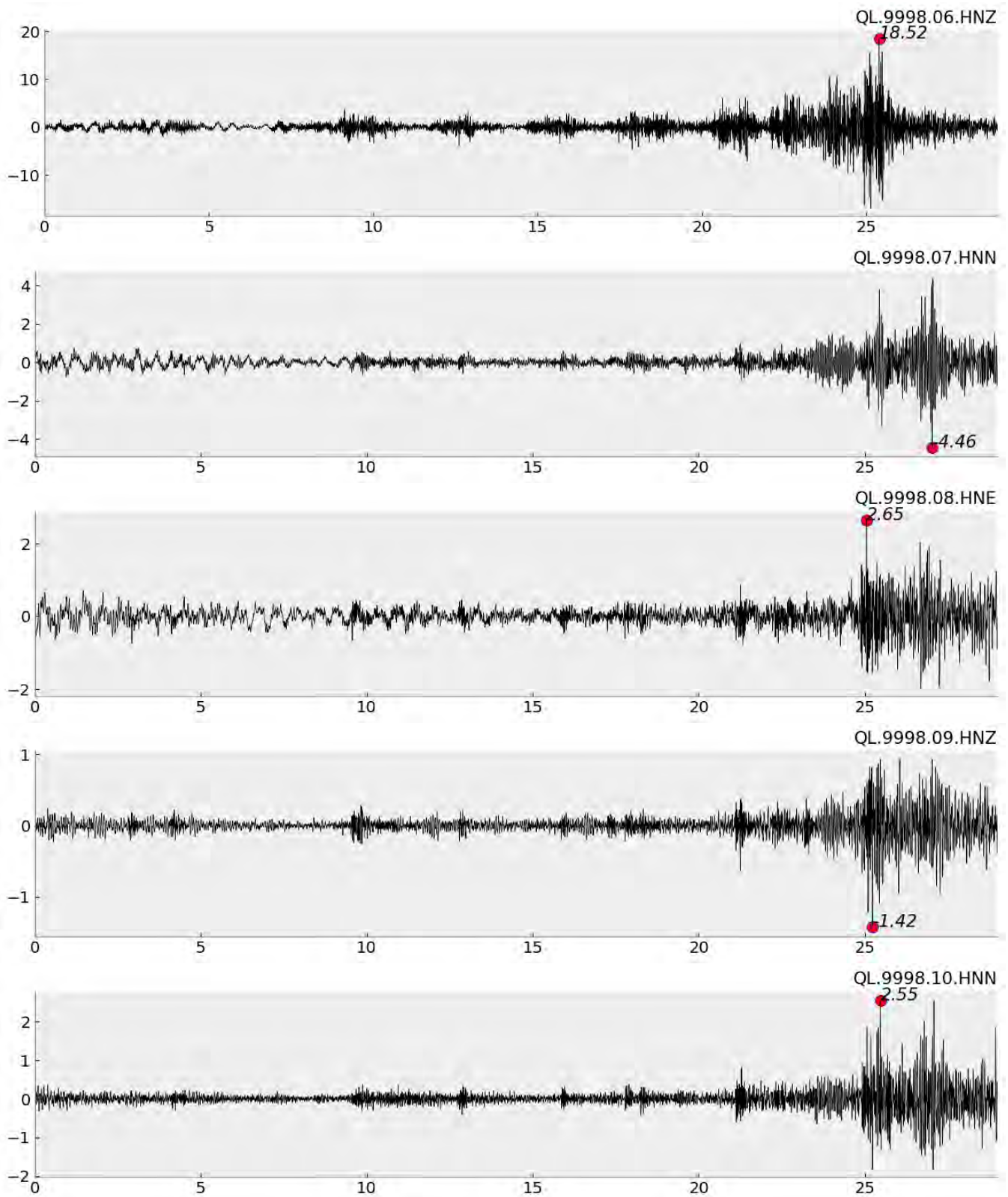
Net.Sta.Chan.Loc.	Sensor	Value (max to min)	Unit
QL.9998.05.HNE	Acceleration	22.26	cm <sup>2</sup> /s
QL.9998.13.HNN	Acceleration	20.57	cm <sup>2</sup> /s
QL.9998.06.HNZ	Acceleration	18.52	cm <sup>2</sup> /s
QL.9998.14.HNE	Acceleration	15.76	cm <sup>2</sup> /s
QL.9998.12.HNZ	Acceleration	13.10	cm <sup>2</sup> /s
QL.9998.15.HNZ	Acceleration	12.45	cm <sup>2</sup> /s
QL.9998.27.HNZ	Acceleration	10.01	cm <sup>2</sup> /s
QL.9998.20.HNE	Acceleration	7.95	cm <sup>2</sup> /s
QL.9998.19.HNN	Acceleration	6.07	cm <sup>2</sup> /s
QL.9998.28.HNN	Acceleration	5.26	cm <sup>2</sup> /s
QL.9998.18.HNZ	Acceleration	5.15	cm <sup>2</sup> /s
QL.9998.21.HNZ	Acceleration	4.86	cm <sup>2</sup> /s
QL.9998.07.HNN	Acceleration	4.46	cm <sup>2</sup> /s
QL.9998.01.HNN	Acceleration	4.34	cm <sup>2</sup> /s
QL.9998.16.HNN	Acceleration	4.28	cm <sup>2</sup> /s
QL.9998.08.HNE	Acceleration	2.65	cm <sup>2</sup> /s
QL.9998.29.HNE	Acceleration	2.63	cm <sup>2</sup> /s
QL.9998.02.HNE	Acceleration	2.56	cm <sup>2</sup> /s
QL.9998.10.HNN	Acceleration	2.55	cm <sup>2</sup> /s
QL.9998.22.HNN	Acceleration	2.05	cm <sup>2</sup> /s
QL.9998.30.HNZ	Acceleration	2.01	cm <sup>2</sup> /s
QL.9998.23.HNE	Acceleration	1.83	cm <sup>2</sup> /s
QL.9998.25.HNN	Acceleration	1.72	cm <sup>2</sup> /s
QL.9998.26.HNE	Acceleration	1.57	cm <sup>2</sup> /s
QL.9998.09.HNZ	Acceleration	1.42	cm <sup>2</sup> /s
QL.9998.17.HNE	Acceleration	1.16	cm <sup>2</sup> /s
QL.9998.03.HNZ	Acceleration	0.93	cm <sup>2</sup> /s
QL.9998.11.HNE	Acceleration	0.89	cm <sup>2</sup> /s
QL.9998.24.HNZ	Acceleration	0.84	cm <sup>2</sup> /s
QL.9998.04.HNN	Acceleration	0.79	cm <sup>2</sup> /s
QL.9998.32.HNE	Acceleration	0.73	cm <sup>2</sup> /s

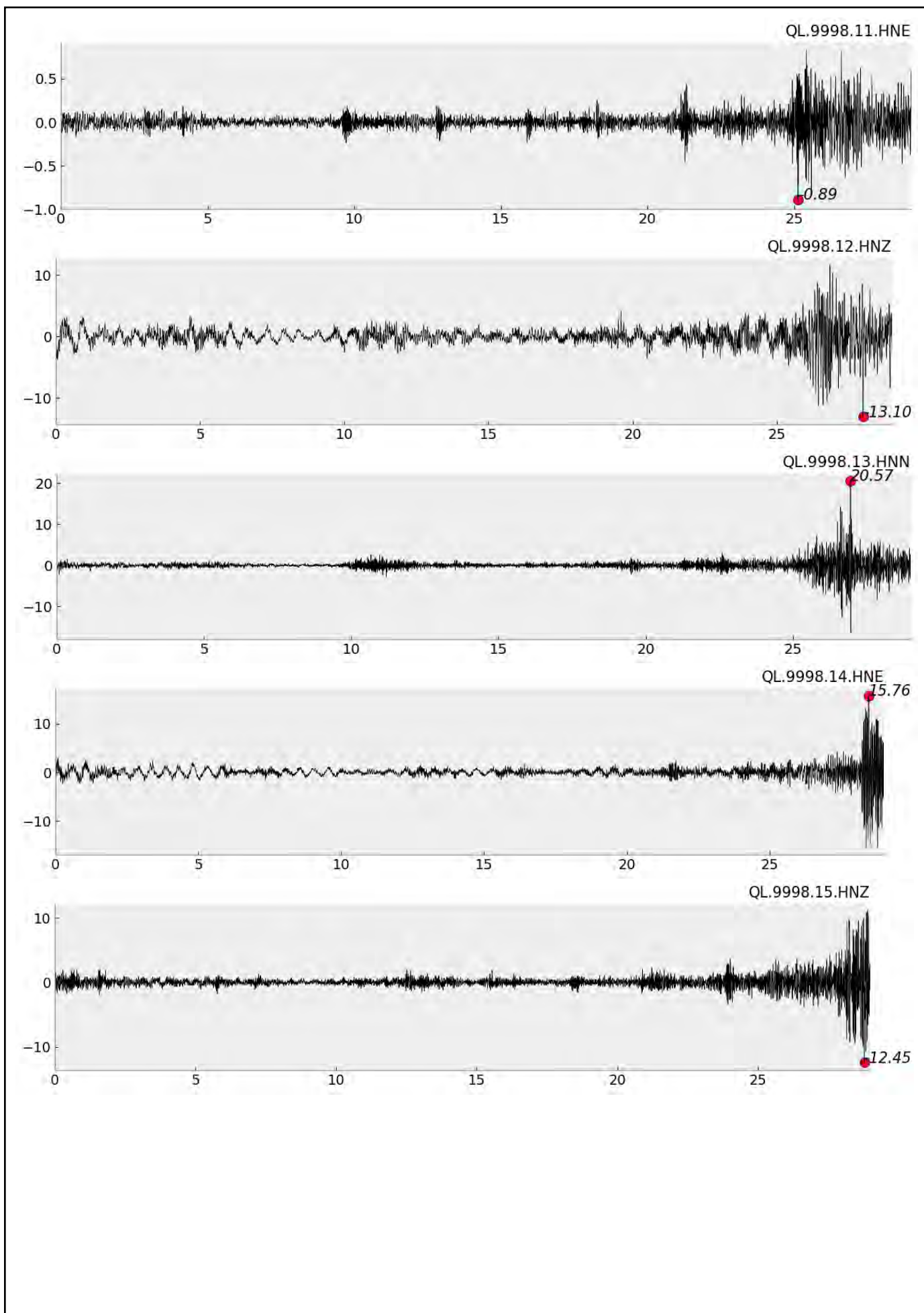
QL.9998.31.HNN	Acceleration	0.56	cm <sup>2</sup> /s
QL.9998.33.HNZ	Acceleration	0.52	cm <sup>2</sup> /s

| Acceleration Waveforms (cm/s<sup>2</sup>)

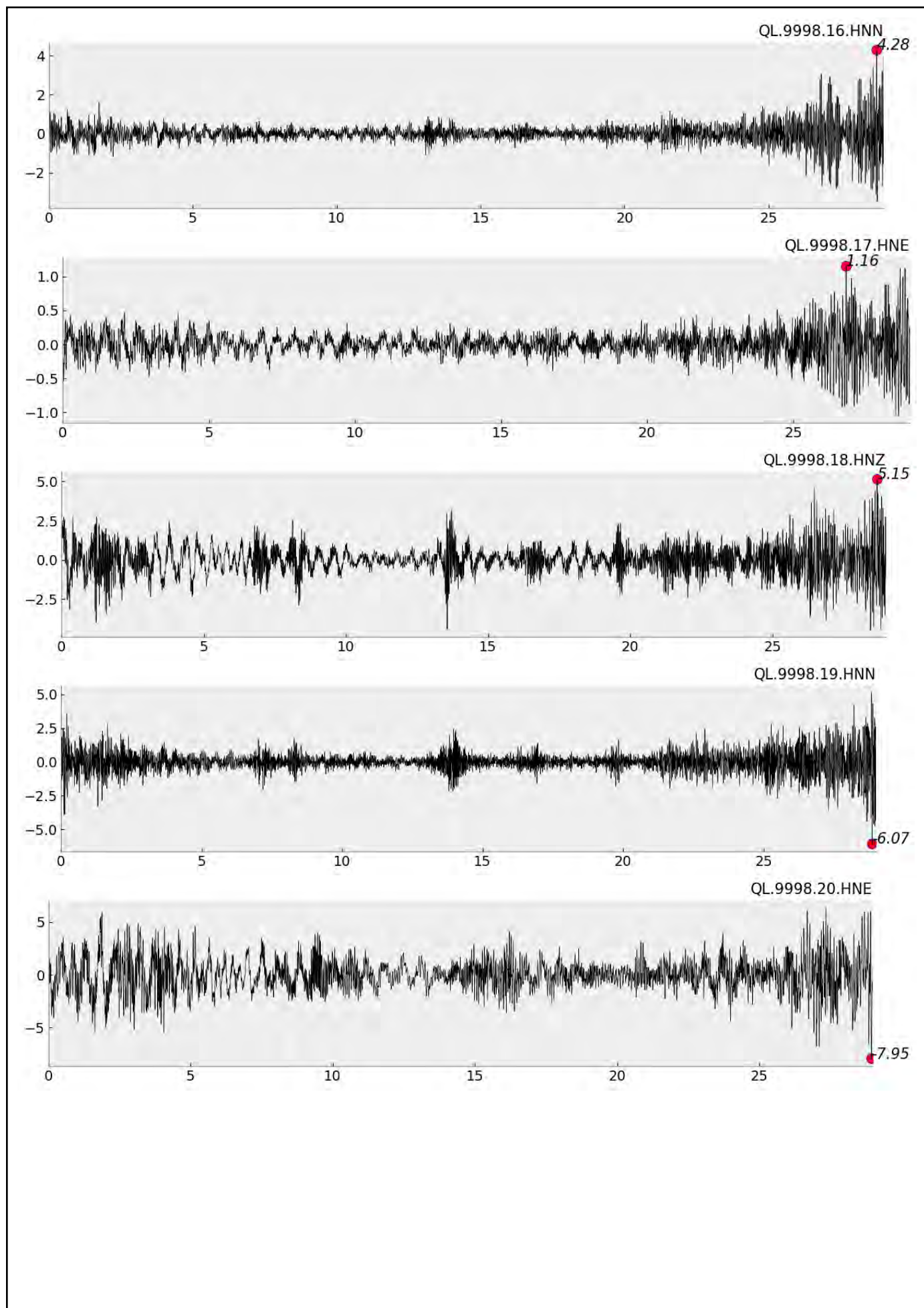
Origin Time 2022.03.11 15:42:47 -0800 PST

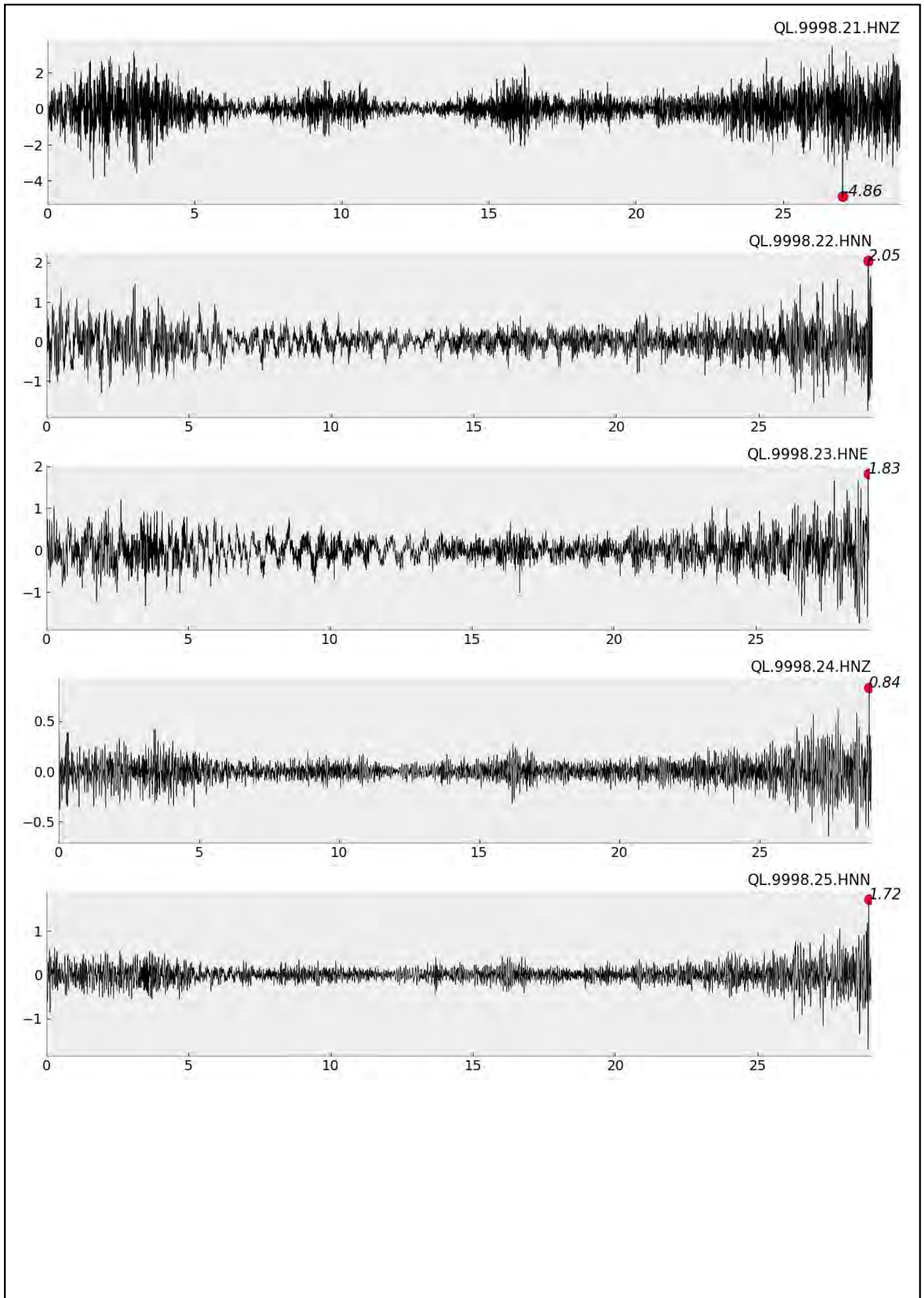




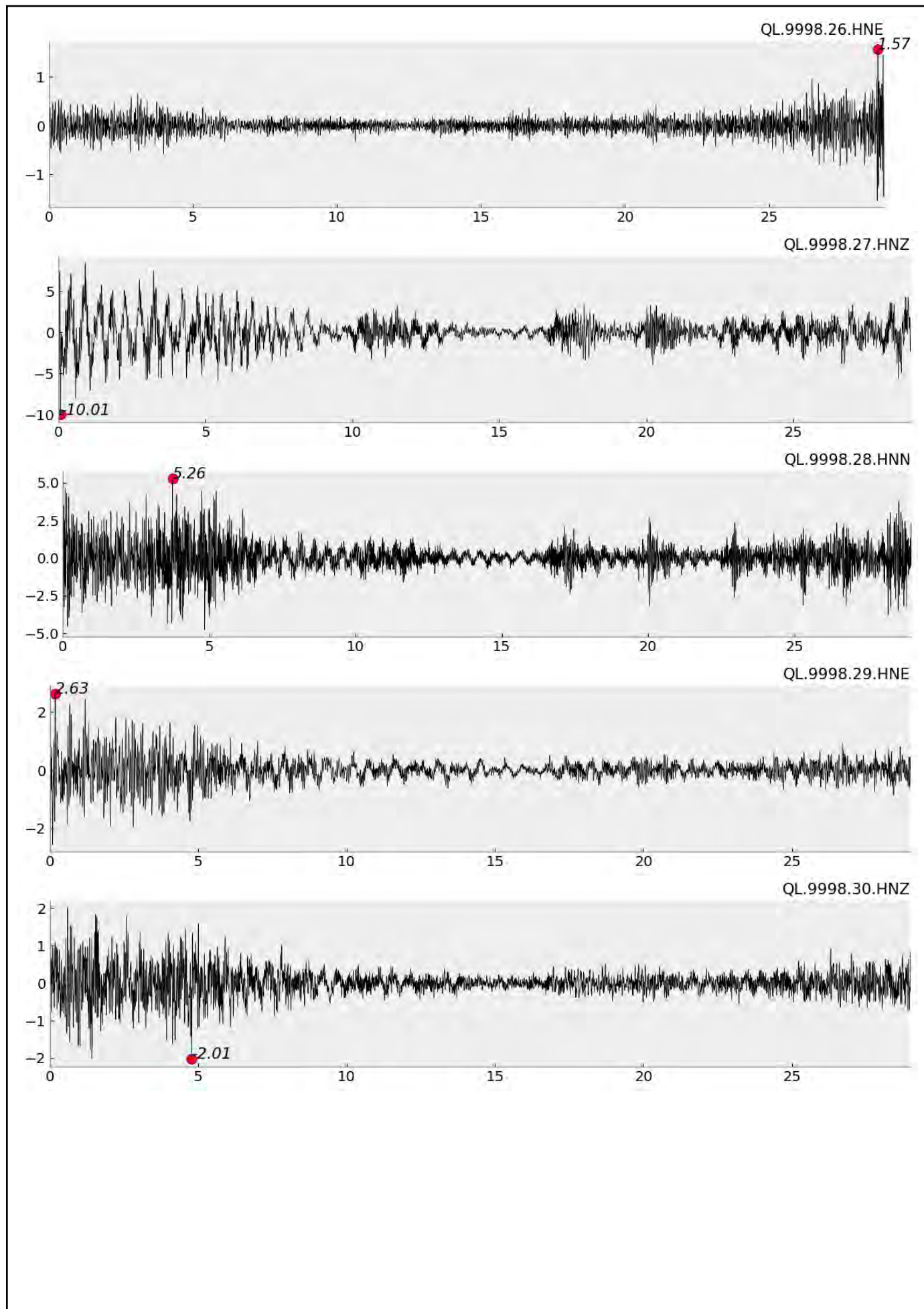


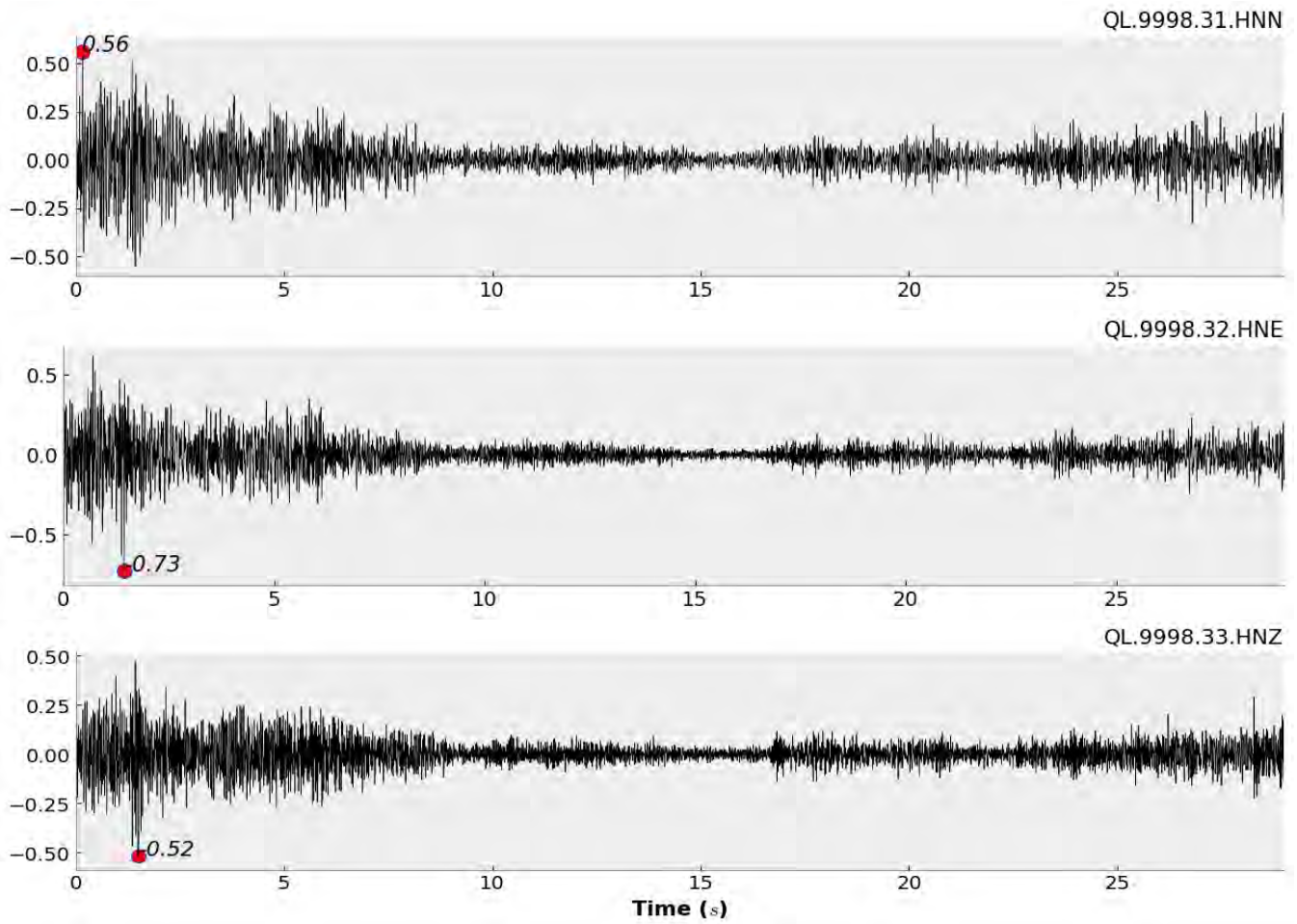










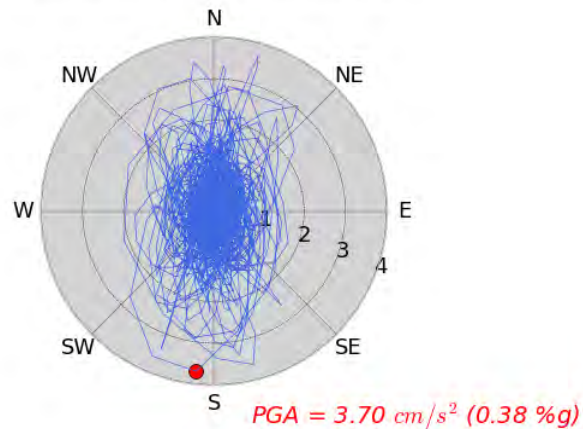


## | Resultant Ground Acceleration, Velocity & Displacement Plots

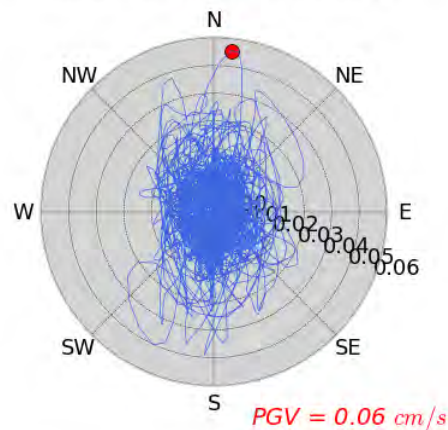
Para visualizar la polarización del movimiento del suelo, los diagramas de hodógrafo de los componentes horizontales. se trazan Los datos de aceleración de tierra se detriende por filtración.

### QL.9998.01.HNN & QL.9998.02.HNE

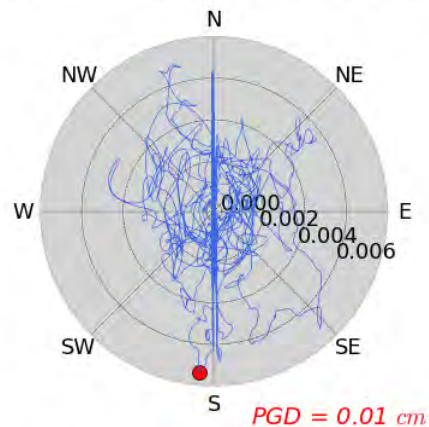
Resultant Horizontal Acceleration



Resultant Horizontal Velocity

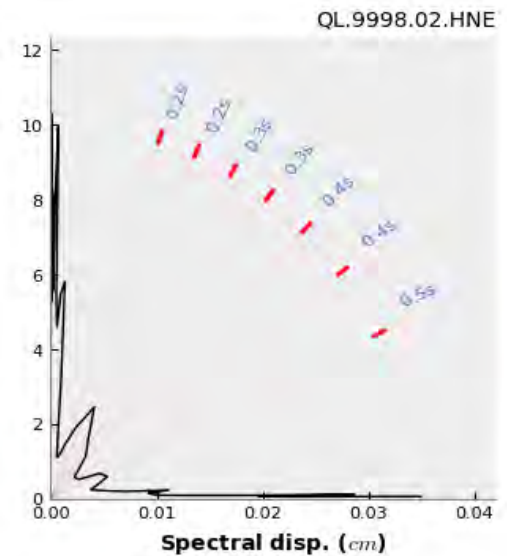
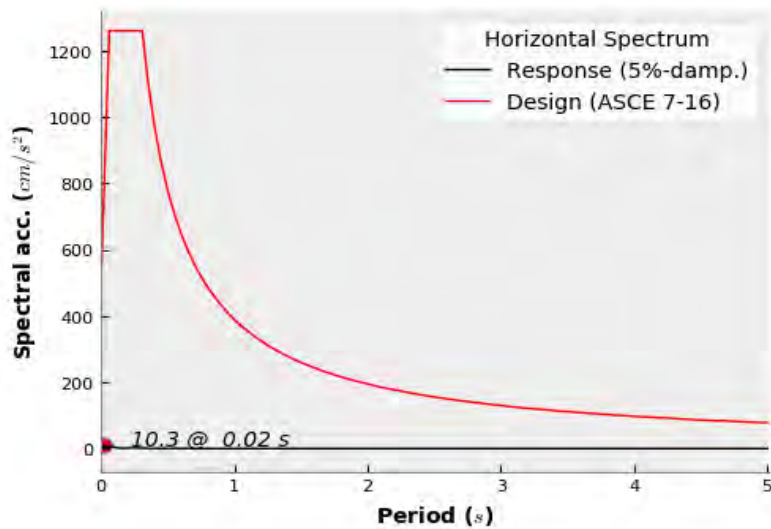
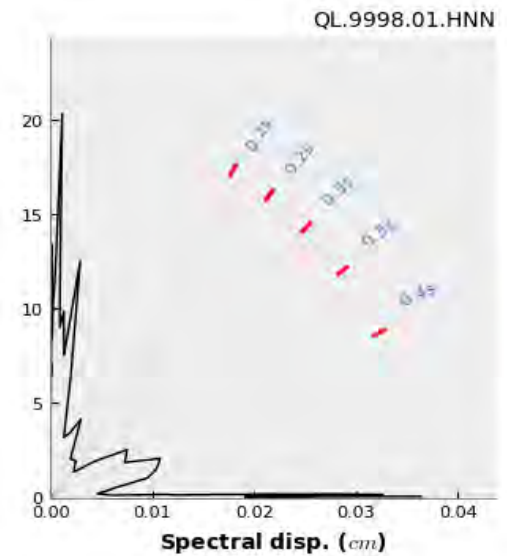
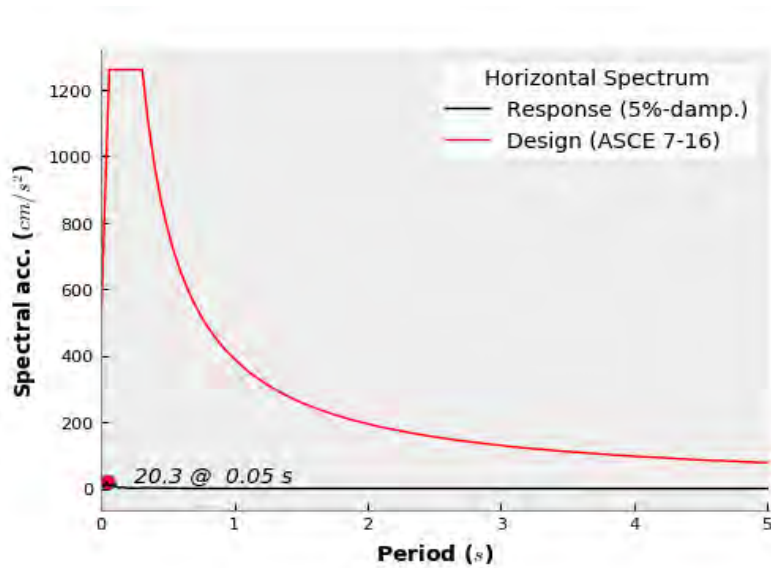


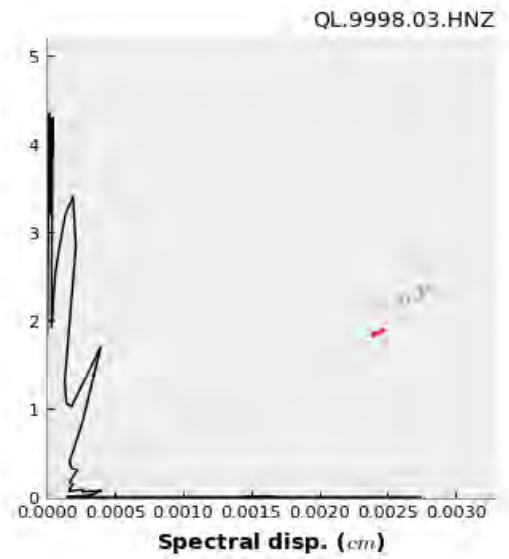
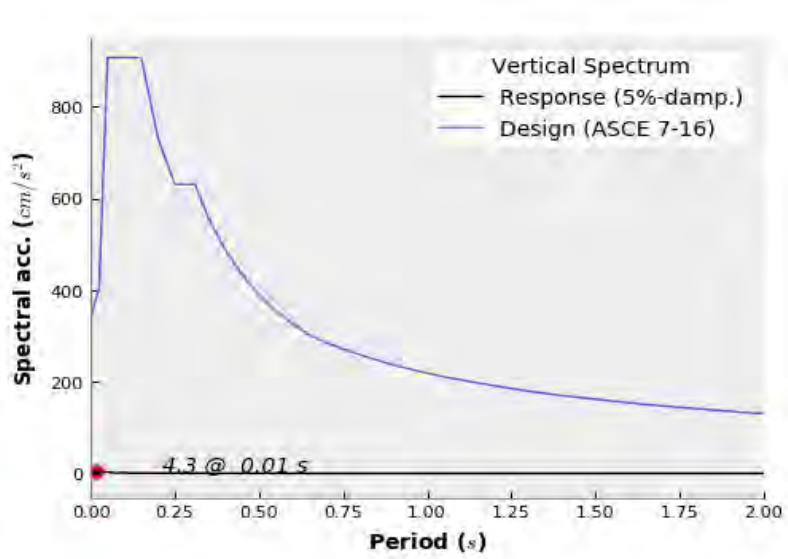
Resultant Horizontal Displacement



## | 5%-damped Pseudo-acceleration & Displacement Response Spectra Plots

Para visualizar la polarización del movimiento del suelo, los diagramas de hodógrafo de los componentes horizontales. se trazan Los datos de aceleración de tierra se detriende por filtración.

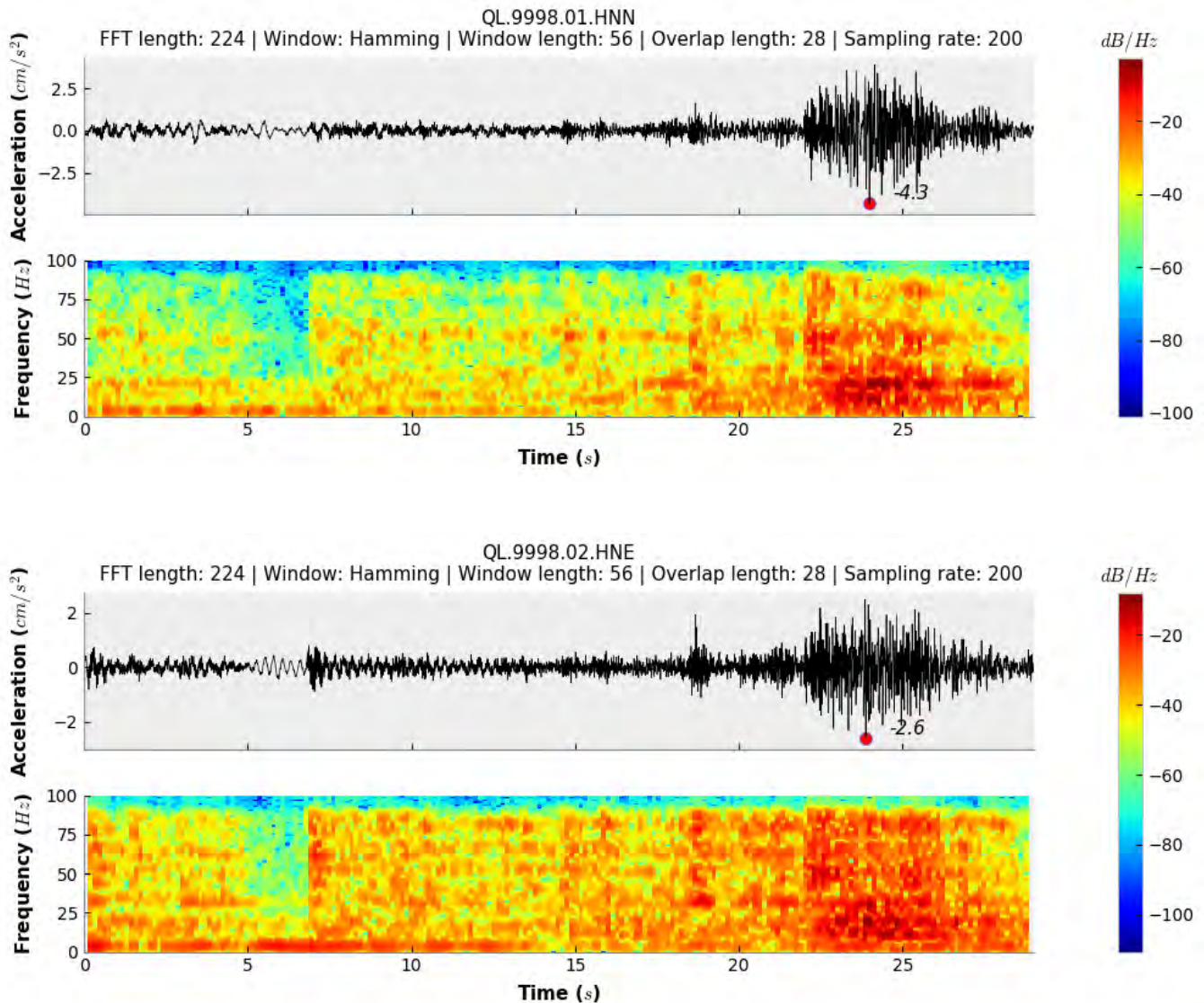


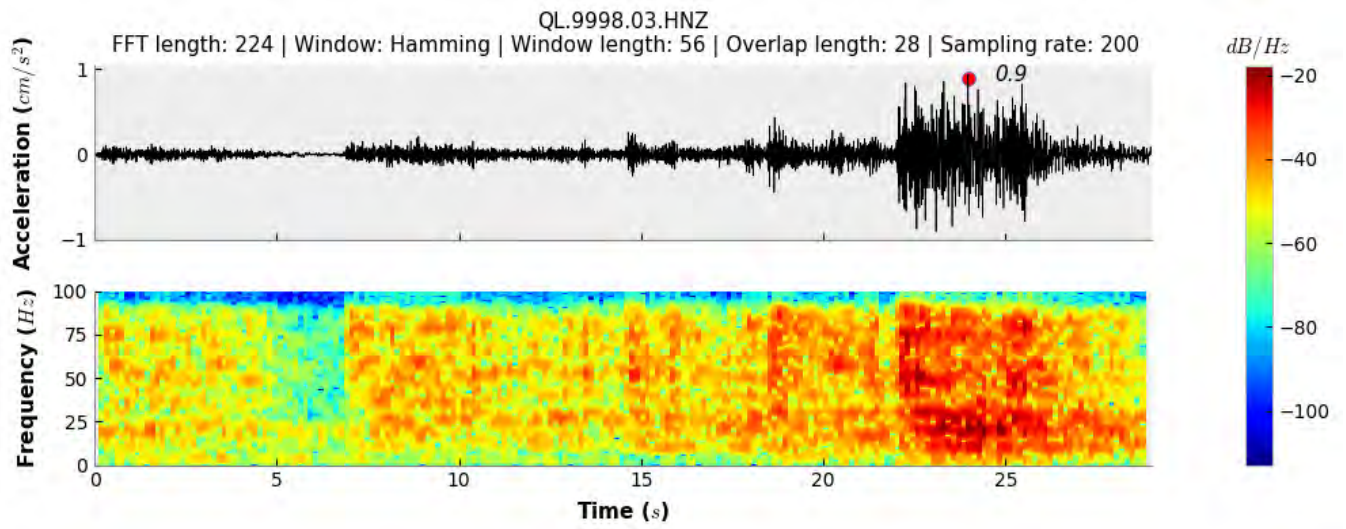




## | Acceleration Waveform & Spectrogram Plots

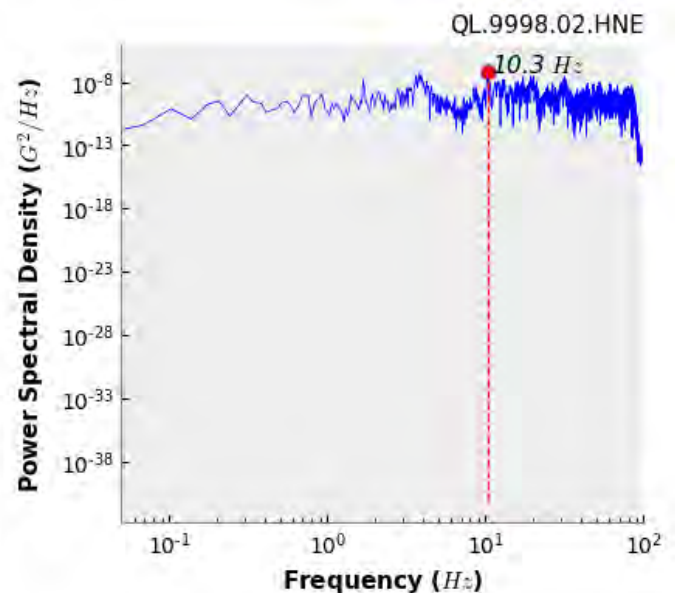
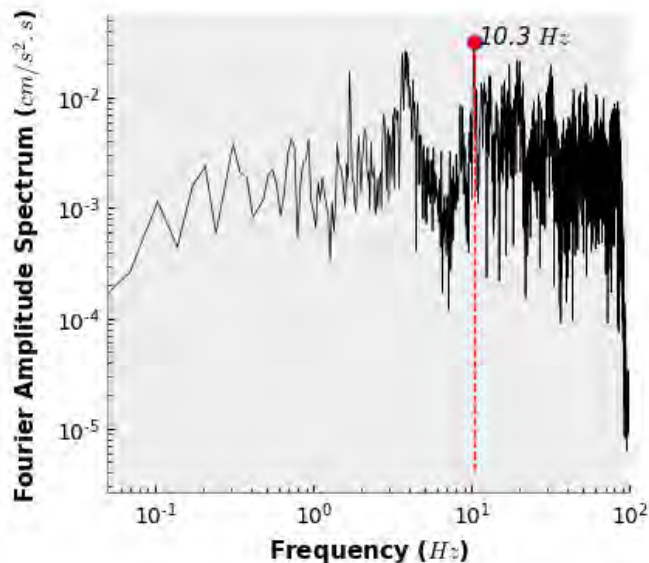
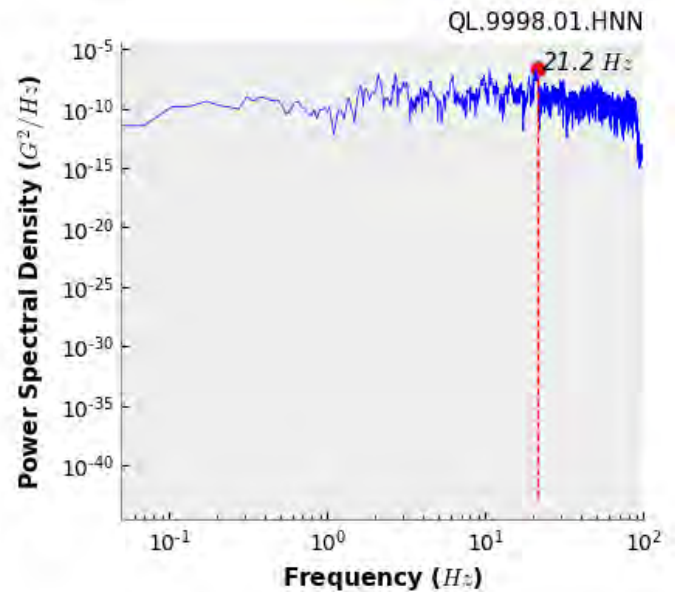
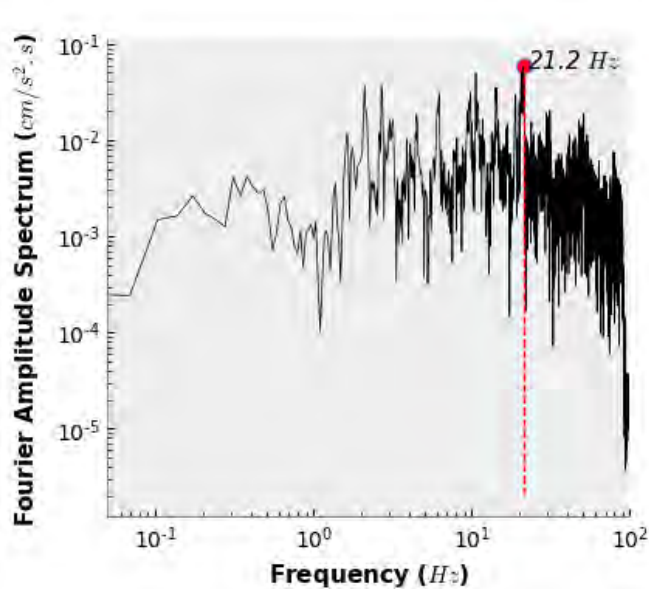
Spectrogram is a visual representation of the spectrum of frequencies of acceleration as they vary with time. Not only one can see whether there is more or less energy at, for example, 2 Hz vs 10 Hz, but one can also see how energy levels vary over time



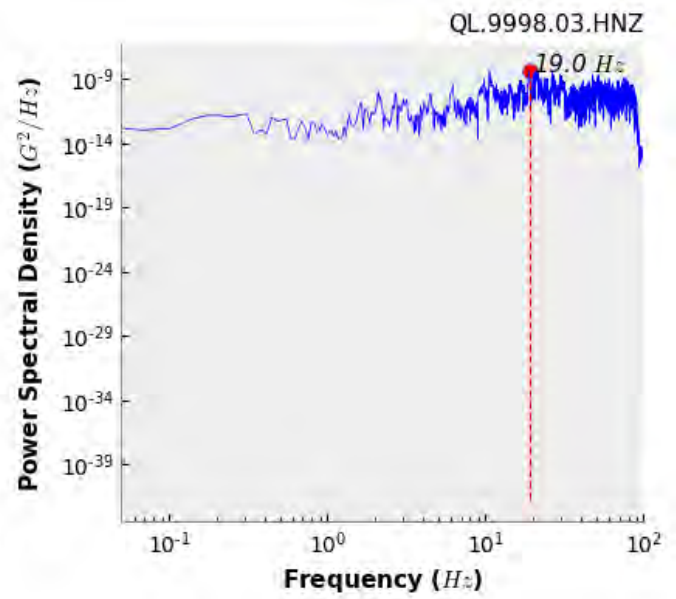
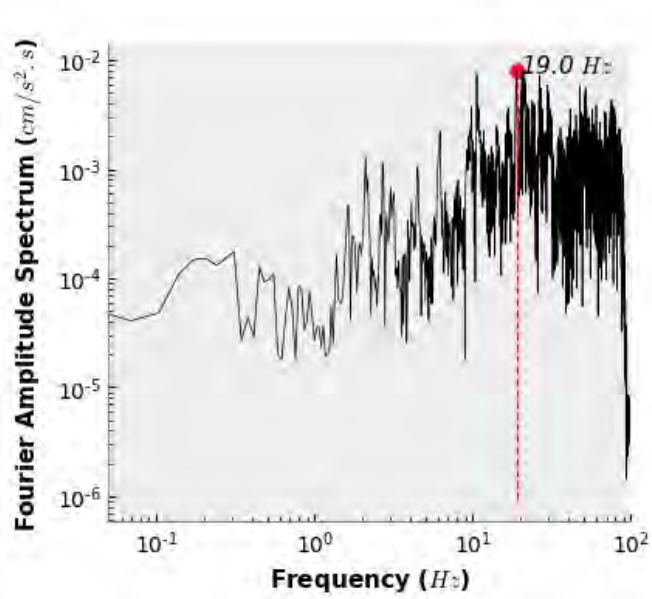


## | Fourier Amplitude and Power Spectrum Density Plots

Fourier amplitude spectrum demonstrates fundamental description of the frequency content of ground motion. The power spectrum describes the distribution of power into frequency components composing the waveform.







## | Abbreviation List

Chan:	channel code
dB:	decibel
FFT:	fast Fourier transform
Loc:	location code
Net:	network code
Sta:	station code
SHM:	structural health monitoring

---

## | Legal Disclaimer

This structural health monitoring (SHM) report is provided for your convenience, for informational purposes only, and is provided “as is” and without warranties of any kind. The data included herein has been obtained from limited number of sensors in the user's facility. The information developed and results produced are subjected to analyses assumptions and uncertainties. While QuakeLogic Inc. has made every effort to use data and information from reliable sources and widely accepted methodologies, QuakeLogic Inc. does not make any representations or warranties as to the accuracy, completeness, reliability, currency, or quality of any information and results provided herein. QuakeLogic Inc. does not intend, nor should anyone interpret, the information and data provided by this report to replace the sound judgment of a competent professional structural engineer, having knowledge and experience in the field of structural performance assessment and damage detection, nor to substitute for the standard of care required of such professionals in interpreting and applying the contents of this report and its supplementary data. In using this report and data, you expressly assume all risks associated with your use. Under no circumstances shall QuakeLogic Inc. or its officers, directors or employees be liable to you or any other person for any direct, indirect, special, incidental, or consequential damages arising from or related to your use of, or reliance on, the report, data or any information obtained therein. To the fullest extent permitted by law, you agree to release and hold harmless QuakeLogic Inc. from any and all liability of any nature arising out of or resulting from any use of data provided by this report.

## | Dashboard Sign In

A copy of this report and corresponding data are available at your dashboard. Visit Knowledge Base section of the dashboard for FAQs, tutorials and information about technical content of this report. **CLICK HERE** or copy and paste the following URL <http://dashboard.quakelogic.net> on your browser to log in. Questions? Feel free to contact us at [support@quakelogic.net](mailto:support@quakelogic.net).

**APPENDIX B:**  
**MANUFACTURER SPECIFICATION SHEETS FOR THE INSTALLED**  
**SENSORS**

# ES-U2

## Uniaxial Force Balance Accelerometer

### For use in a variety of applications

The EpiSensor ES-U2 force balance accelerometer is a uniaxial surface package designed primarily for structural engineering applications. However, it can be used in a variety of applications for measuring accelerations up to  $\pm 4g$  and down to the ambient noise level. With full-scale recording ranges of  $\pm 0.25$  to  $\pm 4g$  (user selectable) the ES-U2 provides on-scale recording of earthquake motions even at near-fault locations and in a wide variety of structure types.

Because the ES-U2 is extremely low-noise, it can detect motions of the ambient vibration field at most urban sites and civil structures from 1 Hz to 200A Hz. This makes the ES-U2 a unique sensor at a great price. The output of the ES-U2 is an amplified, conditioned signal—it requires no external electronics other than a data acquisition system.

The significantly improved bandwidth of DC to 200 Hz allows engineers and scientists to study motions at higher frequencies while maintaining the very important DC response that allows simple field calibration and reduces processing confusion.

Output circuitry is also significantly enhanced. Four types of outputs can be field-selected by the user:  $\pm 2.5V$  single-ended,  $\pm 10V$  single-ended,  $\pm 5V$  differential or  $\pm 20V$  differential.

The sensor has a number of full scale outputs to match the traditional Kinemetrix earthquake recording instruments, as well as the most modern Kinemetrix' Rock+ series and Quanterra's Q330 series of dataloggers.

EpiSensor force balance accelerometers are also available in triaxial surface and borehole (the FBA ES-SB shallow and FBA ES-DH deep) packages.



### FEATURES

- Low noise
- Extended bandwidth - DC to 200Hz
- User-selectable full-scale range
- Calibration coil (standard)
- Single-end or differential output (user selectable)



## SPECIFICATIONS

<b>Dynamic range:</b>	155 dB+
<b>Bandwidth:</b>	DC to 200Hz
<b>Calibration coil:</b>	Standard
<b>Full-scale range:</b>	User selectable at $\pm 0.25g$ , $\pm 0.5g$ , $\pm 1g$ , $\pm 2g$ or $\pm 4g$
<b>Outputs:</b>	User selectable at: $\pm 2.5V$ single-ended $\pm 10V$ single-ended $\pm 5V$ differential $\pm 20V$ differential
<b>Zero adjust:</b>	User-friendly access holes for simple, safe, efficient adjustment
<b>Linearity:</b>	$< 1000 \mu g/g^2$
<b>Hysteresis:</b>	$< 0.1\%$ of full scale
<b>Cross-axis sensitivity:</b>	$< 1\%$ (including misalignment)
<b>Zero point thermal drift:</b>	$< 500 \mu g/^{\circ}C$ (1g sensor)
<b>Power consumption:</b>	Quiescent current $< 9 mA$ from $\pm 12V$
<b>Mounting:</b>	Dual bolt for horizontal or vertical mounting
<b>Operating Temperature:</b>	$-20^{\circ}$ to $70^{\circ}C$ ( $0^{\circ}$ to $160^{\circ}F$ )
<b>Housing:</b>	EMI/RFI Watertight enclosure 55x65x97mm (2.2"x2.6"x3.8")
<b>Weight:</b>	0.35kg (0.77 pounds)



## SPECIFICATIONS

### Channels

Number: 4, 8, 12, 24 and 36  
Input level: 5Vpp, 10Vpp, 40Vpp Differential Input

### Data Acquisition

Type: Individual 24-bit Delta Sigma converter per channel  
bandwidth-optimized 32-bit data path  
Anti-alias filter: Double Precision FIR Filter Causal/Acausal;  
>140 dB attenuation at output Nyquist  
Dynamic range: 200 sps ~127 dB (RMS clip to RMS noise - Typical)  
100 sps ~130 dB (RMS clip to RMS noise - Typical)  
Frequency response: DC to 80 Hz @ 200 sps  
Sampling rates: 1, 10, 20, 50, 100, 200, 250, 500, 1000, 2000, 5000 sps  
Channel skew: None – simultaneous sampling of all channels  
Acquisition modes: Continuous, triggered, time windows  
Output data format: 24 bit signed (3 bytes) in user selectable format  
Parameter calculations: Calculations of key parameters in real-time,  
including JMA intensity  
Real time digital output: Ethernet or RS-232 output of digital stream

### Trigger

Type: IIR bandpass filter (three types available)  
Trigger selection: Independently selected for each channel  
Threshold trigger: Selectable from 0.01% to 100% of full scale  
Trigger voting: Internal, external and network trigger votes with  
arithmetic combination  
Additional trigger: STA/LTA, Time Window

### Timing

Type: Oscillator digitally locked to GPS/GNSS or PTP:  
Integrates completely with system, providing timing,  
internal oscillator correction and position information.  
Shared timing: 3 Ports for shared timing for multiple local units

Accuracy: <1 microseconds of UTC with GPS/GNSS or PTP

### Storage

Data slot: Internal SDHC Card Slot, standard 32 GB  
System slot: Internal SDHC Card Slot, 4 GB  
Recording capacity: Approximately 42 kB per channel per minute on  
Memory Card of 24-bit data @ 200 sps.  
(33 days of 4x200sps recording on 8GB Data card)  
SDHC Format: Linux EXT4  
Data: Offloaded automatically to removable thumb drives  
connected to a USB host port. Parallel recording  
(mirroring) data on an external USB thumb drive.  
USB drives format: FAT32

### Communications

Ethernet interface: Real Time Telemetry (Multiple destinations TCP/IP  
Protocol), Parameter set up, and event retrieval (FTP/  
SFTP) RS-232 interface: Real Time Telemetry (over  
modem, radio, etc.), Parameter set up, and event  
retrieval  
Modem: Built in modem, Remote access, initiated by user or by  
the Obsidian  
Telemetry: Real-time data via DFS, SEEDLink, Earthworm, Antelope  
compatible ORB server, or Altus SDS protocols.

### Instrument Software

Type: Multi-tasking operating system supports simultaneous  
acquisition and interrogation; allows remote  
and automatic firmware upgrades  
Security: Supports SSH and SSL  
System control: Configure sample rate, filter type, trigger type and  
voting, maintains communications and event storage  
File formats: Kinemetrics EVT, MiniSEED, SAC, COSMOS,  
MATLAB, SUDS, SEISAN, ASCII, others  
Intelligent alerting: Initiate communications when an event is detected or if an  
auto-diagnostic failure occurs  
Auto-diagnostics: Continuously check system voltages, temperature, humidity,  
and timing system integrity  
Rapid setup: Can be configured from a parameter file  
System timing: Supports PTP Slave and PTP Master timing (Using  
Internal GPS as Master clock), NTP and External 1PPS

### I/O and Display

Power input: Mil-style connector for DC power input, external  
battery connection, Power over Ethernet (Option)  
Interfaces: 10/100 BaseT Ethernet Port  
(M12 connectors) 3 x USB 2.0 Host Ports  
USB 2.0 Device  
3 x RS-232  
DFS Port (RS232)  
Linux Console (RS232)  
POTS Modem  
3 x Time/Power Ports (1PPS In/Out, Switched Power)  
GPS Antenna (TNC)  
EMI/RFI protection: All I/O lines EMI/RFI and transient protected  
LED: System, power and event status, Ethernet Link & Data



## SPECIFICATIONS

### Power Supply

Type:	Internal high efficiency switched power supply and battery charger system with extensive SOH outputs
DC input:	9-28 VDC (>15.5VDC for Battery Charger Operation)
External AC/DC:	Universal Input 100-250 VAC 50/60 Hz
Power module:	Output 15.5 VDC
Internal battery charger:	Digitally temperature compensated output for External Valve Regulated Lead Acid (VRLA) batteries with reverse protection and deep discharge recovery.
Fuses:	None. Uses resettable Polyswitch protection
Current drain:	180ma @12V (Obsidian 4X w/o sensors)

### Environment

Operating temp: -20° to 70°C Operation  
 Humidity: 0-100% RH (Non-condensing)

### Physical

Size: Obsidian 4X: 14" (L) x 5.5" (D) x 6.8" (H)  
 Obsidian 8X: 19" (L) x 7.5" (D) x 6.8" (H)  
 Enclosure rating: IP67 Equivalent  
 Environmental: RoHS Compliant Unit

### Support Software

File Viewer*:	Multiplatform program for rapid review of waveforms and event information.
Antelope:	Comprehensive commercial network operational and management system for medium and large networks
Earthworm:	Comprehensive public domain network operational and management system for medium and large networks
Rock Monitor Professional:	Rock network operation and monitoring tool
Rockhound:	Commercial open architecture user-extensible real-time data collection and processing software that runs on a variety of computers
PSD:	Commercial Pseudo Spectral Density software for earthquake data analysis
SMA:	Commercial Strong Motion Analyst software for earthquake data analysis and processing
K2COSMOS*:	Conversion software from Altus EVT file format to COSMOS v1.20 format (COSMOS format can also be produced natively from the Obsidian)
Miscellaneous:	Format converters to ASCII and other formats. Web Server for command and control, Optional Software Development Kit and Compilers. Contact Kinemetrix for other options. *No charge

Specifications subject to change without notice



## ETNA 2

### Next Generation of Web Based, Cost Effective, Strong Motion Accelerographs

Kinemetrics' **ETNA** accelerograph established the world's standard for strong motion recording for almost two decades with more than 6000 installations worldwide. The **ETNA 2** represents the next generation of ETNA-class accelerographs offering NEW and cost effective, web based monitoring capabilities paired with another Kinemetrics' established world standard, the exemplary **EpiSensor** accelerometer.

The ETNA 2 is easy to use since it was designed around the Rockhound application software first implemented on the Basalt instruments and continued now on the new Obsidian instruments.

ETNA 2 offers the most essential accelerograph features supporting a wide range of earthquake monitoring applications in a small, lightweight, and simple to use package. If you are interested in Earthquake Early Warning, in structural monitoring, in aftershocks surveys or even in induced earthquake monitoring related to oil and gas, and geothermal fluid injection activities, the ETNA 2 is the right product for you.

And for those whose job it is to maintain large number of stations, we implemented Streamlined Station Maintenance (SSM) that allows you to use your browser to log maintenance activities such as software updates, site inspections, or battery replacements right on the unit. These logs can be automatically uploaded to your data center for archiving, reducing paper work in the field, and eliminating human error.



### FEATURES

- 3 sensor channels with an internal EpiSensor triaxial deck
- 24-bit Delta Sigma converter, one per channel
- Matched to Kinemetrics outstanding EpiSensor accelerometer performance
- Built-in GPS/GNSS and PTP timing options
- Record and communicate multiple sample rates
- Earthquake Early Warning low latency 0.1s packets ready
- Multiple telemetry protocols: ORB natively or public domain Earthworm and SeedLink
- Streamlined Station Maintenance (SSM)
- Data offloaded automatically to removable thumb drive connected to the USB host port. Parallel recording (mirroring) data on an external USB thumb drive.
- Wireless communications via cellular modem
- State-of-health monitoring, including input and system voltages, internal temperature, communication link diagnostics, available storage
- IP Security through SSH and SSL
- Reverse voltage protection and self resettable fuses
- System Status LEDs
- Surviving temporary immersion at 1 m depth (rated IP67)
- Designed for RoHS Compliance and easy re-cycling
- Designed for the lowest Total Cost of Ownership (TCO)





## SPECIFICATIONS

### Sensor

Type: Triaxial EpiSensor force balance accelerometers, orthogonally oriented, internal  
Full scale range: User selectable at  $\pm 1g$ ,  $\pm 2g$  or  $\pm 4g$   
Bandwidth: DC to 200 Hz  
Dynamic range: 155 dB+  
Offset: Factory set, software re-zeroing

### Digitizer

Channels: 3 24-bit sensor channels for the internal sensors  
bandwidth-optimized 32-bit data path  
Dynamic range: ~130 dB at 100 sps (defined as RMS clip to RMS  
shorted- input noise) or  
~139 dB at 100 sps (defined as full scale peak to peak  
to RMS shorted-input noise)  
Primary sample rates: 1, 10, 20, 50, 100, 200, 250, 500 sps  
Secondary sample rates: A second lower sample rate can be  
selected from the primary sample rates  
above

Acquisition modes: Continuous (ring buffer) and triggered  
Calibration & test: Pulse and Sensor Response Test

### Trigger

Trigger selection: Independently selected for each channel Internal  
Trigger: Threshold, selectable from 0.01% to 100%  
of full scale or STA/LTA algorithm  
Trigger voting: Internal and network trigger votes with  
arithmetic combination

### Timing

Type: Oscillator digitally locked to GPS/GNSS or to PTP master  
Accuracy: <1 microseconds of UTC with GPS/GNSS locked

### Storage

Data storage: Internal SDHC Card, 32 GB  
System storage: Internal SDHC Card, 4 GB  
Data: Offloaded automatically to removable thumb drive  
connected to the USB host port. Parallel recording  
(mirroring) data on an external USB thumb drive.  
File formats: MiniSEED, EVT, and ASCII. Other formats  
available.  
USB drive file system: FAT32

### Interfaces and Digital Control

Interfaces: 1 x Ethernet 10/100BaseT  
(M12 connectors) 1 x USB 2.0 Device Port for data access  
1 x USB 2.0 Host Port for peripherals  
1 x RS-232 for factory use only  
Relays: 2 x SPDT relays, software configurable  
LEDs: System, power and event status, Ethernet Link

### Communications

Ethernet interface: Real Time Telemetry (Multiple destinations TCP/IP  
Protocol), web server for parameter setup, event  
retrieval via FTP/SFTP; supports Point of Contact  
(POC) name service  
Modem: External, cellular or POTS, connected via the  
USB 2.0 Host interface; consult factory for details  
Protocols: Real-time data streaming via Antelope compatible ORB  
server or via public domain SEEDLink and Earthworm  
protocols  
State-Of-Health: Input voltage, Super Capacitor voltage, Time  
synchronization, internal temperature, available storage  
Low latency: 1s and 0.1s data packets i.e. for EEWS applications  
Data visualization: Waveform Viewer for continuous waveform display  
and File Viewer for triggered event display;  
consult factory for other support software

### Power Requirements

Consumption: <3W operational  
Voltage range: 9-28 VDC  
Protections: Reverse voltage, over/under voltage, self resettable fuses

### Physical

Mounting: Central bolt, 3 adjustable feet, air bubble leveling  
Dimensions: 6" x 6" x 3" (15cm x 15 cm x 7.5cm)  
Volume: 1.6 liters  
Weight: 3.3 lbs. (1.5 kg)

### Environmental

Temperature range: -20° to 70°C operational  
Humidity: 0-100% RH (non-condensing)  
Enclosure rating: IP67

Specifications subject to change without notice

# HX-P510 SERIES

## 0 to 5, 0 to 10, $\pm 5$ , $\pm 10$ VDC ANALOG OUTPUT

The UniMeasure HX-P510 Series transducer offers a voltage output with wide adjustability to give a 0 to 5, 0 to 10,  $\pm 5$  or  $\pm 10$  VDC output. The device may be powered with an unregulated voltage in the range of 4.9 to 30 VDC. Zero and span adjustment potentiometers are readily accessible. With the zero position set anywhere within the first 30% of total travel, the span may be adjusted to give a full 0 to 5 or 0 to 10 VDC output with the span set anywhere within the last 20% of travel. Alternatively, the zero position may be set anywhere between 10% and 90% of full travel to give an output of  $\pm 5$  or  $\pm 10$  VDC with the span set between 50% to 100% of the longest travel from the zero position.



### SPECIFICATIONS

#### GENERAL

Available Measurement Ranges .....See Supplemental Data<sup>1</sup>, Table 12  
Sensing Device .....Precision Potentiometer  
Connector .....MS3102E-14S-6P  
Mating Connector (included) .....MS3106E-14S-6S

#### PERFORMANCE

Linearity  
2", 3", 4", 5" & 6" Ranges ..... $\pm 0.30\%$  Full Scale  
10", 15", 20" & 25" Ranges ..... $\pm 0.20\%$  Full Scale  
All other ranges ..... $\pm 0.15\%$  Full Scale  
Repeatability ..... $\pm 0.015\%$  Full Scale  
Resolution .....Essentially Infinite

#### ENVIRONMENTAL

Operating temperature .....-40°C to +85°C  
Storage Temperature .....-55° to +100°C  
Operating humidity .....100%  
Vibration .....15 G's 0.1 ms max.  
Shock .....50 G's 0.1 ms max.

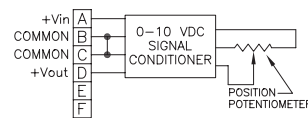
#### INGRESS PROTECTION (Exclusive of Wire Rope Area)

Standard .....IP-65 (NEMA 4)  
Optional .....IP-68 (NEMA 6)

#### ELECTRICAL

Output .....0 to 5 or 10 VDC,  $\pm 5$  or  $\pm 10$  VDC  
Excitation Voltage .....4.9 to 30 VDC  
Excitation Current .....25 mA max.  
Output Impedance .....10 $\Omega$  max.  
Output Load .....5K $\Omega$  min.  
**ADJUSTMENT RANGE-0 to 5 or 0 to 10 VDC**  
Zero .....0 to 30% of Range  
Span .....80% to 100% of Range  
**ADJUSTMENT RANGE- $\pm 5$  or  $\pm 10$  VDC**  
Zero .....10% to 90% of Range  
Span .....50% to 100% of Longest Possible  
Travel from Zero Position  
Protection .....Reversed Polarity  
Temperature Stability .....0.02%/°C of Span

#### CONNECTION DIAGRAM



#### FOOTNOTES TO SPECIFICATIONS

1. Supplemental Data section located at end of HX Series pages.

### MODEL NUMBER CONFIGURATION

**HX-P510-** 0 1 2 3 4 5 6 7 8 9

#### BASIC CONFIGURATION (FOR ALL RANGES)

**HX-P510-50-S10-N0S-1BC**

**0 RANGE**  
Select Measurement Range From Supplemental Data Table 12 (next page), Insert Corresponding Measurement Range Designator

**1 WIRE ROPE**  
S ..... Stainless Steel  
(See Supplemental Data, Table 12)  
N .....  $\varnothing 0.018$  (0.45 mm)  
Nylon Jacketed Stainless Steel  
Ranges to 80" (2m) only. (formerly NJC)  
J .....  $\varnothing 0.037$  (0.94 mm)  
Nylon Jacketed Stainless Steel  
Ranges 100" (2.5m) to 500" (12.7m) only.

**2 WIRE ROPE TENSION**  
1 ..... Standard  
2 ..... Reduced (Ranges to 80" only)

**3 WIRE ROPE EXIT DIRECTION**  
Use Number designators shown  
RANGES TO 80" (2000 mm)

RANGES 100" TO 2000" (2.5 m TO 50 M)

**4 N** ..... Required Designator  
**5 0** ..... Required Designator  
**6 ELECTRICAL OUTPUT POLARITY**  
S ..... Standard (increasing output as wire rope is extended)  
R ..... Reversed (decreasing output as wire rope is extended)

#### NOTES FOR OPTION BOXES 7, 8, and 9

**IP-65 (NEMA 4):** Transducer equipped with body mounted connector and with or without mating connector. Mating connector with electrical cable available separately as part number 10119-xM where 'x' is length of electrical cable in meters.

**IP-68 (NEMA 6):** Transducer equipped with bulkhead fitting and length of electrical cable. Remote end of electrical cable may be outfitted with water proof connector. Mating connector with electrical cable available separately as part number 10424-xM where 'x' is length of electrical cable in meters.

**7 INGRESS PROTECTION**  
1 ..... IP-65 (NEMA 4)  
2 ..... IP-68 (NEMA 6)  
3 ..... IP-68 (NEMA 6) Corrosion Resistant Construction

**8 IP-65-NEMA 4 CONNECTOR**  
B ..... 6 Pin 3102E Body Mounted Connector  
**IP-68-NEMA 6 ELECTRICAL CABLE**  
P ..... Bulkhead Fitting w/ 0.3m (12") Electrical Cable  
3 ..... Bulkhead Fitting w/ 3m (10') Electrical Cable  
4 ..... Bulkhead Fitting w/ 4m (13.5') Electrical Cable  
5 ..... Bulkhead Fitting w/ 5m (16.5') Electrical Cable  
6 ..... Bulkhead Fitting w/ 6m (20') Electrical Cable  
7 ..... Bulkhead Fitting w/ 7m (23') Electrical Cable

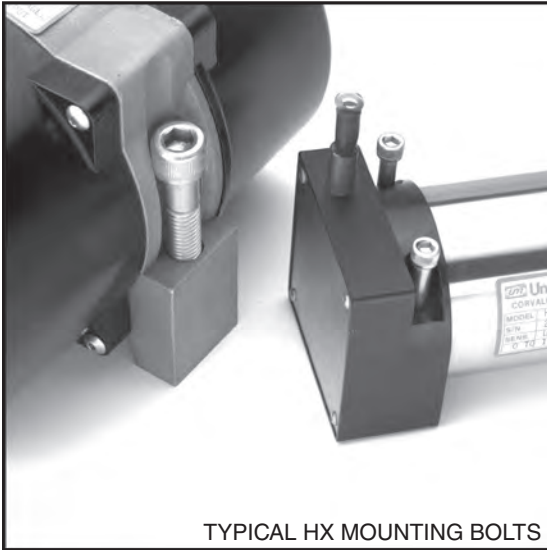
**9 IP-65-NEMA 4 MATING CONNECTOR**  
C ..... IP-65 Mating Connector Included  
K ..... IP-65 Mating Connector Omitted\*  
\*Electrical cable with mating connector may be ordered separately as part number 10119-xM where 'x' is the length required in meters.

**IP-68-NEMA 6 CABLE MOUNTED CONNECTOR**  
N ..... No connector on end of electrical cable  
K ..... IP-68 Cable to cable connector with  
**NO** mating connector\*\*  
\*\*Electrical cable with mating connector may be ordered separately as part number 10424-xM where 'x' is the length required in meters. Mating connector alone unavailable.

# HX SERIES

## SUPPLEMENTAL DATA

### MECHANICAL SPECIFICATIONS



**AVAILABLE MEASUREMENT RANGES** .... See Table 12

#### CONSTRUCTION

Ranges 80" (2 m) and under .....	Anodized Aluminum Mounting Base
	Stainless Steel & Anodized Aluminum Housing
Ranges 100" (2.5 m) and greater .....	Stainless Steel Mounting Base
	High Impact, Corrosion Resistant
	Thermoplastic Housings
Wire Rope Tension.....	See Table 12
Wire Rope Diameter .....	See Table 12
Weight .....	See Table 12
Connector .....	MS3102A-14S-6P
Mating Connector .....	MS3106E-14S-6S
Optional NEMA 6 Capability.....	Bulkhead fitting with shielded twisted pair cable

#### Life<sup>(1)</sup>

Ranges 2" to 6" .....	5,000,000 full stroke cycles
Ranges 10" to 25" .....	500,000 full stroke cycles
Ranges 30" to 400" .....	250,000 full stroke cycles
Ranges 500" to 2000" .....	200x10 <sup>6</sup> lineal inches

#### NOTES:

1. With 1K ohm potentiometer, wire rope misalignment 2° maximum at full stroke, relatively dust free environment, nylon jacketed wire rope on units with ranges 80" and less.

Use value from this column to indicate overall measurement range

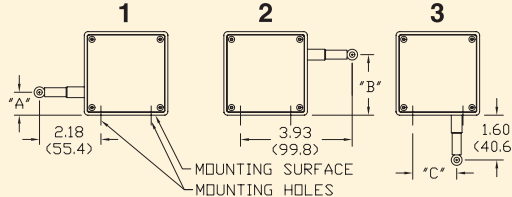
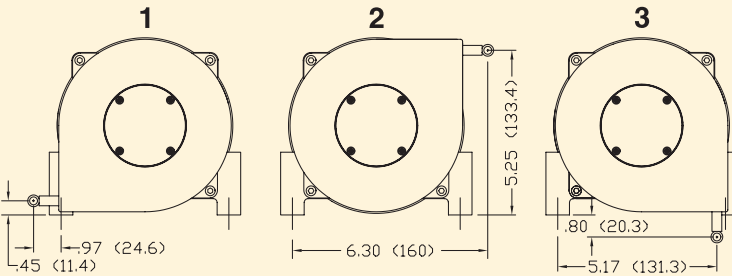


Check mark indicates available measurement range

## TABLE 12

MEASUREMENT RANGE DESIGNATOR	STANDARD MEASUREMENT RANGES (in) (mm)		APPLICABLE SERIES			WIRE ROPE TENSION (NOMINAL) (oz) (N)		WIRE ROPE DIAMETER (in) (mm)		TRANSDUCER WEIGHT (lb) (Kg)		Product Photo
			HX-PA HX-PB HX-P420 HX-P510	HX-EP	HX-V HX-VP							
2	2	50	✓	-	✓	34	9.4	.016	0.4	2	0.9	
3	3	75	✓	-	✓	24	6.7	.016	0.4	2	0.9	
4	4	100	✓	-	✓	24	6.7	.016	0.4	2	0.9	
5	5	125	✓	-	✓	19	5.3	.016	0.4	2	0.9	
6	6	150	✓	-	✓	24	6.7	.016	0.4	2	0.9	
10	10	250	✓	✓	✓	34	9.4	.016	0.4	2	0.9	
15	15	390	✓	-	✓	24	6.7	.016	0.4	2	0.9	
20	20	500	✓	-	✓	24	6.7	.016	0.4	2	0.9	
25	25	640	✓	✓	✓	19	5.3	.016	0.4	2	0.9	
30	30	750	✓	-	✓	24	6.7	.016	0.4	2	0.9	
40	40	1000	✓	-	✓	24	6.7	.016	0.4	2	0.9	
50	50	1250	✓	✓	✓	19	5.3	.016	0.4	2	0.9	
60	60	1500	✓	✓	✓	24	6.7	.016	0.4	2	0.9	
80	80	2.0m	✓	✓	✓	21	5.8	.016	0.4	2	0.9	
100	100	2.5m	✓	✓	✓	36	10.0	.024	0.6	6.8	3.1	
120	120	3.0m	✓	✓	✓	36	10.0	.024	0.6	6.8	3.1	
150	150	3.8m	✓	✓	✓	36	10.0	.024	0.6	6.8	3.1	
200	200	5.0m	✓	✓	✓	36	10.0	.024	0.6	6.8	3.1	
250	250	6.3m	✓	✓	✓	36	10.0	.024	0.6	6.8	3.1	
300	300	7.5m	✓	✓	✓	36	10.0	.024	0.6	6.8	3.1	
350	350	8.8m	✓	✓	✓	36	10.0	.024	0.6	6.8	3.1	
400	400	10.0m	✓	✓	✓	36	10.0	.024	0.6	6.8	3.1	
500	500	12.5m	✓	✓	✓	36	10.0	.024	0.6	8.6	3.9	
600	600	15.2m	✓	✓	✓	36	10.0	.024	0.6	8.6	3.9	
800	800	20.3m	✓	✓	✓	36	10.0	.024	0.6	8.6	3.9	
1000	1000	25.4m	✓	✓	-	36	10.0	.024	0.6	12.0	5.4	
1200	1200	30.4m	✓	✓	-	36	10.0	.024	0.6	12.3	5.6	
1600	1600	40.6m	✓	✓	-	36	10.0	.024	0.6	14.1	6.4	
1800	1800	45.7m	✓	✓	-	36	10.0	.021	0.6	15.9	7.2	
2000	2000	50.8m	✓	✓	-	36	10.0	.021	0.5	16.3	7.4	

Specifications subject to change without notice

### OPTION DESCRIPTIONS

OPTION	OPTION DESIGNATOR	DESCRIPTION																												
NYLON JACKETED WIRE ROPE <u>RANGES TO 80" ONLY</u>	N	Replaces standard stainless steel wire rope with Ø.018 nylon jacketed wire rope. This option increases wire rope life dramatically but may increase non-linearity by as much as ±.05% of full scale.																												
NYLON JACKETED WIRE ROPE <u>RANGES 100" TO 500" ONLY</u>	J	Replaces standard stainless steel wire rope with Ø.037 nylon jacketed wire rope.																												
ALTERNATE WIRE ROPE EXIT <u>RANGES TO 80" (2.0 m)</u>	1, 2, 3	<div><div><div><div>1</div><div>2</div><div>3</div></div><div></div></div><table><thead><tr><th>RANGE</th><th>"A"</th><th>"B"</th><th>"C"</th></tr></thead><tbody><tr><td>2", 10"</td><td>1.12 (28.4)</td><td>1.79 (45.5)</td><td>1.21 (30.7)</td></tr><tr><td>3", 15", 30"</td><td>.96(24.4)</td><td>1.95 (49.5)</td><td>1.37 (34.8)</td></tr><tr><td>4", 20", 40"</td><td>.80 (20.3)</td><td>2.11 (53.6)</td><td>1.53 (38.9)</td></tr><tr><td>5", 25", 50"</td><td>.64 (16.3)</td><td>2.27 (57.7)</td><td>1.69 (42.9)</td></tr><tr><td>6", 60"</td><td>.49 (12.4)</td><td>2.42 (61.5)</td><td>1.84 (46.7)</td></tr><tr><td>80"</td><td>.25 (6.4)</td><td>2.66 (67.6)</td><td>2.08 (52.8)</td></tr></tbody></table><p>Dimensions in brackets are millimeters</p></div>	RANGE	"A"	"B"	"C"	2", 10"	1.12 (28.4)	1.79 (45.5)	1.21 (30.7)	3", 15", 30"	.96(24.4)	1.95 (49.5)	1.37 (34.8)	4", 20", 40"	.80 (20.3)	2.11 (53.6)	1.53 (38.9)	5", 25", 50"	.64 (16.3)	2.27 (57.7)	1.69 (42.9)	6", 60"	.49 (12.4)	2.42 (61.5)	1.84 (46.7)	80"	.25 (6.4)	2.66 (67.6)	2.08 (52.8)
RANGE	"A"	"B"	"C"																											
2", 10"	1.12 (28.4)	1.79 (45.5)	1.21 (30.7)																											
3", 15", 30"	.96(24.4)	1.95 (49.5)	1.37 (34.8)																											
4", 20", 40"	.80 (20.3)	2.11 (53.6)	1.53 (38.9)																											
5", 25", 50"	.64 (16.3)	2.27 (57.7)	1.69 (42.9)																											
6", 60"	.49 (12.4)	2.42 (61.5)	1.84 (46.7)																											
80"	.25 (6.4)	2.66 (67.6)	2.08 (52.8)																											
ALTERNATE WIRE ROPE EXIT <u>RANGES 100" (2.5 m) and GREATER</u>	1, 2, 3	<div><div><div><div>1</div><div>2</div><div>3</div></div><div></div></div><p>Dimensions in brackets are millimeters</p></div>																												
NON-STANDARD POTENTIOMETER <u>APPLIES TO HX-PA &amp; HX-VPA ONLY</u>	3, 4	<p>Non-standard potentiometer linearity is as follows:</p> <table><thead><tr><th>RANGE</th><th>LINEARITY</th></tr></thead><tbody><tr><td>5" and Below</td><td>±1.00% of full scale</td></tr><tr><td>10" to 25"</td><td>±0.50% of full scale</td></tr><tr><td>30" and above</td><td>±0.25% of full scale</td></tr></tbody></table> <p><b>Note:</b> This option is subject to potentiometer availability.</p>	RANGE	LINEARITY	5" and Below	±1.00% of full scale	10" to 25"	±0.50% of full scale	30" and above	±0.25% of full scale																				
RANGE	LINEARITY																													
5" and Below	±1.00% of full scale																													
10" to 25"	±0.50% of full scale																													
30" and above	±0.25% of full scale																													
REVERSED OUTPUT	R	Output is at a maximum when wire rope is fully retracted. Output decreases as wire rope is extended. Does not apply to velocity signal.																												
IP-68, (NEMA 6) CAPABILITY	2	<div><p>Connector is replaced with a bulkhead fitting and a designated length of urethane jacketed, shielded, twisted pair cable. Retraction mechanism and electrical components are sealed to IP-68, (NEMA 6) capability.</p></div>																												
CORROSION RESISTANT CONSTRUCTION	3	<p>All external anodized aluminum parts of transducer are replaced with stainless steel and corrosion resistant plastic. Transducer is sealed to IP-68 (NEMA 6) capability. Urethane jacketed, shielded, twisted pair cable exits unit. No connector on unit.</p> <div></div>																												

### DIMENSIONAL INFORMATION

#### HX SERIES – RANGES TO 80" (2 m)

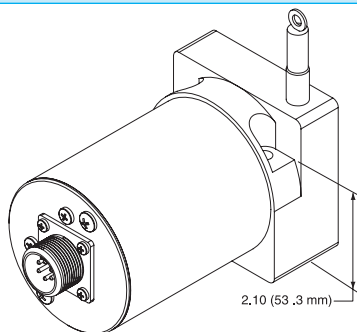
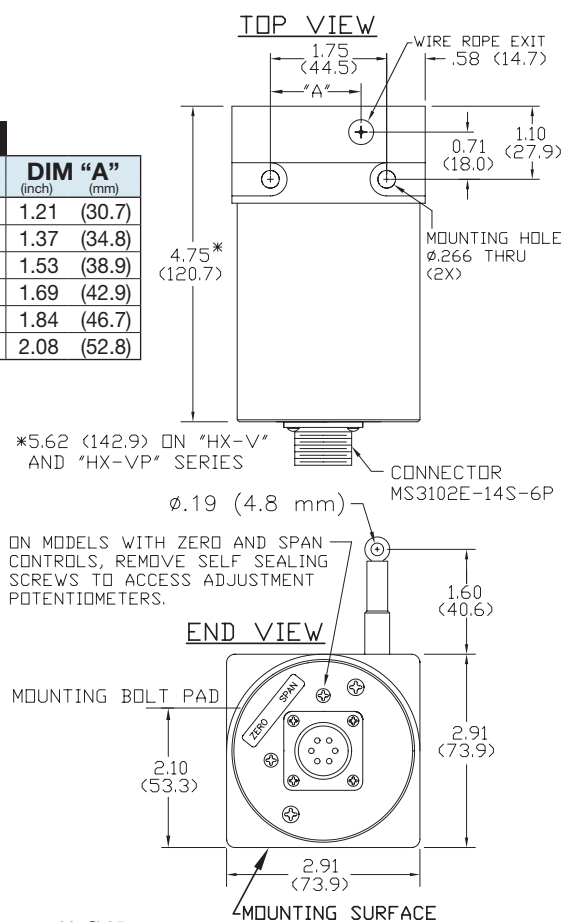


**FIG. 1**

**TABLE 13**

RANGE	DIM "A"	DIM "A"
(inch)	(mm)	
2", 10"	1.21	(30.7)
3", 15", 30"	1.37	(34.8)
4", 20", 40"	1.53	(38.9)
5", 25", 50"	1.69	(42.9)
6", 60"	1.84	(46.7)
80"	2.08	(52.8)



**NOTES:**

1. Transducer mounts with Ø.25 or M6 Socket head cap bolts.

Dimensions in brackets are millimeters

**TABLE 14**

RANGE	DIM "A"	DIM "B"
(inch)	(mm)	(inch)
Ranges to 800"	7.70 (196)	3.80 (97)
1000" to 2000"	11.0 (280)	5.60 (142)

**NOTES:**

1. Transducer mounts with Ø.50 or M12 socket head cap bolts.
2. Dimension "C" is the cable offset that occurs as the cable is extended from the transducer. For "C" in inches,  $C = .0016 \times E$  where E = extension in inches. For "C" in millimeters,  $C = .0016 \times E$  where E = extension in mm.

#### HX SERIES – RANGES GREATER THAN 80" (2 m)

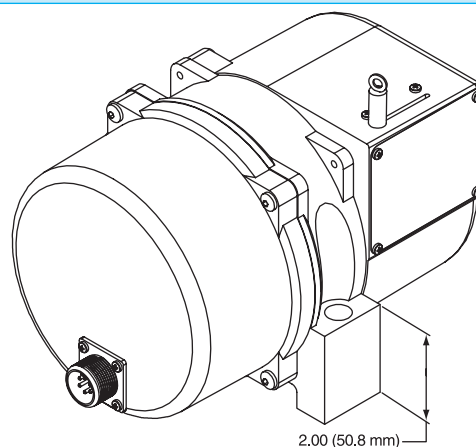
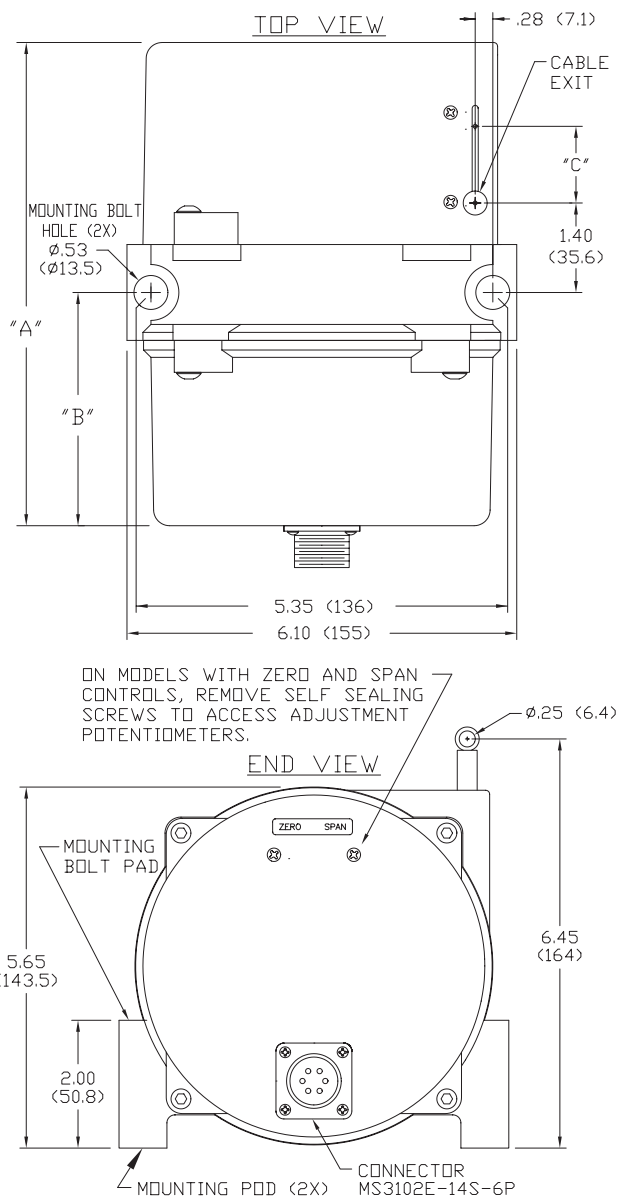


**FIG. 2**



Dimensions in brackets are millimeters



## Accurate, User-Configurable, All-in-One Inclinometer

### DESCRIPTION

The H6 inclinometer provides highly accurate, dual axis inclination sensing in a rugged environmentally protected housing. This unit incorporates MEMS sensing elements referenced to gravity with integrated temperature compensation over the entire industrial operating range of -40° to +85°C.

The H6 provides two continuous and fully configurable analog outputs. These outputs can be individually set to current, voltage or open collector switch modes. The voltage output can be set to any value between 0V and 10V, the current output can be set to any value between 0mA and 24mA - either to any angle range between ±180°. The current and voltage outputs are linear with respect to the input angle directly.

The open collector switch output connects to signal common and can be set to trip above, below, between, or outside any angle threshold or window range. The transistor output can be used directly or to drive an external relay (up to 250mA drive capability)

The H6 also includes a polled, half-duplex (2-wire), RS-485 digital interface for angle measurements and configuration. Also available upon request, the H6 has CAN bus hardware available for customer specified protocols (including J1939 and CanOPEN).

All analog output parameters can be configured via the RS-485 interface at the factory to meet your specifications or through the Flex Series Development Kit and software allowing the end customer to modify the sensor as needed right from a PC - providing full flexibility for R&D and OEM production lines.

Used as integrated devices by original equipment manufacturers (OEMs) or as standalone sensors for test and measurement, the H6 is made for applications where high accuracy and long-term stability are required in noisy and wide temperature changing environments. For use with most applications including commercial, industrial, and military applications.



### FEATURES

- Dual Axis
- Horizontal and Vertical Mount
- Scalable Angle Range up to ±180°
- Fully Temperature Compensated
- Multiple, Simultaneous, Configurable Outputs
  - Current
  - Voltage
  - Open Collector Switch
  - RS-485
  - CAN bus
  - Optional Logging to SD Card
- Daisy-chain Multiple Sensors
- Vibration and shock resistant
- Environmentally sealed IP68
- Rugged Aluminum housing
  - Optional Stainless Steel 316
- EMC protected to 100V/m
- Reverse Polarity Protection
- Overvoltage/overcurrent protection
- -40° to +85°C Operating Temperature
- CE Certified

### INDUSTRIES

- Aerospace & Defense
- Construction
- Mining
- Offshore
- Transportation

**Rieker Rugged. Rieker Reliable.™**

RIEKER INC • 34 MOUNT PLEASANT ROAD • ASTON • PA • 19014 • USA

610-500-2000

fax: 610-500-2002

[inquiry@riekerinc.com](mailto:inquiry@riekerinc.com)

[www.riekerinc.com](http://www.riekerinc.com)



# Flex Series - H6

## General Information Brochure

Page 2 of 5

**TABLE 1: H6 SENSOR SPECIFICATIONS**

INPUT PARAMETERS			
SUPPLY VOLTAGE	+11..36 VDC Non-Regulated		
SUPPLY CURRENT <sup>1</sup>	22mA @ 24VDC (Digital Output only)		
	30mA nominal @ 24VDC (Analog Output - no load)		
	75mA max @ 24VDC (Analog and Digital Outputs enabled)		
	85mA max @ 12VDC (Analog and Digital Outputs enabled)		
ANALOG MEASURING RANGE	Scalable within 360°		
DIGITAL MEASURING RANGE	±180°		
INPUT PROTECTION	Reverse Polarity, ESD & Surge Protected		
ABSOLUTE ACCURACY OVER FULL OPERATING TEMPERATURE			
RANGE: ±180°	±0.1° typical, ±0.2° absolute max		
RESOLUTION	0.05°		
RESPONSE TIME	6 user-configurable options from 4Hz to 0.3Hz		
ANALOG CURRENT & VOLTAGE OUTPUT PARAMETERS			
OUTPUT RANGES	Current	4..20 mA, 0..20 mA (Configurable within 0..24mA)	$R_{sense} \leq \frac{V_{supp}}{000} \frac{5}{R_{wire}}$
	Voltage	0..5 V, 0..10V (Configurable within 0..10V)	1kΩ load min.
SENSITIVITY <sup>2</sup>	Relative to Scaled Range		
NULL (0°)	Fully Configurable		
SWITCH OUTPUT PARAMETERS			
OUTPUT MODE	Open Collector Switch to Signal Common		
TRIP MODES	Fully Configurable (Window, Threshold, etc.)		
SWITCH CAPABILITY	250mA @ 36V max		
DIGITAL OUTPUT PARAMETERS			
OUTPUT TYPE	RS-485 Half Duplex (2-wire)		
INCLINATION OUTPUT	32-Bit IEEE Packetized Float		
BAUD RATE	125K Default (Configurable from 9600 to 250K)		
BYTE FORMAT	8 Data Bits, No Parity, 1-stop Bit, No Flow Control		
PACKET FORMAT	See Installation Manual for Packet Details and Commands		
INFORMATION RATE	Polled (up to 20 times/sec)		
LOGGING CAPABILITY (OPTIONAL)			
SUPPLY CURRENT	Additional 20mA @24VDC		
LOGGING RESOLUTION	Configurable in one minute increments		
CARD TYPE	μSD		

**Rieker Rugged. Rieker Reliable.™**

RIEKER INC • 34 MOUNT PLEASANT ROAD • ASTON • PA • 19014 • USA

610-500-2000

fax: 610-500-2002

[inquiry@riekerinc.com](mailto:inquiry@riekerinc.com)

[www.riekerinc.com](http://www.riekerinc.com)

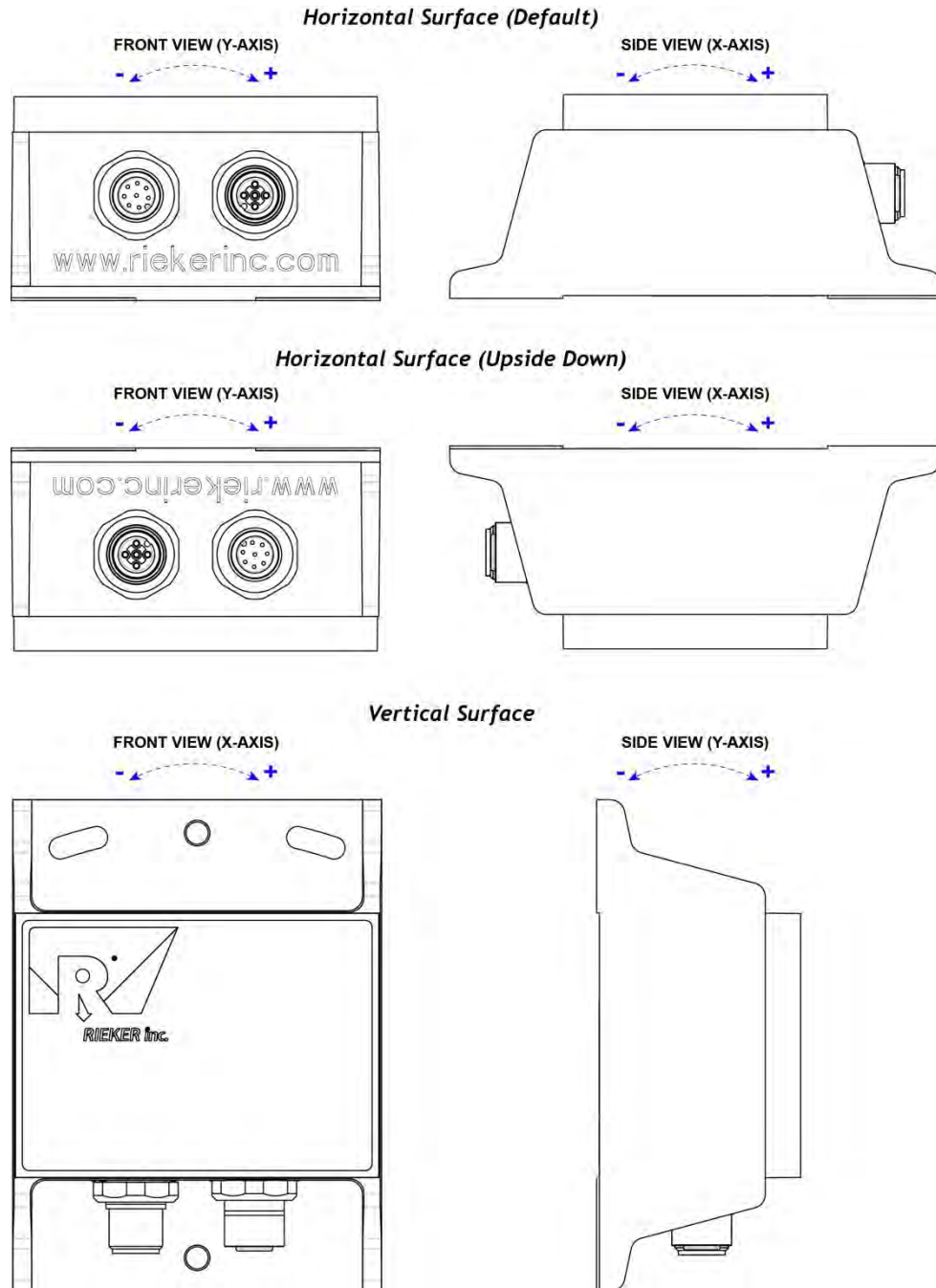




### FIGURE 2: Mounting Positions

**Note:** The factory default settings for mounting position (either horizontal or vertical) must be selected at time of order. Default output polarity shown is configurable at the factory (defined at time of order) or by the end user via the Flex Dev Kit that includes Rieker Flexware app, sold separately.

- Special H6MM Multi-Mount model (available exclusively through Digi-Key) allows the end user to select between horizontal and vertical mounting positions via a special Flex Dev Kit that includes Rieker Flexware app, also sold separately through Digi-key.



**Rieker Rugged. Rieker Reliable.™**

RIEKER INC • 34 MOUNT PLEASANT ROAD • ASTON • PA • 19014 • USA

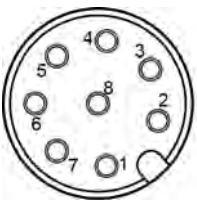
610-500-2000

fax: 610-500-2002

[inquiry@riekerinc.com](mailto:inquiry@riekerinc.com)

[www.riekerinc.com](http://www.riekerinc.com)

**TABLE 2: MALE 8 PIN INPUT CONNECTOR**

PIN	FUNCTION	 <p>M12 (male 8-pin) Pin Assignment FRONT VIEW</p>
1	SUPPLY VOLTAGE +11.. +36VDC	
2	POWER / SIGNAL COMMON	
3	RS485 D+ OR CAN HI	
4	RS485 D- OR CAN LO	
5	NO CONNECTION OR CAN SHIELD	
6	ANALOG OUTPUT 1 (DEFAULT: X-AXIS)	
7	ANALOG OUTPUT 2 (DEFAULT: Y-AXIS)	
8	NO CONNECTION	



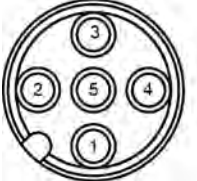


**TABLE 3: FEMALE 5 PIN DIGITAL OUTPUT DAISY CHAIN CONNECTOR**

PIN	FUNCTION	 <p>M12 (female 5-pin) Pin Assignment FRONT VIEW</p>
1	CAN SHIELD	
2	SUPPLY VOLTAGE +11..+36VDC	
3	POWER COMMON	
4	RS485 D+ OR CAN HI	
5	RS485 D- OR CAN LO	

**TABLE 4: CURRENT SENSE**

<p>Rsense is dependent upon supply voltage and cable/wire resistance. Ensure the following equation is met:</p> $R_{sense} \leq \frac{V_{supply} - 2.5}{0.020} - R_{wire}$	QUICK REFERENCE	
	SUPPLY VOLTAGE	SENSE RESISTOR
	12V	200-350 OHMS
	24V	200-1000 OHMS
	28V	200-1000 OHMS

**TABLE 5: ACCESSORIES (SOLD SEPARATELY)**

	<p><b>Flex Series Configurator Kit</b></p> <ul style="list-style-type: none"> <li>Flexware™ Toolkit Applications</li> <li>USB Interface Cable from Sensor to PC</li> <li>Also available through Digi-Key (pn Dev-Kit-C)</li> </ul>
	<p><b>Input / Output Interface &amp; Daisy-chain Cables</b></p> <ul style="list-style-type: none"> <li>I/O Cable, mating connector to sensor, varying cable lengths w/ pigtail leads for input power and output.</li> <li>Daisy-chain cable, M12 8-pin to M12 5-pin, varying cable length for sensor to sensor connection.</li> </ul>
	<p><b>Termination Resistor for Daisy-Chain Configuration</b></p> <ul style="list-style-type: none"> <li>Terminating Resistor M12 5-pin male</li> </ul>
	<p><b>Display Box</b></p> <ul style="list-style-type: none"> <li>Single or Dual Line LCD</li> <li>0.1° Resolution</li> <li>Battery or 12..24VDC input supply</li> </ul>

**Rieker Rugged. Rieker Reliable.™**

RIEKER INC • 34 MOUNT PLEASANT ROAD • ASTON • PA • 19014 • USA

610-500-2000

fax: 610-500-2002

[inquiry@riekerinc.com](mailto:inquiry@riekerinc.com)

[www.riekerinc.com](http://www.riekerinc.com)

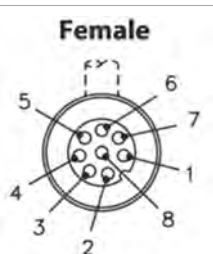
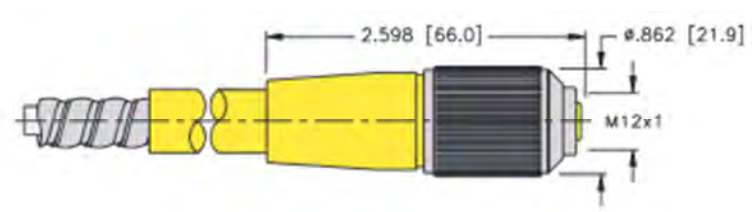
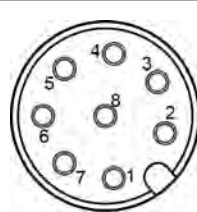
### Cable P/N **CBL-H6-X** External Power Input & Sensor Output

For use with applicable H6 Dual Axis Inclinometer models with

- 11-36VDC input power supply
- dual analog current 4-20mA outputs
- Digital Serial RS-485 Outputs
- Euro M12 type connector
- “-X” = cable length (ie CBL-H6-6 is a 6-ft cable)

#### Description:

- One (1) cable from one (1) 8-pin M12 Female mating connector for power input and output via pigtail leads.

CABLE WIRING TABLE		
CONNECTOR / PIN	DESCRIPTION	TERMINATION
PIN 1	SUPPLY VOLTAGE +11.. +36VDC	WHITE
PIN 2	POWER / SIGNAL COMMON	BROWN
PIN 3	RS485 D+	GREEN
PIN 4	RS485 D-	YELLOW
PIN 5	NO CONNECTION	GRAY
PIN 6	ANALOG OUTPUT 1 (DEFAULT: X AXIS)	PINK
PIN 7	ANALOG OUTPUT 2 (DEFAULT: Y AXIS)	BLUE
PIN 8	NO CONNECTION	RED
<div style="display: flex; align-items: center;"> <div style="margin-right: 20px;"> <p><b>Female</b></p>  </div> <div>  </div> </div>		
H6 Male 8 Pin Input Connector Notes		
<p><b>NOTES:</b></p> <ul style="list-style-type: none"> <li>• The front and back of the connector may not have any pin markings in the actual connector. The user will need to look at the front-side keyway (see drawing) to determine pin outs.</li> <li>• The termination wire colors reference the cable sold by Rieker.</li> </ul>		 <p>M12 (male 8-pin) Pin Assignment FRONT VIEW</p>



# Flex H6 Cable Accessories

## Specifications & Wiring

Page 2 of 2

STOCK CABLE PART NUMBERS FOR ORDERING		
PN	ORDERING DESCRIPTION	EXTENDED DESCRIPTION
CBL-H6-6	CABLE M12(FRA) 8-PIN 6-FT	H6 Cordset, M12, Female Right Angle to Pigtail Leads, 8-Wire, 6-FT (2m)
CBL-H6-6-B	CABLE M12(FSTR) 8-PIN 6-FT	H6 Cordset, M12, Female Straight to Pigtail Leads, 8-Wire, 6-FT (2m)
CBL-H6-13	CABLE M12(FRA) 8-PIN 13-FT	H6 Cordset, M12, Female Right Angle to Pigtail Leads, 8-Wire, 13-FT (4m)
CBL-H6-13-A	CABLE M12(FSTR) 8-PIN 13-FT	H6 Cordset, M12, Female Straight to Pigtail Leads, 8-Wire, 13-FT (4m)
CBL-H6-26	CABLE M12(FRA) 8-PIN 26-FT	H6 Cordset, M12, Female Right Angle to Pigtail Leads, 8-Wire, 26-FT (8m)
CBL-H6-26-A	CABLE M12(FSTR) 8-PIN 26-FT	H6 Cordset, M12, Female Straight to Pigtail Leads, 8-Wire, 26-FT (8m)
CBL-H6-75	CABLE M12(FRA) 8-PIN 75-FT	H6 Cordset, M12, Female Right Angle to Pigtail Leads, 8-Wire, 75-FT (23m)
CBL-H6-75-A	CABLE M12(FSTR) 8-PIN 75-FT	H6 Cordset, M12, Female Straight to Pigtail Leads, 8-Wire, 75-FT (23m)
CBL-H6-100	CABLE M12(FRA) 8-PIN 100-FT	H6 Cordset, M12, Female Right Angle to Pigtail Leads, 8-Wire, 100-FT (30m)
CBL-H6-100-A	CABLE M12(FSTR) 8-PIN 100-FT	H6 Cordset, M12, Female Straight to Pigtail Leads, 8-Wire, 100-FT (30m)
CBL-H6-164	CABLE M12(FRA) 8-PIN 164-FT	H6 Cordset, M12, Female Right Angle to Pigtail Leads, 8-Wire, 164-FT (50m)
CBL-H6-164-A	CABLE M12(FSTR) 8-PIN 164-FT	H6 Cordset, M12, Female Straight to Pigtail Leads, 8-Wire, 164-FT (50m)
CBL-H6DC-50	CABLE M12(FSTR) 8P(F)-5P(M) 50FT	H6 Daisy Chain Cordset, M12, 8-Pin Female Straight to 5-Pin Male Straight, 50-FT (15m)

NOTE: Custom cable lengths available upon request, lead times and pricing subject to change.

The information and material presented may not be published, broadcast, rewritten, or redistributed without the express written consent of Rieker® Inc.  
©2018 Rieker® Inc. All Rights Reserved.  
FORM NUMBER: H60010\_01/15 UPDATED: 4/27/18

<b>Rieker Rugged. Rieker Reliable.™</b>			
RIEKER INC • 34 MOUNT PLEASANT ROAD • ASTON • PA • 19014 • USA			
<b>610-500-2000</b>	fax: 610-500-2002	<b>inquiry@riekerinc.com</b>	<b>www.riekerinc.com</b>



# MODEL 41342VC/VF

## PLATINUM TEMPERATURE PROBE, 0-1V Output

INSTRUCTION SHEET 41342V-90  
REV: C111215

### INTRODUCTION

The Model 41342VC/VF Platinum Temperature Probe is an accurate 1000 ohm Platinum RTD temperature sensor and low power voltage interface circuit mounted in a weatherproof junction box. The probe is available in Celsius or Fahrenheit calibration. Output signal is 0-1 VDC full scale. The probe is designed for easy installation in YOUNG Multi-plate and Aspirated Radiation Shields.

### INSTALLATION

For accurate measurements, the temperature probe should be installed in a protective radiation shield. Use of the probe without a radiation shield may result in large errors. YOUNG naturally ventilated or motor aspirated shields are recommended. For best performance, the probe and shield should be placed in a location with good air circulation clear of large masses (buildings, pavement, solar panels...), Exhaust vents, electrical machinery, motors, water fountains and sprinklers.

### MAINTENANCE

The temperature probe is designed to offer years of service with minimal maintenance. Temperature calibration should be accurate for the life of the probe. If necessary, the probe may be periodically checked or recalibrated using normal bath calibration methods. NIST traceable calibration is available from YOUNG at nominal cost.

### WARRANTY

This product is warranted to be free of defects in materials and construction for a period of 12 months from date of initial purchase. Liability is limited to repair or replacement of defective item. A copy of the warranty policy may be obtained from R. M. Young Company.

### CE COMPLIANCE

This product has been tested and complies with European CE Requirements for the EMC Directive. Please note that shielded cable must be used.

### EMC COMPLIANCE

This device complies with Part 15 of the FCC Rules. Operation is subject to the following two conditions: (1) this device may not cause harmful interference, and (2) this device must accept any interference received, including interference that may cause undesired operation.

This equipment has been tested and found to comply with the limits for a Class A digital device, pursuant to part 15 of the FCC Rules. These limits are designed to provide reasonable protection against harmful interference when the equipment is operated in a commercial environment. This equipment generates, uses, and can radiate radio frequency energy and, if not installed and used in accordance with the instruction manual, may cause harmful interference to radio communications. Operation of this equipment in a residential area is likely to cause harmful interference in which case the user will be required to correct the interference at his own expense.

This ISM device complies with Canadian ICES-001.

Cet appareil ISM est conforme à la norme NMB-001 du Canada.

EN55011/CISPR 11, Group 1, Class B device.

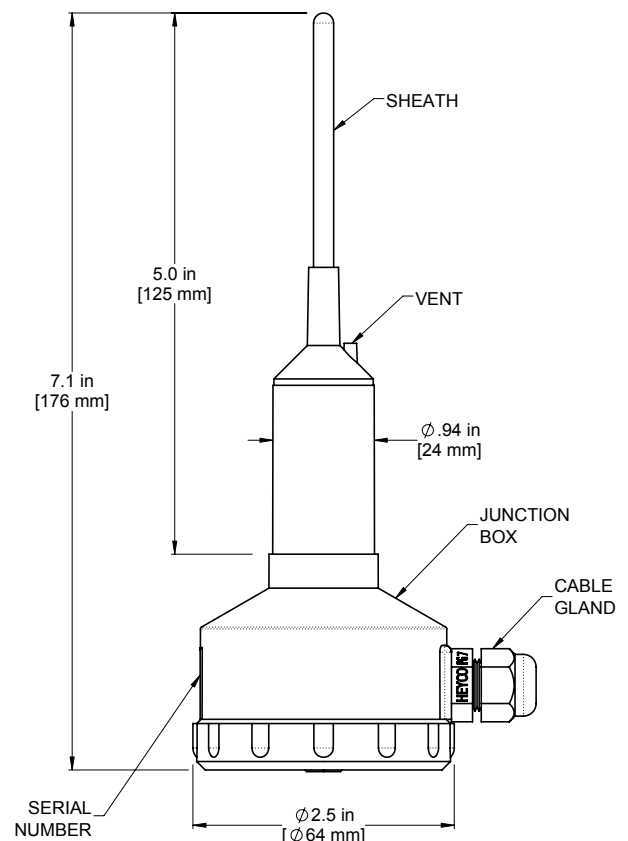
Class B equipment is suitable for use in domestic establishments and in establishments directly connected to a low voltage power supply network which supplies buildings used for domestic purposes.

To meet EMC Compliance, (2) YOUNG 18500 ferrite chokes must be installed on the cable, one near the sensor, and one near the recording instrument. (Each choke must have the cable pass through the center hole at least 2 times, creating 1 loop around the outside as shown in the diagram on the back page.)

### SPECIFICATIONS

Power Requirement:	8 - 24 VDC, 5mA
Calibrated measuring range:	-50 to +50°C (suffix C) -50 to +150°F (suffix F)
Accuracy at 0°C:	±0.3°C (Differential Measurement)
Time Constant:	42 seconds in 43502 shield.
Sensor type:	1000Ω Platinum RTD
Output signal:	0-1 VDC
Recommended Cable:	2 pair shielded, 22 AWG (#18723)

Recommended Radiation Shields:	
Model 43502	Aspirated Radiation Shield
Model 41003P	Multi-Plate Radiation Shield



R. M. YOUNG COMPANY

2801 Aero Park Drive , Traverse City, Michigan 49686 USA

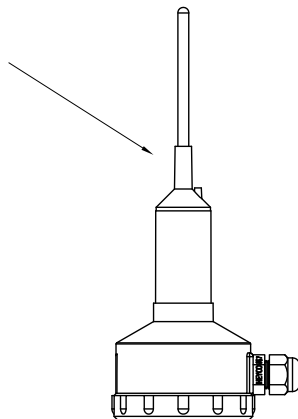
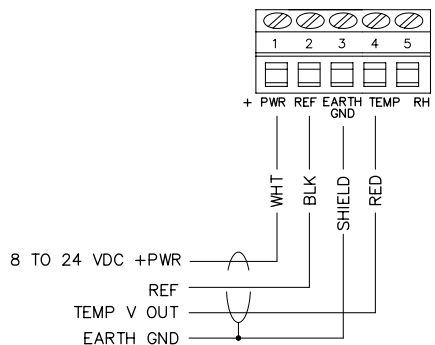
TEL (231) 946-3980 FAX (231) 946-4772



## WIRING INFORMATION

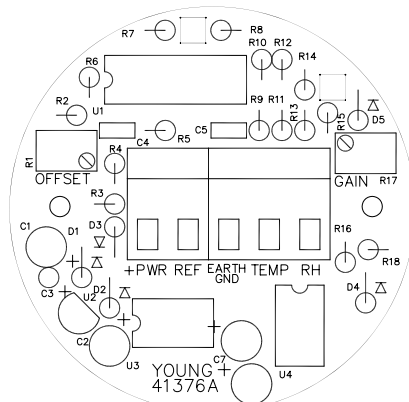
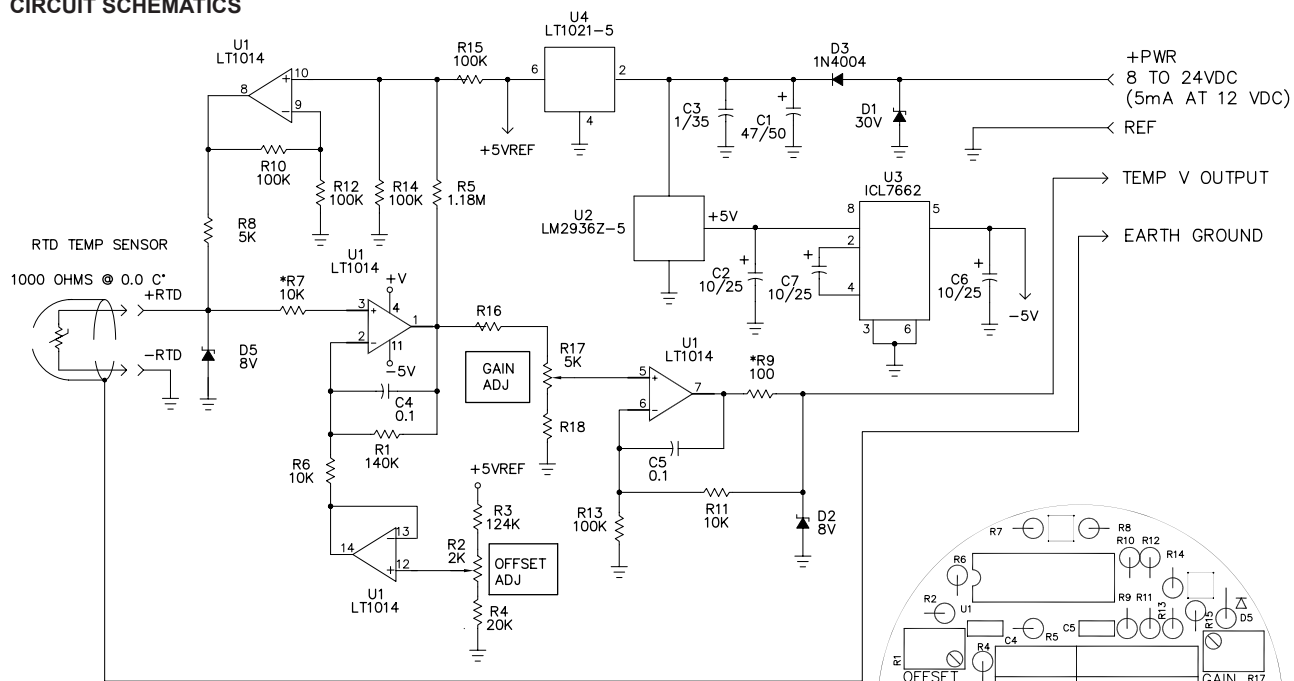
MODEL 41342V TEMPERATURE SENSOR

### WIRING INFORMATION



18500 FERRITE CHOKE (2)  
(SEE EMC SECTION FOR USAGE)

### CIRCUIT SCHEMATICS



RESISTOR VALUES		
MODEL	41342VC	41342VF
RANGE	CELSIUS (-50° TO +50°)	FAHRENHEIT (-50° TO +150°)
OUTPUT	0 TO 1.000V	0 TO 1.000V
R16	95.3K	100K
R18	20K	17.7K

#### NOTES:

- ALL RESISTORS ARE 5ppm, 0.1% UNLESS OTHERWISE NOTED.
- RESISTORS MARKED WITH "\*" ARE 100ppm
- ALL CAPACITORS ARE IN uF OR uF/WV, UNLESS OTHERWISE NOTED.

#### RTD TEMP SENSOR CALIBRATION POINTS:

-50° C	807.873 OHMS
0° C	1000.000 OHMS
+50° C	1189.005 OHMS
-50° F	825.093 OHMS
0° F	932.069 OHMS
+150° F	1247.192 OHMS



# METEOROLOGICAL INSTRUMENTS

## INSTRUCTIONS

### ULTRASONIC ANEMOMETER MODEL 86000





# OPERATING INSTRUCTIONS

Model 86000 Ultrasonic Anemometer

---

## Contents

SECTION	DESCRIPTION	PAGE
1.0	<b>SPECIFICATIONS</b>	1
2.0	<b>INTRODUCTION</b>	1
3.0	<b>BEFORE INSTALLATION</b>	1
4.0	<b>INSTALLATION</b>	2
4.1	Placement	2
4.2	Mounting and Alignment	2
4.3	Wiring Connections	2
5.0	<b>OPERATION</b>	2
5.1	Analog Outputs	2
5.2	With YOUNG Wind Tracker Display	2
5.3	Serial Output Formats and Protocols	2
5.4	Low Power Operation	3
6.0	<b>SETTING SERIAL OUTPUTS AND OPERATING PARAMETERS</b>	
6.1	Setup using YOUNG 86SETUP program	3
6.2	Setup using terminal program	3
6.3	Command Overview	3
6.4	Command Details	4
7.0	<b>EXAMPLE SETTINGS</b>	5
8.0	<b>EMC COMPLIANCE</b>	5
9.0	<b>WARRANTY</b>	5
<b>APPENDIX</b>		
A	<b>WIRING CONNECTIONS</b>	6
B	<b>SENSOR ORIENTATION AND DIMENSIONS</b>	9





## MODEL 86000 ULTRASONIC ANEMOMETER



### 1.0 SPECIFICATIONS

#### WIND SPEED

Range: 0-75 m/s (156 mph)  
Resolution: 0.01 m/s  
Accuracy: 0 to 30 m/s  $\pm 2\%$  or 0.1 m/s  
30 to 75 m/s  $\pm 3\%$

#### WIND DIRECTION

Azimuth Range: 0-360 degrees  
Resolution: 0.1 degree  
Accuracy:  $\pm 2$  degrees

#### SERIAL OUTPUT (Selectable)

Interface Type: RS-232 or RS-485/422  
Formats: ASCII Text (polled and continuous)  
RMYT (YOUNG Wind Tracker)  
NMEA  
Baud Rates: 1200, 4800, 9600, 19200 and 38400

#### ANALOG OUTPUT (Selectable)

Polar Speed: 0-5000mV or 4-20 mA (0 to 100 m/s)  
Polar Direction: 0-5000mV or 4-20 mA (0 to 360° or 0 to 540°)  
Cartesian UV: 0-5000mV or 4-20 mA (-100 m/s to +100 m/s)

#### GENERAL

Output rate: 0.1-20 Hz, 1 Hz typical  
Power Supply: 10 to 30 VDC,  
20 mA typical, 85 mA max  
Protection Class: IP65  
EMC Compliance: FCC Class A digital device  
IEC standard 61326-1  
Dimensions: 29 cm high x 11 cm wide  
Weight: 0.4 kg (0.9 lb)  
Shipping Weight: 1.6 kg (3.5 lb)  
Operating Temperature: -40 to +60°C

### 2.0 INTRODUCTION

The YOUNG 86000 Ultrasonic Anemometer is a 2-axis, no-moving-parts wind sensor. It is ideal for general meteorological applications requiring accurate and reliable measurement. The sensor features wide operating range, compact size, easy installation and low power operation.

The 86000 measures wind speed and direction based on the transit time of ultrasonic pulses between three transducers.

Measurement results are available as calibrated analog output signals, or serial data using RS-232 or RS-485. Continuous serial output or polled operation may be used. Serial format options include direct connection to YOUNG Wind Tracker displays, marine NMEA systems, data loggers, or other compatible serial communication devices.

Operating parameters are easily set using the 86SETUP program provided. All 86000 parameter settings are stored internally in non-volatile memory.

The sensor is constructed using ultraviolet-stabilized thermoplastic for superior environmental resistance. It is easily mounted on standard 1 inch (IPS) pipe. An orientation ring preserves mounting position when the sensor is removed.

### 3.0 BEFORE INSTALLATION

The 86000 arrives fully calibrated and ready to use. Unless otherwise specified, the sensor is configured as follows:

#### FACTORY DEFAULT CONFIGURATION

##### Analog Voltage Outputs:

- Channel V11: Wind Speed  
0-5000 mV = 0-100 m/sec
- Channel V12: Wind Direction  
0-5000mV = 0-360 Deg

If using the sensor with a datalogger or other device requiring 0-5000 mV outputs, no further action is required. Simply connect the device as shown in Appendix A, figure A1.

If using the sensor with a YOUNG Wind Tracker, jumpers must be moved as shown in figure A5. The sensor will then provide RS485 serial output in RMYT format.

Other options are described in APPENDIX A. These are accomplished using various jumper combinations and configuring settings using the 86SETUP program available at [www.youngusa.com](http://www.youngusa.com).

**Note: Always connect and bench test a complex system before installation in the field.**

## 4.0 INSTALLATION

### 4.1 PLACEMENT

Proper instrument placement is important. Eddies from buildings, trees, or other structures can influence measurements. For most applications, locate the sensor well above or upwind of obstructions. As a general rule, air flow around a structure is disturbed to 2 times the height of the structure upwind, 6 times the height downwind, and up to 2 times the height of the structure above ground.

### 4.2 MOUNTING AND ALIGNMENT

Mount the sensor to standard 1-inch (IPS) pipe that has an outside diameter of 1.34 inches (34 mm).

Most applications require aligning the sensor to geographic north (0 degrees). In this orientation the sensor junction box faces SOUTH (180 degrees). See the diagram in APPENDIX B.

- 4.2.1 Place orientation ring over pipe with guide pin up.
- 4.2.2 Place sensor mounting post over pipe.
- 4.2.3 Using the transducers as a sighting aid, align the sensor with a feature on the horizon that represents the proper orientation. After alignment, tighten the mounting post band clamp to secure the position. DO NOT OVER-TIGHTEN.
- 4.2.4 Slide the orientation ring up so its guide pin is fully engaged in the sensor mounting post notch. Tighten the orientation ring band clamp to secure its position. DO NOT OVER-TIGHTEN.

If the sensor needs to be removed later, leave the orientation ring on the pipe to preserve sensor alignment.

### 4.3 WIRING CONNECTIONS

With long cable lengths, resistance in the power supply wires reduces the available voltage at the sensor. Power at the sensor must be in the range of 10 to 30 VDC when the sensor is operating. See WIRING DIAGRAMS in APPENDIX A.

## 5.0 OPERATION

### 5.1 ANALOG OUTPUTS

As supplied, the sensor is configured for VOLTAGE OUTPUT, Wind Speed and Wind Direction. The sensor may also be set up for 4-20 mA CURRENT output by changing internal settings. Details are in section 6.0.

Analog VOLTAGE or 4-20mA CURRENT outputs may be connected to a datalogger or other device such as a YOUNG 26800 Meteorological Translator. See APPENDIX A for connection details.

Analog outputs may be used simultaneously with RS-232 serial connection. RS-485 serial output may not be used simultaneously with analog outputs since they share connection terminals in the junction box.

Analog outputs may be configured for either Polar (speed and direction) or Cartesian (UV) output format.

For voltage output with cable lengths greater than 3m (10 ft.), measure the signal differentially. Current output signals may be measured single-ended.

### 5.2 USE WITH YOUNG WIND TRACKER DISPLAY

The factory default serial output format is RMYT which is compatible with the YOUNG Model 06201 Wind Tracker display. Set the Wind Tracker input to 'INP 09' and connect as shown in the Wiring diagram, Fig A5, Appendix A. Note that jumpers need to be moved so the RS-485 output is available at the connection terminals. Wind speed and direction measurements appear on the Wind Tracker display. See the Wind Tracker manual for display options and other details.

### 5.3 SERIAL OUTPUT FORMATS

Available serial output formats include RMYT, ASCII, ASCII polled, and NMEA. The factory default format is RMYT for use with the YOUNG Wind Tracker display. Other formats may be selected using the 86SETUP program described in Section 6.0.

#### 5.3.1 RMYT

RMYT is a 6-byte binary data format sent at 9600 baud using RS-485 OUTPUT ONLY mode. This is the factory default serial format for use with the YOUNG Model 06201 Wind Tracker.

#### 5.3.2 ASCII

ASCII output format provides continuous wind measurement data in text format at any of the available baud rates.

ASCII output appears either in POLAR (default) or CARTESIAN UV format. With POLAR format, the wind speed threshold, wind speed units, and resolution are user-selectable. With CARTESIAN the wind threshold is ignored and wind speed units are always meters per second (m/s).

#### ASCII POLAR FORMAT

```
a www.w ddd ss*cc<CR>      Low resolution
a www.ww ddd.d ss*cc<CR>    High resolution
```

where

a	= Sensor address
www.ww	= Wind speed
ddd.d	= Wind direction
ss	= Status code
*	= Asterisk (ASCII 42)
cc	= Checksum
<CR>	= Carriage return (ASCII 13)

#### ASCII CARTESIAN (UV) FORMAT

```
a uu.uu vv.vv ss*cc<CR>
```

where

a	= Sensor address
±uu.uu	= U-axis wind speed (m/s)
±vv.vv	= V-axis wind speed (m/s)
ss	= Status code
*	= Asterisk (ASCII 42)
cc	= Checksum
<CR>	= Carriage return (ASCII 13)

CHECKSUM is a two-character hexadecimal value (in printable ASCII format) generated by taking the exclusive-or of all characters up to the asterisk. STATUS CODE shows a non-zero value when the sensor cannot acquire sufficient samples or a measurement error has occurred.

#### 5.3.3 ASCII POLLED

ASCII POLLED is like ASCII format described above except just one serial output string is sent for each polling command received. The polling command is Ma! where 'a' is the sensor address (valid characters: 0-9, A-Z, a-z). The default address is '0' (ASCII 48).

NMEA format provides continuous wind measurements in standard NMEA marine sentences at 4800 baud. Use RS-485 OUTPUT ONLY serial output mode with YOUNG Model 06206 Marine Wind Tracker or other NMEA-capable device.

## \$WTMWV,ddd,B,www,w,N,A\*GG&lt;CB&gt;&lt;I,F&gt;

CHECKSUM is the two-character printable hexadecimal value generated by taking the exclusive-or of all characters between ' \$ ' and ' \* '.

Average current consumption with default settings is about 20 mA. This configuration uses minimal power and enables all features even though they may not be used. This is suitable for many low power applications.

## 6.0 SETTING OUTPUTS AND OPERATING PARAMETERS

The YOUNG 86SETUP program is available from the factory web site at [www.youngusa.com](http://www.youngusa.com). It provides an easy method for checking and configuring sensor operation. Install the program on a Windows PC and follow instructions that appear on the program screen to retrieve current sensor settings or send new settings.

A general purpose text-based serial communications program like HyperTerminal may be used to manually configure the sensor by sending simple text commands.

The YOUNG sensor and communication program must operate at the same baud rate and be properly connected. Sensor RS-232 mode must be enabled. See the RS-232 Wiring diagram, Fig A3, in Appendix A.

Factory default sensor baud rate is 9600, but may be set to 1200, 4800, 19200 or 38400. Configure the serial communications program for NO handshaking and 1 start, 8 data, 1 stop bit.

The sensor must be in COMMAND MODE in order to set parameters. Enter COMMAND MODE by sending three ESC characters (ASCII 27) in quick succession while the sensor is running. When the sensor is in COMMAND MODE, it sends a '>' prompt character indicated that it is ready to accept commands.

If the prompt does not appear after sending three ESC characters, re-check wiring and communication program setup. If the sensor baud rate is unknown, try sending the ESC characters at each of the five available baud rates (1200, 4800, 9600, 19200 and 38400). It is also possible that sensor parameters have been purposely configured to disable RS-232 mode. If this the case, the following method must be used.

To use this feature, set your serial communication program baud rate to 38400. Remove power then wait 5 seconds. Re-apply power to the sensor. The sensor will transmit four asterisks immediately after power up. After the asterisks appear, send three ESC characters. The COMMAND MODE '>' prompt should appear.

After the '>' prompt appears, send '??' to display a list of available commands. Send 'RPTV' to report current settings. (Note that some values in the report are for factory settings cannot be changed by the user.)

After receiving the carriage return, the sensor will evaluate the command. Valid commands will be executed. Current settings can be evaluated at any time by sending RPTV to get a new report.

The YOUNG 86SETUP program automatically saves all settings to flash memory when they are sent to the sensor. Settings that are changed manually must be saved to flash with the SET77 command.

## 6.4 COMMAND DETAILS

COMMAND	DESCRIPTION
---------	-------------

SET01nn	Set OUTPUT MODE
01	Enable voltage output
03	Enable current output
04	Enable RS-232
08	Enable RS-485 output only
16	Enable RS-485 half duplex
24	Enable RS-485 full duplex

SET02n	Set OUTPUT FORMAT
1	RMYT
2	ASCII
3	ASCII POLLED
4	NMEA

SET03nn	Set BAUD RATE
12	1200
48	4800
96	9600
19	19200
38	38400

SET04n	Set ASCII WS UNITS
1	MPH
2	KNOTS
3	KMPH
4	M/S

SET05c	ASCII character sensor address (0-9, A-Z, a-z)
SET06nnnn	Wind speed threshold for polar output (cm/s)
SET07nnnnnn	Wind speed scale (nnnnn/10000)
SET08nnnnnn	Direction offset (±nnnnn degrees x 10)
SET09nn	Damping factor
SET10nnnnn	Output interval (0-9999 milliseconds)
SET11nn	Direction VOUT (36=0-360, 54=0-540 degrees)
SET12nnn	Sample count (3 to 200)
SET13n	Wind output format (0/1=Polar/UV)
SET14n	Analog error code (1/2/3=None/Lo/Hi)
SET15n	ASCII serial resolution(0/1=Lo/Hi)
SET16n	Force analog out (0/1/2=Lo/Mid/Hi)
SET77	SAVE SETTINGS

XX	Go to OPERATE MODE
RPT	Report parameter settings
??	Command Help list

### 6.4.1 SET01nn SET OUTPUT MODE

This enables and disables 0-5000 mV output, 4-20 mA current output, RS-232, and RS-485. Only one of the two analog output types (voltage or current) may be enabled at one time. Both RS-232 and RS-485 can be enabled at the same time but only one serial output may be used.

Add together values shown in 6.4 COMMANDS SET01 to configure multiple compatible modes. For example, to enable voltage output and RS-232, add the code for each one: 01 + 04 = 05, SET0105. To enable only RS-232, SET0104.

To conserve power, enable only those modes that are needed

### 6.4.2 SET02n OUTPUT FORMAT

This parameter determines the serial output format.

### 6.4.3 SET03nn BAUD RATE

Sets the baud rate for RS-232 and RS-485 serial communication. Make sure this baud rate is the same as the connected device.

### 6.4.4 SET04n ASCII and NMEA WIND SPEED UNITS

Sets wind speed units for polar ASCII, ASCII POLLED, and NMEA serial outputs.

### 6.4.5 SET05c POLL ADDRESS CHARACTER

Sets the sensor address for ASCII POLLED serial format. The default is '0' (ASCII 48). This is the address recognized when the 'Ma' polling command is received ('a' is the address character). Valid address characters include 0-9, A-Z, and a-z.

### 6.4.6 SET06nn WIND SPEED THRESHOLD

Sets the wind speed threshold for polar outputs (wind speed and direction) to minimize erratic wind direction indications at very low wind speeds. This allows the sensor output to mimic a mechanical wind vane that retains its orientation when there is no wind.

Wind below the threshold is reported as zero, while the wind direction angle is held at the last value when wind speed was above threshold. Set threshold in centimeters per second (m/s x 100). The default setting is 25 cm/s (0.25 m/s, 0.56 mph).

### 6.4.7 SET07nnnnn WIND SPEED MULTIPLIER

All wind speed measurements are multiplied by this parameter. The default value is 10000 for a multiplier of 1.0000.

### 6.4.8 SET08nnnnn WIND DIRECTION OFFSET

Use this parameter to add or subtract a wind direction offset. Value is degrees x 10 and may be positive or negative. Wind direction is always re-scaled to a 0-360 range after offset is applied. The default value is 00000.

### 6.4.9 SET09nn DAMPING FACTOR

Wind measurement outputs are damped using the following formula:

$$S_{\text{damped}} = [(d-1) * S_{\text{damped}} + S_{\text{sample}}] / d$$

where:

$S_{\text{damped}}$  = New or last damped wind speed

$S_{\text{sample}}$  = New wind speed speed

d = Damping factor

The default value is 00. This means no damping is applied. High damping values at long output intervals can slow the rate at which indicated wind values change.

### 6.4.10 SET10nnnnn OUTPUT INTERVAL

Sets the time interval between measurements in one millisecond increments. Lower values increase power consumption when continuous measurements are taken.

### 6.4.11 SET11nn ANALOG DIRECTION SCALE

Sets wind direction analog output scale to 0-360 or 0-540 degrees. Use the 0-540 scale whenever possible to avoid full-scale analog output swings between 0 and 360 in variable north wind. (Data loggers or display systems may otherwise obtain samples midpoint during these transitions causing erroneous readings.)

Logged data in 0-540 form may be re-scaled to 0-360 by subtracting 360 degrees from any value greater than or equal to 360. The default parameter setting is 0-360 for systems that cannot re-scale the 0-540 output.

### 6.4.12 SET12nnn SAMPLE COUNT

The rate at which the sensor internally takes complete sonic wind samples is greater than 200 times per second. This command sets the number of internal samples used to calculate the median measurement result.

More internal samples consume more power while providing greater immunity to conditions like turbulent high-speed wind. Fewer samples consume less power while providing less immunity to disruptive conditions.

This command interacts with the OUTPUT INTERVAL setting. More samples may require a longer output interval.

#### 6.4.13 SET13n ASCII and ANALOG OUTPUT FORMAT

This setting determines whether ASCII and ASCII POLLED serial outputs and analog outputs provide wind data in either Polar (speed and direction) or Cartesian (UV) form.

#### 6.4.14 SET14n ANALOG OUTPUT STATUS

Serial ASCII and ASCII POLLED formats report a STATUS CODE where non-zero values indicate insufficient samples or measurement error. SET14n determines how the STATUS CODE is indicated by the analog output.

#### 6.4.15 SET15n ASCII RESOLUTION

Sets low or high wind speed and direction resolution.

#### 6.4.16 SET16n FORCE ANALOG OUTPUT

This command forces both analog output channels to LO, MID, or HI scale. This may be used to calibrate or check the operation of externally connected analog measurement devices.

#### 6.4.17 SET77 SAVE SETTINGS

Use this command to save current parameter settings to non-volatile memory. Any settings which have not been saved will be lost when power is removed. Saved settings are loaded at power up. This command may be used any time the sensor is in COMMAND MODE.

#### 6.4.16 XX, RPTV, and ??

XX Returns the sensor to OPERATE MODE.  
RPT Reports the current parameter settings.  
?? Shows a list of commands.

## 7.0 EXAMPLE SETTINGS

Suggested settings. Not all possible setting combinations are shown. Using YOUNG 86SETUP program for changing parameters is recommended. See wiring diagrams for jumper settings.

### 7.1 FACTORY DEFAULT

RS-232	Enabled
RS-485 Output Only	Enabled
Voltage Output:	Enabled
Current Output:	Disabled
Serial Output Format:	RMYT
Output Interval	250
Sample Count:	16

### 7.2 MINIMUM POWER

RS-232	Enabled
RS-485	Disabled
Voltage Output:	Disabled
Current Output:	Disabled
Serial Output Format:	ASCII
Output Interval	1000
Sample Count:	16

### 7.3 4-20 mA OUTPUT

RS-232	Enabled
RS-485	Disabled
Voltage Output:	Disabled
Current Output:	Enabled
Output Interval	1000
Sample Count:	50

### 7.4 RS-485 POLLED ASCII OUTPUT

RS-232	Enabled
RS-485 (Full Duplex)	Enabled
Voltage Output:	Disabled
Current Output:	Disabled
Serial Output Format:	ASCII POLLED
Sample Count:	50

### 7.5 HIGH WINDS

Output Delay:	1000
Sample Count:	200

## 8.0 EMC COMPLIANCE

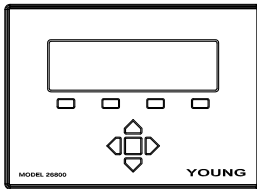
This sensor complies with limits for a Class A digital device, pursuant to part 15 of the FCC Rules, and IEC standard 61326-1. This sensor generates, uses, and can radiate radio frequency energy and, if not installed and used in accordance with the instruction manual, may cause harmful interference to radio communications. Sensor operation may be temporarily affected by radio frequency and transient interference sources, but will revert to proper operation when the source of interference is removed.

## 9.0 WARRANTY

This product is warranted to be free of defects in materials and construction for a period of 12 months from date of initial purchase. Liability is limited to repair or replacement of the defective item. A copy of the warranty policy may be obtained from R. M. Young Company.

## APPENDIX A: WIRING CONNECTIONS

Fig. A1: VOLTAGE OUTPUT



Model 26800 Translator, Datalogger,  
or other voltage measuring device

### SETTINGS

Output Mode: VOUT

WD Output Scale: 0-360 or 0-540 degrees

Wind Format: Polar or UV

Analog Output Error Code: None, Low, or High

### CALIBRATION:

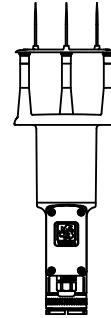
Polar Wind Speed: 0 to 5000 mV

Wind Direction: 0 to 100 m/s

U or V: 0 to 360° or 0 to 540°

-100 m/s to +100 m/s

For best accuracy measure output voltage differentially as shown. Use shielded cable. Connect cable shield to earth ground as shown.



Model 86000 / 86106  
Ultrasonic Anemometer

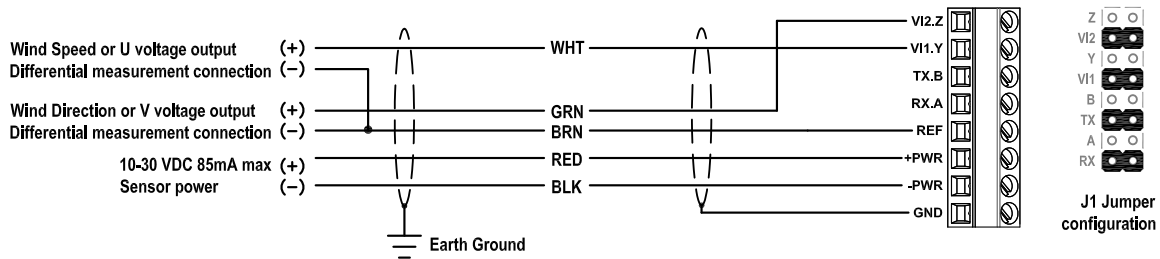
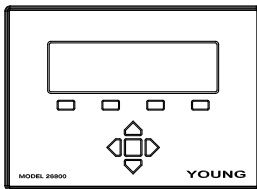


Fig. A2: 4-20 mA CURRENT OUTPUT



Model 26800 Translator, Datalogger,  
or other current measuring device

### SETTINGS

Output Mode: IOUT

WD Output Scale: 0-360 or 0-540 degrees

Wind Format: Polar or UV

Analog Output Error code: None, Low, or High

### CALIBRATION:

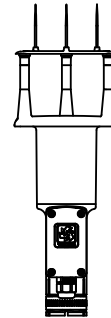
Polar Wind Speed: 4.00 to 20.00 mA

Wind Direction: 0 to 100 m/s

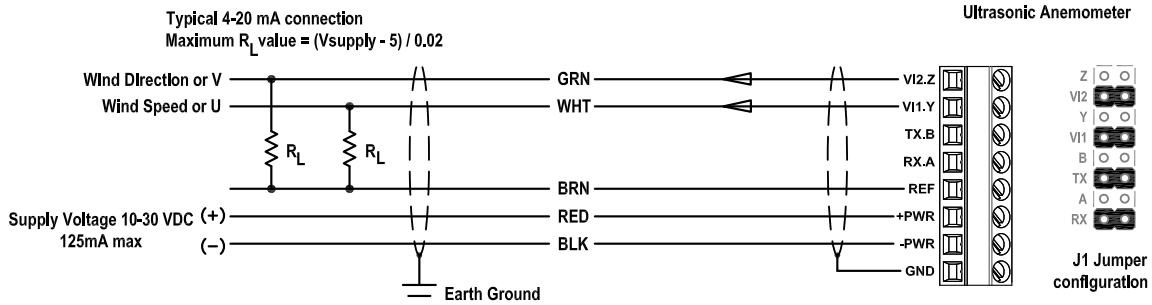
U or V: 0 to 360° or 0 to 540°

-100 m/s to +100 m/s

Use shielded cable. Connect cable shield to earth ground as shown.

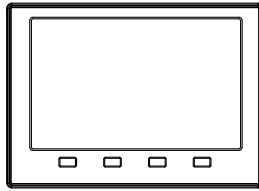


Model 86000 / 86106  
Ultrasonic Anemometer



## APPENDIX A: WIRING CONNECTIONS

Fig. A3: RS-232 SERIAL CONNECTION

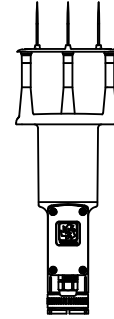


Serial Device

**SETTINGS**  
 Output Mode: RS-232  
 Output Format: ASCII, ASCII POLLED, NMEA, or RMYT  
 Baud Rate: 1200, 4800, 9600, 19200 or 38400

Set connected serial device baud rate to match sensor.  
 1 start bit, 8 data bits, no parity, 1 stop bit, no flow control.

Use shielded cable. Connect cable shield to earth ground as shown.



Model 86000 / 86106  
Ultrasonic Anemometer

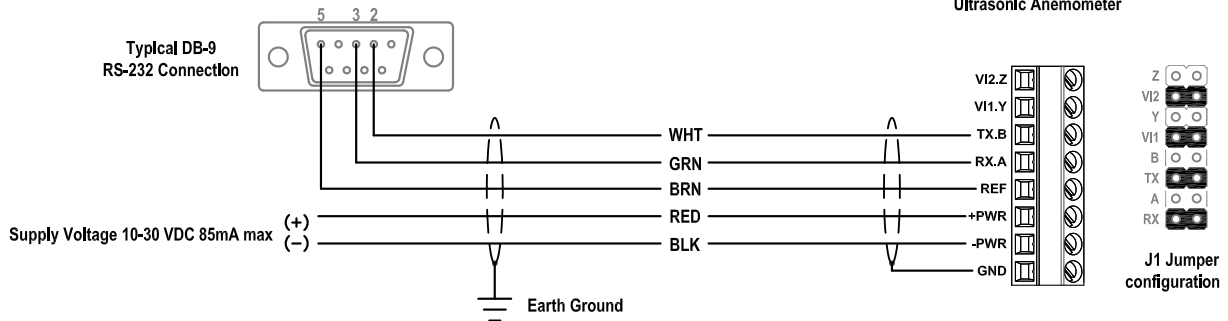
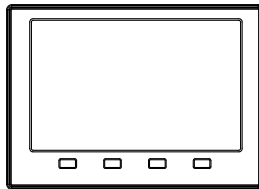


Fig. A4: RS-485 SERIAL CONNECTION

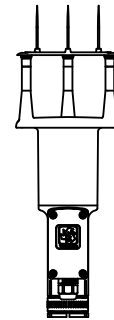


Serial Device

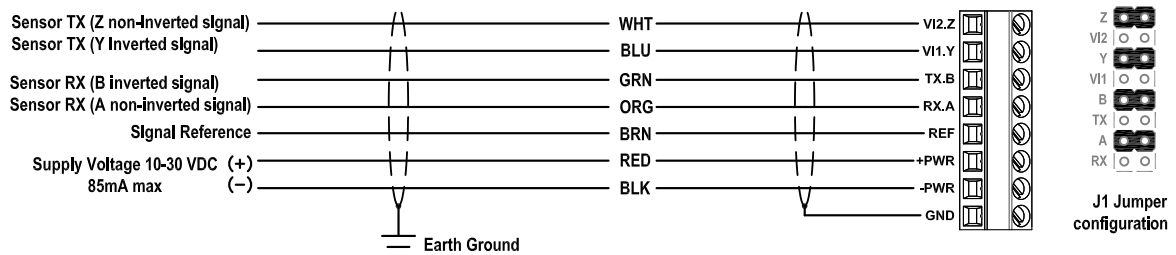
**SETTINGS**  
 Output Mode: RS-485 Full Duplex  
 Output Format: ASCII, ASCII POLLED\*, NMEA, or RMYT  
 Baud Rate: 1200, 4800, 9600, 19200 or 38400

Set connected device baud rate to match sensor.  
 1 start bit, 8 data bits, no parity, 1 stop bit, no flow control.

Use shielded cable. Connect cable shield to earth ground as shown.



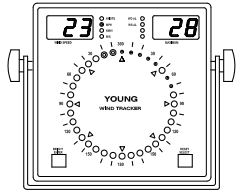
Model 86000 / 86106  
Ultrasonic Anemometer





## APPENDIX A: WIRING CONNECTIONS

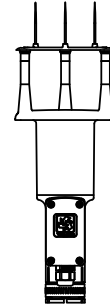
Fig. A5: 06201 WIND TRACKER



Model 06201  
Wind Tracker

SETTINGS:  
Output Mode: RS-485 Output Only  
Output Format: RMYT  
Baud Rate: 9600

These are the default sensor settings as shipped unless otherwise requested. Use shielded cable. Connect earth ground as shown.



Model 86000 / 86106  
Ultrasonic Anemometer

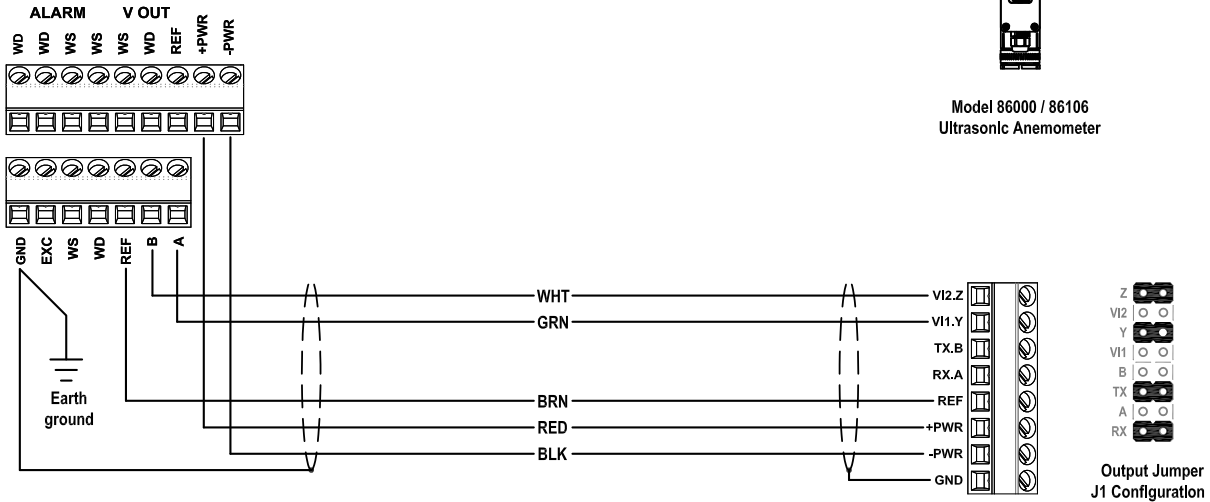
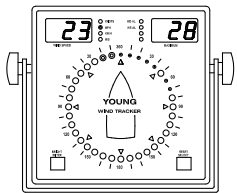


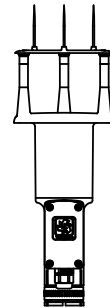
Fig. A6: 06206 MARINE WIND TRACKER



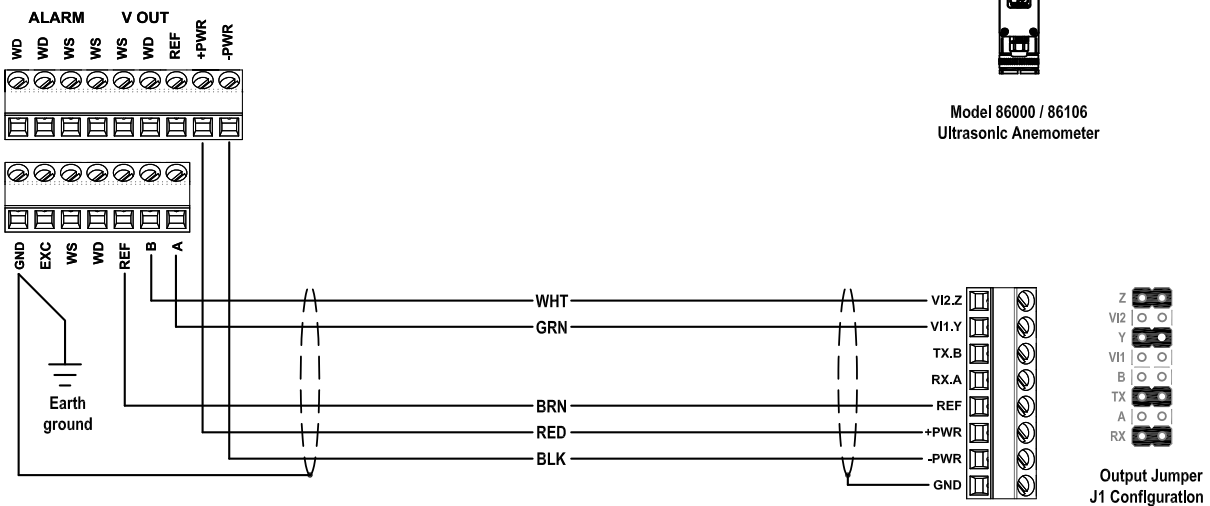
Model 06206  
Wind Tracker

SETTINGS:  
Output Mode: RS-485 Output Only  
Output Format: NMEA  
Baud Rate: 4800

Use shielded cable. Connect earth ground as shown.

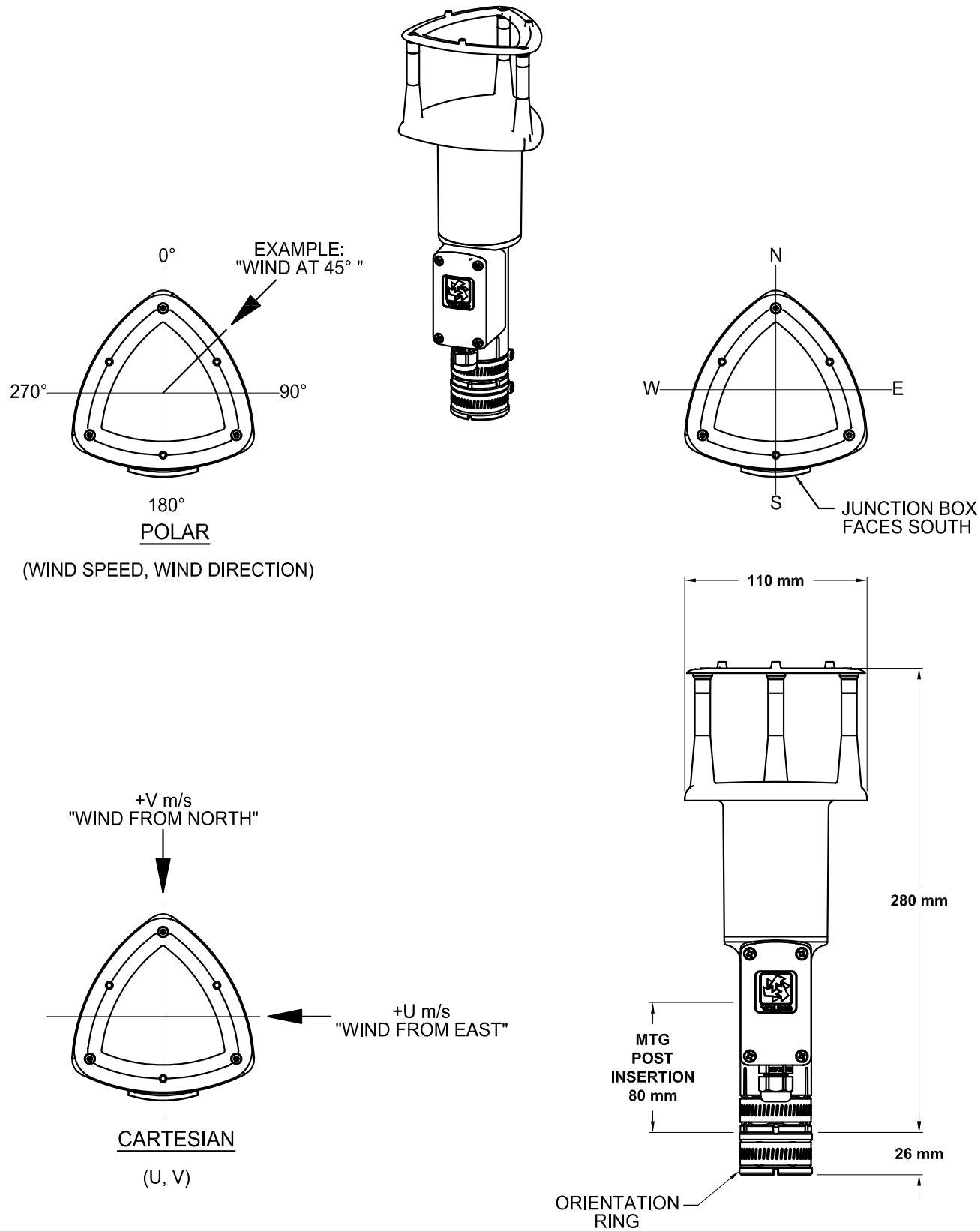


Model 86000 / 86106  
Ultrasonic Anemometer





**APPENDIX B: SENSOR ORIENTATION AND DIMENSIONS**



## **APPENDIX C: CALCULATIONS**

## Galena Creek Bridge Dead Load Calculations

$$\rho_{conc} := 150 \frac{lb}{ft^3}$$

Density of Concrete

$$L := 525 \text{ m}$$

Length of Bridge

### Barrier Rails

$$A_{box} := 0.45 \text{ m} \cdot 1.07 \text{ m}$$

$$cut_1 := 0.1675 \text{ m} \cdot 0.815 \text{ m}$$

$$cut_2 := 0.77 \text{ m} \cdot 0.075 \text{ m}$$

$$cut_3 := 0.18 \text{ m} \cdot 0.125 \text{ m} \cdot 0.5$$

$$A_{barrier\_rail} := A_{box} - cut_1 - cut_2 - cut_3 = 0.276 \text{ m}^2$$

$$line\_load := A_{barrier\_rail} \cdot \rho_{conc} = 6.503 \frac{kN}{m}$$

$$W_{barrier\_rail} := 4 \cdot L \cdot line\_load = 13.657 \text{ MN}$$

The cross sectional area of the barrier rail was taken by taking the full 450 mm x 1070 mm area and subtracting areas where there is no concrete.

Multiplied by a factor of 4. The NB structure and SB structure both have two barrier rails.

### Future Wearing Surface

Assume 3 in thick hot mix asphalt as wearing surface

$$area\_load := 3 \text{ in} \cdot \rho_{conc} = 1.796 \frac{kN}{m^2}$$

$$lane\_width := 18 \text{ m}$$

$$W_{FWS} := 2 \cdot L \cdot lane\_width \cdot area\_load = 33.935 \text{ MN}$$

$$W_{loads} := W_{FWS} + W_{barrier\_rail} = 47.592 \text{ MN}$$

## Superstructure

### Box Girder

Cross sectional area computed by CSI Bridge

$$A_{box\_girder} := 8.4664 \text{ m}^2$$

$$W_{box\_girder} := A_{box\_girder} \cdot \rho_{conc} \cdot 525 \text{ m} \cdot 2$$

$$W_{box\_girder} = 209.47 \text{ MN}$$

### Diaphragms

$$A_{diaph} := \frac{3.192 \text{ m} + 5.283 \text{ m}}{2} \cdot 2.6 \text{ m} \cdot 2$$

Diaphragm Thicknesses

$$t_{intermediate} := 0.25 \text{ m}$$

$$t_{hinge} := 5.8 \text{ m}$$

$$t_{abut} := 1.6 \text{ m}$$

$$t_{fillet} := 0.5 \text{ m}$$

$$t_{crown} := 0.3 \text{ m}$$

$$t_{total} := 2 \cdot (2 \cdot t_{hinge} + 2 \cdot t_{fillet} + 2 \cdot t_{crown} + 7 \cdot t_{abut} + 8 \cdot t_{intermediate}) = 52.8 \text{ m}$$

$$W_{diaph} := 2 \cdot A_{diaph} \cdot t_{total} \cdot \rho_{conc} = 54.829 \text{ MN}$$

### Link Slab

$$V_{link\_slab} := 0.2 \text{ m} \cdot 2.02 \text{ m} \cdot 240 \text{ m}$$

$$W_{link\_slab} := \rho_{conc} \cdot V_{link\_slab} = 2.285 \text{ MN}$$

$$W_{superstructure} := W_{box\_girder} + W_{diaph} + W_{link\_slab} = 266.583 \text{ MN}$$

Properties	
Base Material 4500Psi (31MPa) v	
A	8.4664
J	24.581
I33	10.7151
I22	176.3352
I23	0.
AS2	3.0022
AS3	6.5324
S33(+face)	10.6375
S33(-face)	5.3772
S22(+face)	18.6598
S22(-face)	18.6598
Z33	7.567
Z22	31.8184
r33	1.125
r22	4.5637
Xcg	9.45
Ycg	1.9927
Xpna	9.45
Ypna	2.7437
OK	

## Substructure

### Columns

$$A_{column} := 6 \text{ m} \cdot 3 \text{ m} - 1.8 \text{ m} \cdot 4 \text{ m} + 2 \cdot 0.15 \text{ m} \cdot 0.15 \text{ m}$$

$$W_{NB\_col\_1} := \rho_{conc} \cdot A_{column} \cdot 19.2 \text{ m}$$

$$W_{SB\_col\_1} := \rho_{conc} \cdot A_{column} \cdot 16.6 \text{ m}$$

$$W_{NB\_col\_2} := \rho_{conc} \cdot A_{column} \cdot 38.0 \text{ m}$$

$$W_{SB\_col\_2} := \rho_{conc} \cdot A_{column} \cdot 38.0 \text{ m}$$

$$W_{NB\_col\_3} := \rho_{conc} \cdot A_{column} \cdot 38.8 \text{ m}$$

$$W_{SB\_col\_3} := \rho_{conc} \cdot A_{column} \cdot 38.8 \text{ m}$$

$$W_{NB\_col\_4} := \rho_{conc} \cdot A_{column} \cdot 34.4 \text{ m}$$

$$W_{SB\_col\_4} := \rho_{conc} \cdot A_{column} \cdot 22.0 \text{ m}$$

$$W_{NB\_col\_5} := \rho_{conc} \cdot A_{column} \cdot 31.3 \text{ m}$$

$$W_{SB\_col\_5} := \rho_{conc} \cdot A_{column} \cdot 22.2 \text{ m}$$

$$W_{NB\_col\_6} := \rho_{conc} \cdot A_{column} \cdot 23.9 \text{ m}$$

$$W_{SB\_col\_6} := \rho_{conc} \cdot A_{column} \cdot 16.5 \text{ m}$$

$$W_{NB\_columns} := W_{NB\_col\_1} + W_{NB\_col\_2} + W_{NB\_col\_3} + W_{NB\_col\_4} + W_{NB\_col\_5} + W_{NB\_col\_6}$$

$$W_{SB\_columns} := W_{SB\_col\_1} + W_{SB\_col\_2} + W_{SB\_col\_3} + W_{SB\_col\_4} + W_{SB\_col\_5} + W_{SB\_col\_6}$$

$$W_{columns} := W_{NB\_columns} + W_{SB\_columns} = 86.808 \text{ MN}$$

### Link Beams

$$V_{link\_beam} := 4 \text{ m} \cdot 6 \text{ m} \cdot 13.92 \text{ m}$$

$$W_{link\_beams} := 2 \cdot V_{link\_beam} \cdot \rho_{conc} = 15.744 \text{ MN}$$

Thust blocks were not taken into consideration when computing self weight of structure.

### Arch

$$A_{arch} := 6 \text{ m} \cdot 3.6 \text{ m} - 5.2 \text{ m} \cdot 2.8 \text{ m} + 2 \cdot 0.35 \text{ m} \cdot 0.35 \text{ m}$$

$$W_{arch} := 2 \cdot \rho_{conc} \cdot A_{arch} \cdot (74.911 \text{ m} + 79.615 \text{ m} + 76.119 \text{ m}) = 79.184 \text{ MN}$$

$$W_{arch\_diaph} := 2 \cdot \rho_{conc} \cdot 5.2 \text{ m} \cdot 2.8 \text{ m} \cdot (6.731 \text{ m} + 7.827 \text{ m}) = 9.989 \text{ MN}$$

$$W_{substructure} := W_{columns} + W_{link\_beams} + W_{arch} + W_{arch\_diaph} = 191.724 \text{ MN}$$

## Comparison to CSI Bridge Values

$$W_{total} := W_{loads} + W_{superstructure} + W_{substructure} = 505.899 \text{ MN}$$

$$W_{CSI} := 151711 \text{ kip} + W_{loads} = 722.436 \text{ MN}$$

Note: the current DEAD load case in CSI Bridge does not take into account the barrier rails or future wearing surface.

$$Difference_{CSI} := \frac{W_{CSI} - W_{total}}{W_{total}} = 42.802\%$$

### Additional substructure loads

$$W_{footings} := 8 \cdot \rho_{conc} \cdot 2.75 \text{ m} \cdot 14 \text{ m} \cdot 13.42 \text{ m} = 97.395 \text{ MN}$$

$$W_{thrust\_blocks} := 4 \cdot \rho_{conc} \cdot 12 \text{ m} \cdot 13.4 \text{ m} \cdot 5.7 \text{ m} = 86.388 \text{ MN}$$

$$W_{GCB} := W_{total} + W_{thrust\_blocks} + W_{footings} = 689.682 \text{ MN}$$

$$Difference_{CSI} := \frac{W_{CSI} - W_{GCB}}{W_{GCB}} = 4.749\%$$

Note: the values calculated were slightly under the values reported by CSI Bridge. The difference is attributed to the change in superstructure depth and soffit thickness in the CSI model, which are not accounted for in this report.

### **Column Height Calculations (meters)**

Column heights were evaluated by calculating the difference between the elevation of the bottom of the box girder and the top of the footing at the centeline of the respective pier. All values are in meters unless specified otherwise

SB Pier 1	$1593.072 - 1576.45 = 16.622$	NB Pier 1	$1593.539 - 1574.35 = 19.189$
SB Pier 2	$1592.308 - 1554.259 = 38.049$	NB Pier 2	$1592.727 - 1554.68 = 38.047$
SB Pier 3	$1589.683 - 1550.914 = 38.769$	NB Pier 3	$1590.102 - 1551.333 = 38.769$
SB Pier 4	$1588.833 - 1568.85 = 19.983$	NB Pier 4	$1589.252 - 1554.85 = 34.402$
SB Pier 5	$1588.108 - 1565.95 = 22.158$	NB Pier 5	$1588.527 - 1557.25 = 31.277$
SB Pier 6	$1587.508 - 1571.05 = 16.458$	NB Pier 6	$1587.885 - 1563.95 = 23.935$

## Elastomeric Bearing Stiffness Calculations

$$G := 1.06 \text{ MPa}$$

Section Modulus of 60 Durometer Elastomer

$$E := 4.4 \text{ MPa}$$

Modulus of Elasticity of 60 Durometer Elastomer

### Abutment Bearings

$$b := 640 \text{ mm}$$

Elastomer Length

$$w := 640 \text{ mm}$$

Elastomer Width

$$A := b \cdot w = 0.41 \text{ m}^2$$

Gross Plan Area of Elastomer

$$I := \frac{b \cdot w^3}{12} = 0.014 \text{ m}^4$$

Elastomer Moment of Inertia

$$H_r := 12 \text{ mm} + 7 \cdot 13 \text{ mm}$$

Total Elastomer Thickness

$$H := 119 \text{ mm}$$

Total Bearing Height

$$K_H := \frac{G \cdot A}{H_r} = 4215.301 \frac{\text{kN}}{\text{m}}$$

Lateral Stiffness

$$K_V := \frac{E \cdot A}{H_r} = 17497.476 \frac{\text{kN}}{\text{m}}$$

Vertical Stiffness

$$K_\theta := \frac{E \cdot I}{H} = 516.945 \text{ kN} \cdot \text{m}$$

Rotational Stiffness



## Hinge Bearings

$$b := 710 \text{ mm}$$

Elastomer Length

$$w := 760 \text{ mm}$$

Elastomer Width

$$A := b \cdot w = 0.54 \text{ m}^2$$

Gross Plan Area of Elastomer

$$I := \frac{b \cdot w^3}{12} = 0.026 \text{ m}^4$$

Elastomer Moment of Inertia

$$H_r := 12 \text{ mm} + 13 \cdot 19 \text{ mm}$$

Total Elastomer Thickness

$$H := 287 \text{ mm}$$

Bearing Height

CSiBridge accepts a single input for bearing info at hinges. Multiply values by 3 to determine bearing properties for the three bearings at each hinge.

$$K_H := \frac{3 \cdot G \cdot A}{H_r} = 6625.205 \frac{\text{kN}}{\text{m}}$$

Lateral Stiffness

$$K_V := \frac{3 \cdot E \cdot A}{H_r} = 27500.849 \frac{\text{kN}}{\text{m}}$$

Vertical Stiffness

$$K_\theta := \frac{3 \cdot E \cdot I}{H} = 1194.565 \text{ kN} \cdot \text{m}$$

Rotational Stiffness



## **Nevada Department of Transportation**

Kristina L. Swallow, P.E. Director

Ken Chambers, Research Division Chief

(775) 888-7220

[kchambers@dot.nv.gov](mailto:kchambers@dot.nv.gov)

1263 South Stewart Street

Carson City, Nevada 89712